IDENTIFICATION AND ALTERATION OF GLOBAL RESONANCE MODES IN SHIP STRUCTURES TO REDUCE SOUND RADIATION

by

KEVIN MICHAEL McCOY

B. S., MECHANICAL ENGINEERING
S.U.N.Y. at STONY BROOK
(1978)

Submitted to the Department of
Ocean Engineering
in Partial Fulfillment of the
Requirements of the Degrees of

NAVAL ENGINEER

and

MASTER OF SCIENCE IN MECHANICAL ENGINEERING

at the
MASSACHUSETTS INSTITUTE OF TECHNOLOGY

May 1989

Signature of Author _____
Department of Ocean Engineering, 12 May 1989

Certified by _____
Richard H. Lyon, Thesis Supervisor

Certified by _____
J. Kim Vandiver, Thesis Reader

Accepted by _____
Chairman, Ocean Engineering Departmental Committee

Accepted by _____
Chairman, Mechanical Engineering Departmental Committee

IDENTIFICATION AND ALTERATION OF GLOBAL RESONANCE MODES IN SHIP STRUCTURES TO REDUCE SOUND RADIATION

by

KEVIN MICHAEL McCOY

Submitted to the Department of Ocean Engineering
on 12 May 1989 in partial fulfillment of the
requirements of the Degree of Naval Engineer and
Master of Science in Mechanical Engineering

ABSTRACT

A ship hull and foundation structure will have many vibratory resonance modes. During the shipbuilding process on land or in a drydock, it would be highly advantageous to determine which of these modes have a potential for strong sound radiation when the ship is waterborne.

This research employs an experimental model of a submarine hull and foundation. Small masses are placed on the foundation and hull, and the effects on the vibration spectra of the structure are studied. Based on spectra response, modes are classified as hull modes, foundation modes, or "global" modes. Global modes are well coupled hull and foundation mode pairs which are closely spaced in frequency.

Waterborne testing reveals that global mode pairs are strong waterborne sound radiators. Additionally, the application of small masses is shown to perturb the coupling between the global mode pairs and yield dramatic changes in the radiated sound.

Four foundations of differing size are tested and repeatability of the experimental results is confirmed. As the foundation size increases, global modes are identified on the basis of foundation drive point vibration spectra alone, hull vibration data is not required.

Thesis Supervisor : Richard H. Lyon
Title : Professor of Mechanical Engineering

ACKNOWLEDGEMENTS

Special thanks and deep gratitude to the United States Navy for providing me the opportunity of a lifetime to study at MIT.

Thanks to Professor Richard H. Lyon for his guidance and for allowing me complete freedom to plan and execute this experimental research.

Sincere thanks to Bolt, Beranek, and Newman, Inc. for donating use of their acoustic water tank. Without their generosity and support this work could not have been performed. Special thanks to Dan Nelson, Jeff Doughty, and David Lanfranchi for their assistance with logistics, access, and equipment needs.

Thanks to David Goldsmith of the David Taylor Research Center (DTRC), Annapolis, Maryland for his technical input and for sponsoring three weeks of valuable internship at DTRC during the summer of 1988.

Special thanks to Djamil Boulahbal for all the help he provided during this experiment and for his friendship.

To my father who sparked my interest in engineering at an early age, and whose generosity and encouragement made all the difference in the world these past three years, I am forever grateful.

To my beautiful daughters Kathleen Marie and Jacqueline Maureen whose smiles brightened many a day for me.

Above all, to my wife and best friend, Terry, whose love and support sustained me these past three years, and to whom I owe everything.

TABLE OF CONTENTS

1 INTRODUCTION

1.1 Need for Research

Rotating equipment installed in ships is a major source of noise radiated into the ocean. The radiated noise arises predominantly from vibratory energy transmitted from the rotating equipment, through its foundation and into the ship's hull. The resultant noise contains tones reflecting strong resonance frequency components of the equipment, its foundation and the hull. For a naval vessel, the radiated noise, and in particular the tonal properties of the noise, can result in unwanted detection and classification.

A rigidly connected system consisting of a foundation attached to a hull will have many vibratory mode shapes and many resonance modes yielding large amplitude vibrations. Some of these modes will likely be dominated by hull motion, and some will likely be dominated by foundation motion. Additionally, a few of these resonance modes may be driven by a "global" combination of a pair of closely spaced hull and foundation resonances. Such modes, which represent strong vibratory coupling between the foundation and hull, may result in an efficient generation of noise radiated into the water.

Many of the resonance modes of a foundation and hull structure will likely lie near (i.e., within 5 percent) the operational frequency of equipment to be installed on the foundation. Global mode pairs which exist within this frequency tolerance band may be strongly excited by the operating equipment and present a strong waterborne noise problem. It would be highly advantageous to identify these global modes and alter their close coupling. Ideally, this should

be accomplished during the shipbuilding process, rather than wait until the ship becomes operational. This would minimize costs and rework associated with scheduling a future availability and removing interfering equipment to allow access to the hull and foundation.

Current methods for modifying hull and foundation structures to reduce strong resonances are time consuming and involve development of expensive computer models and/or scale model testing to determine a suitable "fix". Application of these techniques to all the resonance modes found near the equipment operational frequency can therefore become prohibitively time consuming and expensive. A method of identifying these likely efficient radiating global resonance modes and information about the behavior of these modes would be of great benefit. Ideally, such a method should be relatively easy to perform in a shipboard environment.

1.2 Research Goals

Previous research [1] demonstrated that modes can be classified as either hull, foundation, or global by performing foundation drive point measurements. This work was performed on a high mobility model of a foundation (cantilevered beam - 0.16 cm. thick) attached to a hull (0.32 cm. thick aluminum plate). It was found that the spacing between the global resonance peaks could be altered by the addition of small masses. The fact that foundation drive point measurements alone were used to classify the modes is particularly appealing for potential shipboard use. In general, access to a foundation is easier than access to the hull due to structural and equipment interferences.

The goals of this thesis research are to apply the theory developed in [1] to a low mobility structure (i.e, more typical of a shipboard installation) to determine:

a) if global modes in a low mobility structure can be identified on the basis of foundation drive point measurements alone;

b) if global modes can be altered with small masses; and

c) the role global modes and altered global modes have on waterborne sound radiation.

Additionally, global mode response and characteristics should be compared with the structure in water and in air to determine if full scale testing during ship construction on land or in a drydock will likely predict the resonance mode response when the ship is waterborne.

1.3 Thesis Organization and Content

The goals described above form the basis of this thesis research. Chapter 2 describes and defines hull, foundation, and global modes in greater detail than above and outlines the method used to identify each of these mode types. Chapter 3 describes the experimental model, instrumentation, and reverberant water tank used for this research. Chapter 4 defines and calculates the important modal parameters of the model and water tank. Chapter 5 presents the experimental results of testing the model in the water tank and in air. Finally, Chapter 6 presents the conclusions resulting from this research along with recommendations for future research in this subject area.

2 THEORY

2.1 Introduction

As stated in Chapter 1, the initial research aimed at classifying resonance modes as being either predominantly hull, foundation, or a global combination of both the hull and foundation was conducted in [1]. The experimental model used for the research of [1] is depicted in Figure 2.1. The discussion that follows in this chapter is based on the experimental method and results presented in [1].

2.2 Definition of Global Modes

A large structure such as a ship hull will have many resonance modes. Likewise, a foundation will have many resonance modes as well. The independent hull and foundation structures may have resonance modes which are very close together in frequency. When these structures are joined, the closely spaced modes, as well as the other hull and foundation modes, will still be present.

From the standpoint of waterborne noise generated by operating equipment (e.g., a pump and motor) installed on a particular foundation, hull modes are, in general, of most concern since hull displacement results in volume velocity and hence pressure in the surrounding water. However, if closely spaced hull and foundation modes exist, these modes may be a potentially greater source of waterborne noise. This is due to the fact that vibratory energy is being

transmitted from the operating equipment through the foundation which, together with the hull, is undergoing a large amplitude global response. Hence, such closely spaced resonance mode pairs are termed "global" modes.

2.3 Identification of Global Modes

The identification of global modes can be broken down into a three step process involving use of masses at the free end of the foundation and masses at the junction between the hull and foundation. The order in which Steps 2 and 3 identified below are performed can be reversed. Figure 2.2 presents a flow chart summarizing the process of identifying hull, foundation, and global modes.

2.3.1 Step 1 - Obtain As Assembled Spectrum Data

This step consists of exciting the foundation rigidly attached to the hull and obtaining drive point spectrum data. For this research, drive point acceleration measurements were performed vice drive point mobility measurements performed in [1]. As will be shown in Chapter 5, the acceleration spectra of the model correlated directly with the reverberant water tank acoustic pressure spectrum with regard to resonance mode frequencies. Mobility (velocity divided by force) or accelerance (acceleration divided by force) measurements were found to be slightly skewed with regard to resonance mode frequencies compared to water tank pressure. This is due to the fact that the force anti-resonances occurred at slightly higher frequencies than the acceleration resonances.

2.3.2 Step 2 - Apply Tuning Mass to Foundation

This step involves distinguishing global and foundation modes from hull modes. Hull modes should be relatively unaffected by the presence of small masses added to the free end of the foundation (termed "tuning masses" for this research). Foundation modes will naturally be affected by the presence of the tuning mass since the foundation mode shapes and amplitudes will change in response to the tuning mass. Additionally, global mode pairs will likely be affected by the presence of the tuning mass since these modes represent strong coupling between the foundation and hull.

Modes affected (i.e., frequency or amplitude change) by the presence of the tuning mass are classified as either foundation or global modes.

2.3.3 Step 3 - Apply Coupling Mass to Junction

This step involves distinguishing hull and global modes from foundation modes. For a typical shipboard installation, the foundation impedance is much lower than the hull impedance. Therefore, a foundation will behave relatively "fixed" at the junction between the foundation and hull. If a mass were added to the junction, the foundation mode (fixed) will be relatively unaffected (i.e., little or no frequency shift or amplitude change). Global mode pairs (which represent strong coupling between the hull and foundation response) and hull modes will likely be affected by the presence of a mass at the junction which serves to increase the hull impedance at the junction. For the purposes of this research, mass added to the junction is termed "coupling mass" since it perturbs the junction and, as such, tends to alter the coupling between the hull and foundation at the junction. Modes affected by the presence of the coupling mass are classified as either hull or global modes.

By comparing the results of Steps 2 and 3 we can conclude that modes that are affected by both tuning and coupling masses can be classified as global modes. In [1], application of the methods described above enabled classification of modes as either hull, foundation, or global for the experimental model shown in Figure 2.1, where the hull was modeled as a plate (61 cm x 76 cm x 0.32 cm thick aluminum) and the foundation was modeled as a cantilevered beam (61 cm x 5.1 cm x 0.16 cm thick aluminum).

2.4 Alteration of Global Modes

The same coupling and tuning masses used to identify the global mode pairs also serve to alter the response of the global mode pairs by changing the frequency separation between modes comprising the global pair. For example, small tuning masses at the free end of the foundation should effect the foundation dominant mode of the global pair more than the hull dominant mode. Likewise, coupling masses will likely have a greater effect on the hull dominant mode of the global pair than the foundation dominant mode. If there is indeed a strong coupling between the global mode pairs, then the global response (and hence the radiated sound) should increase as the two modes come close together in frequency and amplitude, and decrease as the modes move farther apart.

When altering the resonance modes by the addition of tuning and coupling masses with the intent of comparing acoustic pressure response, care must be taken not to cause gross spectrum changes. A valid comparison between an unperturbed condition and a perturbed condition can only be accomplished when small scale spectrum changes result. Gross changes in resonant mode frequency or mode shape indicate that the original structure has been excessively distorted by the addition of mass.

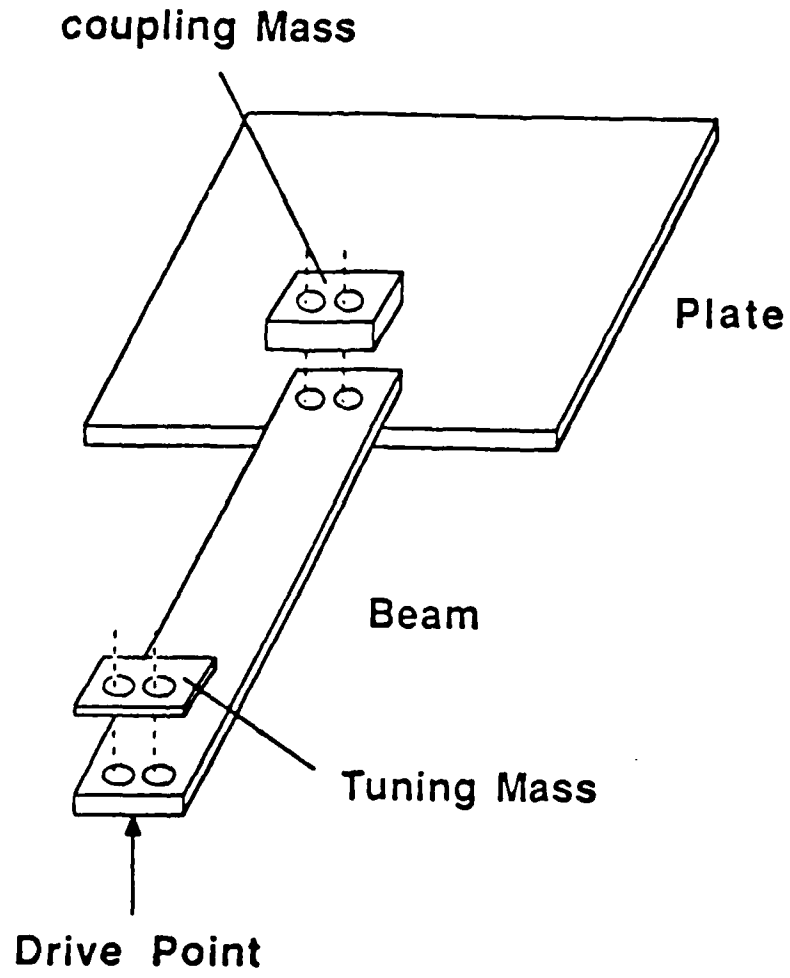

Figure 2.1 Experimental model used for the research conducted in [1]. The plate (61 cm x 76 cm x 0.32 cm thick) and beam (61 cm x 5.1 cm x 0.16 cm thick) are both aluminum. Figure taken from [1].

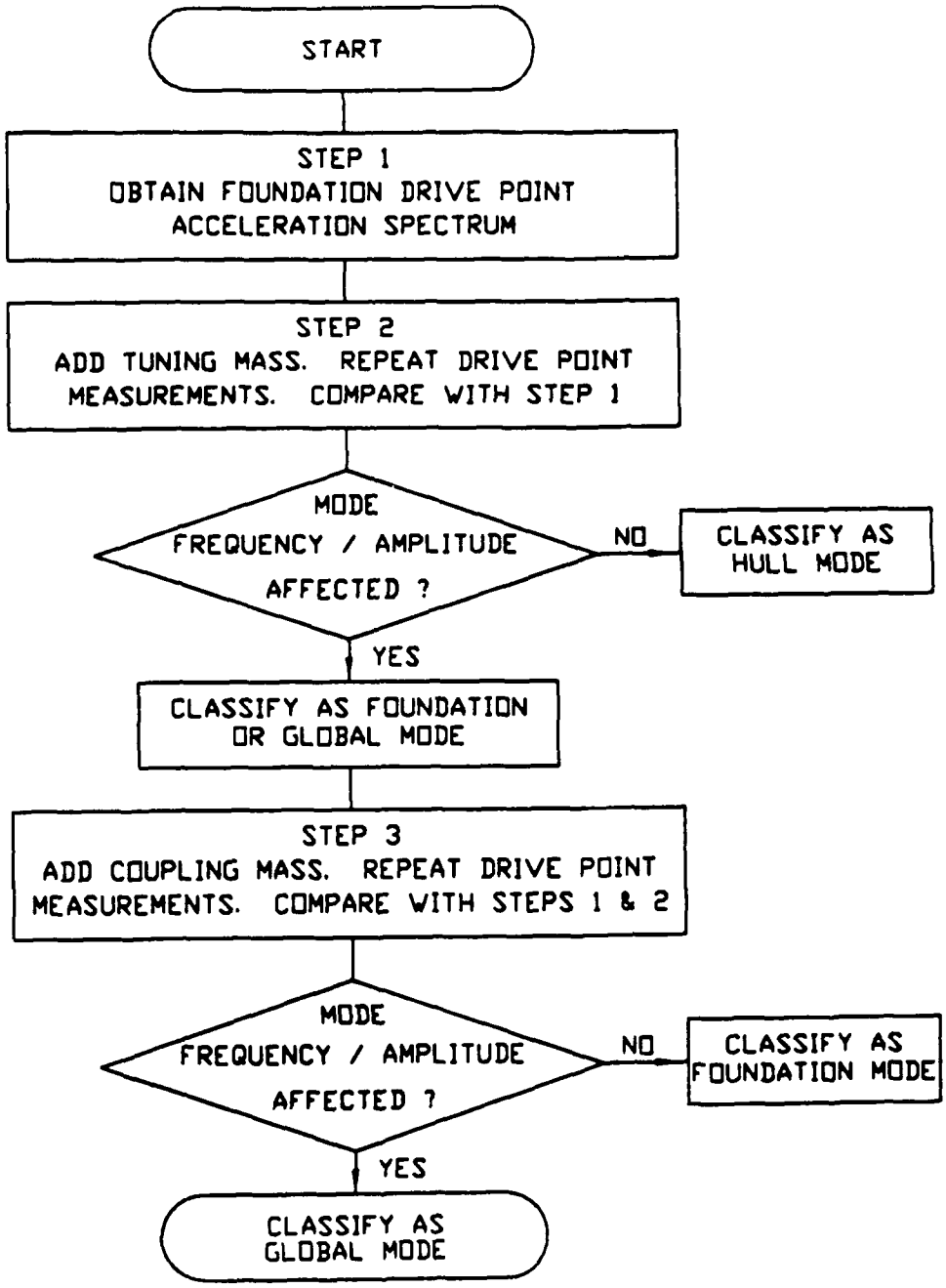

Figure 2.2 Flow chart summarizing the process of identifying hull, foundation and global modes.

3 EXPERIMENTAL MODEL AND INSTRUMENTATION

3.1 Introduction

The experimental model and instrumentation setup used for this research are shown in Figures 3.1 through 3.4. Specific details about the model and instrumentation are described in this chapter.

3.2 Model Scaling Parameters

A 1/4 inch thick steel plate is used to model a submarine pressure hull. This is thick enough to ensure low mobility (high impedance), yet not so thick as to make the model impractical to transport for waterborne testing. As such, the plate is an approximate 1/8 scale model of a submarine hull. Accordingly,

$$\lambda_{plate} = \frac{(h_{plate})_{model}}{(h_{plate})_{ship}} = \frac{1}{8} = \frac{\omega_{ship}}{\omega_{model}} \tag{3.1}$$

where, λ_{plate} = plate scaling parameter

h = plate thickness

ω = radian frequency

The object now is to determine the beam scaling parameter, λ_{beam}. Since the input excitation to the plate will be via a moment applied at the beams, the beams should be scaled such that the ratio of model to ship beam bending moment impedance equals the ratio of model to ship plate bending moment impedance. Therefore,

$$\left(\frac{W_{model}}{W_{ship}}\right)_{beam} = \left(\frac{W_{model}}{W_{ship}}\right)_{plate} \tag{3.2}$$

where, W = bending moment impedance

= ratio of bending moment to angular velocity

From [2] and [3], the moment impedances for an infinite plate and semi infinite beam (neglecting imaginary parts) are

$$W_{beam} = \left(\frac{\rho c_l^2 I}{c_b}\right)_{beam} \tag{3.3}$$

$$W_{plate} = \left(\frac{16\rho\kappa^2 c_l^2 h}{\omega}\right)_{plate} \tag{3.4}$$

where, ρ = material density

c_l = longitudinal wave speed

I = moment of inertia

κ = radius of gyration

h = plate thickness

c_b = bending wave speed $=\sqrt{\omega\kappa c_l}$

For a steel model and ship,

$$\left(\frac{W_{model}}{W_{ship}}\right)_{plate} = \left(\frac{\kappa^2 h}{\omega}\right)_{model}\left(\frac{\omega}{\kappa^2 h}\right)_{ship} \tag{3.5}$$

$$= \frac{\kappa^2_{model}}{\kappa^2_{ship}}\lambda^2_{plate} = \lambda^4_{plate}$$

$$\left(\frac{W_{model}}{W_{ship}}\right)_{beam} = \left(\frac{I}{\sqrt{\omega\kappa}}\right)_{model}\left(\frac{\sqrt{\omega\kappa}}{I}\right)_{ship} \tag{3.6}$$

However, since the ratio of model to ship moment of inertia (I) scales as λ^4_{beam}, the ratio of model to ship radius of gyration (κ) scales as λ_{beam}, and the ratio of model to ship frequency (ω) scales as λ^{-1}_{plate}, the following simplification results:

$$\left(\frac{W_{model}}{W_{ship}}\right)_{beam} = \lambda^{3.5}_{beam}\lambda^{0.5}_{plate} \tag{3.7}$$

Comparing equations 3.2, 3.5 and 3.7 yields

$$\lambda_{beam} = \lambda_{plate} \tag{3.8}$$

In other words, consistent with that of the plate, the beam characteristic dimension for the model should be 1/8 that of the full scale ship to ensure that bending moment impedances are properly modeled.

3.3 Plate

As stated above, the submarine hull is modeled as a 1/4 inch mild steel plate. The plate, originally 4 feet on each side, has had its corners cut slightly as shown in Figure 3.2. The cut corners reduce geometrical similarity to more closely approximate a large structure such as a submarine hull.

The ring frequency of a cylindrical structure such as a submarine hull defines the frequency limit above which the cylindrical structure behaves dynamically as a flat plate. From [4], the ring frequency f_{ring} for a cylinder of diameter d is

$$f_{ring} = \frac{c_l}{\pi d} \tag{3.9}$$

Using a diameter of 4 feet for a 1/8 scale model yields a ring frequency in steel of 1330 Hz. The frequency range used for this research is 400 to 2500 Hz. Accordingly, the model dynamically approximates a 32 foot diameter cylindrical structure in the upper half of the frequency range investigated.

3.4 Beams

Equipment foundations are modeled as beams welded perpendicular to the interior of the steel plate. Four steel pipe beams of varying cross section and approximately one foot long are attached to the plate (hull) via 360 degree welds at their base. As detailed above in section 3.1, the model foundations have a characteristic length equal to 1/8 those of the full scale ship foundations. Table 3-1 lists the model beam dimensions along with those of the

corresponding shipboard pipe type foundations. For comparison, Table 3-2 lists the cross sectional area, moment of inertia, and stiffness (based on cantilevered end condition at the plate) of each model beam. Figure 3.5 provides an exact scale drawing of each beam cross section.

Table 3-3 lists the ratio of beam bending moment impedance to plate bending moment impedance W_{beam}/W_{plate} at 500, 1500, and 2500 Hz. As can be seen, the ratio W_{beam}/W_{plate} is low for beams 1, 2, and 3 and approaches unity for beam 4 over the frequency range investigated. For comparison with shipboard installations, a low value of $W_{foundation}/W_{hull}$ would be typical for foundations for many small to medium sized components, such as an auxiliary sea water or hydraulic pumps. A high value of $W_{foundation}/W_{hull}$ would be expected for foundations for larger components, such as main propulsion elements and turbine generators.

TABLE 3-1 Foundation Dimensions (inches)

Model Beam Foundation	Full Scale Foundation
#1 - 0.313 OD x 0.250 ID	2.50 OD x 2.00 ID
#2 - 0.375 OD x 0.305 ID	3.00 OD x 2.45 ID
#3 - 0.438 OD x 0.365 ID	3.50 OD x 2.90 ID
#4 - 1.000 OD x 0.750 ID	8.00 OD x 6.00 ID

TABLE 3-2 Beam Properties

Beam	Cross Section (in^2)	Moment of Inertia (in^4)	Stiffness (lbf/in)	Mass (grams)
1	0.028	2.76 E-04	14.4	43
2	0.037	5.46 E-04	28.4	57
3	0.046	9.35 E-04	48.7	71
4	0.344	3.36 E-02	1750.0	529

TABLE 3-3 W_{beam}/W_{plate} as a Function of Frequency

Beam	$\frac{W_{beam}}{W_{plate}}$ at 500 Hz	$\frac{W_{beam}}{W_{plate}}$ at 1500 Hz	$\frac{W_{beam}}{W_{plate}}$ at 2500 Hz
1	5.28 E-03	9.02 E-03	1.17 E-02
2	9.45 E-03	1.64 E-02	2.17 E-02
3	1.49 E-02	2.58 E-02	3.31 E-02
4	3.63 E-01	6.24 E-01	8.06 E-01

The first three model beams listed in Tables 3-1, 3-2, and 3-3 are fairly similar to each other with regard to size, bending stiffness, moment impedance, and modal parameters (discussed in Chapter 4). Comparison of the results of testing these three foundations should provide an indication of the repeatability of the experimental method and results. Recall from Chapter 2 that the assumption made for a foundation mode to appear "fixed" at the hull junction (and thus, relatively unaffected by coupling mass) was that the foundation impedance be much lower than that of the hull. From Table 3-3, beams 1, 2, and 3 satisfy this assumption; beam

4 does not. Accordingly, the results of testing beam 4 should provide some indication of the expected range of shipboard foundation sizes to which the results of this research can be applied.

The beam spacing relative to the plate edge (see Figure 3.2) is on the order of, or greater than the bending wave lengths λ_b of the plate over the frequency range investigated. Where,

$$\lambda_b = \frac{c_b}{f} = \frac{\sqrt{\omega \kappa c_l}}{f} \tag{3.10}$$

For a 1/4 inch steel plate, Equation 3.10 reduces to

$$\lambda_b \approx 600\sqrt{\frac{h_{plate}(inches)}{f}}(inches)$$

$$\lambda_b \approx 15 \text{ inches at } 400 \text{ Hz}$$

At the free end of each beam, two threaded fasteners are attached via welds. One fastener is used for attaching the shaker and impedance head, and the other is used for attaching tuning masses. The end of the beam was selected for attaching the shaker and tuning masses since the mode shape is maximum at this location.

3.5 Damping

In [5] it was estimated that the damping loss factor (η) of a large framed structure such as a submarine hull was on the order of 1 to 2 percent. Modeling this damping loss factor was considered essential to this research since, as theorized in [1], highly damped modes may be

indicative of strong sound radiation into the water. The measured damping loss factor of the virgin plate was found to be in the range 0.1 to 0.2 percent over the frequency range 0 to 2500 Hz.

To achieve the required 1 to 2 percent damping loss factor, a constrained damping treatment was applied to the plate as shown in Figures 3.3 and 3.6. The plate surface interior to the 6 inch sides was covered with a 0.070 inch thick sheet of self stick viscoelastic damping material (TEC Damping Sheet, manufactured by Eckel Industries, Inc.) with the exception of four 8 inch diameter circles centered at each of the four beams (areas left open for placement of coupling masses). Distributed on top of the viscoelastic material is a total of 7 square feet of 1/32 inch stainless steel strips attached to the viscoelastic material via contact cement. The stainless steel layer ensures that the viscoelastic layer is shear loaded.

Measured values of the damping loss factor as a function of frequency are discussed in detail in Chapter 4.

3.6 Model Side Walls

Side walls (6 inches high) were fabricated from 3/4 inch plywood and installed on the plate as shown in Figures 3.1 through 3.4. The side walls were waterproofed and attached to the plate with epoxy and screws from the bottom. When waterborne, the sidewalls provided 3 inches of freeboard (i.e. the plate bottom was 3 1/4 inches below the surface) as shown in Figure 3.4.

3.7 Reverberant Water Tank

Waterborne testing was performed in a reverberant water tank at Bolt, Beranek, and Newman (BBN), Incorporated in Cambridge, Massachusetts. This tank holds 11,000 cubic feet of water and has a highly reflective liner (absorption coefficient of 0.05) covering the bottom and sides which acts as a pressure release surface. Figure 3.7 provides tank dimensions and identifies the location of the experimental model and hydrophones (discussed in Section 3.8.4) in the tank. Note that the tank was constructed so that no two walls are parallel. This minimizes echoes and enhances the coupling of sound from one end of the tank to the other.

For the tank to remain reverberant there must be enough resonance modes in the tank to support the reverberant sound field. From [6], the resonance frequencies of the M-th mode (f_M) of a three dimensional space can be determined from the following relation:

$$f_M^2 = \frac{c_{medium}^2}{4} \sum_{j=1}^{3} \frac{m_j^2}{L_j} \tag{3.11}$$

where, $j = 1,2,3$ subscripts apply to the coordinate axes

m_j is the modal integer number

L_j is the length in the j-th coordinate direction

Setting the modal integer numbers to 1 (lowest mode) and using the tank centerline dimensions of 32 by 23 by 14 feet deep yields 217 Hz as the lowest resonance frequency of the tank. For practical purposes, the tank is considered no longer reverberant below the 400 Hz 1/3 octave band. Accordingly, 400 Hz was established as the lower frequency limit for this thesis research.

3.8 Data Acquisition and Analysis

3.8.1 Shaker

A Brüel & Kjaer (B&K) Model 4810 vibration shaker was used to model operating equipment and provide vibration excitation to the beams (foundations). As discussed above, the shaker was installed at the free end of the beams. The shaker was driven with pseudo random noise over the acquisition bandwidth (0-2500 Hz) by the internal signal generator of the GenRad 2515 spectrum analyzer (discussed below). Pseudo random noise is random noise that is periodic with respect to each sampling interval.

3.8.2 Drive Point Force and Acceleration

Drive point force and acceleration was measured by a Wilcoxon Research Model Z602 impedance head attached between the shaker and the beams. As recommended in [7], the impedance head was attached flush against the beam without use of a connecting drive rod which can introduce errors due to drive rod compliance.

3.8.3 Plate Acceleration

Plate acceleration was measured by four B&K Model 4332 accelerometers (28 gram). The accelerometers were mounted on insulated studs which were epoxyed to the plate near the base of each foundation as shown in Figure 3.1 and 3.3. The acceleration power spectrum output from each of the accelerometers was averaged in the GenRad 2515 analyzer to form a spatially averaged acceleration power spectrum.

3.8.4 Waterborne Sound Pressure Level

Waterborne sound pressure level was measured by means of three International Transducer Corporation (ITC) Model 6050C hydrophones. Figure 3.7 depicts the location of the three hydrophones relative to the experimental model in the water tank. The pressure power spectrum output from each of the hydrophones was averaged in the GenRad 2515 analyzer to form a spatially averaged pressure power spectrum.

The distance from each hydrophone to the center of the model is 12.2 feet. The range of acoustic wavelengths in fresh water (sound speed of 4860 ft/sec) over the frequency range 400-2500 Hz is approximately 1.9 to 12.2 feet. Accordingly, each hydrophone is at least one wavelength away (and therefore out of the near field) from the model center over the frequency range investigated.

The 2500 Hz maximum frequency used for this research is considerably below the critical frequency (f_{crit}) of the 1/4 inch steel plate. Where, from [8]

$$f_{crit} = \frac{c_{medium}^2}{2\pi\kappa_{plate} c_l} \tag{3.12}$$

For a 1/4 inch steel plate in water, Equation 3.12 reduces to

$$f_{crit} = \frac{9340}{h_p(inches)} = 37,373Hz$$

Accordingly, the plate radiation will be acoustically slow with low radiation efficiency. However, during this research a signal pressure level of at least 40 dB (factor of 10,000) relative to water tank background noise pressure levels was observed near the resonance frequencies of the foundations (frequencies of interest for this research).

3.8.5 Data Analysis

A GenRad Model 2515 spectrum analyzer (16 channels) was used to process, store and plot all data associated with this research. The storage and programming capabilities of this analyzer were particularly well suited for this research. These capabilities allowed generation of spectrum plots which contain several data runs so as to clearly see the effect of tuning or coupling mass additions on the spectra. For example, the plots in Chapter 5 were produced using the storage and programming capabilities of this analyzer. The plotting program used during this research to display up to six different data ranges on a single plot is listed in APPENDIX B for information and use by others. This program is written in the Time Series Language (TSL2) programming language for the GenRad 2515 analyzer.

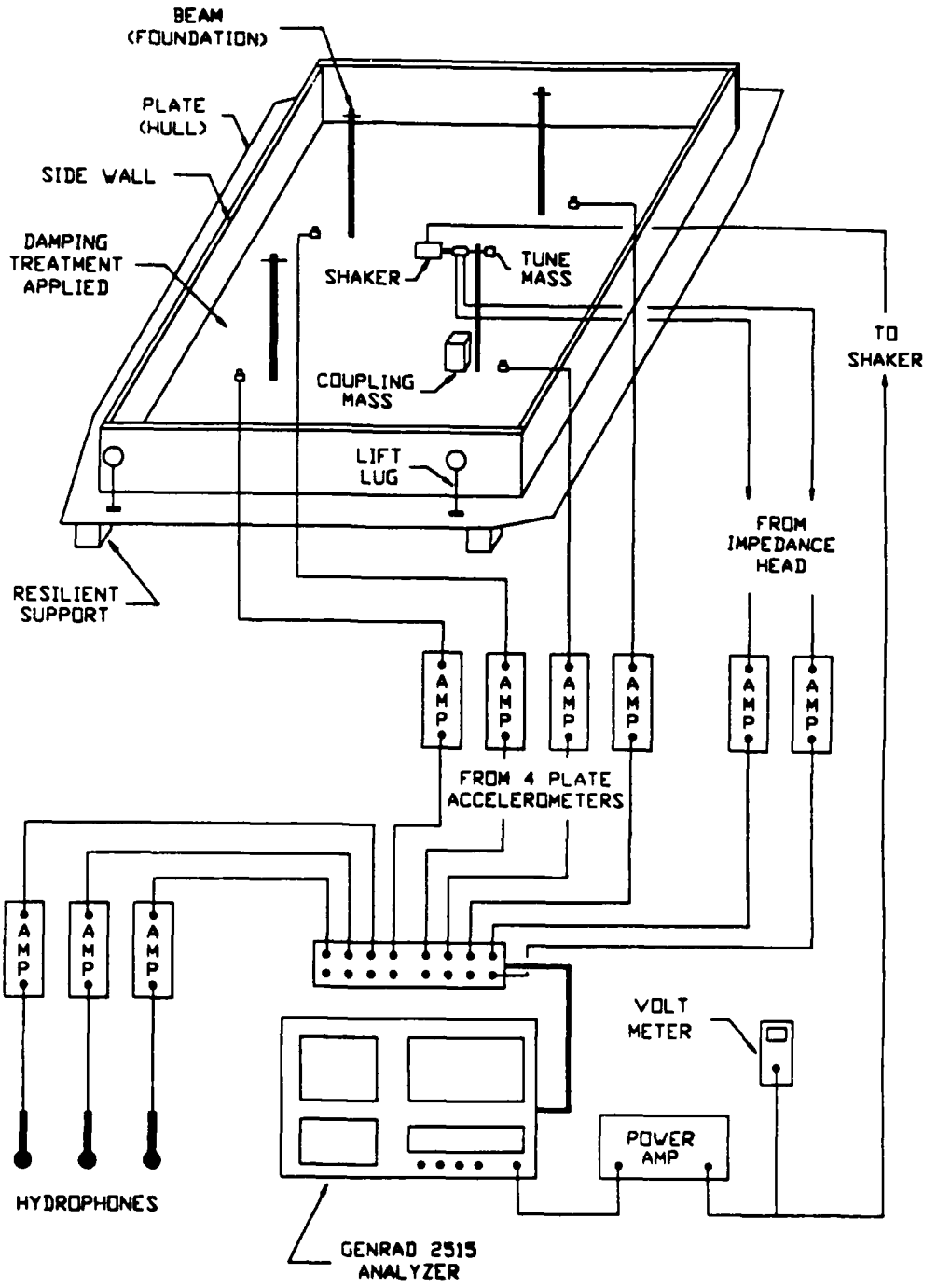

Figure 3.1 Experimental model and instrumentation.

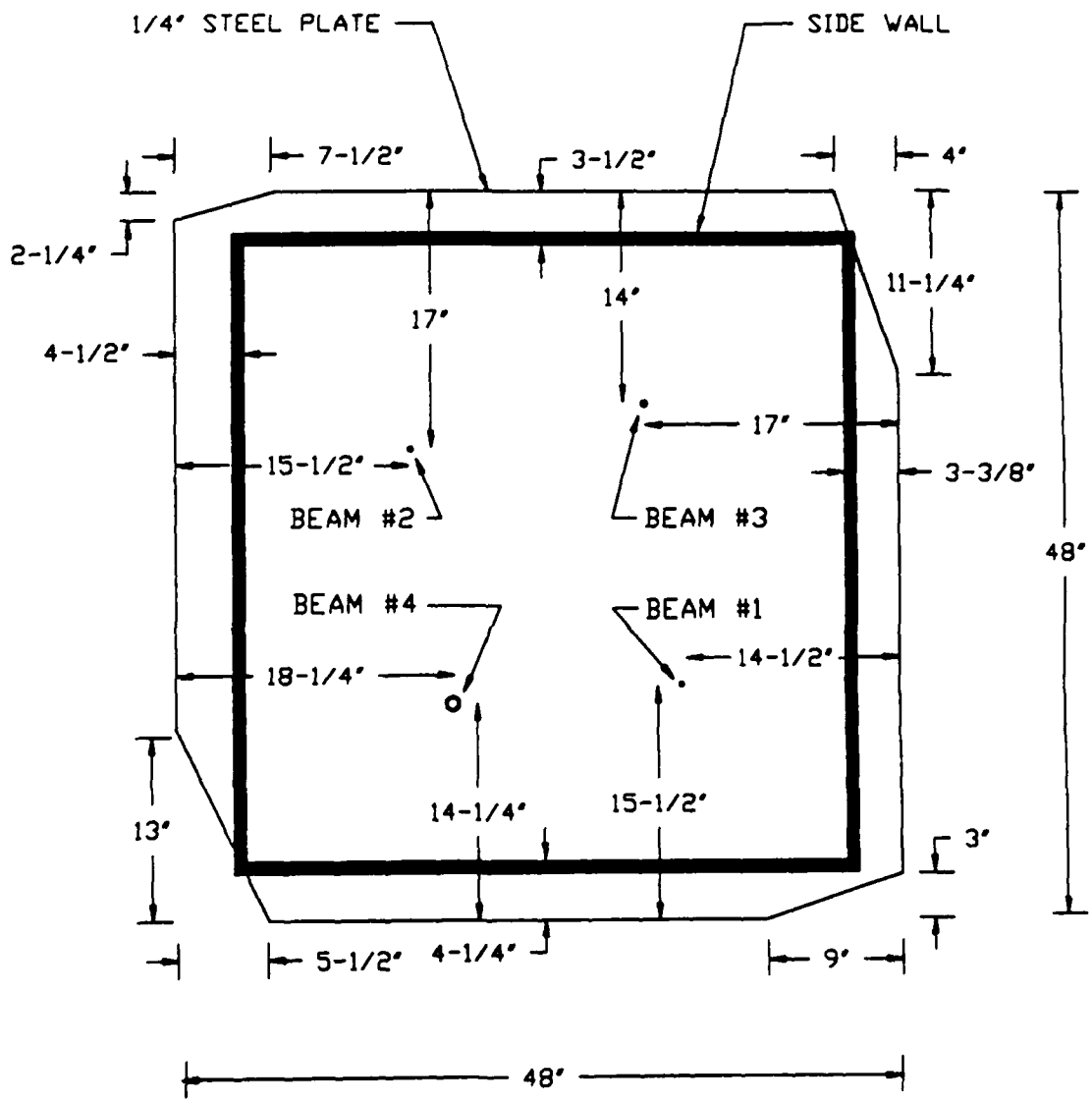

Figure 3.2 Overhead view of the experimental model showing dimensions.

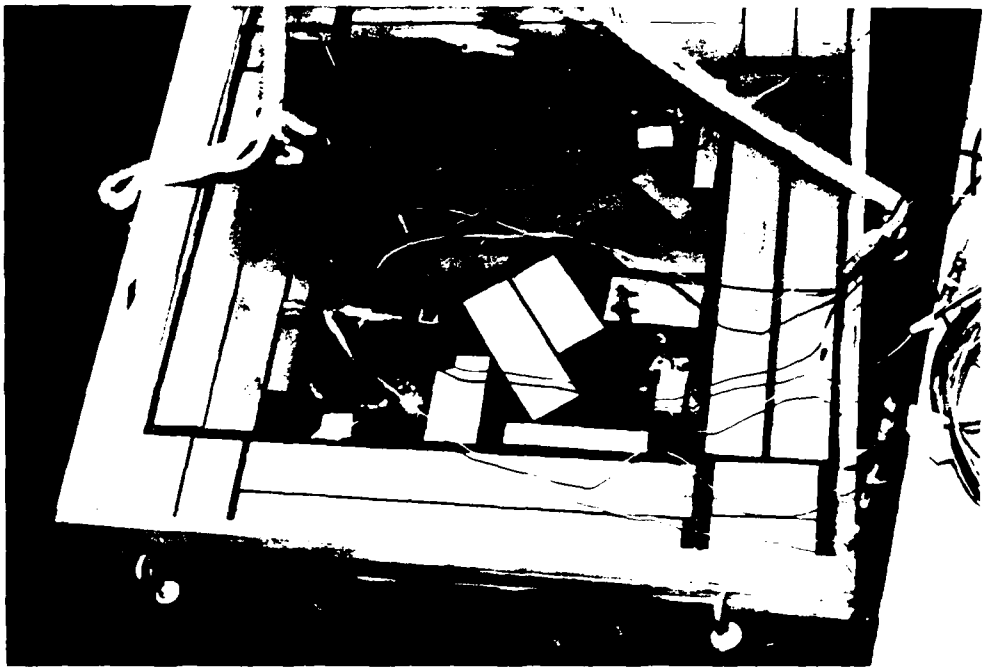

Figure 3.3 Overhead photograph of model showing damping treatment (rectangular sheet steel pieces cemented to TEC Damping Sheet. Shaker, impedance head and tuning mass are mounted on beam 4. Coupling mass is applied at the base of beam 4.

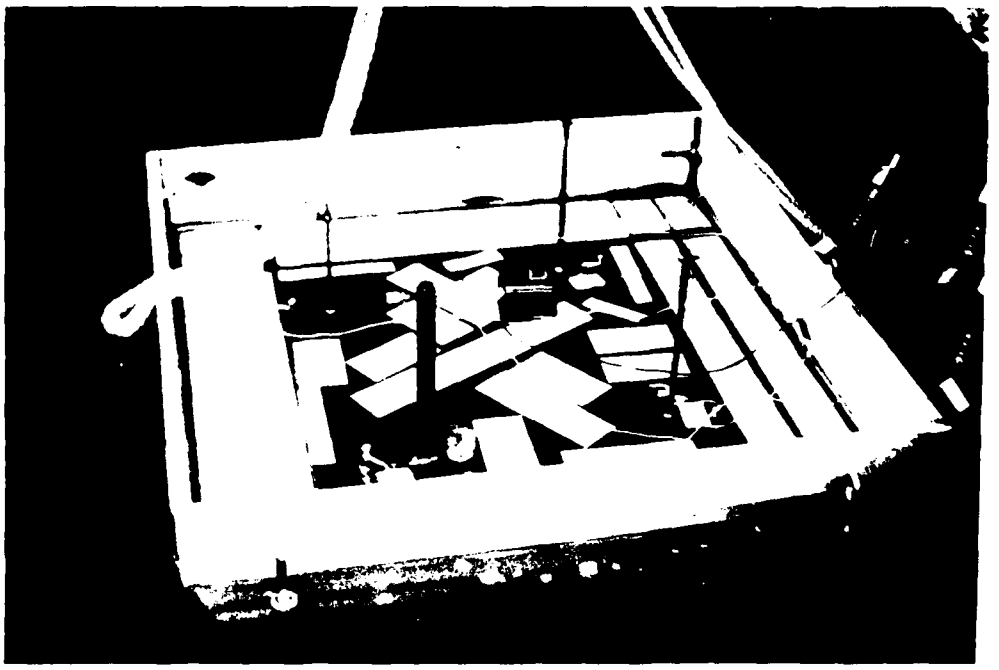

Figure 3.4 Same as Figure 3.3 except a side view of the model in the reverberant water tank.

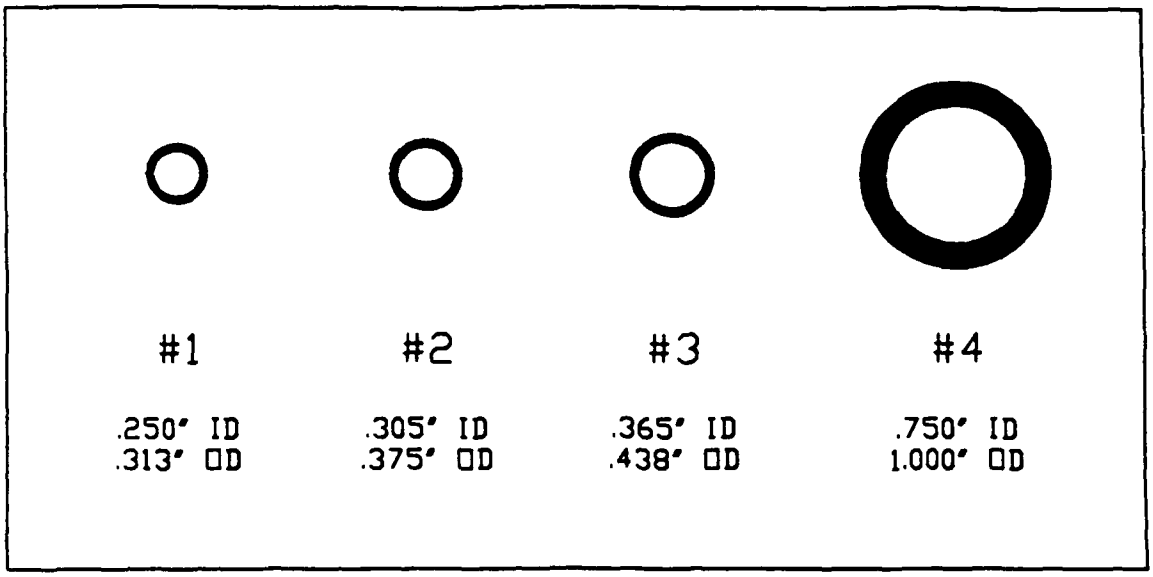

Figure 3.5 Beam cross sections shown actual scale.

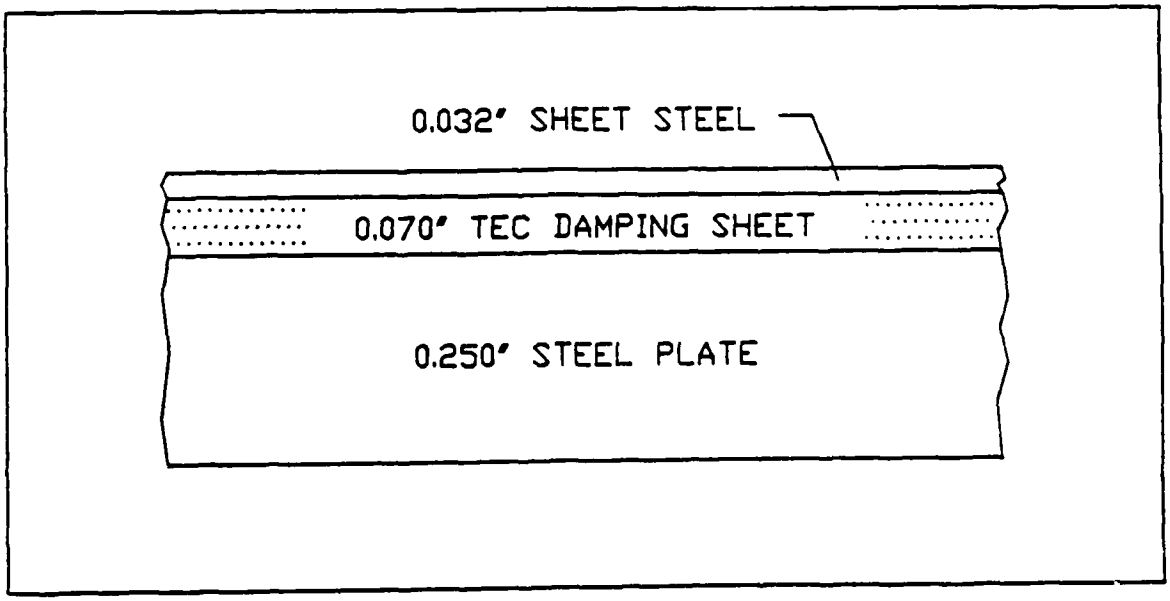

Figure 3.6 Plate damping treatment cross section.

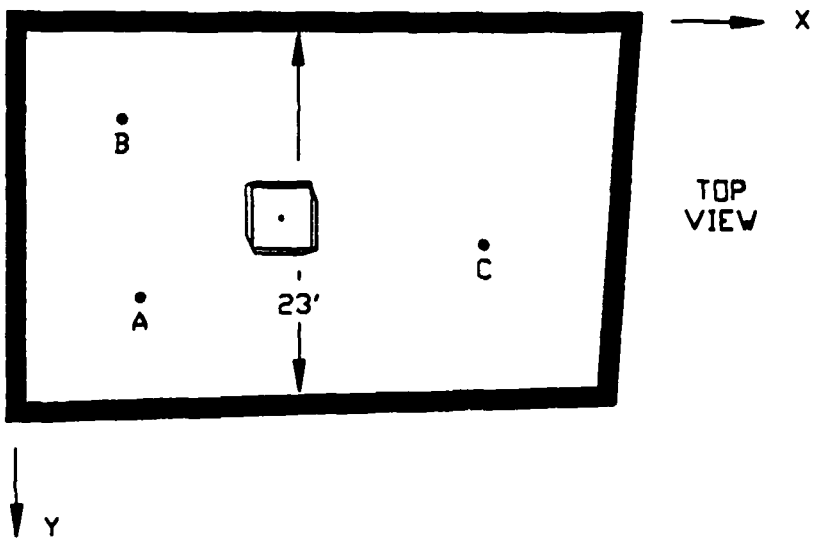

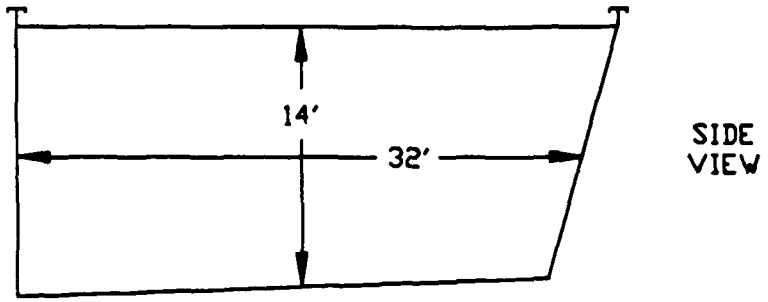

	X	Y	Z
H-PHONE A	7'	15.5'	8'
H-PHONE B	6'	5.5'	6'
H-PHONE C	26.5'	12.5'	4'
MODEL	15'	11'	

Figure 3.7 Top and side view of the reverberant water tank showing hydrophone and model placement. Tank sides and bottom are sloping. Dimensions shown are approximate centerline dimensions. Tank volume is roughly 11,000 cubic feet. Each hydrophone is roughly 12.2 feet from the model center.

4 MODAL PROPERTIES

4.1 Introduction

The purpose of this Chapter is to introduce and define some of the modal parameters important to this research. Specifically, the average frequency separation ($\overline{\delta f}$) between plate and beam modes, the plate damping loss factor (η) and reverberation time (T_{60}), and the acoustic water tank reverberation time as a function of frequency are discussed. Additionally, estimates of the amount of coupling and tuning mass required to noticeably perturb the drive point acceleration spectrum of each beam are made. At the end of this chapter, the experimental sampling period and frequency resolution are discussed and selected based on the modal properties of the experimental model and water tank.

To facilitate calculations, and for consistency with units used during the experiment, MKS units will be used in this chapter and in subsequent chapters.

4.2 Frequency Separation Between Plate Modes

From [4], the average frequency separation between plate (hull) modes can be expressed as

$$\overline{\delta f}_{plate} = \frac{2\kappa c_l}{A_p} = \frac{h_p c_l}{\sqrt{3}A_p} \sim 12.6Hz \tag{4.1}$$

where, A_p = plate area $\approx 1.486\ m^2$

h_p = plate thickness = 0.635 cm

c_l = longitudinal wave speed = 5100 m/sec

Figure 4.1 shows a typical mean acceleration power spectrum for the plate in water in the frequency range 0 to 200 Hz. The vibration source is a shaker mounted on the top of beam 3. Figure 4.2 shows a similar spectrum for the plate in air. Figures 4.1 and 4.2 verify that the calculated average frequency separation between plate modes of 12.6 Hz is consistent with measured results in water and in air.

Figure 4.3 shows a typical mean acceleration power spectrum for the plate in water in the frequency range 0 to 2500 Hz. As the frequency increases, the resonance peaks become rounded and more spread out as individual modes become masked due to modal overlap. If the plate modes are modeled as simple resonators, the effective bandwidth (Δ_e) of each mode of frequency f_n can be evaluated from [6] as,

$$\Delta_e(Hz) = \frac{\pi}{2}\eta f_n \tag{4.2}$$

Modal overlap occurs when Δ_e approaches $\overline{\delta f}_{plate}$ (12.6 Hz). Using an average value of 0.015 for η (see Section 4.6), Δ_e approaches 12.6 Hz for frequencies greater than roughly 500 Hz. This result agrees well with the plate spectrum shown in Figure 4.3

4.3 Frequency Separation Between Beam Modes

From [4], the average frequency separation between beam bending modes can be expressed as

$$\overline{\delta f}_{beam} = \frac{c_b}{L} = \frac{\sqrt{\omega \kappa c_l}}{L} \tag{4.3}$$

where, L = beam length = 0.3048 meters for each beam

Table 4-1 lists $\overline{\delta f}$ for each of the beams at 500 and 1500 Hz. Figure 4.4 shows the drive point acceleration spectrum of beam 3, for example. The distribution of resonance peaks conforms reasonably well to the values listed in Table 4-1.

Having established the average frequency separation between plate and beam modes, these values will be used in Chapter 5 to help distinguish between plate and beam modes.

Table 4-1 $\overline{\delta f}$ for Beams

Beam	$\overline{\delta f}$ at 500 Hz (Hz/mode)	$\overline{\delta f}$ at 1500 Hz (Hz/mode)
1	662	1146
2	727	1260
3	790	1368
4	1170	2026

4.4 Coupling Mass Estimate

To estimate the amount of coupling mass necessary to perturb the beam spectrum, an estimate of the "impedance level" of the junction between the beam and plate must be made. From [1], to estimate the junction impedance, $|Z|_{junction}$, we set

$$|Z|_{junction} \approx |Z|_{plate} + |Z|_{beam} \tag{4.4}$$

Where $|Z|_{plate}$ and $|Z|_{beam}$ refer to average drive point impedances of the plate and beam. From [1] and [4],

$$|Z| \sim 4M\overline{\delta f} \tag{4.5}$$

where, M is the mass of the plate or beam

For the plate, $|Z|$ is independent of frequency (since $\overline{\delta f}$ is constant).

$$|Z|_{plate} = 3717 kg/\sec$$

For the beams, $|Z|$ is a function of frequency. Values of $|Z|$ for the beams at 500, 1500 and 2500 Hz are listed in Table 4-2.

Table 4-2 Average Beam Drive Point Impedances

Beam	$\|Z\|$ at 500 Hz (kg/sec)	$\|Z\|$ at 1500 Hz (kg/sec)	$\|Z\|$ at 2500 Hz (kg/sec)
1	113	195	252
2	168	290	375
3	224	388	501
4	2476	4289	5538

To estimate the amount of coupling mass ($m_{coupling}$) necessary to perturb the junction (and thus the beam spectrum), we set

$$|Z|_{coupling} \approx |Z|_{junction} \tag{4.6}$$

where,

$$|Z|_{coupling} \approx \omega m_{coupling} \tag{4.7}$$

This results in the coupling mass estimates listed in Table 4-3 for each of the foundations. As can be seen, coupling masses on the order of 2 kg or less are estimated. Note that this is an estimate based on $|Z|_{coupling}$ being equal to $|Z|_{junction}$. In [1], with a very low impedance plate and beam model, it was reported that the beam spectrum was noticeably perturbed at values of $|Z|_{coupling}$ equal to roughly 20% of $|Z|_{junction}$. Based on Equation 4.7 and Table 4-3, we see that coupling mass effects should be more pronounced at higher frequencies.

Table 4-3 Coupling Mass Estimates

Beam	$m_{coupling}$ at 500 Hz (kg)	$m_{coupling}$ at 1500 Hz (kg)	$m_{coupling}$ at 2500 Hz (kg)
1	1.22	0.42	0.25
2	1.24	0.43	0.26
3	1.25	0.44	0.27
4	1.97	0.85	0.59

The analysis used above to estimate coupling mass amounts is taken from [1] and makes intuitive sense as long as the impedance of the beam is not so low that the plate appears as an infinite impedance to the beam at the junction (e.g., beam 1 may approach this situation). In

such a case (i.e., ideal cantilevered boundary condition), we can conclude that any additional impedance due to the coupling mass would likely have no effect on the beam. Conversely, if the impedance of the beam approaches that of the plate (e.g., as in the case for beam 4), coupling mass will likely have a pronounced affect. These considerations will be addressed again in Chapter 5.

4.5 Tuning Mass Estimate

To simplify determining the effect of adding tuning masses to the free end of the cantilevered beams under the forced vibration of the shaker, the static case of free vibration can be studied. From [9], the resonance frequency (ω_n) of a uniform cantilevered beam with a lumped mass added to the free end can be approximated as

$$\omega_n \approx \sqrt{\frac{3EI}{L^3(M+0.23m)}} \approx \sqrt{\frac{k}{M+0.23m}} \tag{4.8}$$

where, M = lumped mass; tuning mass for this research

m = beam mass

k = beam stiffness

From Equation 4.8, a 20% reduction in ω_n occurs for a tuning mass equal to roughly 10% of the beam mass. In other words, very small tuning masses have a large effect on the resonance frequency of free vibration, and will likely have a noticeable effect on the resonance frequencies of forced vibration. Based on the beam masses listed in Table 3-2 and the above simplified analysis, tuning masses on the order of 3 grams to roughly 100 grams should be sufficient to noticeably shift the resonant frequencies of the foundations.

The tuning mass applies a moment to the plate at the base of the beam. From [3], the power (Π) transmitted by a given moment (M_o) can be expressed as

$$\Pi = \frac{c_b}{8EI} M_o^2 = \frac{\sqrt{\omega \kappa c_l}}{8EI} M_o^2 \tag{4.9}$$

From Equation 4.9, the transmitted power is proportional to the square root of the frequency. Accordingly, the effects of tuning mass should increase with increasing frequency.

Note that the above discussion ignored any changes to the stiffness of the beam due to the added tuning mass. If the tuning mass should cause an increase in the stiffness, for example, the resonance frequency of the beam could actually increase due to the addition of the tuning mass.

4.6 Plate Damping and Reverberation Time

As discussed in Chapter 3, a constrained layer damping treatment was applied to the plate to achieve a damping loss factor (η) on the order of 1 to 2 percent necessary to properly model a large framed structure such as a submarine hull. Damping loss factor measurements were accomplished using the Integrated Impulse method described in [10]. Reverberation time (T_{60}) calculations were made using the measured plate damping loss factors. Appendix A describes the method and experimental setup used to obtain damping loss factors and reverberation times for each 1/3 octave band from 100 to 2500 Hz center frequencies in air and in water (plate bottom 3 inches below surface). Values of η and T_{60} for frequencies below 400 Hz are included for information only, since they are below the usable frequency range of the acoustic water tank. In general, plate damping loss factors in water were greater than those

in air. This is most likely due to radiation damping effects.

Table 4-5 Plate Damping Loss Factors and Reverberation Times

1/3 Octave Band (Hz)	$\eta - air$	$\eta - water$	$T_{60} - air$ (sec)	$T_{60} - water$ (sec)
100	.015	.011	1.47	2.00
125	.014	.018	1.26	0.98
160	.013	.022	1.06	0.63
200	.017	.025	0.65	0.44
250	.010	.030	0.88	0.29
315	.010	.028	0.70	0.25
400	.016	.024	0.34	0.23
500	.020	.021	0.22	0.21
630	.012	.012	0.29	0.29
800	.017	.019	0.16	0.14
1000	.017	.019	0.13	0.12
1250	.012	.015	0.15	0.12
1600	.011	.017	0.13	0.08
2000	.013	.019	0.08	0.06
2500	.018	.020	0.05	0.04

4.7 Water Tank Reverberation Time

Reverberation time as a function of frequency for the water tank was obtained from [11] and is listed in Table 4-6. Note that the T_{60} data was measured without the model in the water

tank . Due to the small size of the experimental model in relation to the tank size, the T_{60} values listed for the tank alone closely approximate the values for the tank with the model in the water.

Table 4-6 Water Tank Reverberation Times

1/3 Octave Band (Hz)	T_{60} (sec)
400	0.23
500	0.21
630	0.29
800	0.14
1000	0.12
1250	0.12
1600	0.08
2000	0.06
2500	0.04

4.8 Sampling Period and Frequency Resolution

With the GenRad 2515 spectrum analyzer used for this research, the sampling period is the reciprocal of the frequency resolution. The sampling period should be long enough to ensure that amplitudes have decayed to nearly background levels prior to initiating a new sampling run. The frequency resolution should be fine enough to allow adequate discrimination of the vibration modes of interest. To satisfy these considerations, a sampling period of 1 second (and consequently, a frequency resolution of 1 Hz) was selected for this research. This

sampling period allows amplitude decays of greater than 60 dB over the frequency range 400 to 2500 Hz based on the T_{60} values listed in Tables 4-5 and 4-6. Additionally, the resultant 1 Hz frequency resolution allows for sufficient discrimination of plate modes which have a $\overline{\delta f}$ of 12.6 Hz.

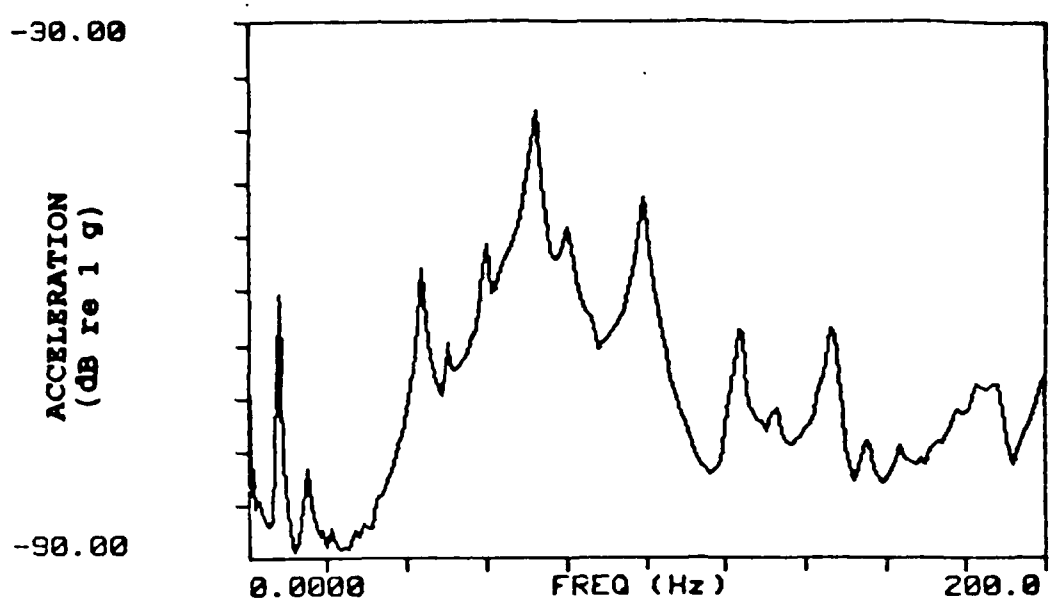

Figure 4.1 Typical mean acceleration power spectrum for the plate in water from 0 to 200 Hz. The measured average frequency separation between plate modes agrees well with the calculated value of 12.6 Hz.

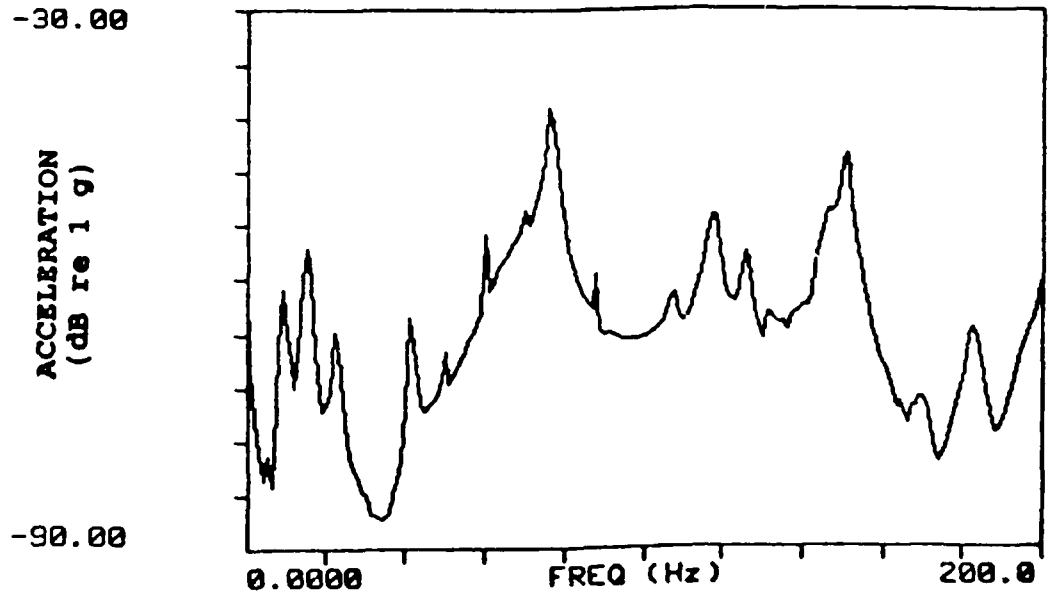

Figure 4.2 Typical mean acceleration power spectrum for the plate in air from 0 to 200 Hz. The measured average frequency separation between plate modes agrees well with the calculated value of 12.6 Hz.

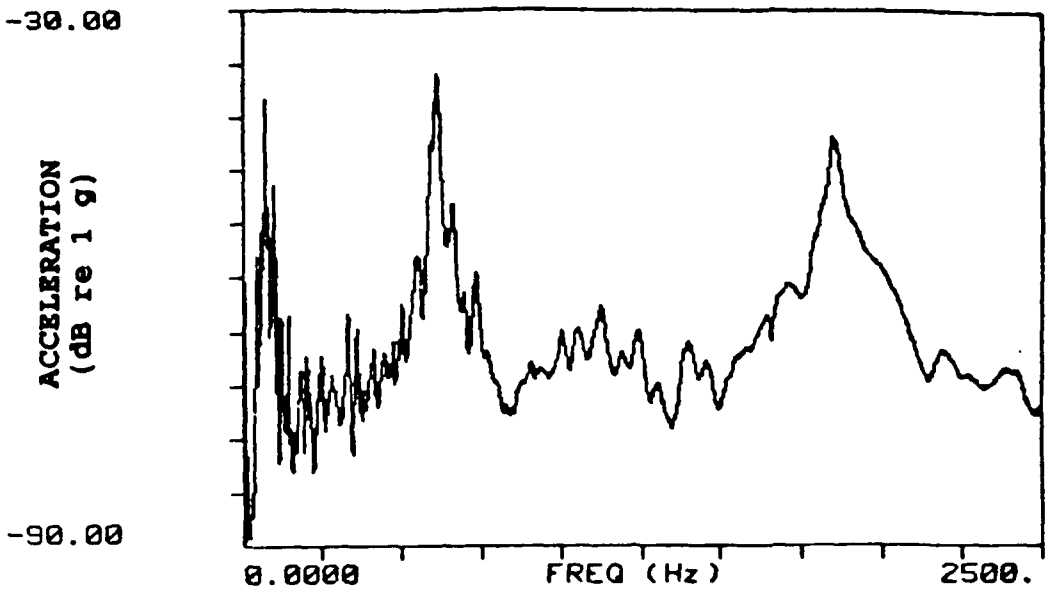

Figure 4.3 Plate acceleration power spectrum as in Figure 4.1 except over the range 0-2500 Hz. This figure shows modal overlap at frequencies greater than about 500 Hz.

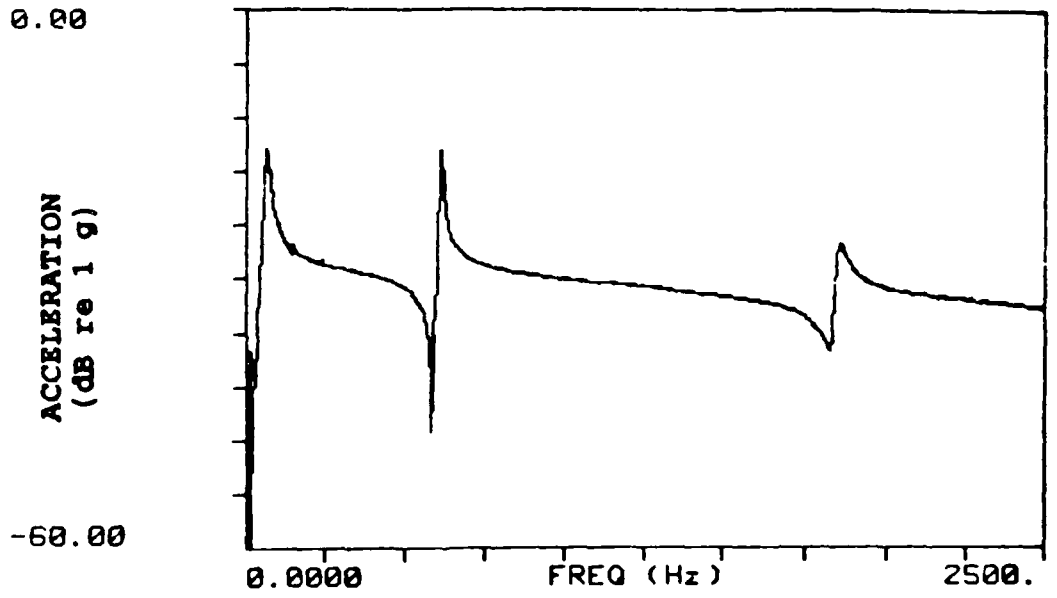

Figure 4.4 Typical drive point acceleration power spectrum for beam 3. The measured average frequency separation between beam modes agrees well with the values listed in Table 4-1.

5 EXPERIMENTAL RESULTS

5.1 Organization and Content

This chapter presents the experimental results obtained from testing the model in water and in air. Experimental results will be presented in the order: beam 3, beam 2, beam 1, and finally, beam 4. This order was chosen based on the following considerations:

a. As previously discussed, it is clear that beams 1, 2,and 3 are very similar in size, stiffness, and impedance. They are therefore expected to behave and interact with the plate in a similar manner. Beam 4 on the other hand, is much larger in cross section and has much greater stiffness and bending moment impedance than the other three beams. Consequently, the response of beam 4 and its interaction with the plate is expected to be markedly different from beams 1, 2, and 3.

b. Beam 3 results are presented first since the presence of plate modes were clearly evident in the drive point acceleration spectrum of this beam, thereby making this beam a logical starting point for analysis. Plate interactions were less evident in the smaller two beams.

To simplify following the numerous figures which will be presented to understand the modal interactions and their affect on the waterborne noise, the figures relative to each individual beam are presented at the conclusion of the discussion for that beam. Note that where multiple spectra of the same type are presented together in the same figure (e.g., Figure 5.1 showing 3 beam spectra), the top spectrum is shown with the correct amplitude value. Sub-

sequent spectra are offset in amplitude an equal amount for display purposes. Where multiple spectra of different types are presented in the same figure (e.g., Figure 5.8), all amplitude values shown are correct.

For all conditions tested and presented in this chapter, the shaker was excited with pseudo random noise over the frequency range 0 to 2560 Hz with a constant shaker input of 2.0 volts. All acceleration spectra presented have magnitude expressed as dB relative to 1 g (9.8 m/s^2). All pressure spectra presented have magnitude expressed as dB relative to water tank ambient background noise. Typical background noise levels recorded in the water tank were on the order of -180 dB relative to 1 micro bar.

5.2 Beam 3 Results

Sections 5.2.1, 5.2.2, and 5.2.3 below discuss in detail the results of testing beam 3 with the model in the water tank. Section 5.2.4 discusses the results of testing beam 3 with the model in air, simply supported at its corners. Section 5.2.5 provides a summary of conclusions reached as a result of testing beam 3 with the model in water and in air.

5.2.1 Beam 3 - Spectra Overview (Waterborne)

Figure 5.1 shows the drive point acceleration spectrum for beam 3 for the conditions of 0, 3, and 7 grams tuning mass added to the free end of the beam (no coupling mass added). Figures 5.2 and 5.3 show the mean plate acceleration and mean water tank acoustic pressure spectra for the 0, 3, and 7 grams tuning mass conditions. The following comments pertain to Figures 5.1, 5.2, and 5.3:

a) The beam acceleration spectrum consists of three dominant resonance modes with frequencies of 67, 613, and 1855 Hz prior to the addition of tuning mass. The frequency spacing between beam modes conforms well to the values calculated in Chapter 4. Application of 3 grams tuning mass reduces these frequencies to 65, 612, and 1850 Hz. The addition of 7 grams tuning mass results in resonance frequencies of 65, 601, and 2048 Hz. As can be seen, the predominant effect of the tuning mass is to lower the resonance frequencies, with the exception of the frequency increase from 1850 to 2048 Hz when changing from 3 to 7 grams tuning mass. This is most likely due to an increase in stiffness due to the 7 grams tuning mass at the high frequency.

b) The plate mean acceleration spectrum has dominant resonance peaks which coincide with those of the beam acceleration spectrum. This will be discussed in detail later in this chapter.

c) The mean water tank acoustic pressure has dominant resonance peaks which coincide with those of the plate (and beam) with the exception of the plate and beam mode near 67 Hz. This low frequency mode is not reflected in the pressure spectrum since the water tank is no longer reverberant (i.e., runs out of modes) below roughly 400 Hz as discussed in Chapter 3. Accordingly, this low frequency mode will not be studied in any further detail.

Figure 5.4 shows the effect of 10, 15, and 22 grams tuning mass on the beam spectrum compared to the zero tuning mass condition. Starting at 10 grams (14 percent of beam mass) the spectrum becomes "distorted" with a new mode appearing at roughly 1020 Hz. The 15 and 22 gram tuning mass conditions accentuate the distortion as beam characteristics and mode shapes likely undergo significant changes due to the presence of the lumped mass at the free end of the beam. Consistent with the philosophy (discussed in Chapter 2) of adding just enough

mass to cause small scale spectrum changes, the 10, 15, and 22 gram tuning mass conditions are considered outside the bounds to allow for reasonable comparison with the unperturbed (i.e., no added mass) condition.

The focus of the discussion that follows will be on the modes originally at 613 Hz and 1855 Hz, with the goal being to follow small scale changes in the beam and plate acceleration spectra and the water tank acoustic pressure spectrum.

5.2.2 Beam 3 - 500-700 Hz Range (Waterborne)

Beam and Plate Acceleration Spectra

Figure 5.5 provides a close-up view of the 613 Hz beam mode showing the effect of 3 and 7 grams tuning mass on the beam and plate acceleration spectra. The unperturbed beam spectrum shows the presence of two modes; a dominant mode at 613 Hz and a less dominant, although well defined mode at 594 Hz. The addition of 3 grams tuning mass reduces the frequency of the dominant mode by 1 Hz. The less dominant mode is relatively unaffected by the 3 grams tuning mass. The addition of 7 grams tuning mass results in the dominant mode frequency of 601 Hz (12 Hz decrease from unperturbed case) and two less dominant modes. The less dominant mode previously observed at 594 Hz experiences little or no frequency shift due to the 7 grams tuning mass. A new sharp peaked mode now appears at roughly 585 Hz. Note that the less dominant modes are closer in amplitude to the dominant mode in the plate spectrum than the beam spectrum. Also, away from the general vicinity of the dominant mode, the tuning mass has very little effect on the plate spectrum.

Based on Table 4-1, the expected average frequency separation between beam modes ($\overline{\delta f}$) near 600 Hz is in excess of 790 Hz. The presence of two modes roughly 20 Hz apart in

the beam spectrum indicates that one mode is likely a beam mode and the other mode (two modes in the 7 gram tuning mass case) is likely a plate mode. The dominant mode (613 Hz) is likely the beam mode since it is 18 dB higher in amplitude and beam acceleration amplitudes are much higher than those of the plate as indicated in Figures 5.1 and 5.2. Additionally, the dominant mode shifts much more in frequency than the other mode. As discussed in Chapter 2, beams modes are expected to be affected greatly by the tuning masses. The fact that the plate mode originally at 594 Hz experiences little or no frequency shift due to the 7 grams tuning mass would indicate (by the discussion in Chapter 2) that it is not a candidate to be a global mode.

Figure 5.6 shows the effect of adding coupling mass amounts of 100, 400, 1200, 2000, and 4000 grams to the base of the beam. The overall trend of the coupling mass is to increase the frequency of the dominant (beam) mode by roughly 4 Hz, and decrease the frequency of the less dominant (plate) mode previously observed at 594 Hz by roughly 7 Hz. Again, this indicates that the less dominant mode (originally at 594 Hz) is likely a plate mode since it is affected more by the presence of the coupling mass. Of more interest is the presence of 2 new modes (likely plate modes) which start to appear in the beam spectrum on both sides of the beam mode as 1200 grams of coupling mass is added. The well defined mode to the left of the dominant mode at 607 Hz at the bottom of the beam spectrum in Figure 5.6 (4000 grams coupling mass case) appears to be more affected by the presence of coupling mass than the dominant beam mode and is likely a plate mode. By inspection of the plate spectrum in Figure 5.6, this mode appears to be "splitting out" of the wide bandwidth peak. The mode appearing to the right of the dominant beam mode is another plate mode which moves roughly 30 Hz to the left as coupling mass is added.

Figure 5.7 shows the successive effects of first adding coupling mass amounts of 1200 and 2000 grams coupling mass and then adding 7 grams of tuning mass. Figures 5.5, 5.6, and 5.7 indicate that the addition of tuning and coupling masses have a noticeable and complicated effect on beam and plate modes. To follow and understand the modal interactions and relate the interactions to the radiated acoustic water pressure, the individual beam and plate acceleration spectra and the water tank acoustic pressure spectrum will be studied in detail for the range of tuning and coupling mass conditions shown in Figure 5.7.

Beam, Plate, and Pressure Spectra

Figures 5.8 through 5.13 show the beam drive point acceleration spectrum, the mean plate acceleration spectrum, and the mean water tank acoustic pressure spectrum for the conditions ranging from no tuning or coupling mass to 7 grams tuning mass and 2000 grams coupling mass. Figures 5.8 through 5.13 reveal that the average plate acceleration spectrum (average of 4 accelerometers) correlates extremely well (generally within 1 Hz) with that of the beam drive point acceleration spectrum regarding resonance mode peak frequencies. To facilitate following the movement and interactions of modes from figure to figure as mass configurations are varied, modes in the beam and plate spectra will be labeled A, B, C, and D, with mode A being the dominant beam mode.

Unperturbed Condition : Figure 5.8 shows that the acoustic pressure peaks near the frequency of the beam mode at 613 Hz (mode A). Additionally, the only plate mode visible in the beam spectrum is mode B at 594 Hz, where the plate acceleration is roughly 10 dB below that of the beam acceleration.

100 Grams Coupling Mass : Figure 5.9 shows the effect of the addition of 100 grams of coupling mass. Comparison with the unperturbed case shows that 100 grams coupling mass has practically no effect on either the beam, plate, or pressure spectra. This is as expected for such a small amount of coupling mass. The purpose of including Figure 5.9 here is to demonstrate that the hydrophone response is repeatable for similar mass configuration schemes and directly related to the beam and plate acceleration spectra.

1200 Grams Coupling Mass : Figure 5.10 shows the effect of 1200 grams coupling mass. Notable changes from Figure 5.8 include:

a) The overall acoustic pressure levels have increased, with the level at mode A increasing 3 dB.

b) Mode C has shifted from 659 Hz to 643 Hz, and along with a 3 Hz increase in frequency at mode A, modes A and C are now roughly 30 Hz apart vice 46 Hz apart prior to adding the coupling mass. Additionally, mode C is now starting to become visible in the beam spectrum, even though the plate acceleration is roughly 24 dB less in amplitude than the beam acceleration at that frequency. The acoustic pressure near mode C has increased 10 dB. The fact that the pressure at mode C increases dramatically as mode C approaches mode A indicates that there may be strong coupling between modes A and C.

c) The frequency separation between modes A and B increases 3 Hz. However, the acoustic pressure at mode B increases by roughly 7 dB . This trend tends to indicate that modes A and B are probably not well coupled and that the frequency spacing between these two modes does not control the acoustic pressure. Recall that this was previously suspected based on the fact that mode B did not respond to tuning mass as shown in Figure 5.5. The

acoustic pressure increase observed at mode B might be due to the overall increase in pressure observed near mode A; possibly in response to the fact that modes A and C are now closer together and reacting globally to increase the sound over the entire frequency region.

2000 Grams Coupling Mass : Figure 5.11 shows the effect of 2000 grams coupling mass. Comparison with Figure 5.10 reveals a new plate mode (mode D) now appears in the beam spectrum as beam mode A has shifted 1 Hz to the right. Comparison of Figure 5.11 with Figure 5.8 (unperturbed condition) reveals two obvious changes. The first is that the addition of 2000 grams coupling mass causes 3 plate modes to show up in the beam spectrum, vice 1 plate mode for the unperturbed case. The second change is that the acoustic pressure levels have increased considerably over the frequency range bounded by modes B, D, A, and C in Figure 5.11. This increase occurs even though the peak beam acceleration amplitude has actually decreased by 3 dB and the peak plate acceleration amplitude has decreased by roughly 1 dB. Additional comments relative to Figure 5.11 are as follows:

a) It appears that mode D was previously masked along with mode A in the plate spectrum due to modal overlap. Note that the acoustic pressure near mode D decreases slightly as mode D breaks away from beam mode A.

b) The frequency separation between modes A and C has now decreased to 19 Hz and the acoustic pressure in the region between modes A and C has increased roughly 4 dB. This again points to the possibility that close coupling of modes A and C is responsible for the large pressure increases.

c) The acoustic pressure increases again near mode B (by about 4 dB) while the frequency separation between mode B and beam mode A increases by about 1 Hz over that in Figure

5.10. Again, the fact that the acoustic pressure at mode B increases as mode B moves away from mode A indicates that some mechanism other than strong coupling with beam mode A must be responsible for the acoustic pressure increases.

3 Grams Tuning Mass Plus 2000 Grams Coupling Mass : Figure 5.12 shows the effect of 3 grams tuning mass plus 2000 grams coupling mass. Comparison of Figure 5.12 with Figure 5.11 reveals that the 3 grams tuning mass has caused mode D to completely split away from mode A and overlap with mode B. Note the reduced bandwidth at the peak of mode A as compared to Figure 5.11. Additional specific comments are as follows:

a) The 3 grams tuning mass lowered the frequency of the beam and plate modes; mode A decreased 3 Hz, mode C decreased 3 Hz and mode D decreased 16 Hz. Here it appears that the tuning mass had as much or more affect on the plate modes as on the beam mode.

b) The acoustic pressure in the frequency range between modes B and D was reduced by 12 dB as a result of mode D splitting away from beam mode A. This would indicate that mode D was likely well coupled to mode A and that high acoustic pressure levels at mode B previously observed in Figures 5.10 and 5.11 might have been due to the close proximity of mode B to mode D. In effect mode B may have been "carried along" by the close coupling of modes A and D.

c) Mode D is 6 dB higher in amplitude than mode C in the plate acceleration spectrum. However, the acoustic pressure at mode B is 13 dB less than at mode C. This shows that modes which exhibit high vibration amplitude are not necessarily efficient sound radiators; and vice versa.

7 Grams Tuning Mass Plus 2000 Grams Coupling Mass : Figure 5.13 shows the effect of 7 grams tuning mass plus 2000 grams coupling mass. Comparison with Figure 5.12 reveals the following:

a) As expected, the 7 grams tuning mass causes the biggest change in beam mode A (6 Hz reduction in frequency). Plate mode D has a roughly 4 dB increase in amplitude (in the plate spectrum). Modes A and D are now 7 Hz closer together than in Figure 5.12 and, along with this, a 6 dB increase in acoustic pressure is observed at plate mode D. However, the acoustic pressure at beam mode A has now decreased by 8 dB. A possible explanation for this decrease is presented below. An interesting observation from Figure 5.13 is that modes A and D are of equal magnitude in both the plate and pressure spectra.

b) Previous figures have shown that the acoustic pressure increases as modes A and C have been brought together in frequency. In Figure 5.13 we see that these two modes are shifted 5 Hz farther apart by the 7 grams tuning mass relative to the condition shown in Figure 5.12. As a result, the acoustic pressure decreases 8 dB at mode A and 6 dB at mode B. A disturbing observation from Figure 5.13 (as well as Figure 5.12) is that plate mode C now dominates the acoustic pressure spectrum. However, mode C is not distinctly visible in the beam drive point acceleration spectrum. In other words, this mode which appears very well coupled to the beam mode and, in turn, to the sound field, would not be detected by beam (or foundation in the case of a full scale ship) drive point measurements alone.

c) Mode B is now obscured and no longer distinct in either the beam or plate spectrum.

5.2.3 Beam 3 - 1750-1950 Hz Range (Waterborne)

Beam and Plate Acceleration Spectra

The 613 Hz mode previously discussed was rich with modal interactions and movements observable in both the beam and plate spectra. Due to modal overlap as a result of a damping loss factor of roughly 0.19, the 1855 Hz mode provides little or no insight into the effect of tuning and coupling masses on the modal interactions, spacings, or movements. Figure 5.14 shows both the beam and plate acceleration spectra for the unperturbed and 3 grams tuning mass conditions. Recall from Equation 4.2 that the effective bandwidth (Δ_e) of the 1855 Hz mode can be calculated from:

$$\Delta_e = \frac{\pi}{2}\eta f = 55.4Hz \tag{4.2}$$

This effective bandwidth greatly exceeds $\overline{\delta f}$ for the plate (12.6 Hz). Accordingly, on the order of 4 to 5 plate modes are masked in this frequency range.

The 3 grams tuning mass reduced the resonance frequency of the dominant beam mode by 5 Hz; compared to 1 Hz for the 613 Hz mode previously studied. Figure 5.15 shows the effect of coupling mass on the beam spectrum. Note that both the 2000 gram and 4000 gram coupling mass conditions result in an 8 Hz increase in resonance frequency compared to the unperturbed condition. In Figure 5.6, both the 2000 gram and 4000 gram coupling masses resulted in a 4 Hz increase in frequency over the unperturbed 613 Hz mode. These comparisons confirm the predictions of Chapter 4 that tuning and coupling masses will have a greater effect on altering resonance mode frequency at higher frequencies. Additionally, the comparisons

suggest that coupling mass may reach a "saturation level", whereby, after a certain amount is added (2000 grams in the case of the 613 and 1855 Hz modes) additional mass results in no additional frequency shift.

Pressure Spectrum

As discussed above, the high modal overlap at the 1855 Hz mode renders it impossible to follow the interaction of the beam and plate modes to determine their impact on the acoustic pressure. However, even though these vibratory modes may be masked, we can assume that the tuning and coupling masses are indeed altering both the frequency and amplitude characteristics of these modes. Accordingly, consistent with what was observed for the 613 Hz mode, we should observe noticeable changes in the acoustic pressure spectrum as tuning and coupling masses are applied.

Figures 5.16 through 5.21 follow the changes in the acoustic pressure spectrum for mass configurations ranging from the unperturbed case to 3 grams tuning mass plus 4000 grams coupling mass. These figures show that the acoustic pressure increases steadily near the beam mode as coupling mass amounts of 400 and 1200 grams are applied (9 dB increase after 1200 grams). As additional coupling mass is applied up to 4000 grams, the acoustic pressure decreases by 5 dB. The acoustic pressure then increases 3 dB as 3 grams tuning mass is added to the 4000 gram coupling mass condition. These significant changes in the pressure spectrum in response to little or no changes in vibration amplitudes support the theory that modal spacing and interactions play a dominant role in how the vibration field of a structure couples to the radiated sound field.

5.2.4 Beam 3 - Results in Air

Spectra Overview

Figures 5.22 and 5.23 show the beam drive point acceleration spectrum in air for tuning mass amounts ranging from the unperturbed condition to 22 grams. Comparison with Figures 5.1 and 5.4 for the waterborne case reveals that the results in air are very similar to the results in water relative to the appearance of the beam spectrum. The resonance peaks in air are reduced slightly in frequency from those in water. For example, the unperturbed condition in air has modes at 67, 609, and 1847 Hz, vice 67, 613, and 1855 Hz for the waterborne case.

The beam spectrum "distortion" due to 10, 15, and 22 grams tuning mass is similar in both the waterborne and airborne cases. Also, for both the waterborne and airborne cases, 7 grams of tuning mass increases the resonance frequency of the high frequency mode by roughly 200 Hz. Figure 5.24 depicts the mean plate acceleration spectrum in air. Comparison with figure 5.2 shows that, on a gross scale, the overall plate acceleration spectrum frequency and amplitude characteristics are comparable between the waterborne and airborne cases.

On a gross scale, it appears that the boundary condition differences between the waterborne and airborne cases do not result in significant acceleration spectra differences. The goal now is to follow individual modes in the beam and plate spectra and compare the waterborne and airborne cases on a mode by mode basis. To accomplish this, only the mode near 600 Hz will be studied. Fortunately, near 600 Hz the damping loss factor for the waterborne and airborne cases is the same (0.012). This should simplify comparing the waterborne and airborne spectra and identifying corresponding modes. The modes near 60 and 1850 Hz will not be studied further. As previously discussed, the mode near 60 Hz is outside the frequency range of this research, and modal interactions near 1850 Hz are masked by modal overlap.

500-700 Hz Range

Figures 5.25 through 5.31 compare beam and plate spectra in the frequency range 500-700 Hz for the waterborne and airborne cases as various combinations of tuning and coupling masses are applied. The top graph in each figure applies to the waterborne case; the bottom graph in each figure applies to the airborne case. In each figure, the waterborne graph has previously been presented and discussed, and is included here again to facilitate comparison. In all cases, individual modes are labeled A, B, C, D, etc, consistent with what was presented previously.

Figure 5.25 shows beam response to tuning mass amounts of 3 and 7 grams. The waterborne and airborne spectra appear similar with the exception of a sharp well defined plate mode to the left of the beam mode anti-resonance. Additionally, the plate mode to the left of the dominant beam mode is not distinct in the airborne case until 7 grams tuning mass is applied. The 7 grams tuning mass reduces the beam mode frequency 12 Hz for the waterborne case and 10 Hz for the airborne case. The tuning mass has very little effect on the other (plate) modes visible in both cases.

Figure 5.26 compares beam spectrum response to coupling mass amounts up to 4000 grams. Again, a similar response between the waterborne and airborne cases is observed, with one exception. For the waterborne case, 2000 grams of coupling mass resulted in a well defined plate mode close in amplitude and slightly to the left of the beam mode. This is not observed in the airborne case. However, the rounded shape of the spectrum just to the left of the beam mode indicates that this mode is likely present but masked. Both the 2000 gram and 4000 gram coupling masses increased the frequency of the beam mode in air by 2 Hz. This again supports the possibility that coupling mass may reach a "saturation level".

Unperturbed and 1200 Grams Coupling Mass Conditions : Figure 5.27 compares beam and plate spectra for the unperturbed (no mass) condition. Figure 5.28 compares response to 1200 grams coupling mass. Note that mode C in the airborne case is much closer to the beam mode than in the waterborne case. Subsequent figures will support that the mode to the right of the beam mode in Figure 5.28 (airborne case) corresponds to mode C previously identified in the waterborne case. Observe that the amplitude of the beam mode is virtually identical in the beam and plate spectra of both the waterborne and airborne cases. The fluid loading apparently has no affect on the vibration amplitude.

2000 Grams Coupling Mass: Figures 5.29 and 5.30 show the response to 2000 grams of coupling mass followed by the addition of 3 grams of tuning mass. The notable change is that plate mode D starts to split away from beam mode A (in Figure 5.30) in the airborne case, consistent with what is observed for the waterborne case. Again, the relative frequency spacing between the modes in air and water is different. Modes A and D are much closer together in the airborne case.

7 Grams Tuning Mass Plus 2000 Grams Coupling Mass : Figure 5.31 shows the addition of 7 grams tuning mass along with 2000 grams of coupling mass. In the airborne case, mode D is now distinct from mode A, like in the waterborne case. In both cases mode B now becomes obscured. Observe again that in the airborne case, modes A and D are much closer together than in the waterborne case.

Comparison of Figures 5.27 through 5.31 reveal that beam mode A and plate modes C and D undergo significant frequency changes along with some amplitude changes in response to coupling and tuning masses. Plate modes B and E respond much less, with mode B essentially being obscured as mass is added. Accordingly, modes A, C, and D fit the definition of "global" modes.

5.2.5 Beam 3 - Summary

Based on the previous discussion and the overall trends depicted in Figures 5.1 through 5.31, the following general conclusions can be made based on waterborne and airborne testing of beam 3.

a) Mode A is a beam dominant mode and modes B, C, D, and E are plate dominant modes. Modes A, C, and D are affected noticeably by both tuning and coupling masses and, as such, are considered global modes. The acoustic pressure increases considerably as modes A and D are brought closer together, and also increases as modes A and C are brought closer together. Conversely, acoustic pressure decreases considerably as the frequency separation between these mode pairs increases. We have observed acoustic pressure changes in excess of 12 dB (factor of 16) as a result of small frequency shifts among these global modes.

b) Plate modes with high amplitude vibration levels generally are visible in the beam drive point acceleration spectrum. This holds even when the plate acceleration is roughly about 20 dB less than that of the beam. However, as Figures 5.12 and 5.13 demonstrate, plate modes which dominate the acoustic pressure spectrum can be invisible to the beam drive point acceleration spectrum if their vibration amplitude is low.

c) As detailed in Figure 5.12, plate modes which exhibit high amplitude vibration are not necessarily efficient radiators.

d) Very small amounts of tuning mass (3 and 7 grams) resulted in a noticeable shift in the beam resonance frequency. Additionally, relatively small amounts (400 grams) of coupling mass were required to noticeably perturb the beam spectrum.

e) Beam, plate, and global modes appear to respond in a similar manner regardless of whether waterborne or airborne, although the spacing between global mode pair appears to vary considerably between the airborne and waterborne cases. Peak acceleration amplitudes were identical for the waterborne and airborne cases, and therefore, were not affected by fluid loading.

f) Addition of tuning masses decreases the resonance frequency of beam and plate modes. Addition of coupling masses increases the resonance frequency of beam modes, and decreases the resonance frequency of plate modes. Additionally, tuning and coupling masses have a more pronounced effect on the spectra at higher frequencies.

g) It appears that coupling mass may reach a "saturation level". For both the waterborne and airborne cases, coupling mass in excess of 2000 grams did not cause further frequency shifts. This applies to both high and low frequency modes.

h) Modal overlap at high frequencies due to damping makes it impossible to identify or follow individual modes. However, modes are likely affected by tuning and coupling masses since the acoustic pressure spectrum experiences significant amplitude changes in response to the masses.

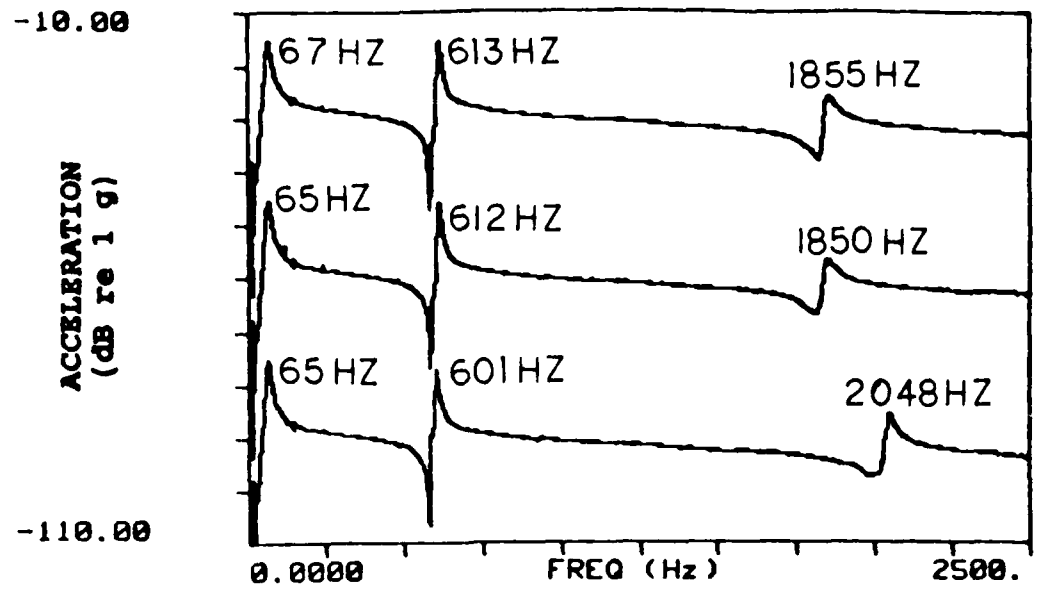

Figure 5.1 Beam 3 Waterborne. Beam drive point acceleration. From top: 0, 3, and 7 grams tuning mass.

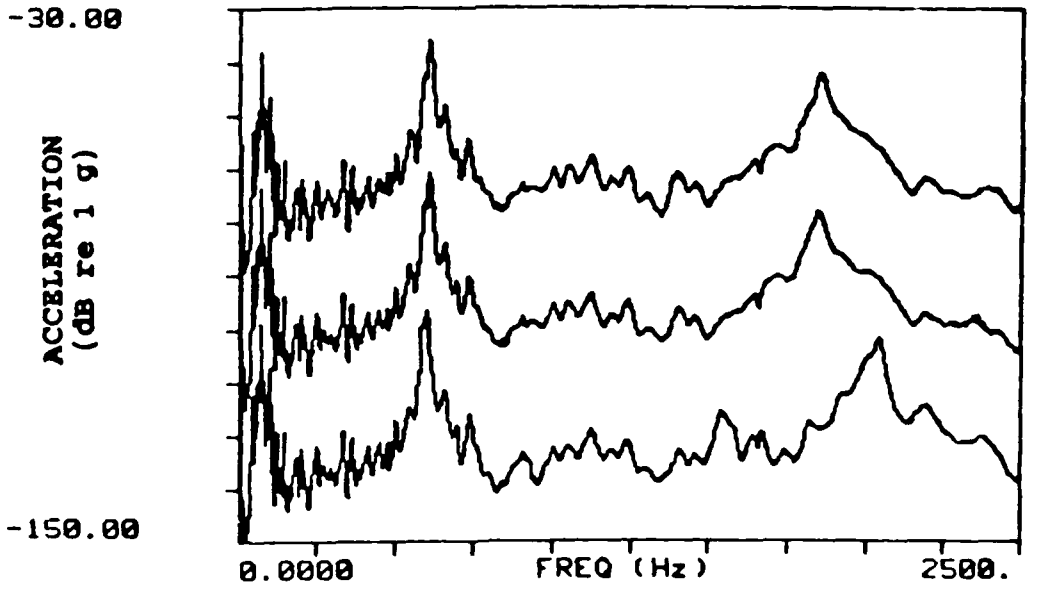

Figure 5.2 Beam 3 Waterborne. Mean plate acceleration. From top: 0, 3, and 7 grams tuning mass.

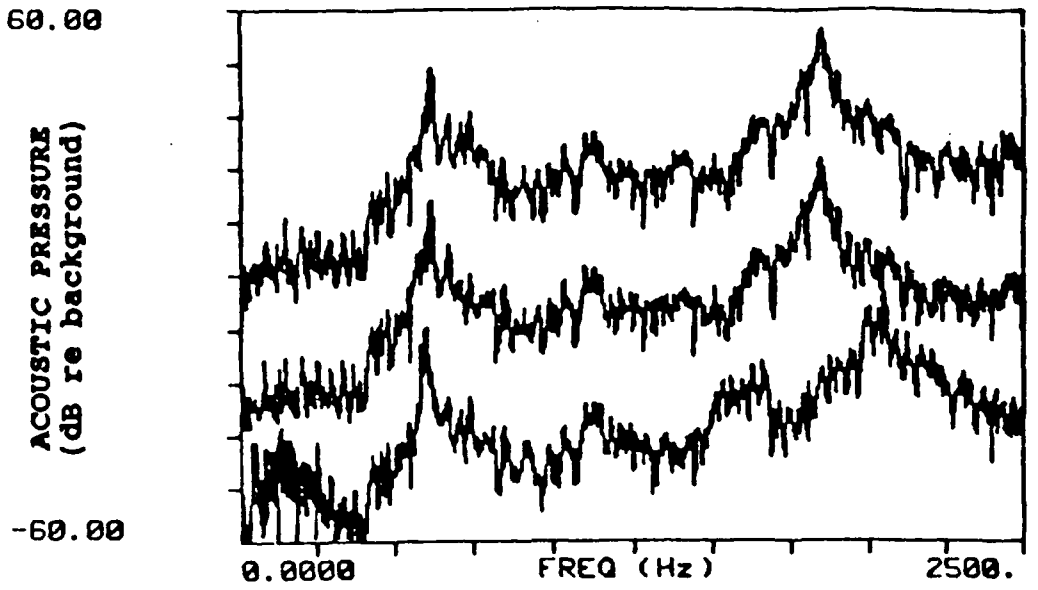

Figure 5.3 Beam 3 Waterborne. Mean acoustic pressure. From top: 0, 3, and 7 gram tuning mass.

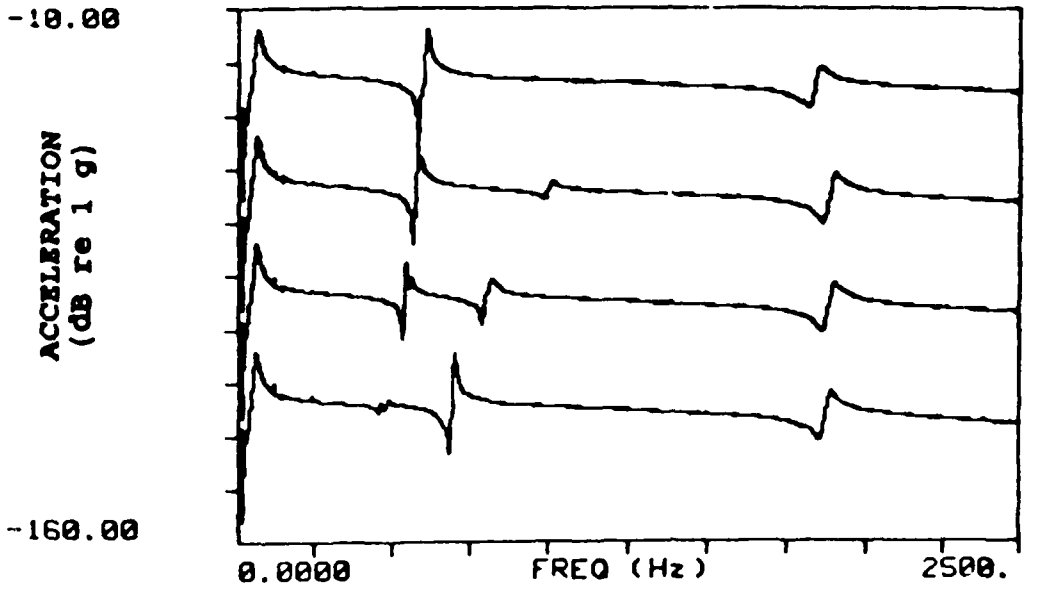

Figure 5.4 Beam 3 Waterborne. Beam drive point acceleration. From top: 0, 10, 15, and 22 grams tuning mass.

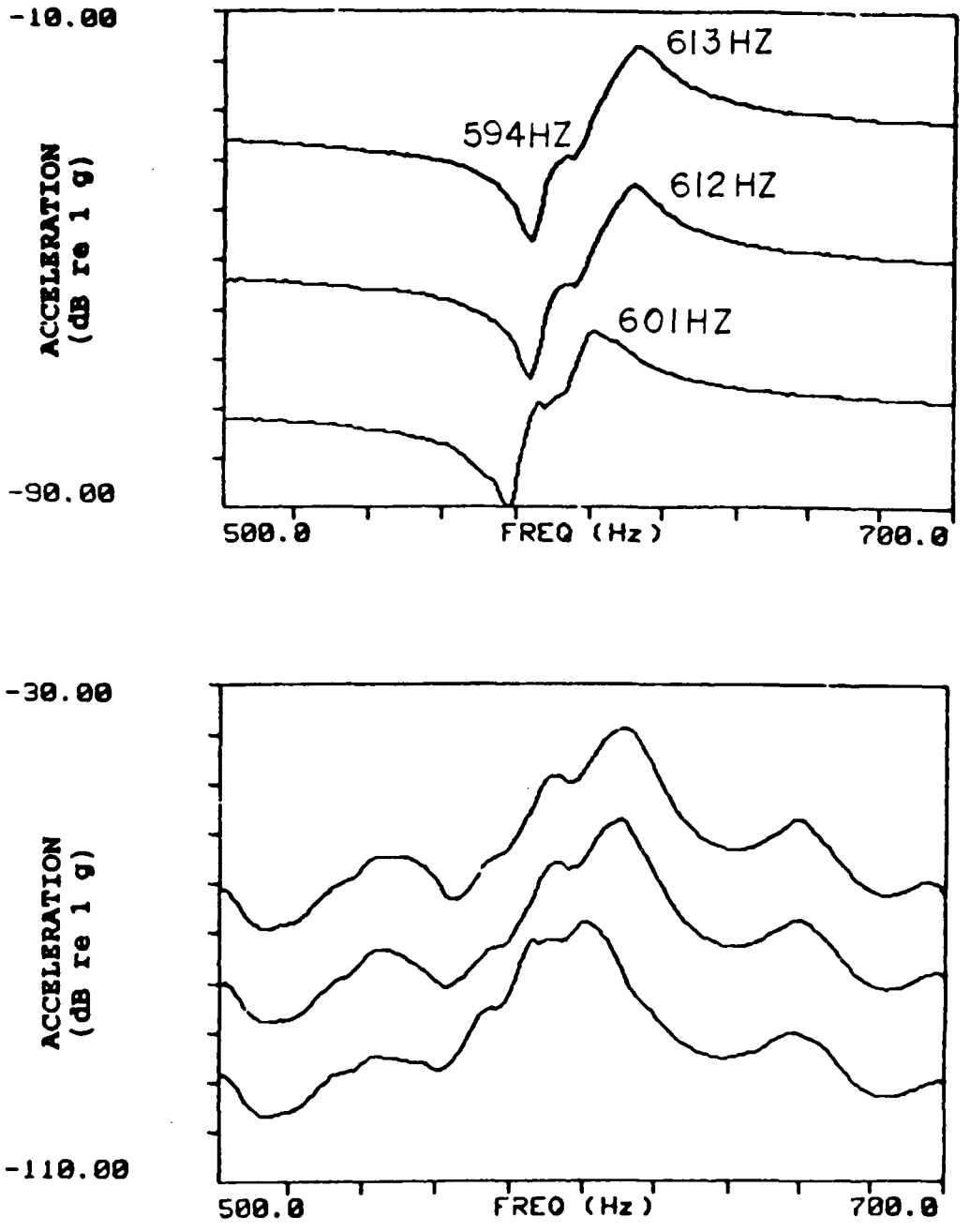

Figure 5.5 Beam 3 Waterborne. Beam drive point acceleration (top graph) and mean plate acceleration (bottom graph). From top in each graph: 0, 3, and 7 grams tuning mass.

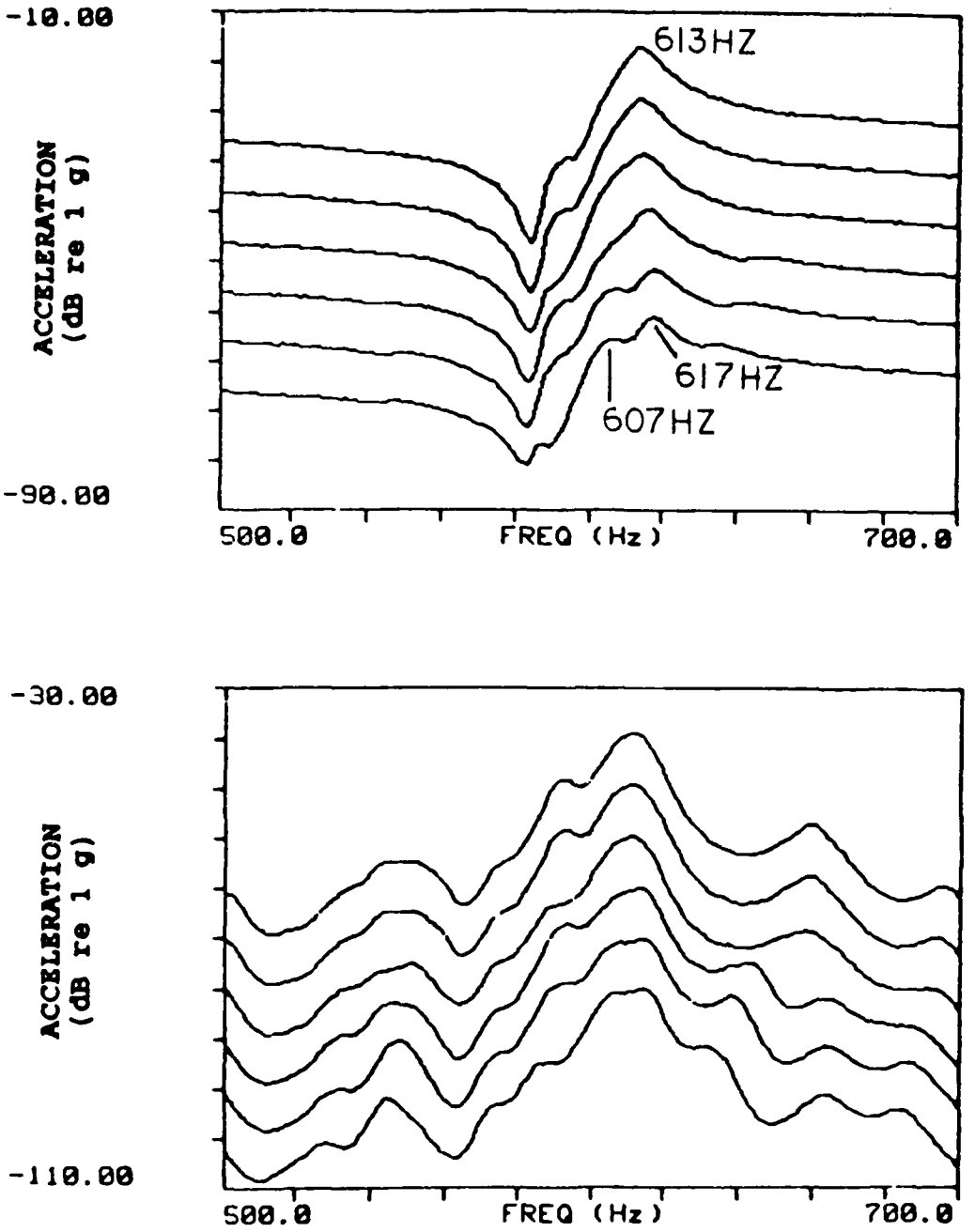

Figure 5.6 Beam 3 Waterborne. Beam drive point acceleration (top graph) and mean plate acceleration (bottom graph). From top in each graph: 0, 100, 400, 1200, 2000, and 4000 grams coupling mass.

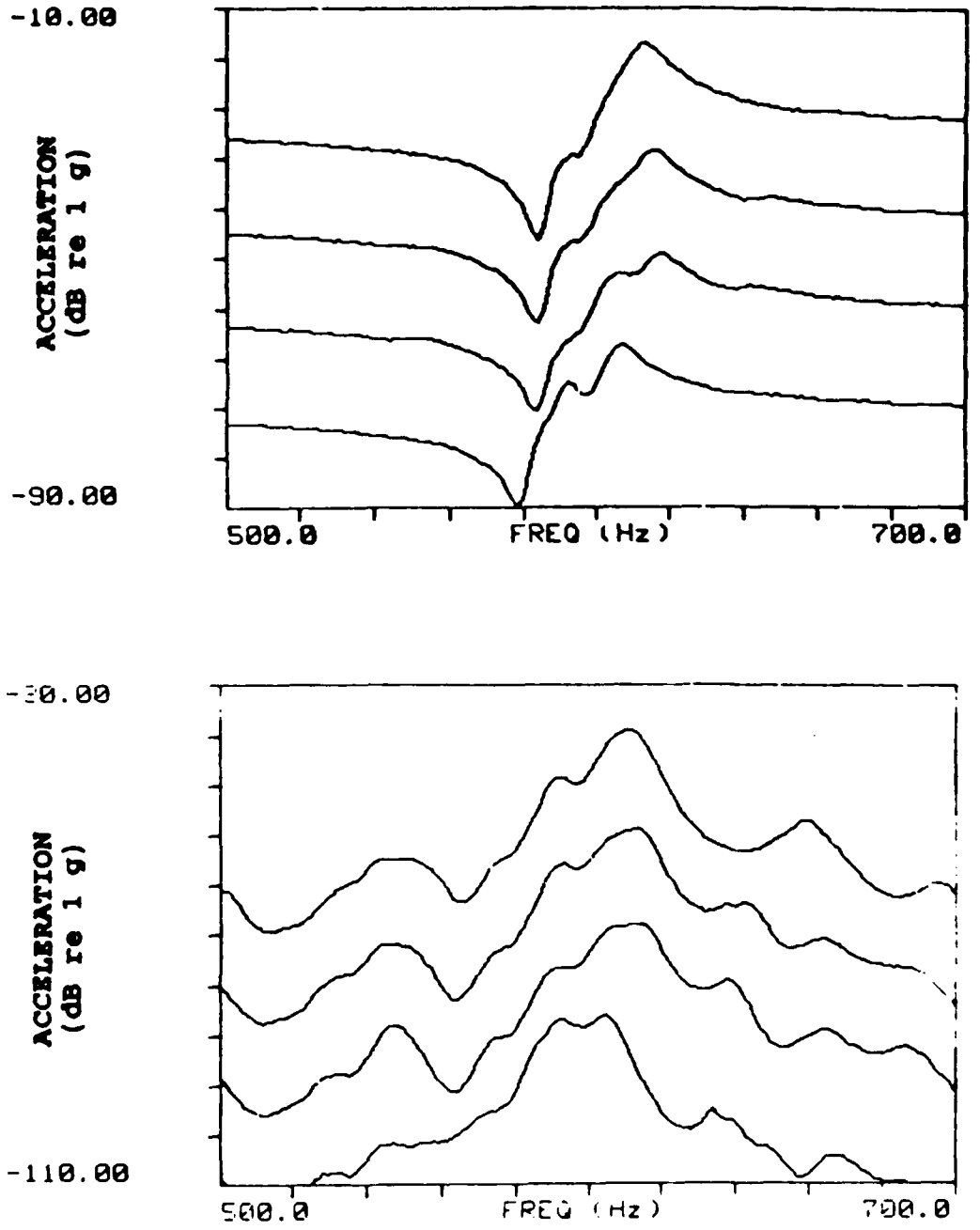

Figure 5.7 Beam 3 Waterborne. Beam drive point acceleration (top graph) and mean plate acceleration (bottom graph). From top in each graph: 0, 1200, and 2000 grams coupling mass, 7 grams tuning mass plus 2000 grams coupling mass.

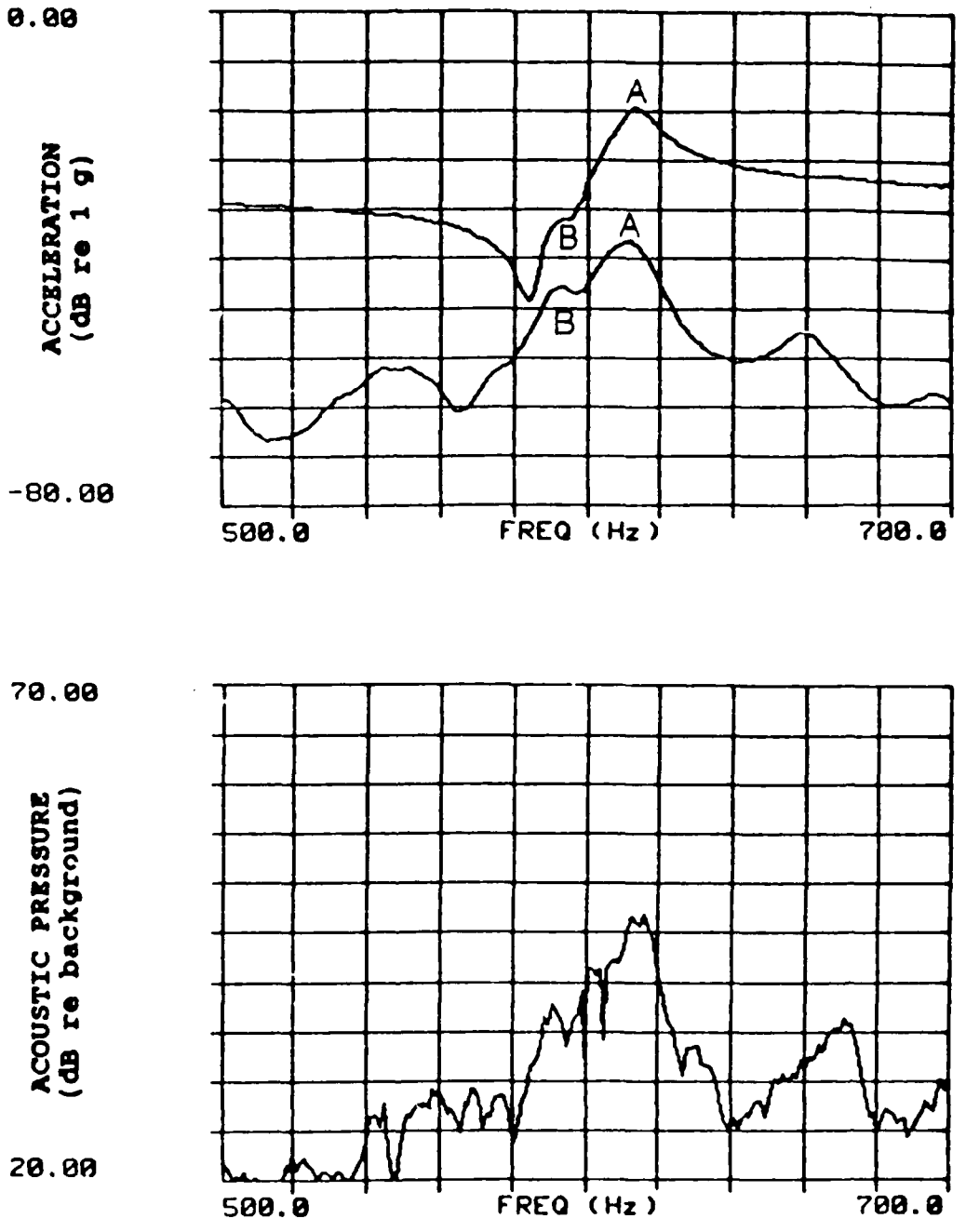

Figure 5.8 Beam 3 Waterborne. Unperturbed condition (no mass). From top: beam acceleration, mean plate acceleration, and mean acoustic pressure.

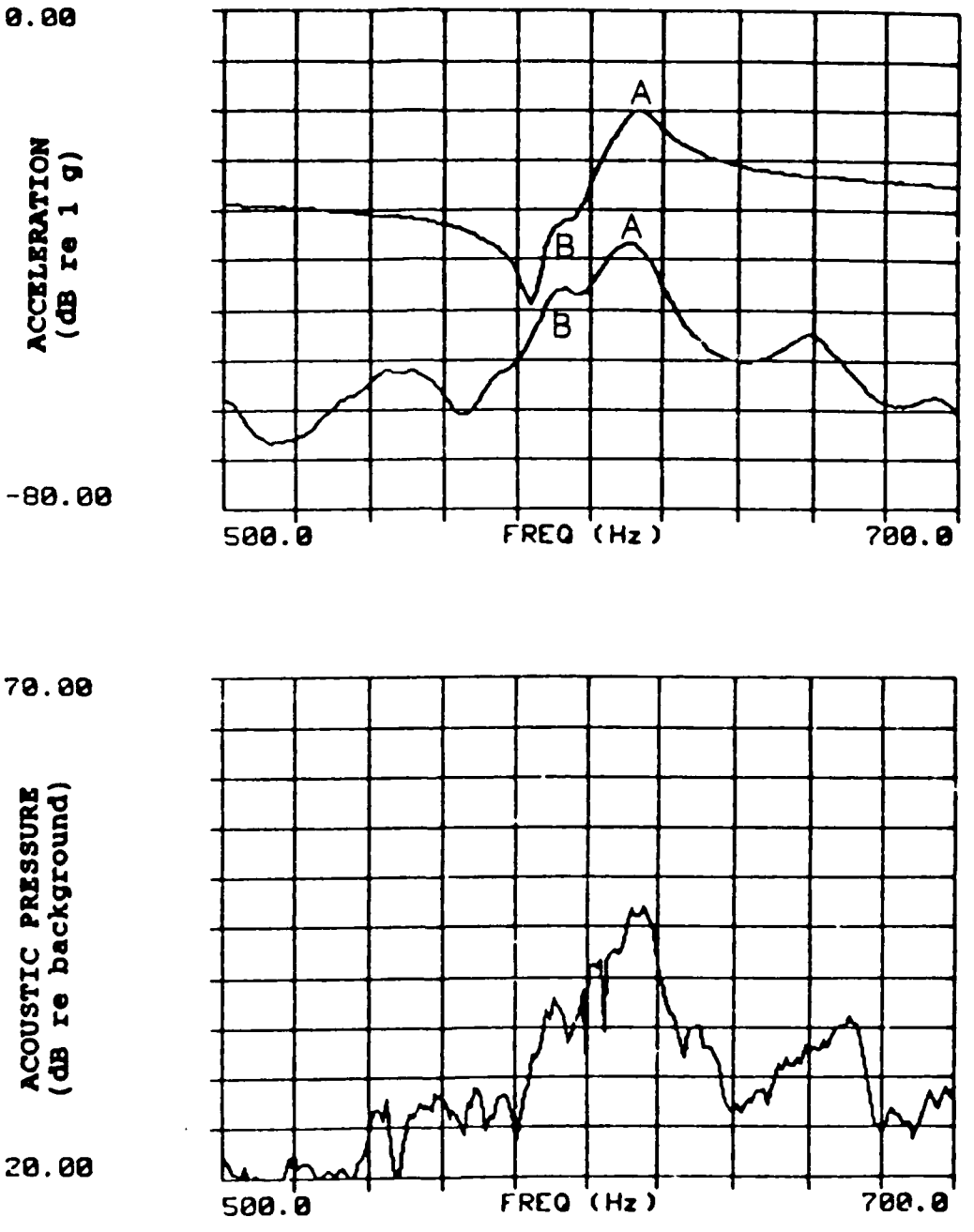

Figure 5.9 Beam 3 Waterborne. 100 grams coupling mass. From top: beam acceleration, mean plate acceleration, and mean acoustic pressure.

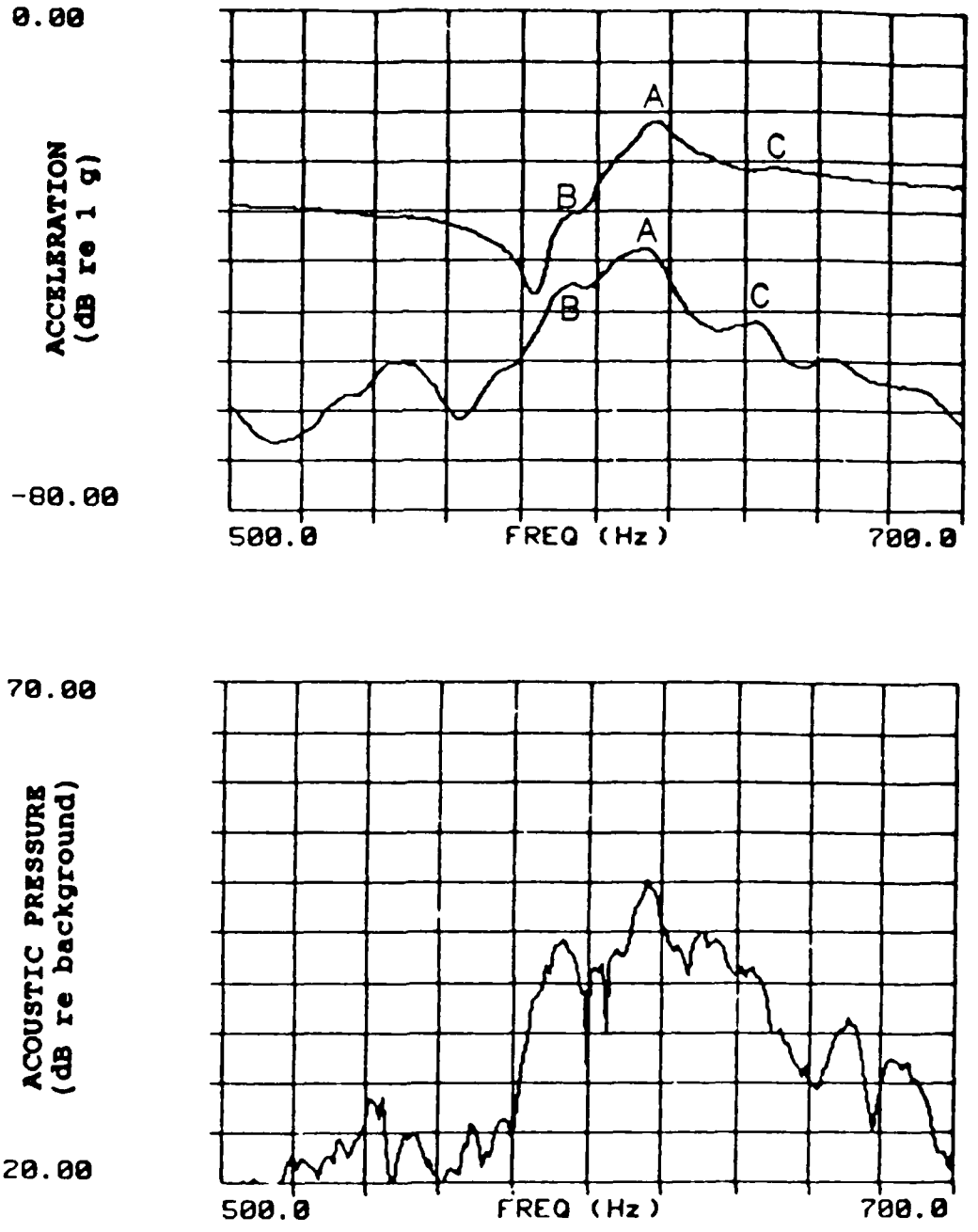

Figure 5.10 Beam 3 Waterborne. 1200 grams coupling mass. From top: beam acceleration, mean plate acceleration, and mean acoustic pressure.

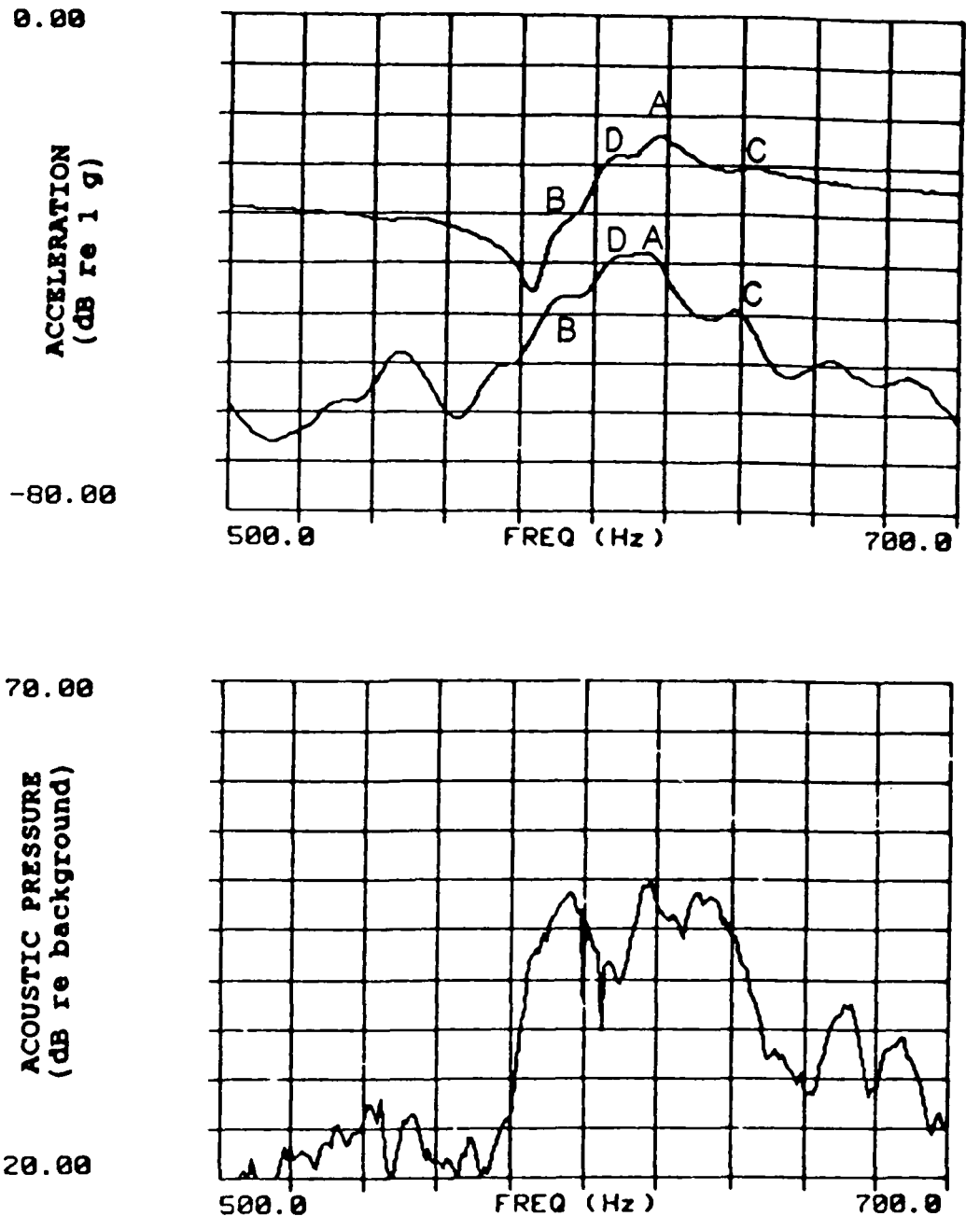

Figure 5.11 Beam 3 Waterborne. 2000 grams coupling mass. From top: beam acceleration, mean plate acceleration, and mean acoustic pressure.

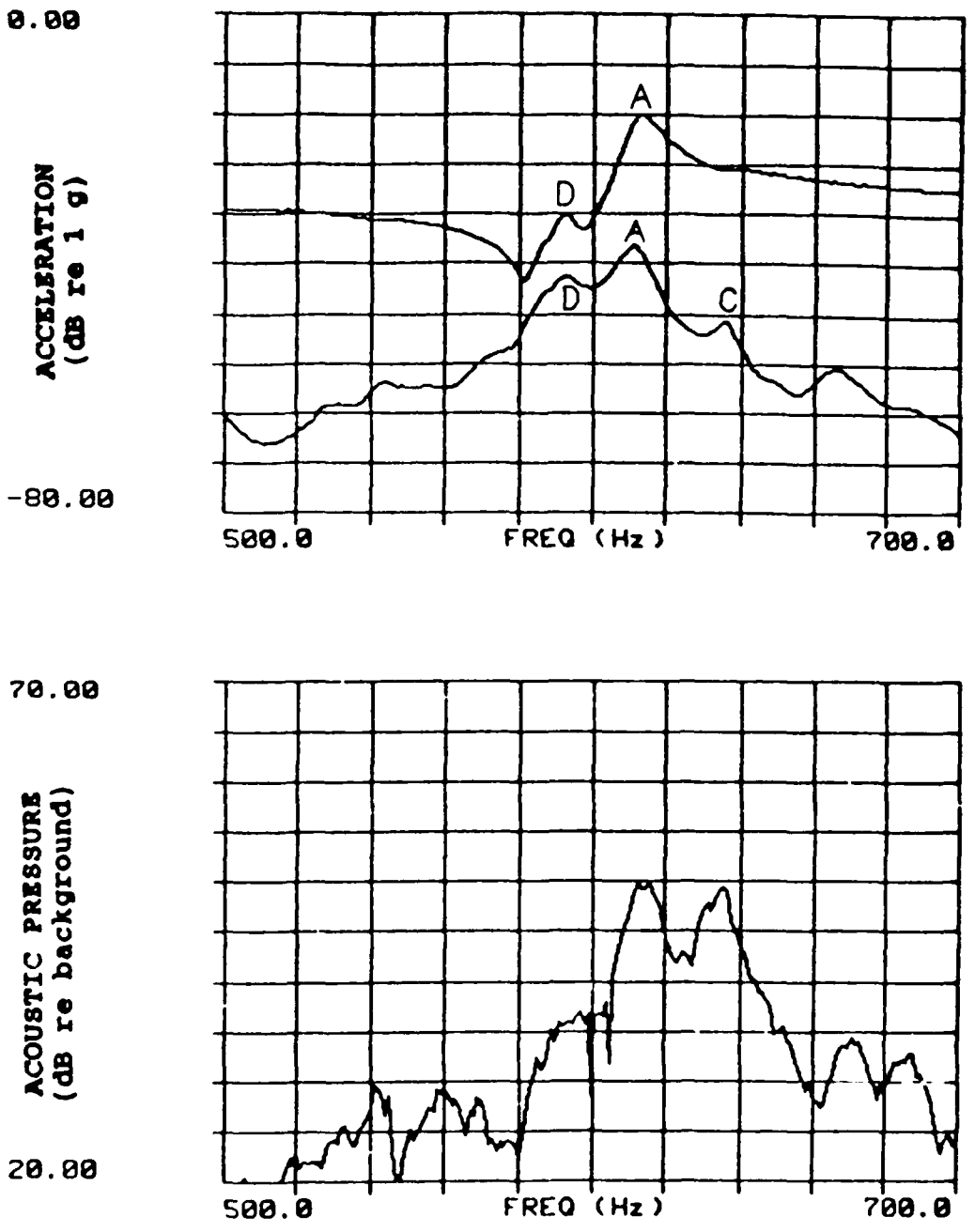

Figure 5.12 Beam 3 Waterborne. 3 grams tuning mass plus 2000 grams coupling mass. From top: beam acceleration, mean plate acceleration, and mean acoustic pressure.

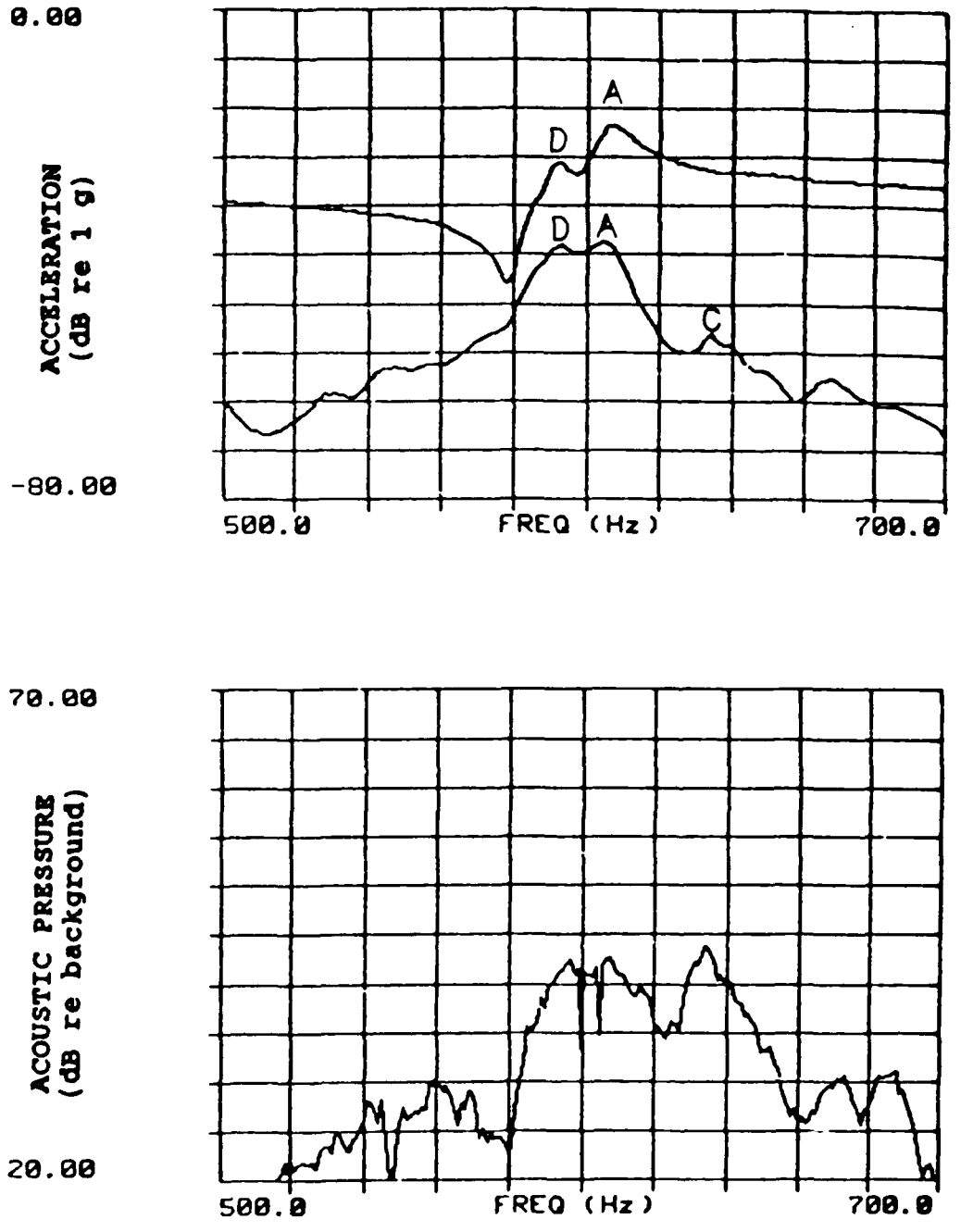

Figure 5.13 Beam 3 Waterborne. 7 grams tuning mass plus 4000 grams coupling mass. From top: beam acceleration, mean plate acceleration, and mean acoustic pressure.

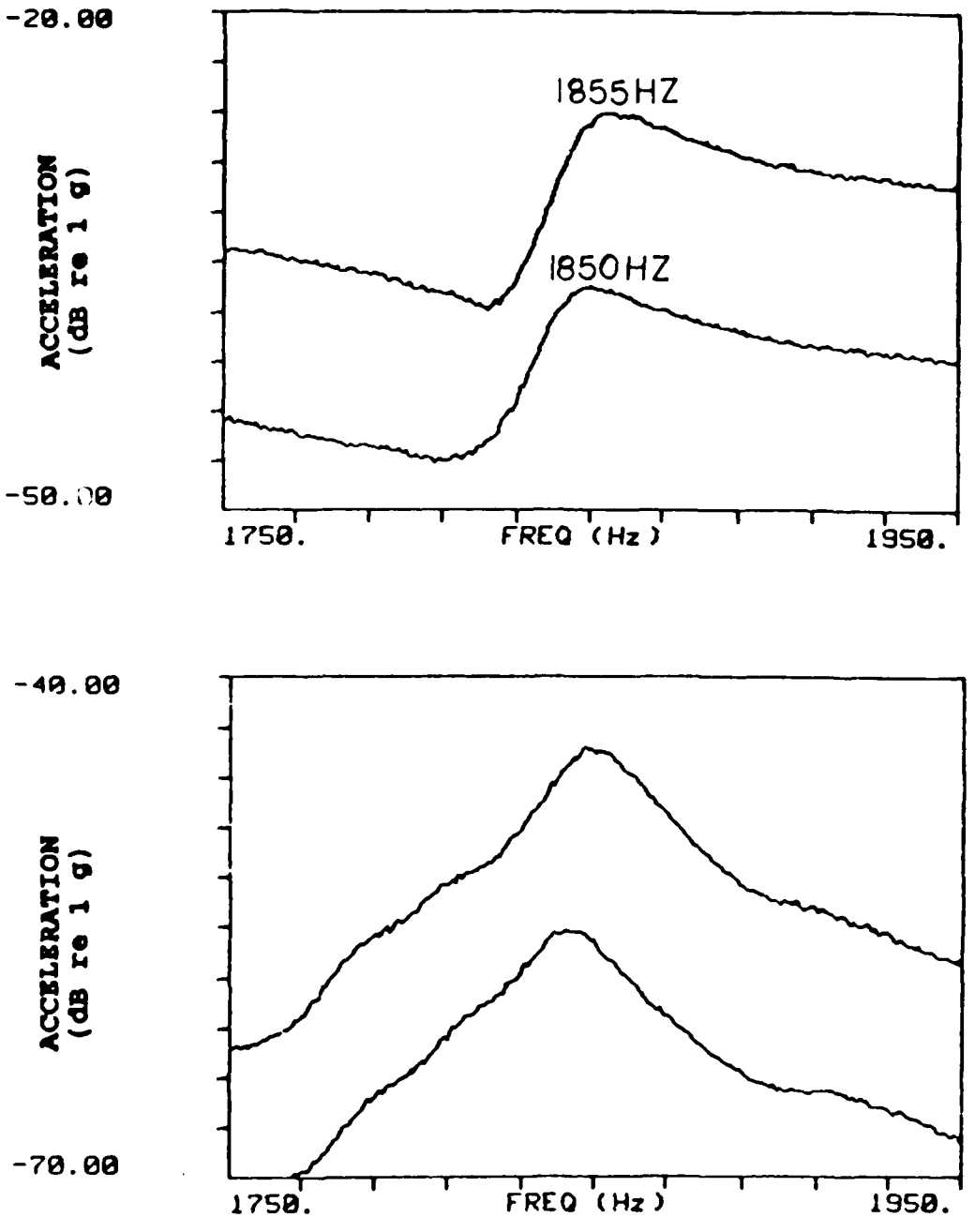

Figure 5.14 Beam 3 Waterborne. Beam drive point acceleration (top graph) and mean plate acceleration (bottom graph). From top in each graph: 0 and 3 grams tuning mass.

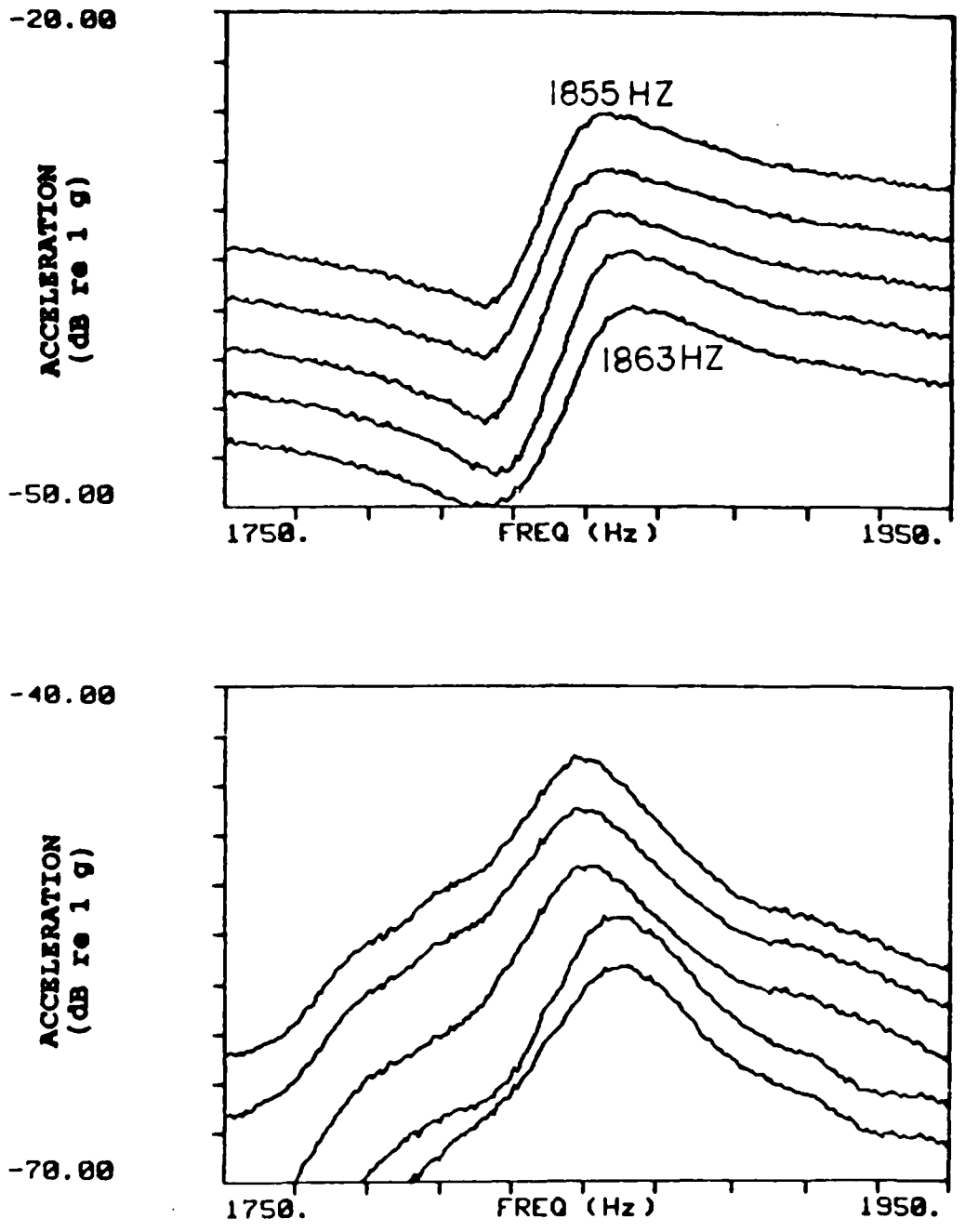

Figure 5.15 Beam 3 Waterborne. Beam drive point acceleration (top graph) and mean plate acceleration (bottom graph). From top in each graph: 0, 100, 400, 2000, and 4000 grams coupling mass.

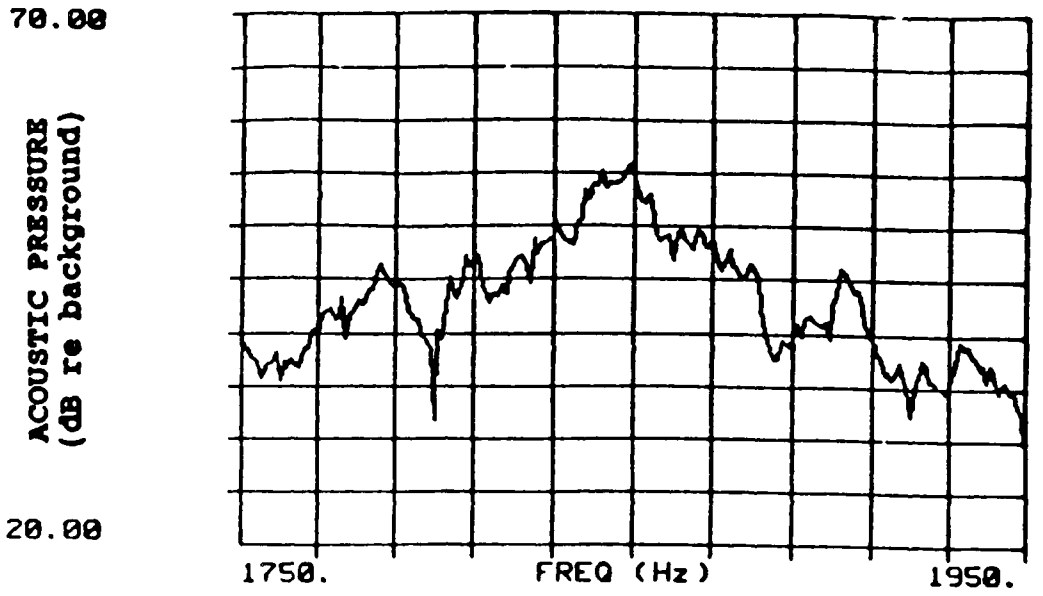

Figure 5.16 Beam 3 Waterborne. Unperturbed condition (no mass). Mean acoustic pressure.

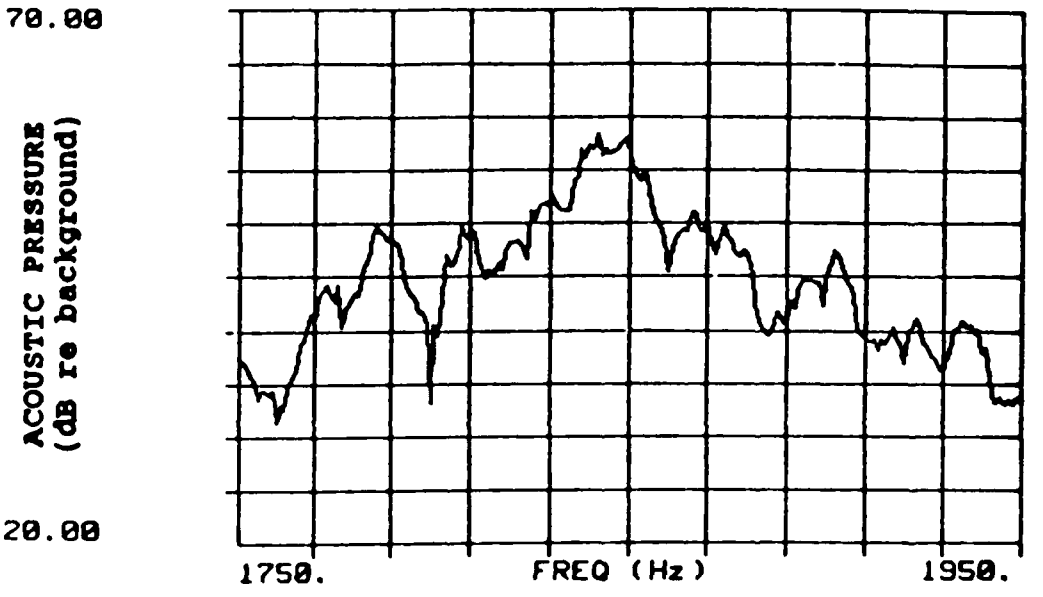

Figure 5.17 Beam 3 Waterborne. 400 grams coupling mass. Mean acoustic pressure.

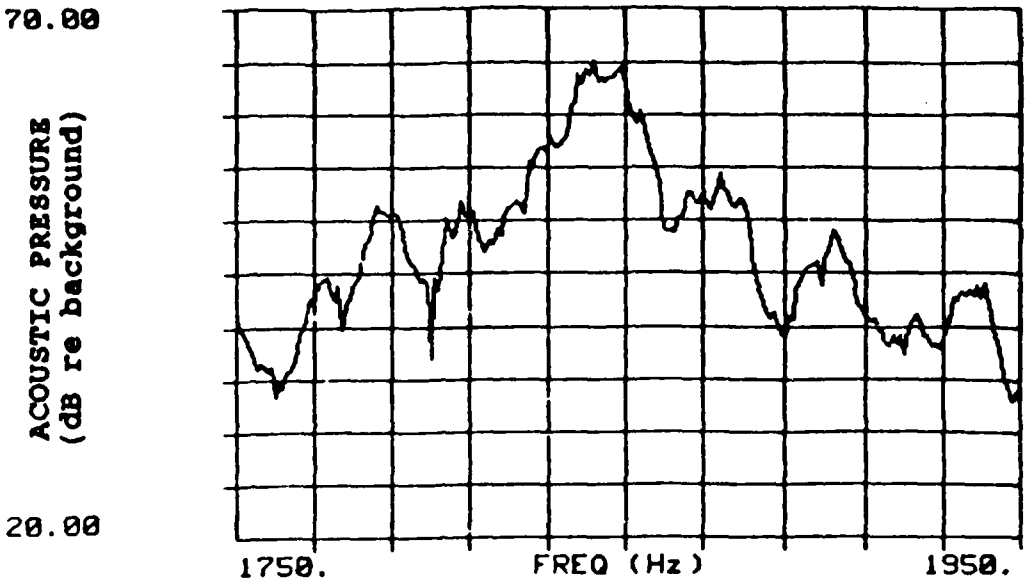

Figure 5.18 Beam 3 Waterborne. 1200 grams coupling mass. Mean acoustic pressure.

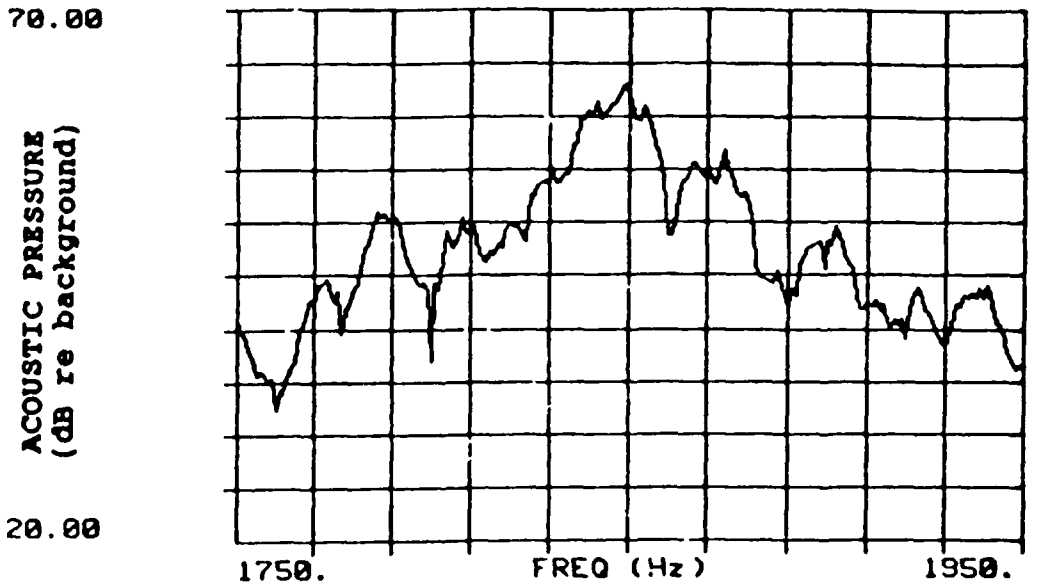

Figure 5.19 Beam 3 Waterborne. 2000 grams coupling mass. Mean acoustic pressure.

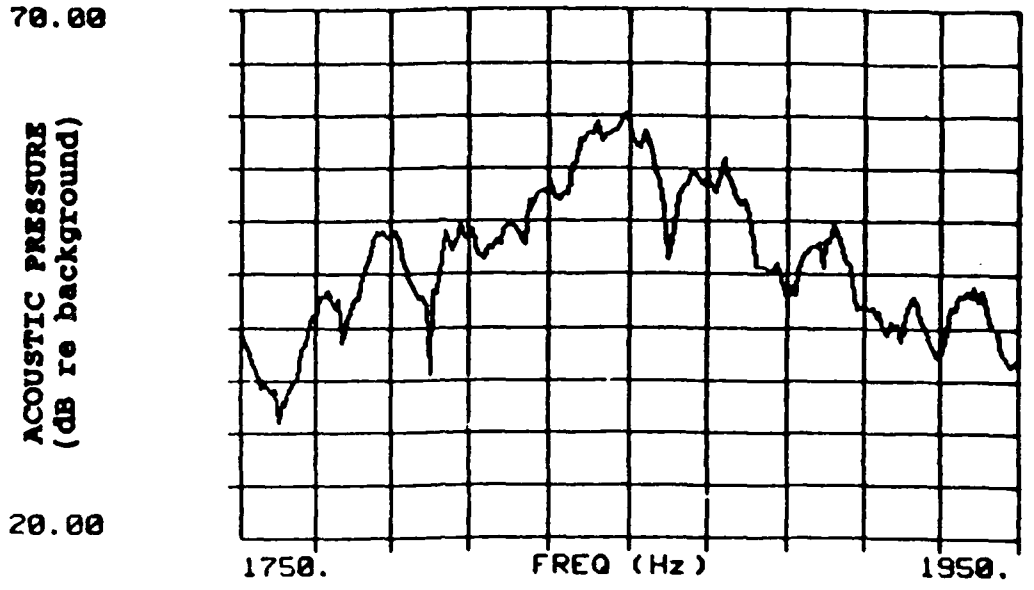

Figure 5.20 Beam 3 Waterborne. 4000 grams coupling mass. Mean acoustic pressure.

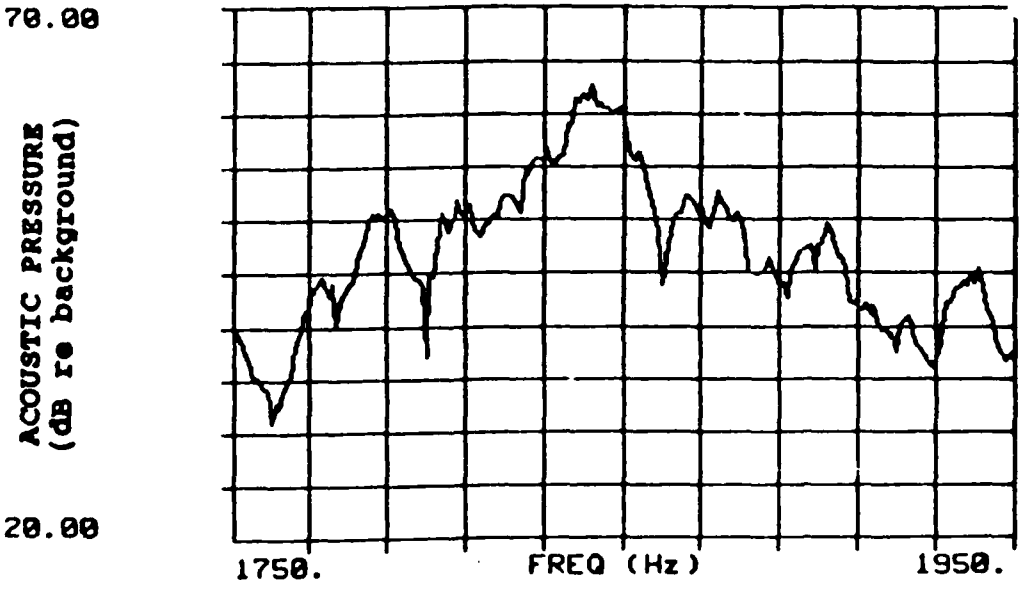

Figure 5.21 Beam 3 Waterborne. 3 grams tuning mass plus 4000 grams coupling mass. Mean acoustic pressure.

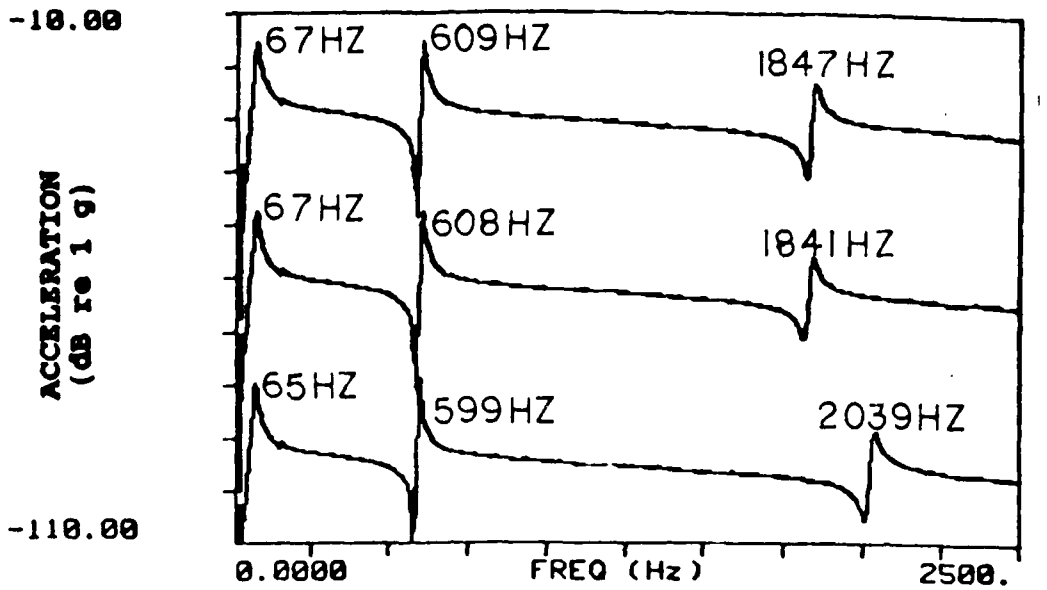

Figure 5.22 Beam 3 Airborne. Beam drive point acceleration. From top: 0, 3, and 7 grams tuning mass.

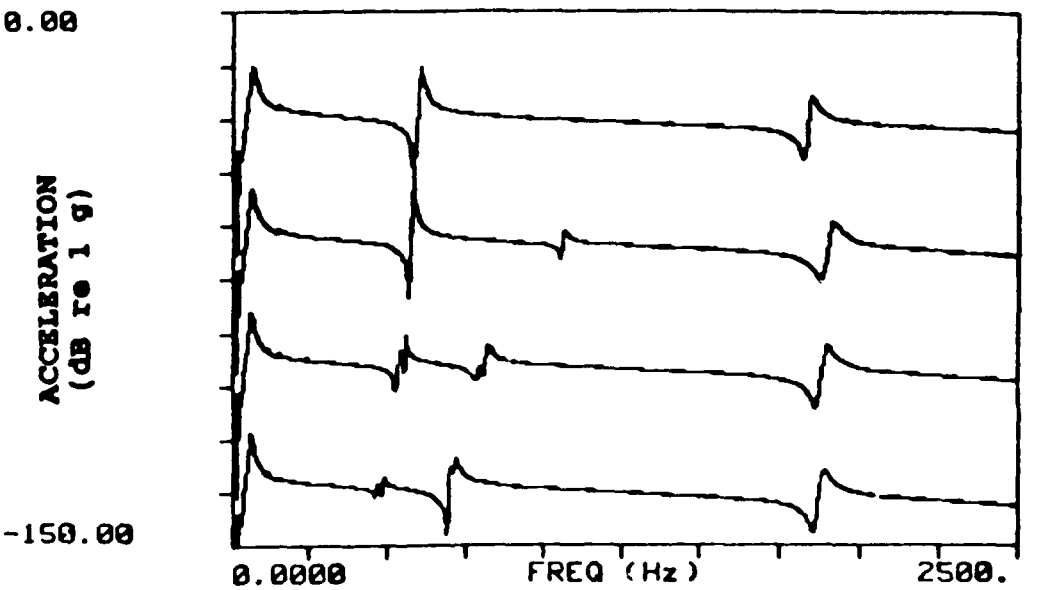

Figure 5.23 Beam 3 Airborne. Beam drive point acceleration. From top: 0, 10, 15, and 22 grams tuning mass.

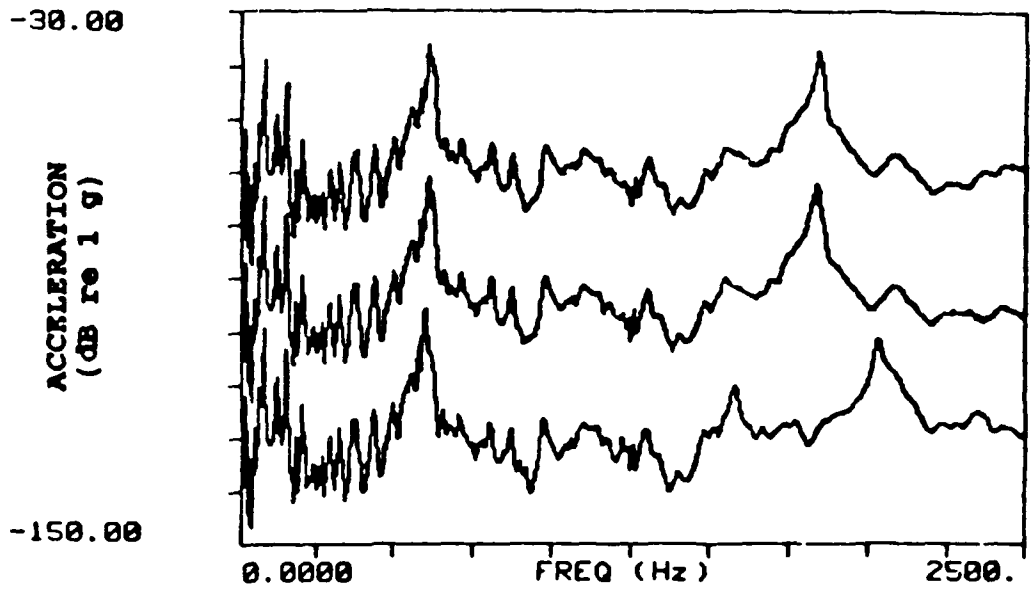

Figure 5.24 Beam 3 Airborne. Mean plate acceleration. From top: 0, 3, and 7 grams tuning mass.

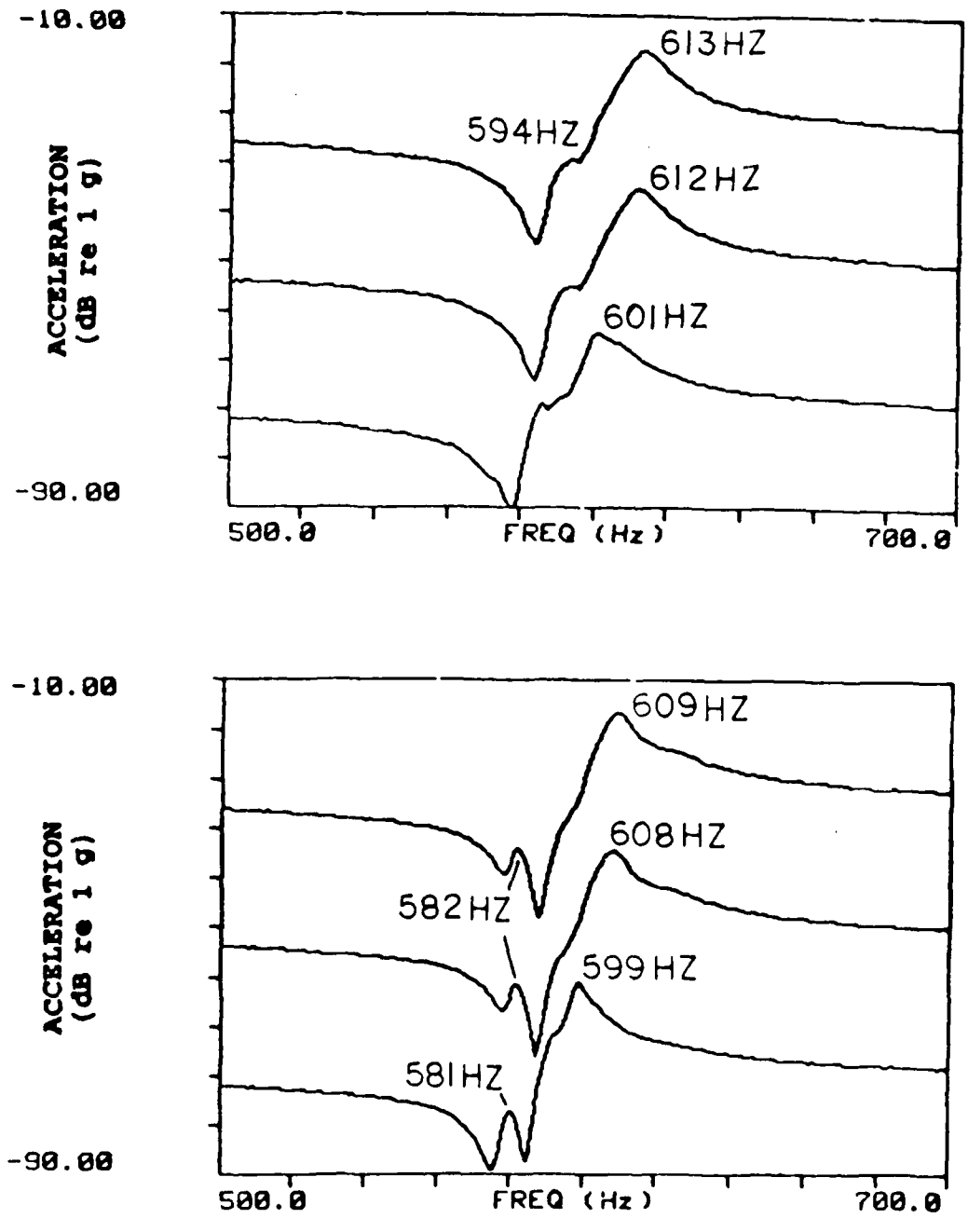

Figure 5.25 Beam 3 Waterborne (top graph) and Airborne (bottom graph). From top in each graph: 0, 3, and 7 grams tuning mass.

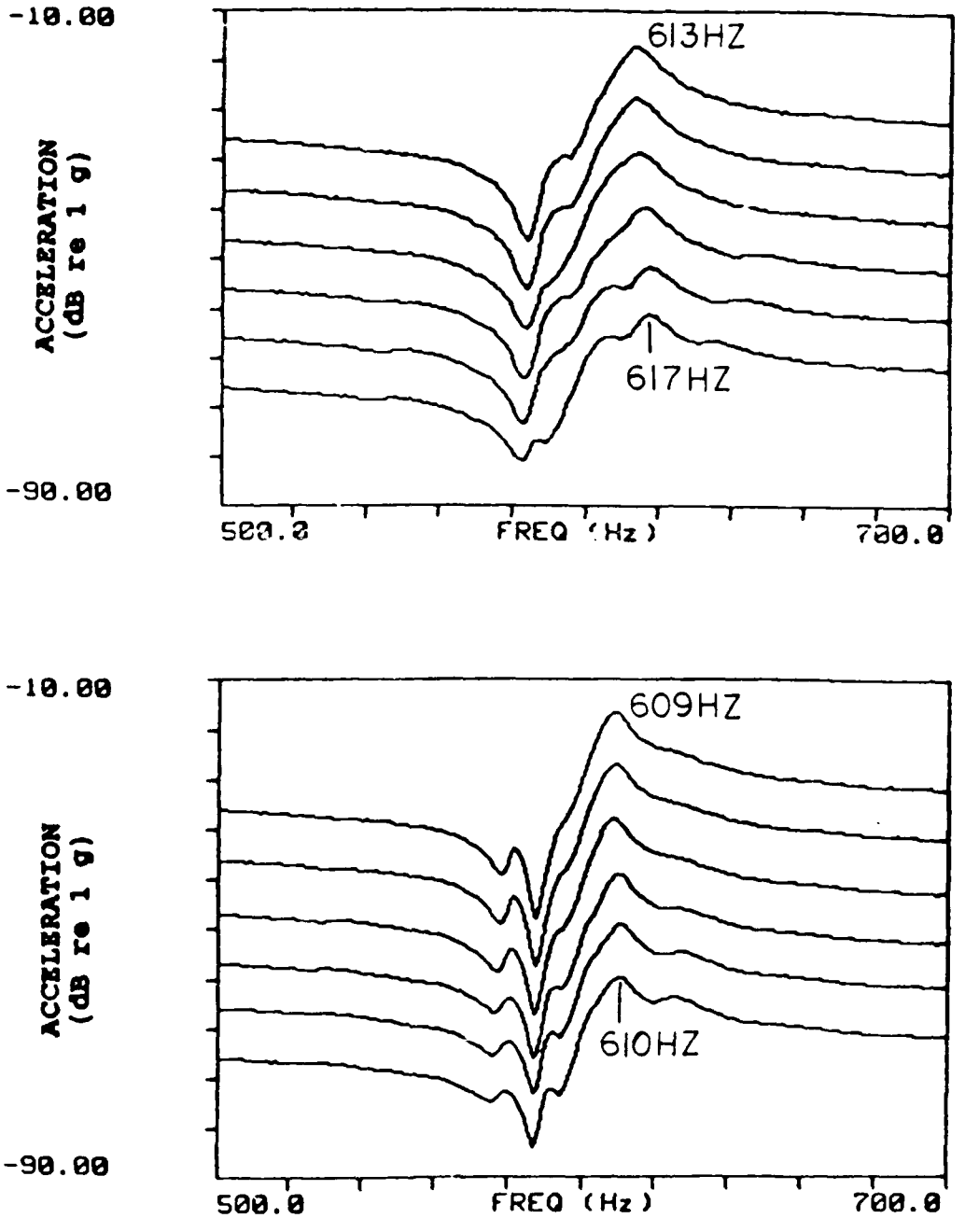

Figure 5.26 Beam 3 Waterborne (top graph) and Airborne (bottom graph). From top in each graph: 0, 100, 400, 1200, 2000, and 4000 grams coupling mass.

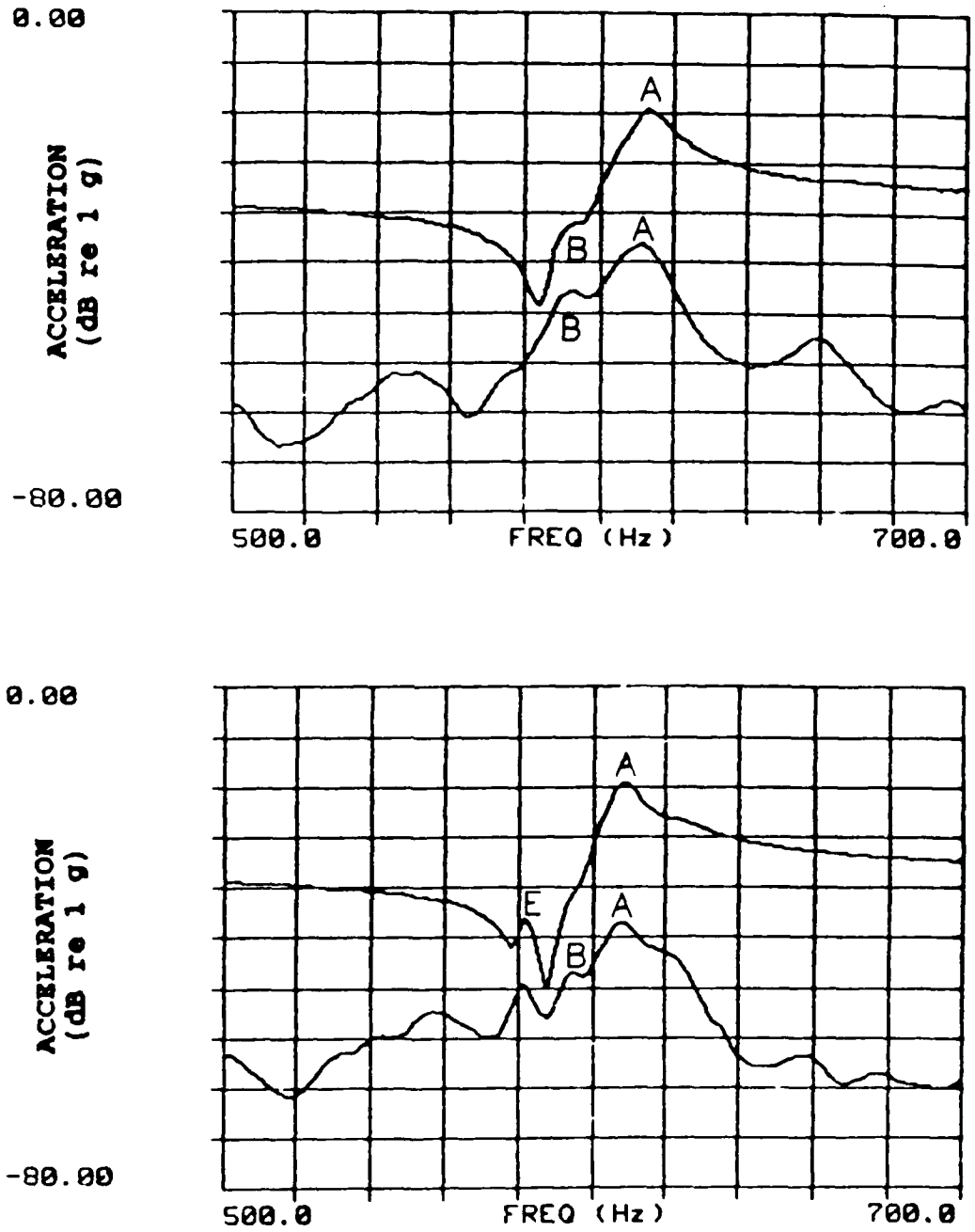

Figure 5.27 Beam 3 Waterborne (top graph) and Airborne (bottom graph). Unperturbed condition (no mass). From top in each graph: beam drive point acceleration, and mean plate acceleration.

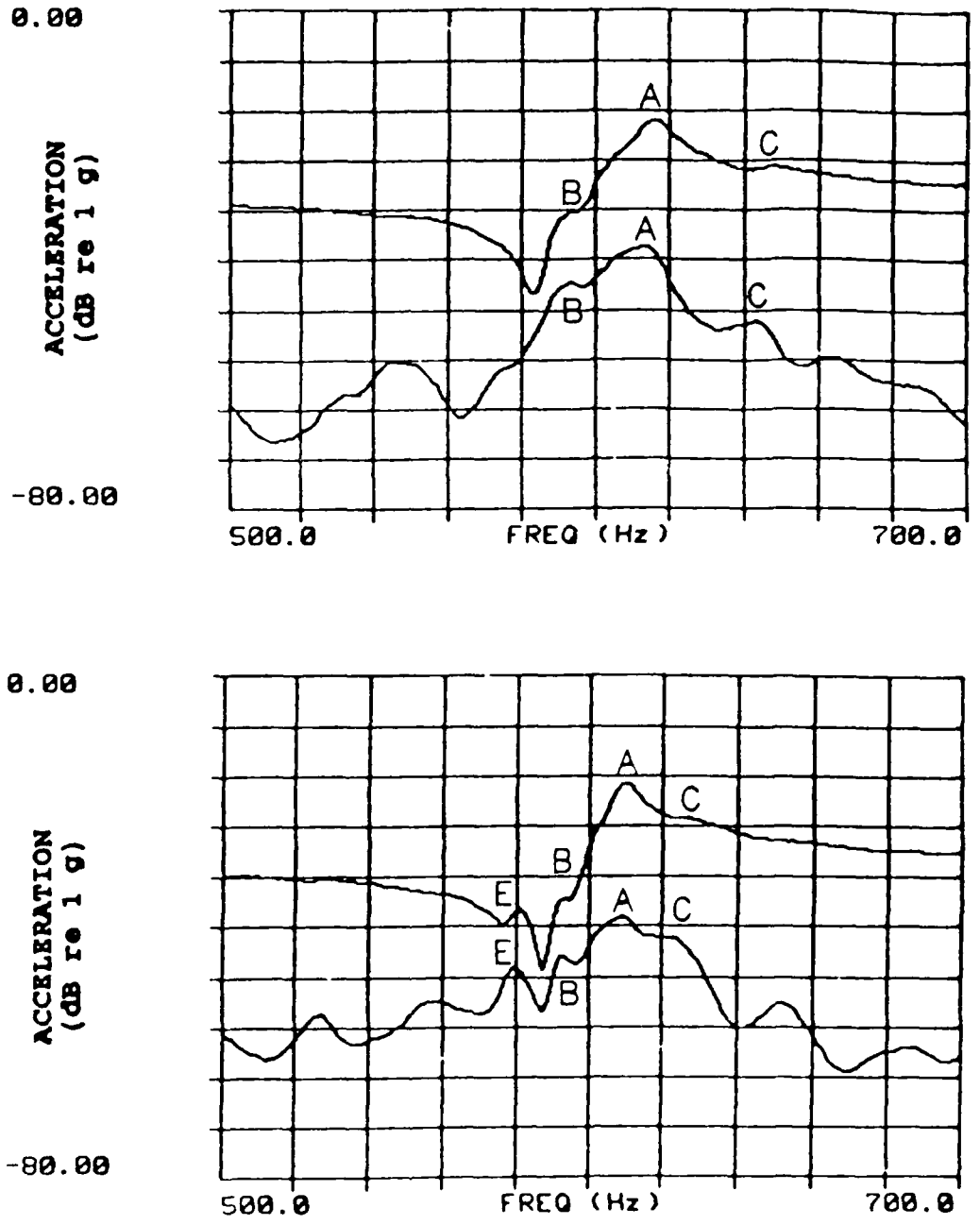

Figure 5.28 Beam 3 Waterborne (top graph) and Airborne (bottom graph). 1200 grams coupling mass. From top in each graph: beam drive point acceleration, and mean plate acceleration.

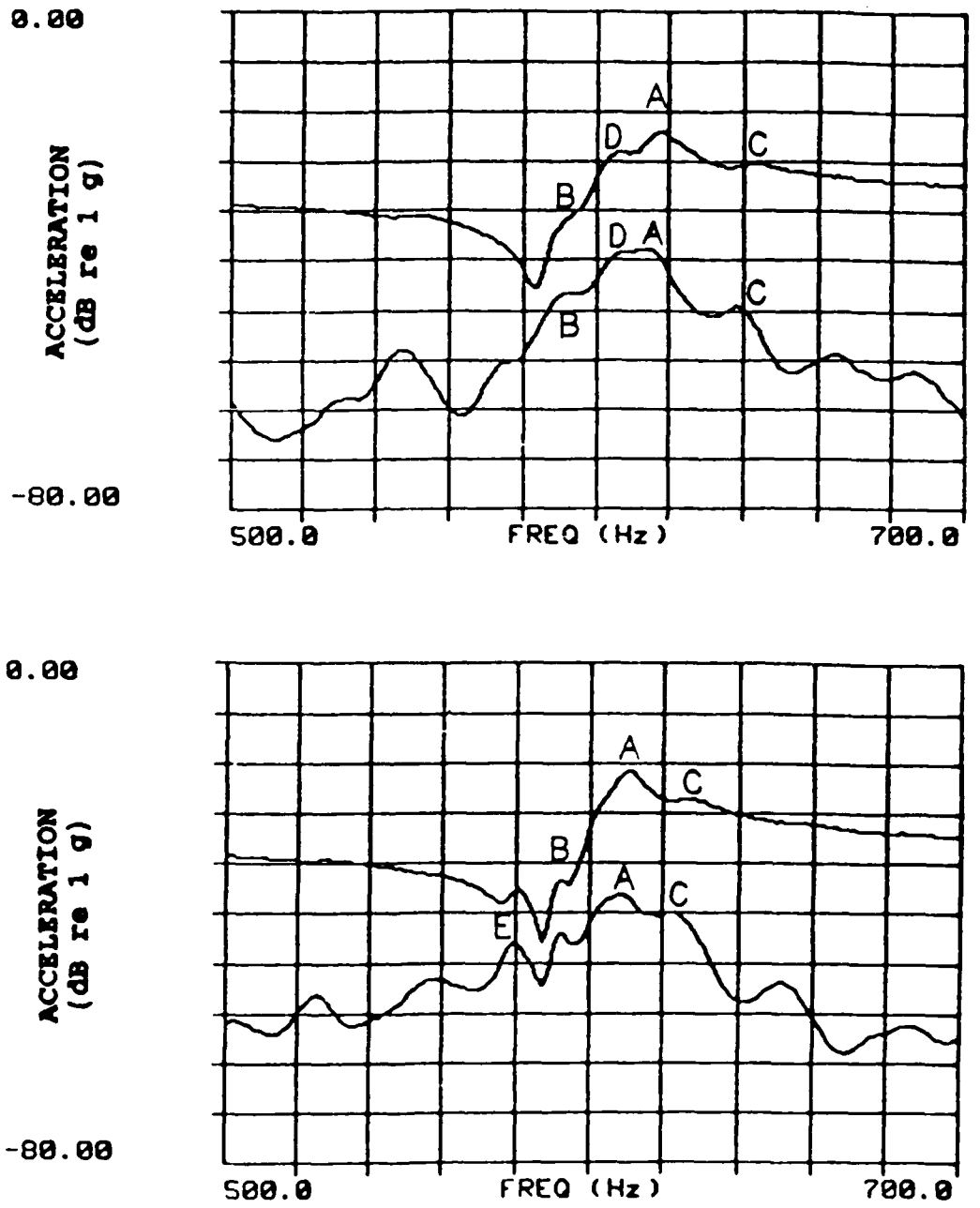

Figure 5.29 Beam 3 Waterborne (top graph) and Airborne (bottom graph). 2000 grams coupling mass. From top in each graph: beam drive point acceleration, and mean plate acceleration.

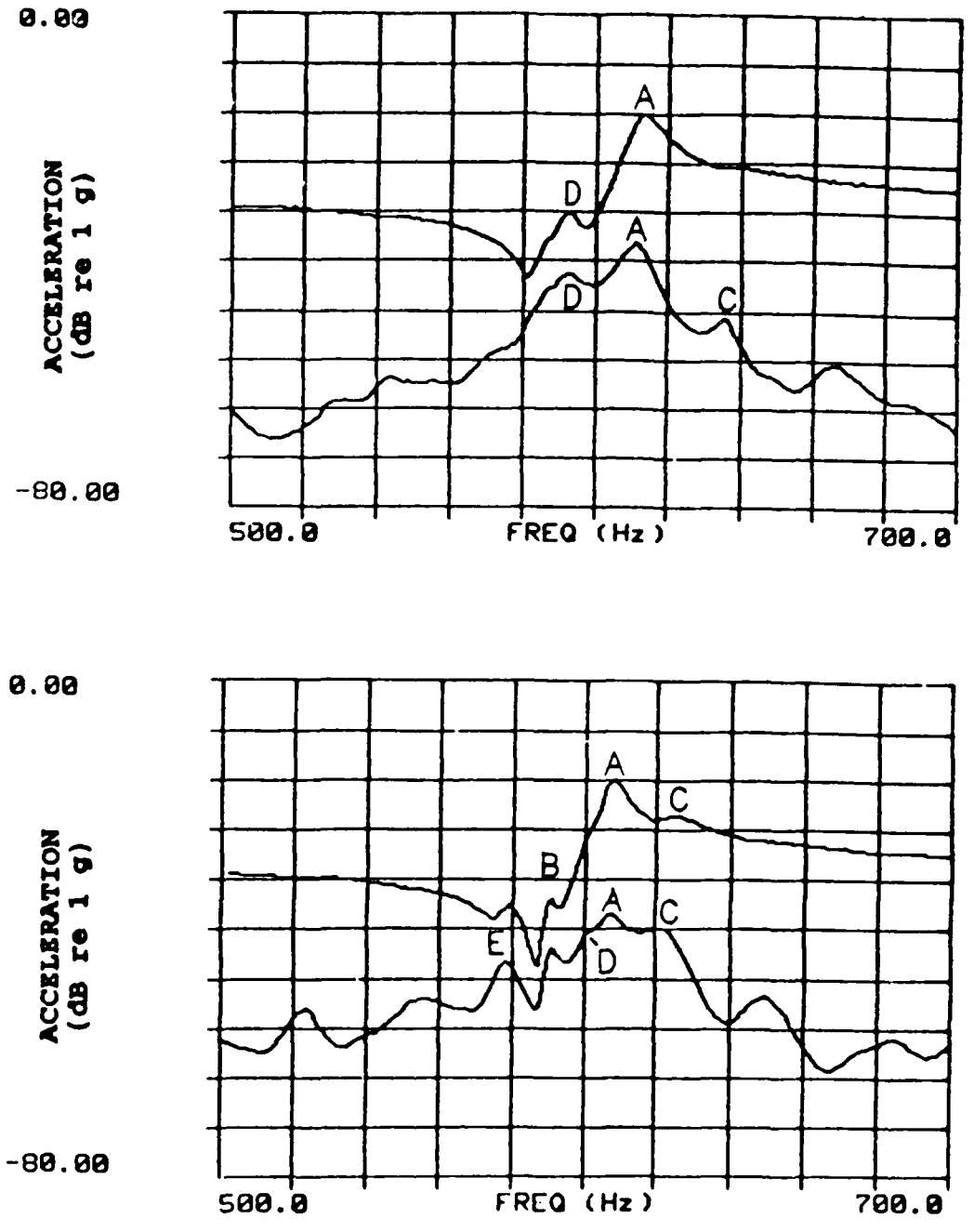

Figure 5.30 Beam 3 Waterborne (top graph) and Airborne (bottom graph). 3 grams tuning mass plus 2000 grams coupling mass. From top in each graph: beam drive point acceleration, and mean plate acceleration.

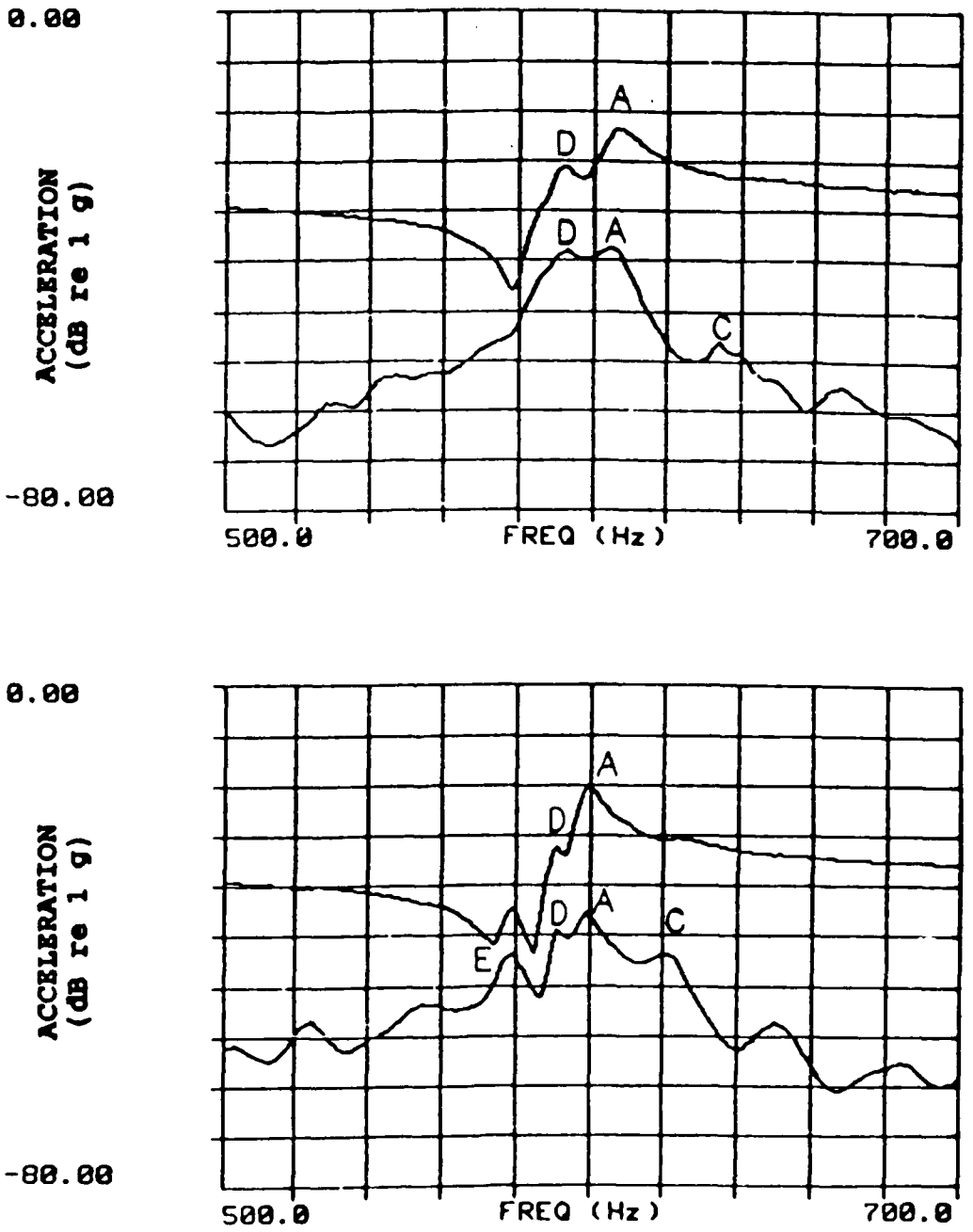

Figure 5.31 Beam 3 Waterborne (top graph) and Airborne (bottom graph). 7 grams tuning mass plus 2000 grams coupling mass. From top in each graph: beam drive point acceleration, and mean plate acceleration.

5.3 Beam 2 Results

Sections 5.3.1 through 5.3.4 present the results of testing with the shaker mounted on beam 2. Results in water and in air are discussed. The focus of the discussion is to compare the beam 2 results with those obtained for beam 3 to evaluate the repeatability of the experimental results.

5.3.1 Beam 2 - Spectra Overview (Waterborne)

Figure 5.32 shows the drive point acceleration spectrum for beam 2 for the conditions of 0, 3, and 7 grams tuning mass added to the free end of beam 2 (no coupling mass added). Figures 5.33 and 5.34 show the mean plate acceleration and mean water tank acoustic pressure spectra for the 0, 3, and 7 grams tuning mass conditions. The following comments pertain to Figures 5.32, 5.33, and 5.34:

a) Figure 5.32 shows that the drive point acceleration spectrum of beam 2 is less affected by the tuning mass than beam 3. The unperturbed spectrum consists of three dominant resonance modes with frequencies of 64, 560, and 1687 Hz (all lower frequency than beam 3). Application of 3 grams tuning mass results in no frequency change to the first two modes and a 6 Hz decrease in the frequency of the original 1687 Hz mode. Application of 7 grams tuning mass results in resonance mode frequencies of 63, 553, and 1908 Hz. As in the case for beam 3, 7 grams tuning mass greatly increased the frequency of the higher frequency mode. Additionally, Figures 5.33 and 5.34 reveal that 7 grams tuning mass alters the plate acceleration spectrum and the acoustic pressure spectrum near 1500 Hz to produce a strong resonance not visible in the beam spectrum.

b) Comparison of Figures 5.32, 5.33, and 5.34 with Figures 5.1, 5.2, and 5.3 reveal that the beam and plate acceleration levels and water tank pressure levels are higher for beam 2 than for beam 3.

c) Figure 5.35 shows the effect of 10, 15, and 22 grams tuning mass on the beam spectrum. Comparison with Figure 5.4 shows that, consistent with beam 3, the beam spectrum starts to become "distorted" with the addition of 10 grams tuning mass. This distortion increases as additional tuning mass is added.

Figures 5.32 and 5.34 reveal wide bandwidths in both the beam and plate acceleration spectra for the 1687 Hz mode. Consistent with what was previously determined for beam 3, very little useful information can therefore be obtained from studying this mode due to excessive modal overlap. Accordingly, only the 560 Hz mode will be investigated in detail. (Recall that the 64 Hz mode is below the usable frequency range of the acoustic tank.)

5.3.2 Beam 2 - 450-650 Hz Range (Waterborne)

Beam and Plate Acceleration Spectra

Figure 5.36 shows a close-up view of the 560 Hz mode in both the beam and plate acceleration spectra and the effect of 3 and 7 grams tuning mass. Comparison with Figure 5.5 for beam 3 reveals three main differences: the beam 2 amplitude is 5 dB higher; the beam mode frequency is reduced 7 Hz by 7 grams tuning mass, vice 12 Hz for beam 3; and most notably, there are no plate modes detectable in the beam drive point spectrum. Plate modes are detectable in the plate spectrum, however, they are relatively unaffected by the presence of the tuning mass.

Figure 5.37 shows the effect of adding coupling mass amounts of 100, 400, 1200, 2000, and 4000 grams to the base of the beam with no tuning mass applied. Unlike what was observed for beam 3, the coupling mass does not change the resonance frequency of the beam mode. However, the increasing coupling mass does reduce the amplitude of the beam mode (6dB decrease after 4000 grams). Note that 4000 grams was considered the upper limit for coupling mass to minimize the list experienced by the model when waterborne (4000 grams yielded a 1/2 inch list). Note in Figure 5.37 that as coupling mass is increased, two plate modes start to appear in the beam spectrum; one to the right of the dominant beam mode and one to the left of the beam anti-resonance. In the plate spectrum in Figure 5.37 we can see that the increased coupling mass decreases the frequency of the plate modes in the vicinity of the beam mode. Other plate modes farther away in frequency are relatively unaffected.

Figures 5.36 and 5.37 reveal that tuning mass did not noticeably shift the resonance frequencies of plate modes, and that coupling mass did not noticeably shift the resonance frequency of the beam mode. This is contrary to what was observed for beam 3 in Figures 5.5 and 5.6. This necessitates additional testing of the modal response to tuning and coupling masses. Figure 5.38 shows the effect of 0, 3, and 7 grams tuning mass in addition to a constant 4000 gram coupling mass applied to each case. Here, we see a small frequency shift and an amplitude change for the plate modes as tuning mass is applied to the beam. Figure 5.39 shows the effect of 0, 100, 400, 1200, 2000, and 4000 grams coupling mass in addition to a constant 7 grams tuning mass applied. Here, we see no frequency change at the beam mode until 4000 grams coupling mass is applied and an 1 Hz increase is observed.

Beam, Plate, and Pressure Spectra

Figures 5.38 and 5.39 showed that tuning mass has a small effect on plate modes and coupling mass has a small effect on the beam mode. For beam 2, these modes react much less than what was observed for beam 3. We will now follow the individual modes and their effect on the radiated sound as various mass configurations are applied. To accomplish this, Figures 5.40 through 5.45 present the beam 2 drive point acceleration spectrum, the mean plate acceleration spectrum, and the mean water tank acoustic pressure spectrum for mass configurations ranging from the unperturbed condition to 7 grams tuning mass plus 4000 grams coupling mass.

Unperturbed Condition : Figure 5.40 shows that the acoustic pressure peaks at the dominant beam mode (labeled mode F). Note that the beam mode has a narrow band width compared to the beam mode shown in Figure 5.8 for beam 3. This indicates that only one mode (the beam mode) is present here vice the mode "splitting off" observed for beam 3. Also, for comparison with Figure 5.8 for beam 3, the peak beam acceleration is 5 dB higher, the peak plate acceleration is 2 dB higher, and the peak acoustic pressure is 8 dB higher for beam 2.

To the right of beam mode F, the plate spectrum shows the presence of "ripples" along with a well defined mode. For identification purposes, the rippled area will be labeled mode G and the well defined mode will be labeled mode H. In subsequent figures, modes G and H will tend to merge together and become difficult to distinguish.

100 Grams Coupling Mass : Figure 5.41 shows the effect of adding 100 grams coupling mass. Comparison with the unperturbed case shows practically no effect on either the beam, plate, or pressure spectra. Consistent with what was previously observed for beam 3, hydrophone response is repeatable for similar beam and plate acceleration spectra.

2000 Grams Coupling Mass : Figure 5.42 shows the effect of 2000 grams coupling mass. Comparison with the unperturbed case (Figure 5.40) shows that beam mode F has decreased about 3 dB in amplitude in the beam spectrum. The plate spectrum near modes G and H has increased about 4 dB in amplitude and is starting to be reflected in the beam spectrum, even though the plate acceleration is roughly 20 dB below that of the beam at this frequency. Modes G and H have moved roughly 2 Hz closer to mode F as a result of the mass addition. Associated with this, the acoustic pressure near these modes has increased roughly 10 dB, and the acoustic pressure near mode F has increased 5 dB. Additionally, a new mode (mode I) appears in both the beam and plate spectra to the left of beam mode F. Associated with this, the acoustic pressure near mode I increases 8 dB.

4000 Grams Coupling Mass : In Figure 5.43, modes G and H continue to move closer to beam mode F in both frequency and amplitude, resulting in a 5 dB increase in acoustic pressure near modes G and H. Here modes G and H are indistinguishable in the plate spectrum. Note that modes F, G, and H are now very close in amplitude in the beam, plate, and pressure spectra. This results in a roughly 20 Hz wide peak in the acoustic pressure. Mode I is moved 4 Hz farther away from beam mode F, resulting in a small decrease in the sharp pressure peak near mode I.

7 Grams Tuning Mass Plus 4000 Grams Coupling Mass : Figure 5.44 shows the effect of adding 7 grams tuning mass to the condition shown in Figure 5.43. Here, beam mode F is reduced 7 Hz in frequency and modes G and H are increased roughly 4 Hz in frequency. As

a result, the pressure near modes G and H is reduced roughly 6 dB. Additionally, even though mode I moves 2 Hz to the left, modes F and I are now 19 Hz apart (vice 24 Hz apart in Figure 5.43) and the acoustic pressure at mode I increases about 3 dB.

5.3.3 Beam 2 - Results in Air

Spectra Overview

Figures 5.45 and 5.46 show the beam drive point acceleration spectrum in air for tuning mass amounts ranging from the unperturbed condition to 22 grams. Comparison with Figures 5.32 and 5.35 for the waterborne case reveals that the results in air are very similar to those in water relative to beam spectrum appearance. For example, the unperturbed condition in air has modes at 64, 560, and 1673 Hz, vice 64, 560, and 1687 Hz for the waterborne case. Notice that, similar to what was observed for beam 3, the fluid loading in the waterborne case has more of an effect on the high frequency mode resulting in frequency increases on the order of 10 Hz at higher frequency, compared to roughly 4 Hz or less at the lower frequency modes. Additionally tuning mass has more of an effect on the higher frequency mode as previously observed for beam 3.

The beam spectrum "distortion" due to 10, 15, and 22 grams tuning mass is similar for both the waterborne and airborne cases. Additionally, the large frequency increase at the high frequency mode due to 7 grams tuning mass observed in the waterborne case (and for beam 3) is also observed here.

450-650 Hz Frequency Range

Figure 5.47 shows a close-up view of the 560 Hz mode in both the beam and plate acceleration spectra and the effect of 3 and 7 grams tuning mass. Comparison with Figure 5.36 (waterborne case) reveals that a plate mode (previously identified as mode I) is now visible in the beam spectrum. This plate mode changes shape and amplitude under the presence of the tuning mass. Additionally, to the right of the beam mode in the plate spectrum, we see a plate mode becoming distinct as tuning mass is added.

Figure 5.48 shows the effect of adding coupling mass amounts of 100, 400, 1200, 2000, and 4000 grams to the base of the beam with no tuning mass applied. Here we see a 1 Hz increase in the resonance frequency of the beam mode as well as frequency, amplitude, and shape changes for the plate modes. As in the waterborne case, the airborne case shows that the beam mode is only slightly affected by coupling mass, and neighboring plate modes to the right and left of the beam mode are only slightly affected by tuning mass.

Figures 5.49 through 5.52 compare beam and plate spectra for the waterborne and airborne cases as various combinations of tuning and coupling masses are applied. The top graph in each figure applies to the waterborne case; the bottom graph in each figure applies to the airborne case. In each figure, the waterborne graph has previously been presented and discussed, and is included again here to facilitate comparison. Individual modes are labeled F, G, H, and I, consistent with what was presented previously for the waterborne case.

Unperturbed Condition : Figure 5.49 compares beam and plate spectra for the unperturbed (no mass) condition. Consistent with what was observed for beam 3, the beam and plate peak acceleration amplitudes are virtually identical in the airborne and waterborne cases.

Mode H is clearly visible in both plate spectra, although it is about 4 Hz closer to mode F in the waterborne case. In the airborne case, mode I is distinct and visible in the beam and plate spectra, whereas in the waterborne case it is masked.

2000 Grams Coupling Mass : Figure 5.50 compares response to 2000 grams coupling mass. Mode I is now visible in the beam and plate spectra in the waterborne case. In the airborne case, modes G and H are not distinct in the plate spectrum, although it appears mode G is now being reflected in the beam spectrum. In the waterborne case, modes G and H are visible in the beam spectrum. Again, we see plate modes visible in the beam spectrum even though the plate acceleration at the frequency of the modes is roughly 20 dB below the beam acceleration.

4000 Grams Coupling Mass : Figure 5.51 compares response to 4000 grams coupling mass. We can see that mode I has been reduced in frequency compared to previous figures in both the airborne and waterborne cases. Modes G and H are not distinct in either plate spectra, although mode H appears visible in the waterborne beam spectrum.

7 Grams Tuning Mass Plus 4000 Grams Coupling Mass : Figure 5.52 compares response to 7 grams tuning mass plus 4000 grams coupling mass. In both the airborne and waterborne cases, the 7 gram tuning mass reduced the beam mode (mode F) frequency from 560 to 554 Hz. Additionally, in both the airborne and waterborne cases modes G and H are now more distinct in the plate spectrum, although they are not visible in either of the beam spectra.

5.3.4 Beam 2 - Summary

The results of testing beam 2 show some similarities and some differences with the results obtained for beam 3. The similarities and differences are as follows:

Similarities with Beam 3 Results

a) Beam and plate modes were relatively easy to classify in the plate acceleration spectrum based on response to tuning and coupling masses. Plate modes which were within roughly 20 dB of the beam acceleration spectrum appeared in the beam spectrum. However, plate modes can be strong sound radiators and not be detectable in the beam spectrum.

b) Beam mode F appears to react globally with plate modes G, H, and I. As these modes are brought closer to mode F, acoustic pressure increases significantly (on the order of 15 dB was observed). Conversely, as these modes are separated from mode F, the acoustic pressure decreases sharply.

c) Tuning mass decreased the frequency of beam and plate modes. Coupling mass tended to decrease the frequency of plate modes, and increase the frequency (although slightly) of the beam mode.

d) Airborne and waterborne response of beam, plate, and global modes is similar. Corresponding modes can be identified for the waterborne and airborne cases. However, the spacing between global mode pairs again varied between the waterborne and airborne cases. For example, in Figure 5.49 mode H is roughly 7 Hz closer to mode F in the waterborne case compared to the airborne case. Recall again that around 560 Hz, the plate damping was measured to be identical for the airborne and waterborne conditions.

Differences from Beam 3 Results

The major differences observed for beam 2 is that the modes which appear to act globally from an acoustic pressure standpoint, are affected very little by the presence of tuning and

coupling masses. This fact would make it hard to identify modes F, G, and H as global without the benefit of the acoustic data. This problem is compounded by the fact that modes G and H tend to be nondistinctive and hard to follow.

In Table 3-3 we saw that the bending moment impedance of beam 2 was roughly 60 percent that of beam 3 near 500 Hz, and roughly 1 percent that of the plate. The relative insensitivity to coupling mass that beam 2 experienced may be due to the fact that the plate is already appearing as an infinite impedance to the beam. Addition of coupling mass may have no effect since the beam may be approaching an ideal cantilevered boundary condition at the plate.

The relative insensitivity of plate modes to tuning mass is puzzling. The reduced bending moment impedance and stiffness of beam 2 over those of beam 3 do not appear to be the cause. Beam 2 generates a 2 dB higher plate acceleration level than beam 3, and as such, appears to be efficient at imparting a moment to the plate. Based on this, we would expect plate modes to be fairly sensitive to tuning mass effects.

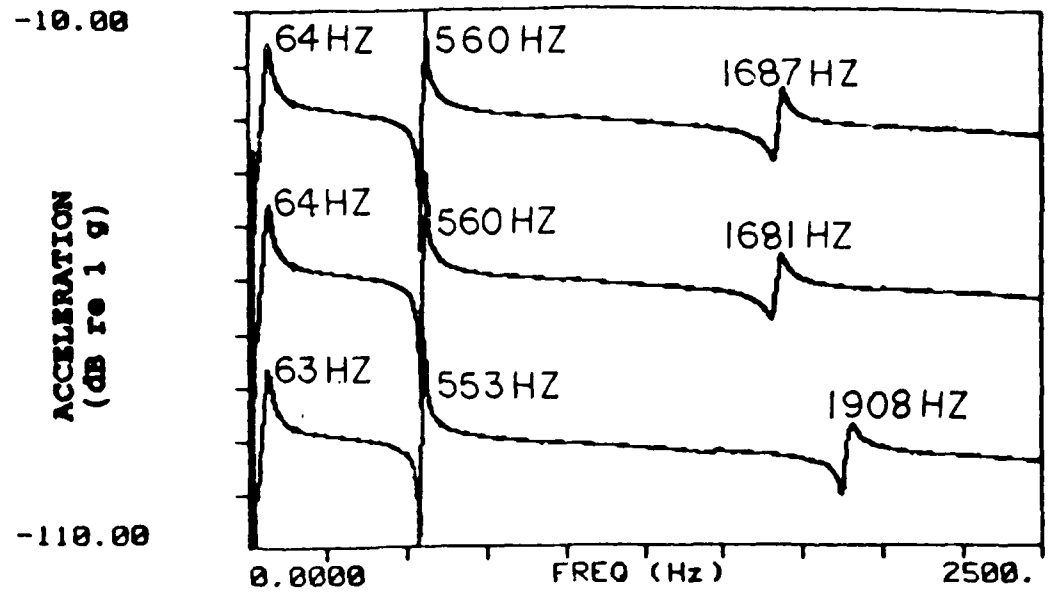

: 5.32 Beam 2 Waterborne. Beam drive point acceleration. From top: 0, 3, and 7
; tuning mass.

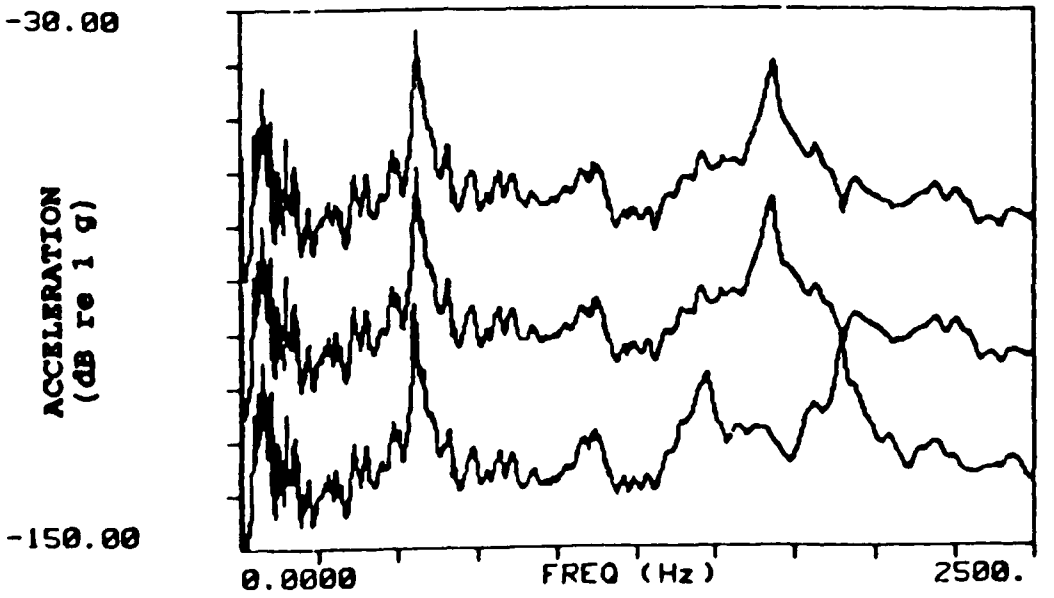

: 5.33 Beam 2 Waterborne. Mean plate acceleration. From top: 0, 3, and 7 grams
; mass.

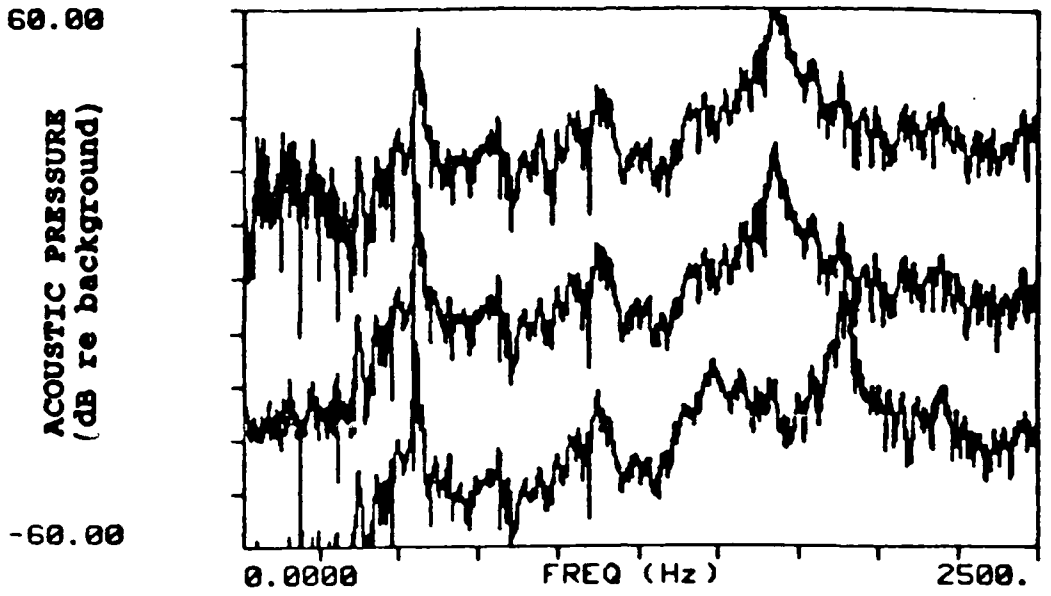

Figure 5.34 Beam 2 Waterborne. Mean acoustic pressure. From top: 0, 3, and 7 gram tuning mass.

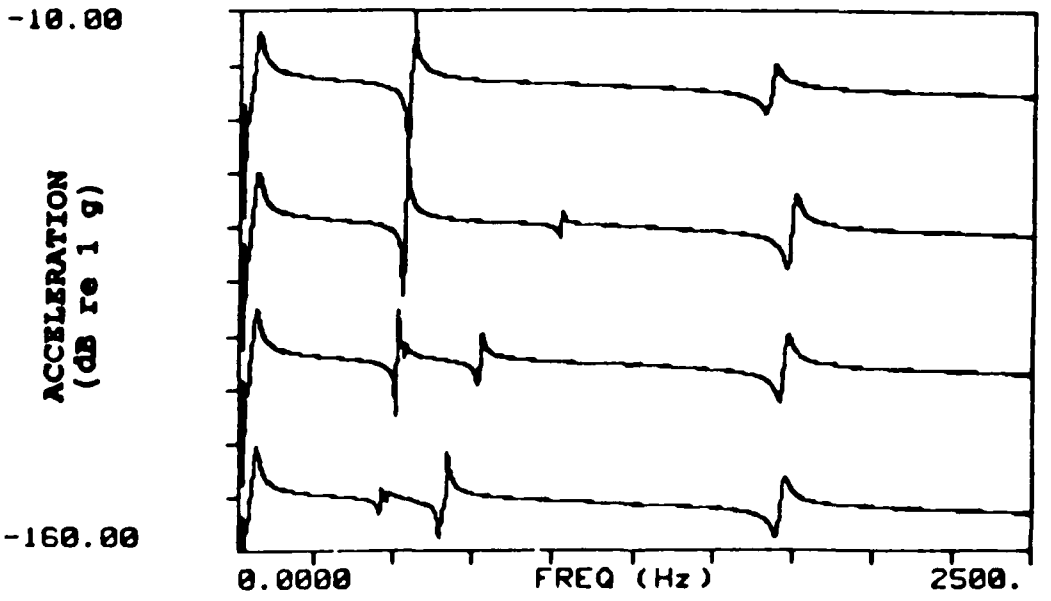

igure 5.35 Beam 2 Waterborne. Beam drive point acceleration. From top: 0, 10, 15, and 2 grams tuning mass.

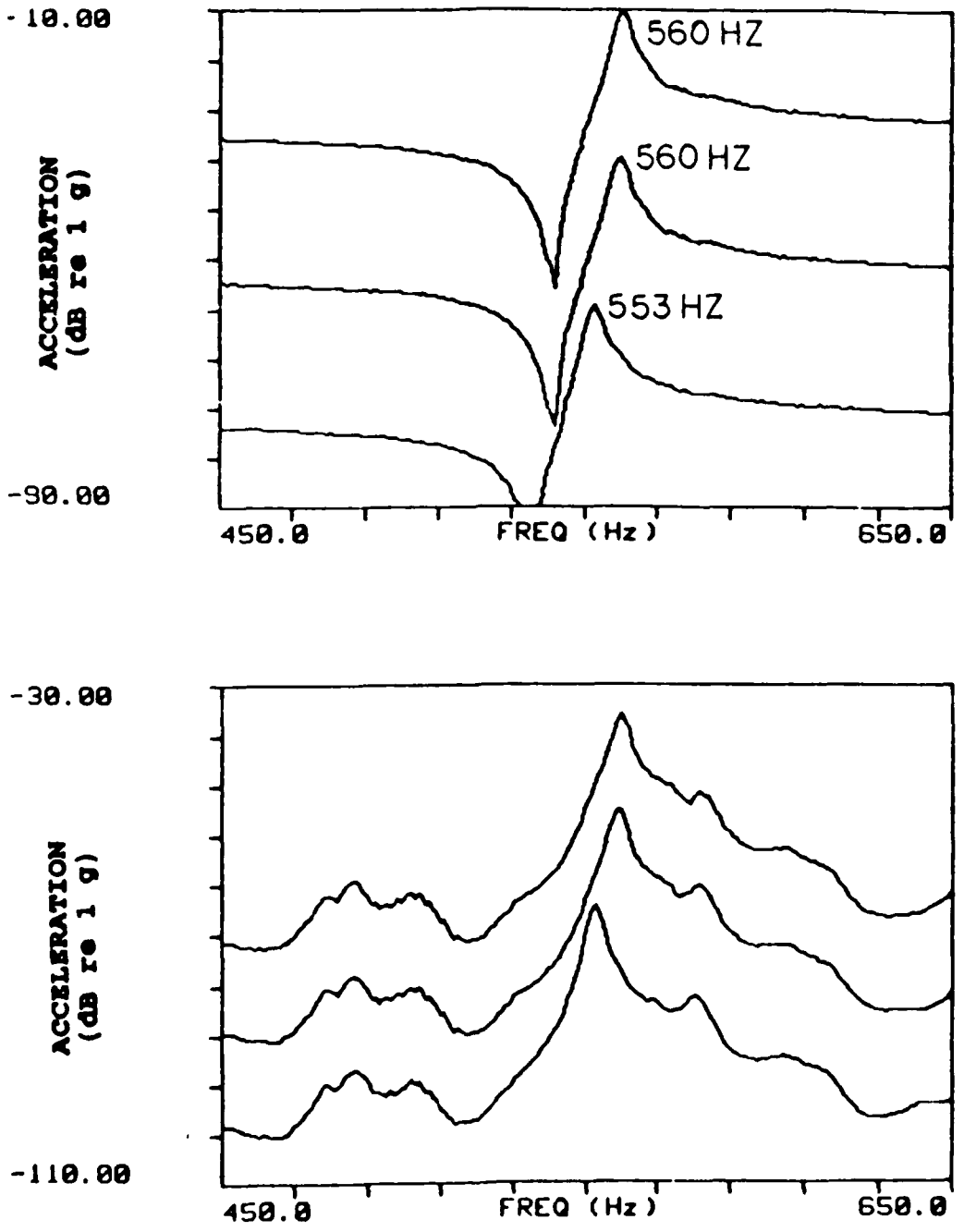

Figure 5.36 Beam 2 Waterborne. Beam drive point acceleration (top graph) and mean plate acceleration (bottom graph). From top in each graph: 0, 3, and 7 grams tuning mass.

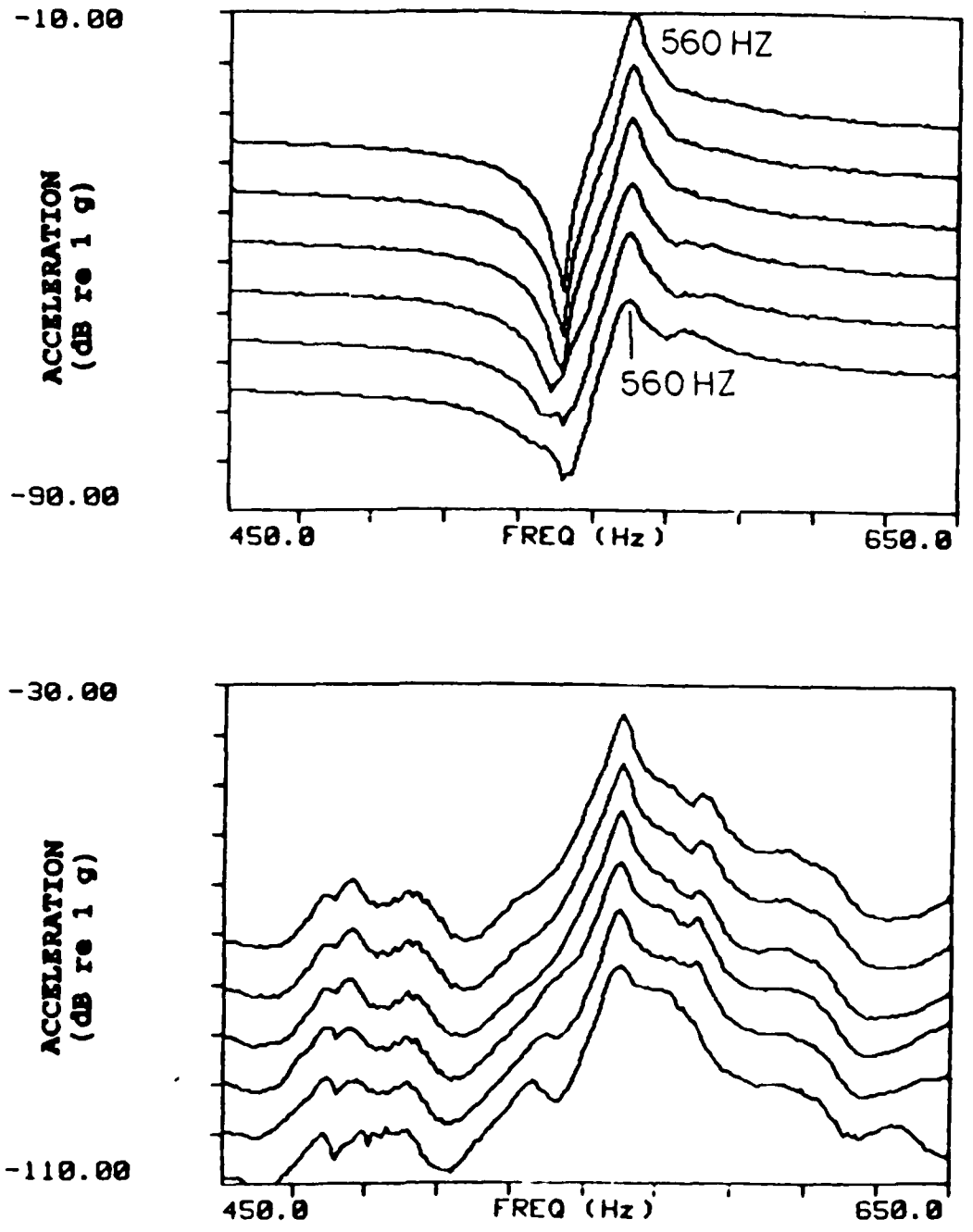

Figure 5.37 Beam 2 Waterborne. Beam drive point acceleration (top graph) and mean plate acceleration (bottom graph). From top in each graph: 0, 100, 400, 1200, 2000, and 4000 grams coupling mass.

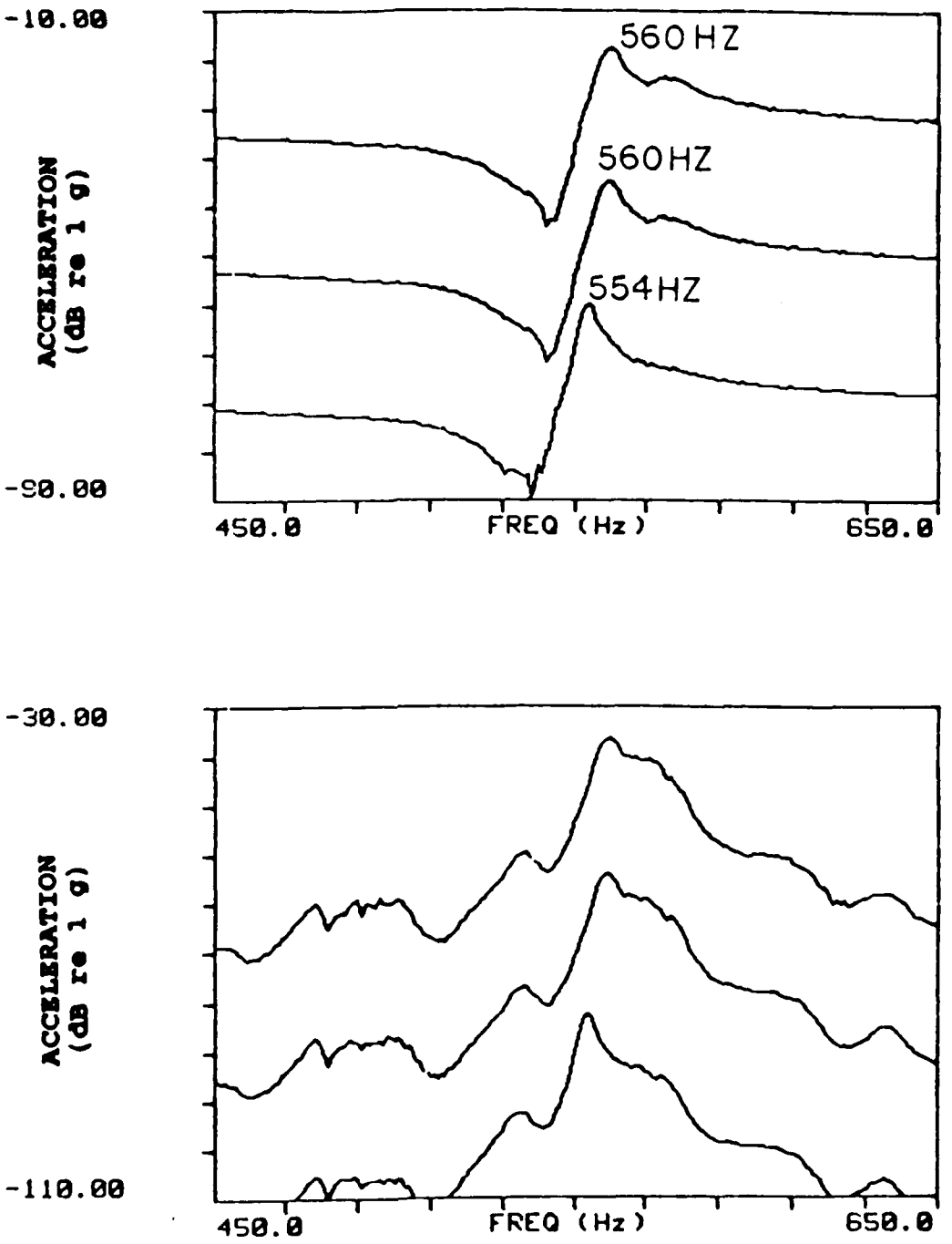

Figure 5.38 Beam 2 Waterborne. Beam drive point acceleration (top graph) and mean plate acceleration (bottom graph). All plots shown have 4000 grams coupling mass added in addition to tuning mass. From top in each graph: 0, 3, and 7 grams tuning mass.

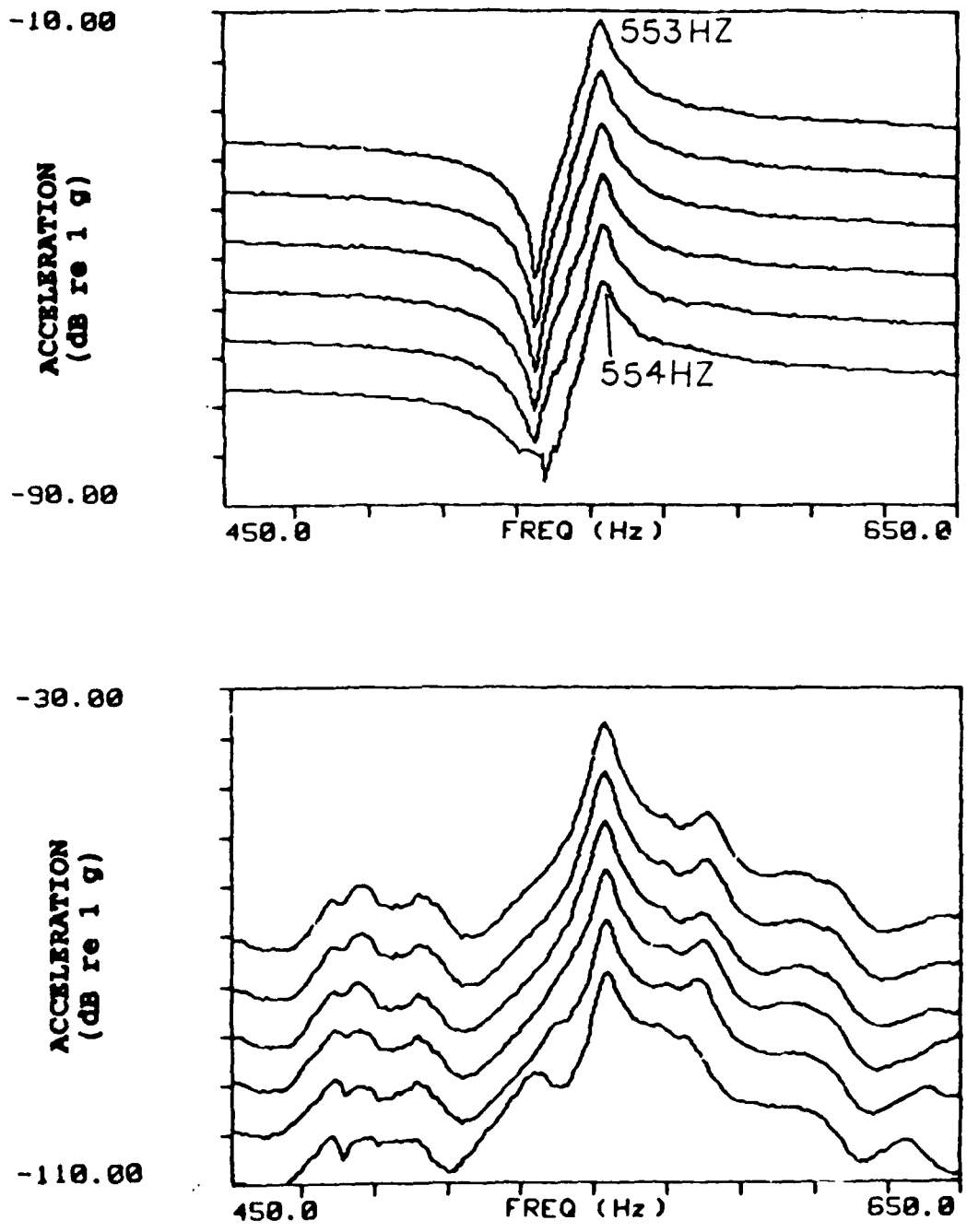

Figure 5.39 Beam 2 Waterborne. Beam drive point acceleration (top graph) and mean plate acceleration (bottom graph). All plots shown have 7 grams tuning mass added in addition to coupling mass. From top in each graph: 0, 100, 400, 1200, 2000, and 4000 grams coupling mass.

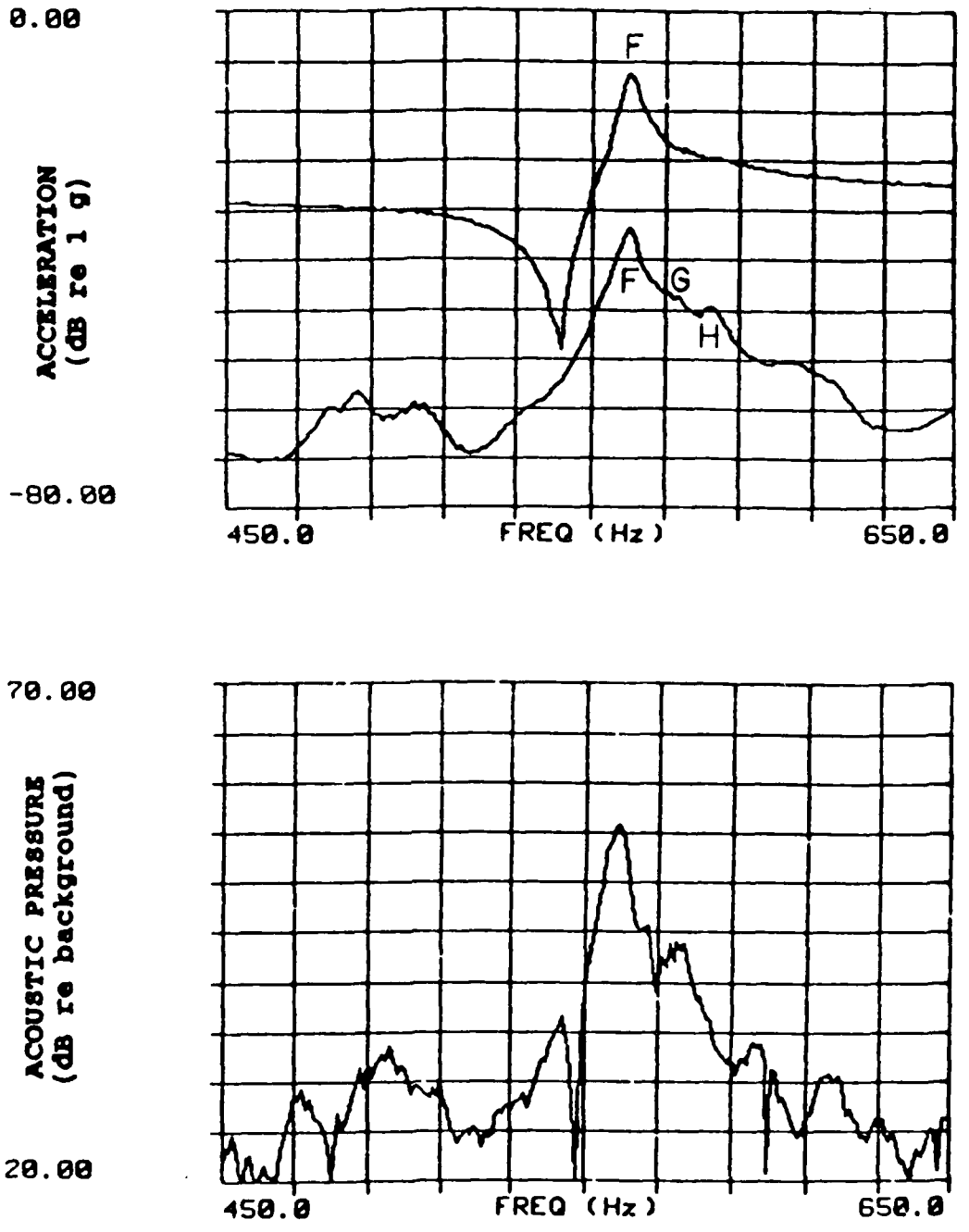

Figure 5.40 Beam 2 Waterborne. Unperturbed condition (no mass). From top: beam acceleration, mean plate acceleration, and mean acoustic pressure.

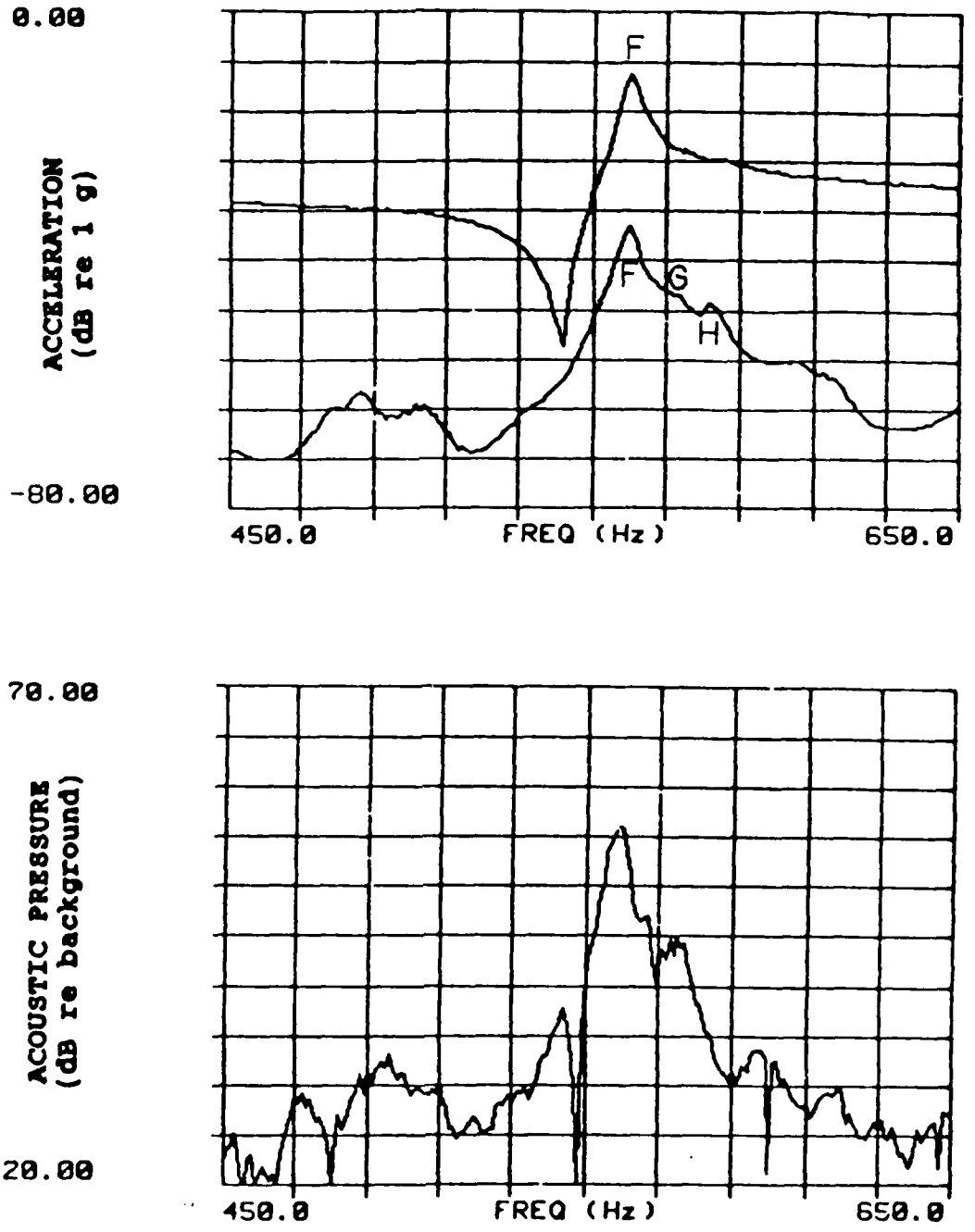

Figure 5.41 Beam 2 Waterborne. 100 grams coupling mass. From top: beam acceleration, mean plate acceleration, and mean acoustic pressure.

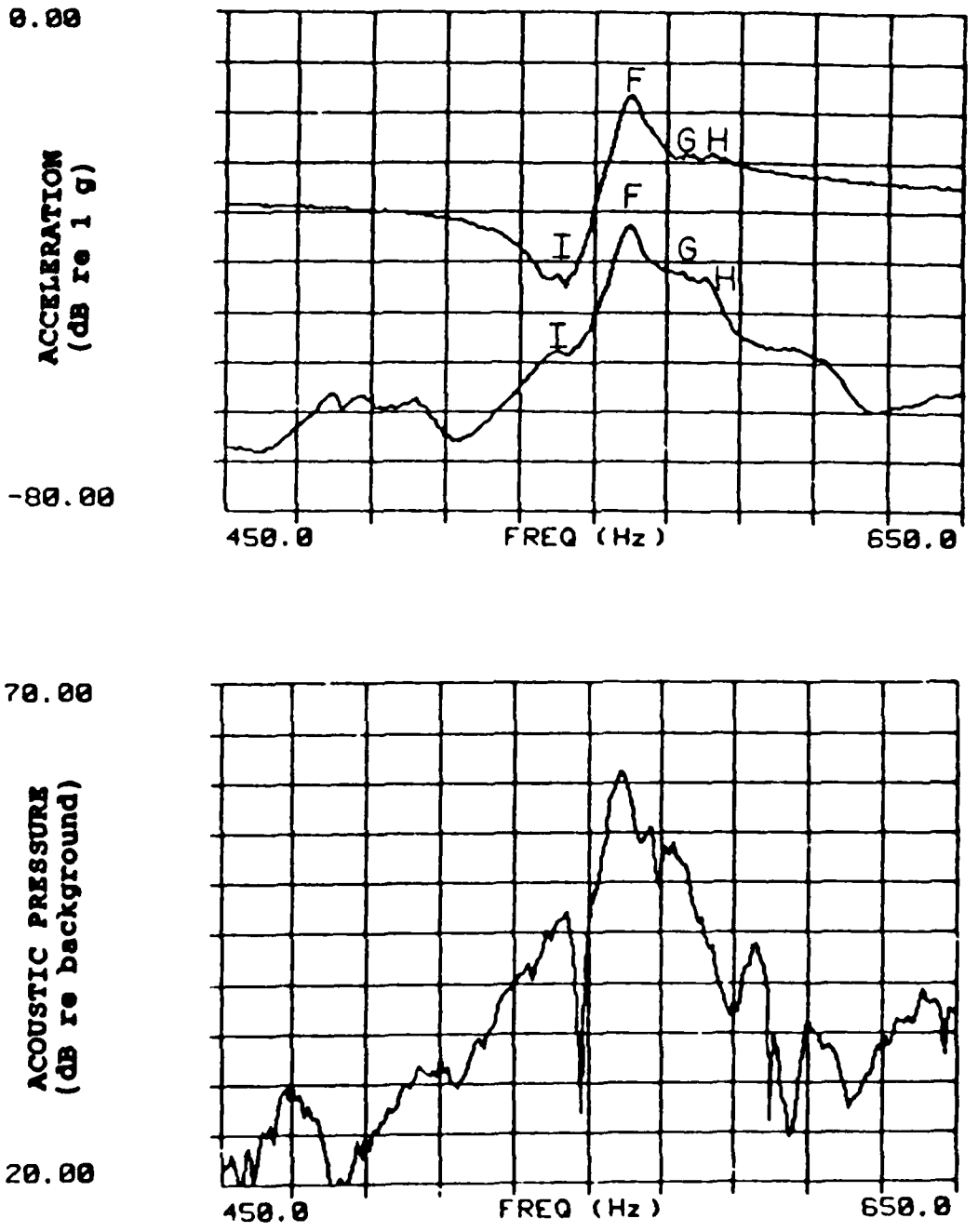

Figure 5.42 Beam 2 Waterborne. 2000 grams coupling mass. From top: beam acceleration, mean plate acceleration, and mean acoustic pressure.

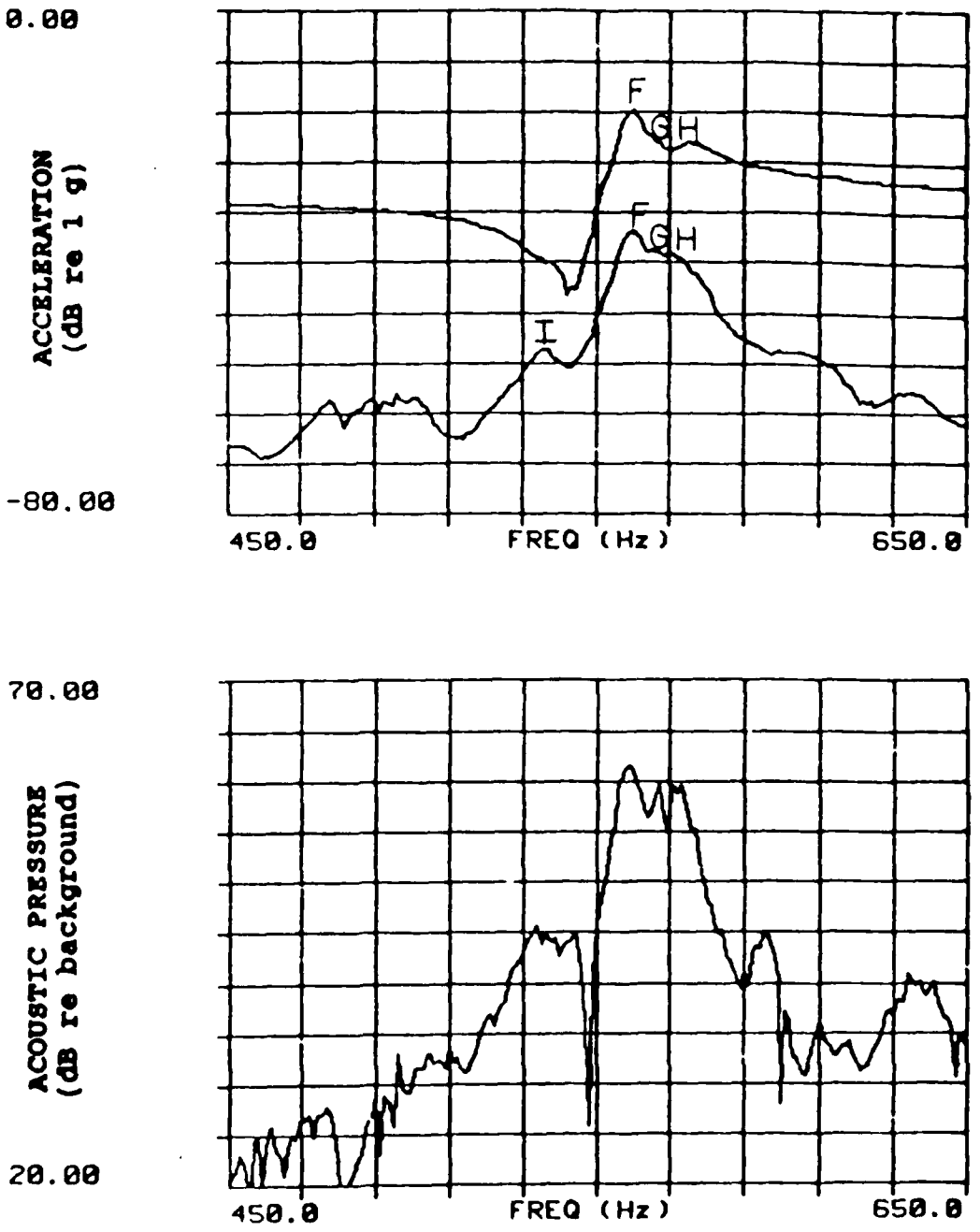

Figure 5.43 Beam 2 Waterborne. 4000 grams coupling mass. From top: beam acceleration, mean plate acceleration, and mean acoustic pressure.

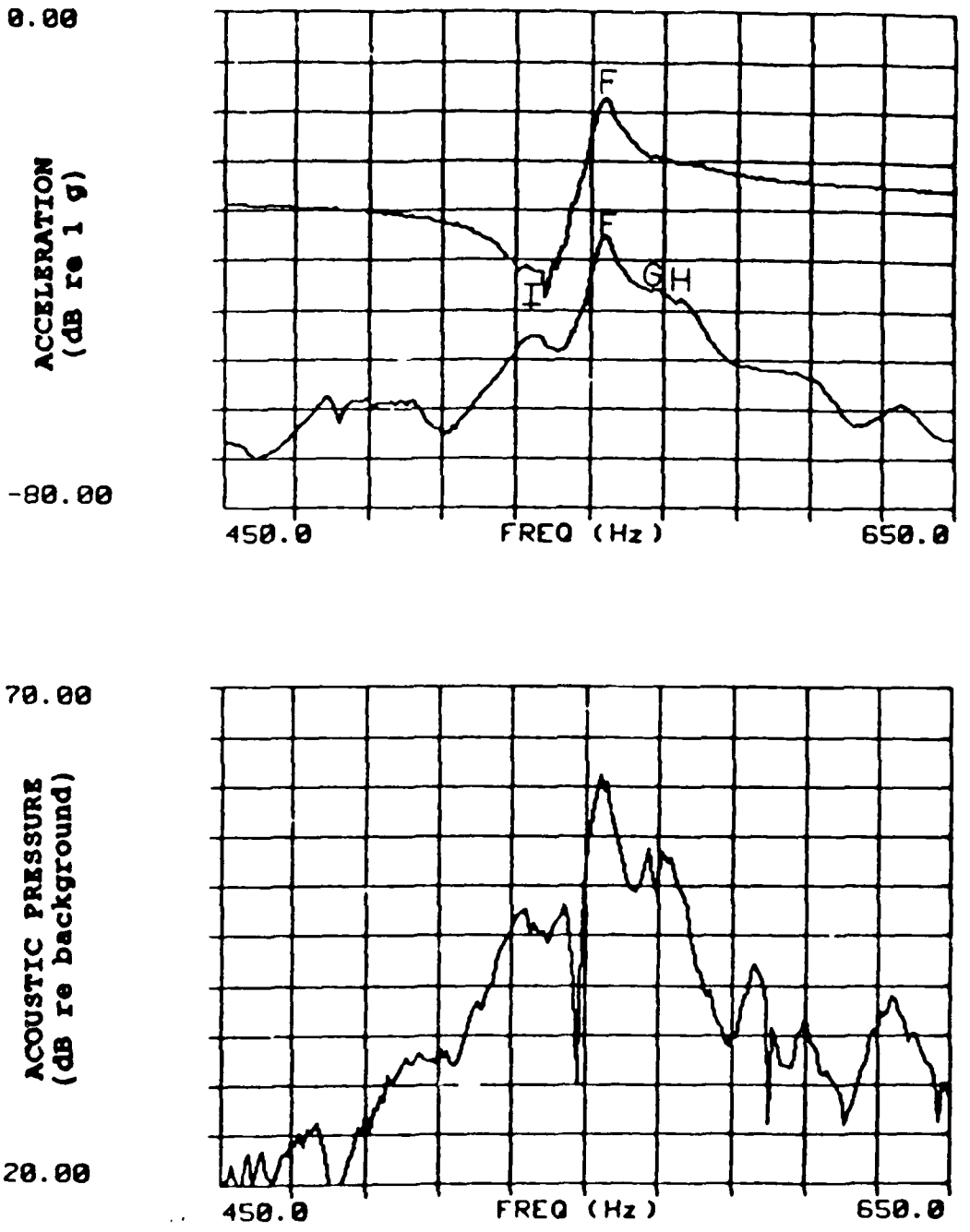

Figure 5.44 Beam 2 Waterborne. 7 grams tuning mass plus 4000 grams coupling mass. From top: beam acceleration, mean plate acceleration, and mean acoustic pressure.

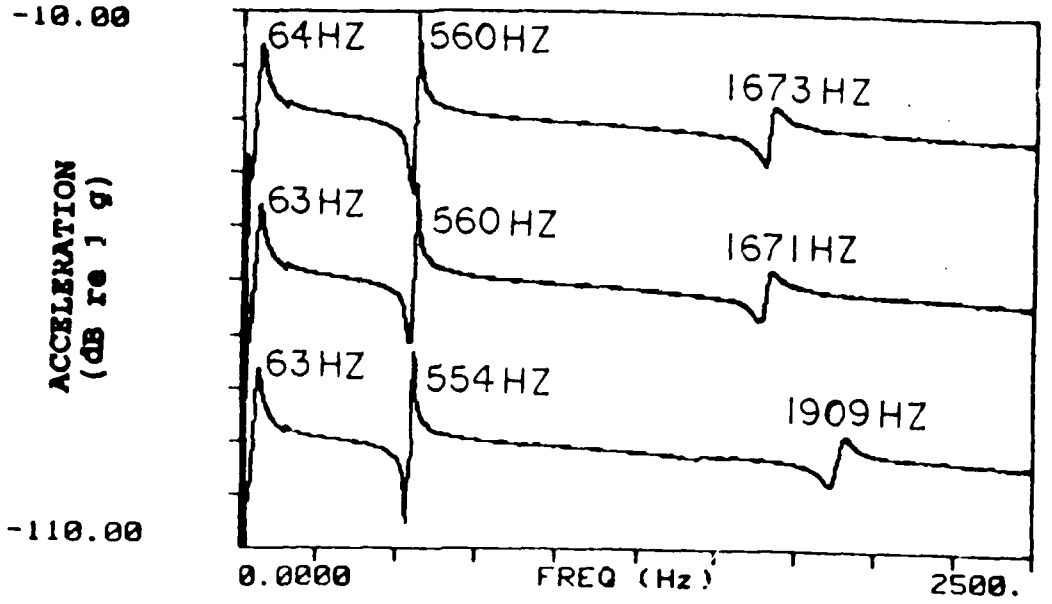

Figure 5.45 Beam 2 Airborne. Beam drive point acceleration. From top: 0, 3, and 7 grams tuning mass.

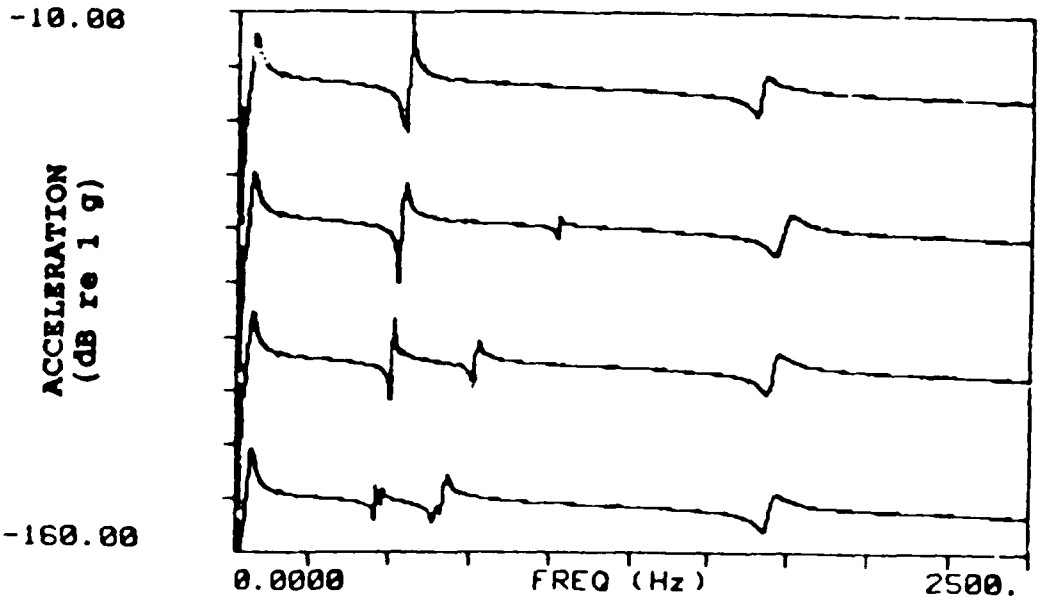

Figure 5.46 Beam 2 Airborne. Beam drive point acceleration. From top: 0, 10, 15, and 22 grams tuning mass.

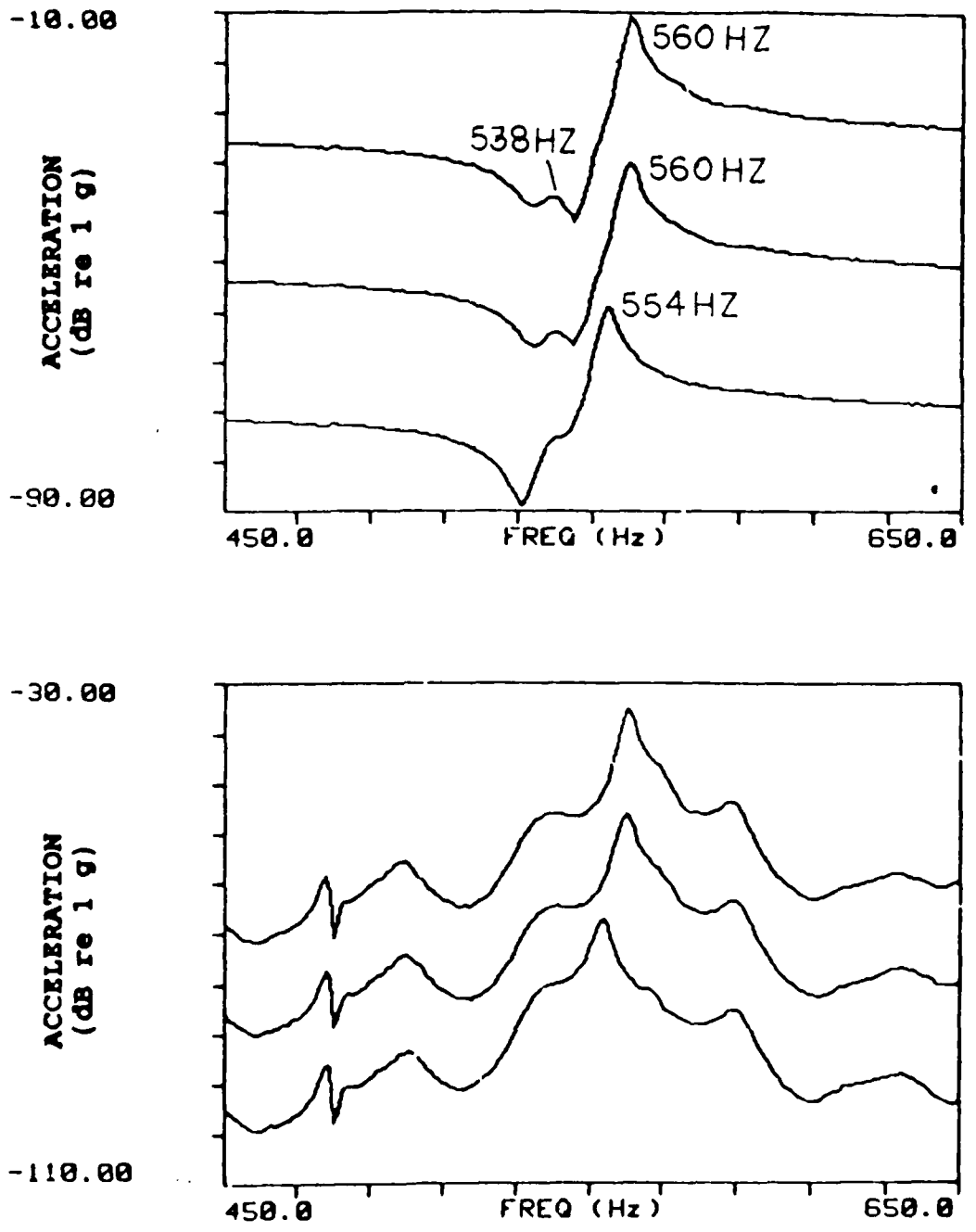

Figure 5.47 Beam 2 Airborne. Beam drive point acceleration (top graph) and mean plate acceleration (bottom graph). From top in each graph: 0, 3, and 7 grams tuning mass.

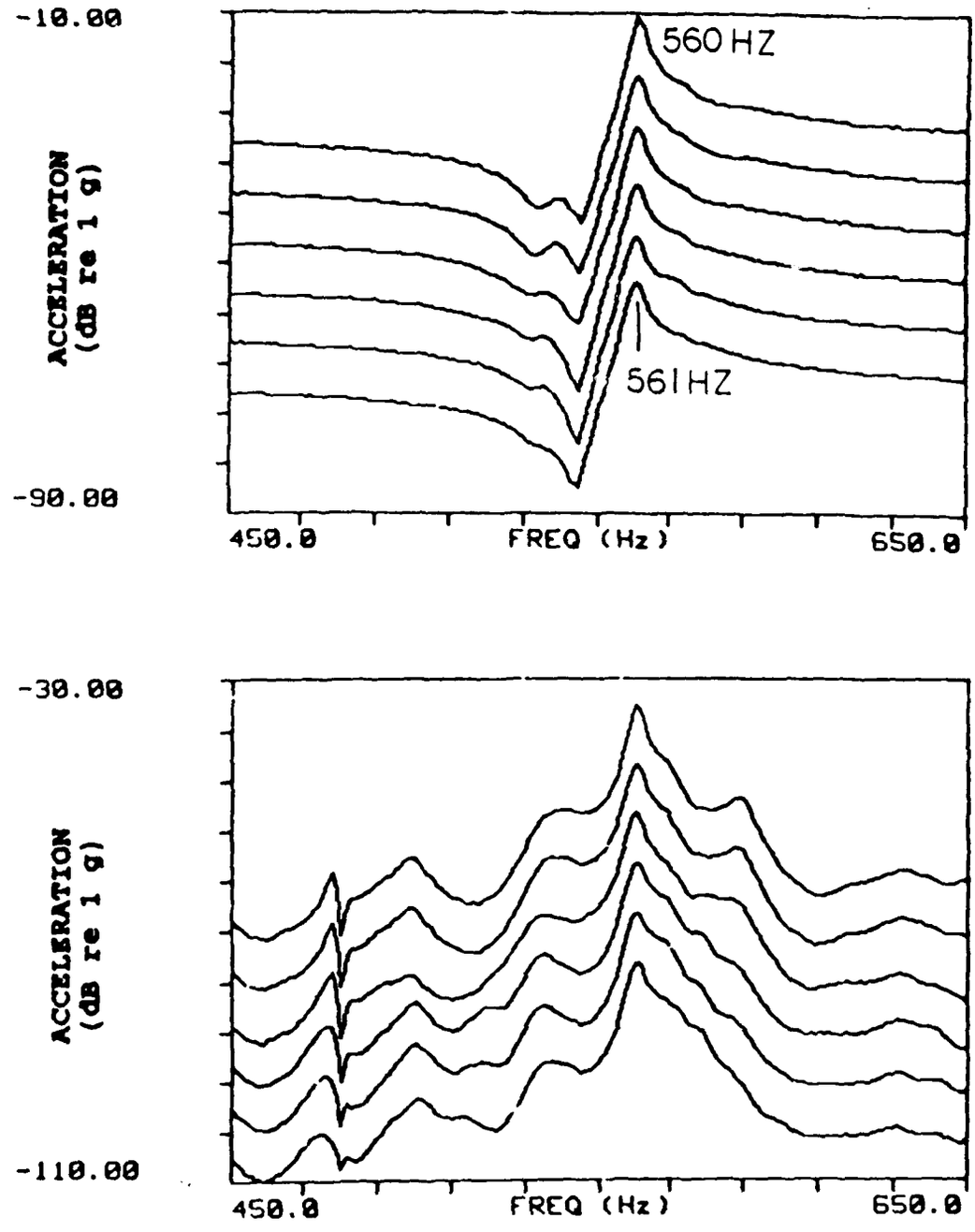

Figure 5.48 Beam 2 Airborne. Beam drive point acceleration (top graph) and mean plate acceleration (bottom graph). From top in each graph: 0, 100, 400, 1200, 2000, and 4000 grams coupling mass.

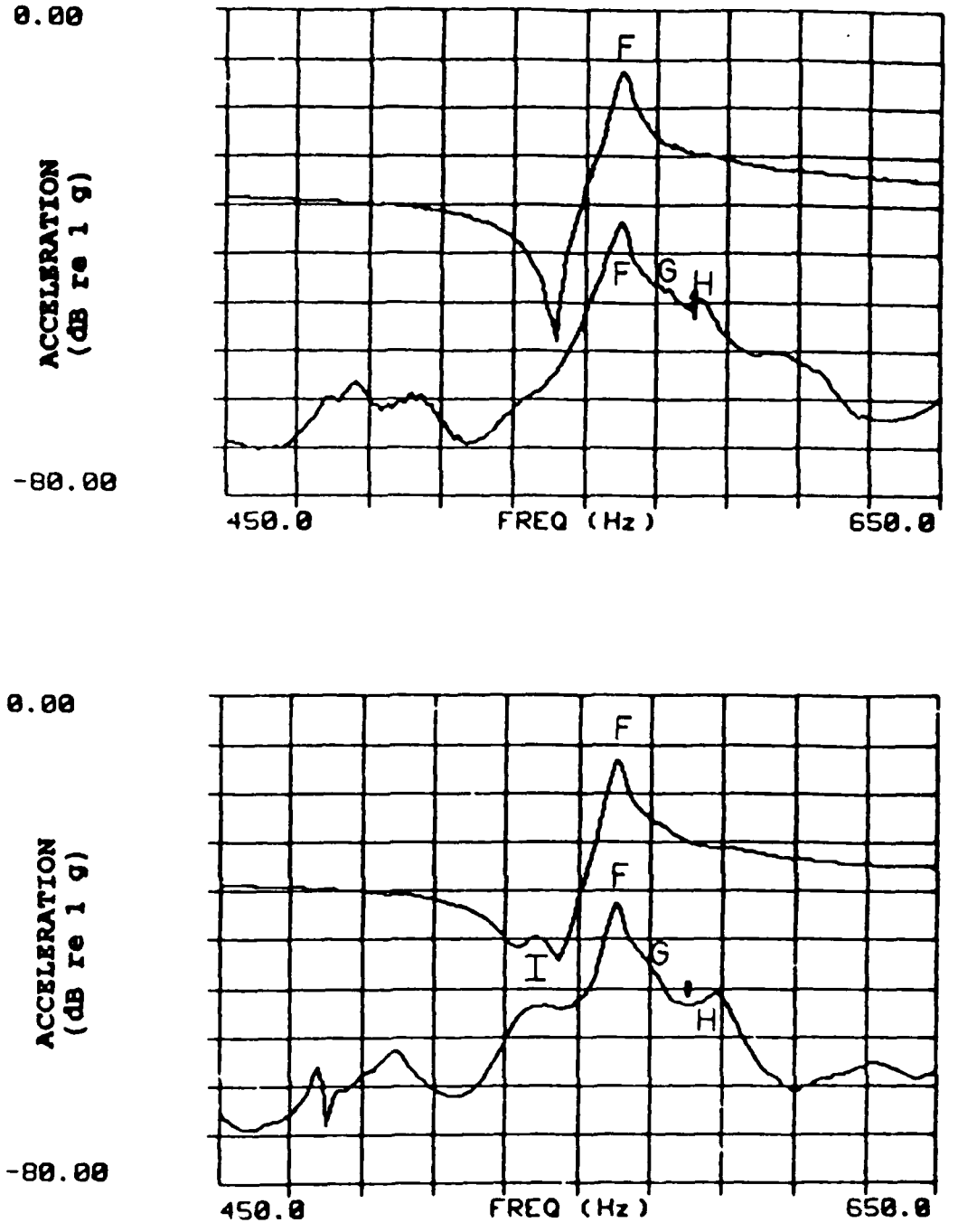

Figure 5.49 Beam 2 Waterborne (top graph) and Airborne (bottom graph). Unperturbed condition (no mass). From top in each graph: beam drive point acceleration, and mean plate acceleration.

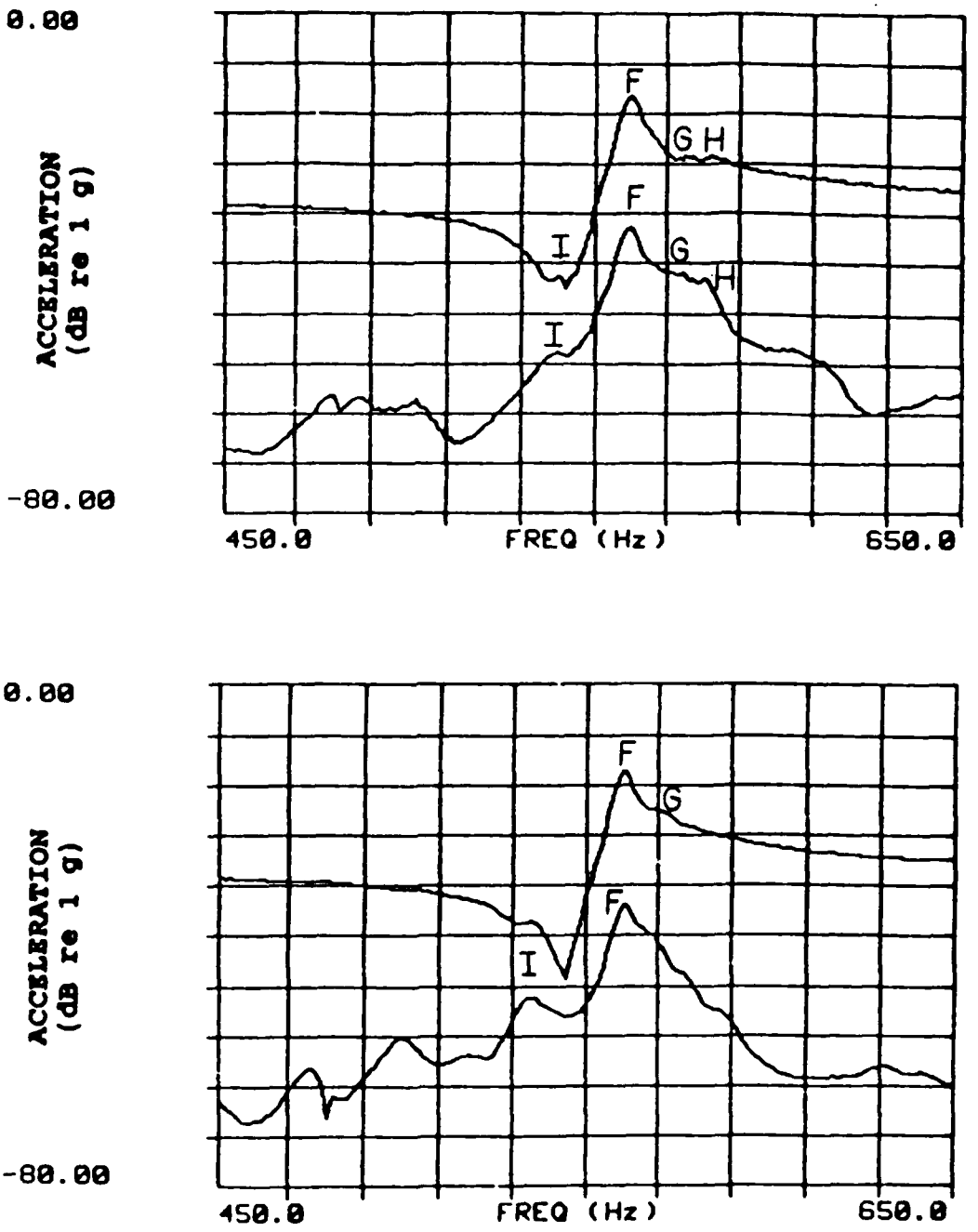

Figure 5.50 Beam 2 Waterborne (top graph) and Airborne (bottom graph). 2000 grams coupling mass. From top in each graph: beam drive point acceleration, and mean plate acceleration.

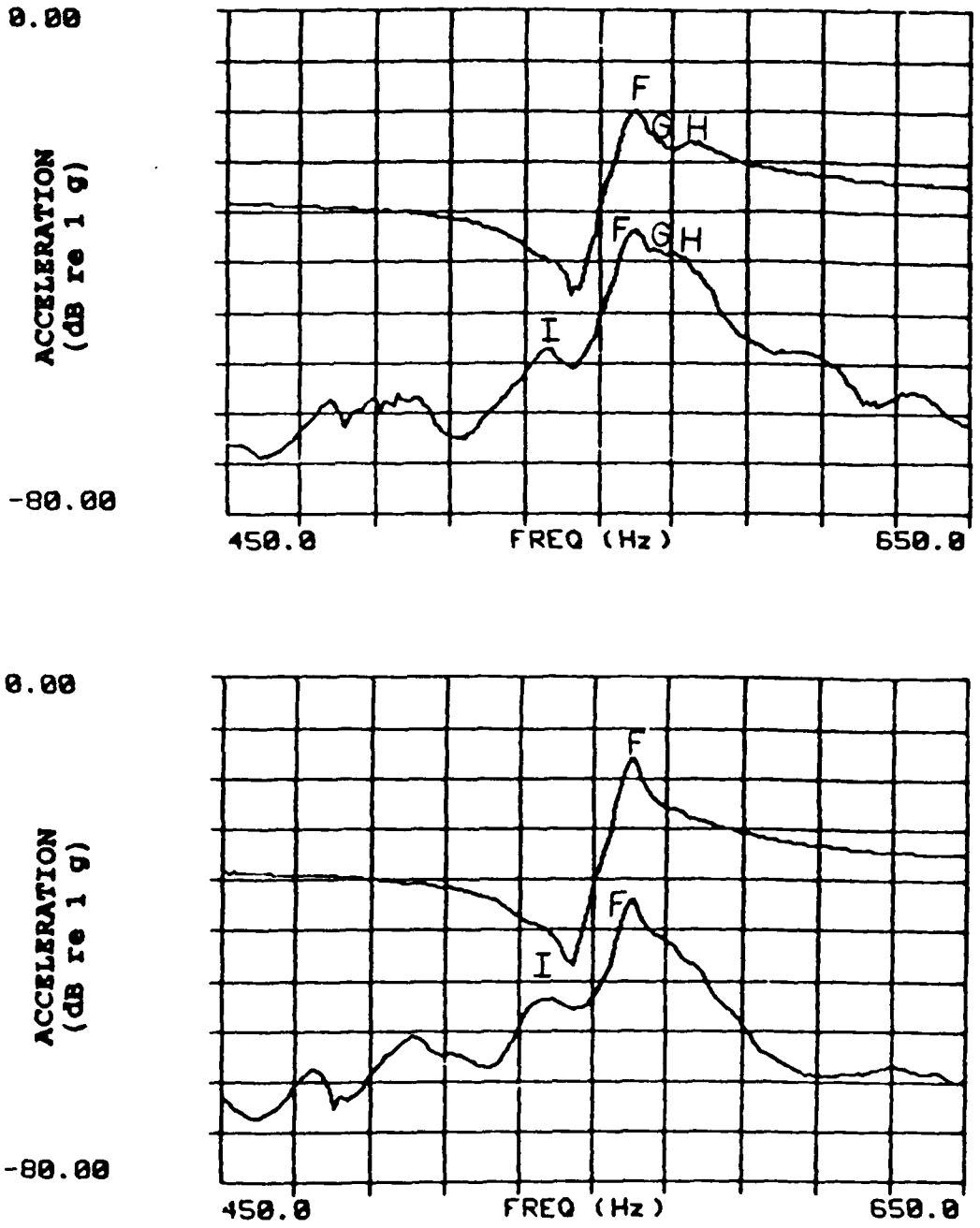

Figure 5.51 Beam 2 Waterborne (top graph) and Airborne (bottom graph). 4000 grams coupling mass. From top in each graph: beam drive point acceleration, and mean plate acceleration.

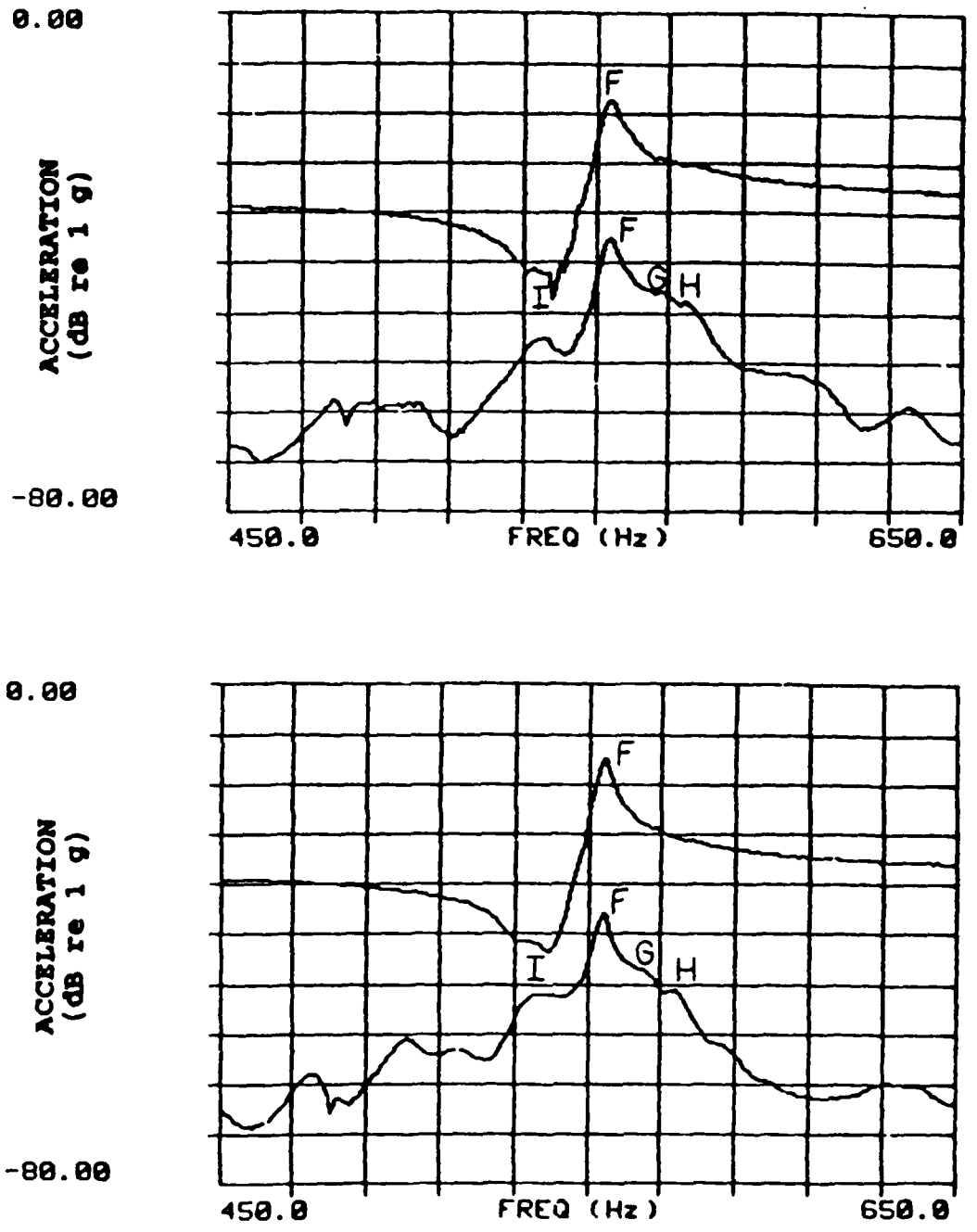

Figure 5.52 Beam 2 Waterborne (top graph) and Airborne (bottom graph). 7 grams tuning mass plus 4000 grams coupling mass. From top in each graph: beam drive point acceleration, and mean plate acceleration.

5.4 Beam 1 Results

Sections 5.4.1 through 5.4.4 present the results of testing with the shaker mounted on beam 1. Results in water and air are discussed. In this section we will briefly compare the results of testing beam 1 with results obtained for beam 3 and beam 2.

5.4.1 Beam 1 - Spectra Overview (Waterborne)

Figure 5.53 shows the drive point acceleration spectrum for beam 1 for the conditions of 0, 3, and 7 gram tuning mass added to the free end of beam 1 (no coupling mass added). Figures 5.54 and 5.55 show the mean plate acceleration and mean acoustic pressure spectrum for the 0, 3, and 7 gram tuning mass conditions. The following comments pertain to Figures 5.53, 5.54, and 5.55:

a. Figure 5.53 shows that beam 1 reacts to tuning mass in a similar manner to beam 2, and reacts less to tuning mass than beam 3. The unperturbed spectrum consists of three dominant resonance modes with frequencies of 54, 502 and 1485 Hz (all lower in frequency than beams 2 and 3). As in the case for beam 2, application of 3 grams tuning mass results in no frequency change to the first two modes and a 3 Hz decrease in the frequency of the original 1485 Hz mode. Application of 7 grams tuning mass results in resonance mode frequencies of 52, 495 and 1766 Hz. Here again, the 7 grams tuning mass greatly increased the frequency of the higher frequency mode. Additionally, with the 7 gram tuning mass the beam spectrum is starting to become "distorted". Note the addition of a low amplitude mode near 850 Hz.

b. Similar to what was observed for beam 2, the 7 gram tuning mass condition alters the plate spectrum near 1300 Hz to yield a strong resonance which is reflected in the acoustic pressure spectrum.

Consistent with what was observed for beams 3 and 2, modal overlap due to damping yields wide bandwidths in both the beam and plate acceleration spectra at the high frequency mode. Such wide bandwidths mask the movements of individual beam and plate modes. Accordingly, only the 502 Hz mode will be investigated in detail.

5.4.2 Beam 1 - 400-600 Hz Range (Waterborne)

Beam and Plate Acceleration Spectra

Figure 5.56 shows a close-up view of the 502 Hz mode in both the beam and plate acceleration spectra and the effect of 3 and 7 grams tuning mass. Here again, it appears obvious that the dominant mode is a beam mode. No plate modes are clearly visible in the beam spectrum, although the plate spectrum shows a closely neighboring plate mode at 489 Hz. The application of 7 grams tuning mass results in the beam and plate mode merging and a noticeable change in the appearance of the plate spectrum in this region.

Figure 5.57 shows the effect of adding coupling mass amounts of 100, 400, 1200, 2000, and 4000 grams to the base of the beam with no tuning mass applied. Here we see that the resonance frequency of the beam mode does not change until 2000 grams coupling mass is added and a 1 Hz reduction in frequency is observed. Increasing the coupling mass amount to 4000 grams resulted in no further frequency change. The "saturation" effect of increasing coupling mass observed for beam 3 also occurs here for beam 1. However, contrary to what was observed for beams 3 and 2, application of coupling mass to beam 1 resulted in a reduction

of the beam mode frequency. For beams 3 and 2 we observed a frequency increase. Consistent with the results for beam 3 and 2, plate modes are in general reduced in frequency as increasing coupling mass is applied.

Having established that the 502 Hz beam mode is slightly affected (i.e., 1 Hz reduction after 4000 grams) by coupling mass and that the neighboring plate mode just to the left of the beam mode is affected by tuning mass, it appears that these two modes could likely form a global mode pair. We will now follow these modes as various configurations of tuning and coupling mass are applied and study the effect on the radiated sound.

Unperturbed Condition : Figure 5.58 shows that the acoustic pressure peaks at the dominant beam mode at 502 Hz (labeled mode J). The neighboring plate mode is at 489 Hz (labeled mode K). Figure 5.58 for beam 1, and Figures 5.8 and 5.40 for beams 3 and 2 respectfully, provide the acceleration and acoustic pressure level comparisons listed in Table 5-1.

Table 5-1 Beam Mode Characteristics (Unperturbed Condition)

	Beam 1	Beam 2	Beam 3
Beam Mode Frequency (Hz)	502	560	613
Beam Acceleration (dB re 1 g)	-16	-10	-15
Plate Acceleration (dB re 1 g)	-42	-35	-37
Acoustic Pressure (dB re Background)	48	55	47

We see that beam 1 has unperturbed (no mass) acceleration and acoustic pressure levels far below those of beam 2. Beam 1 is comparable to beam 3 with regard to beam acceleration and acoustic pressure, however, it generates a plate acceleration level 5 db lower (factor of 3.2). Here we see that among similar beams, similar beam or plate acceleration levels do not necessarily yield similar acoustic pressure levels.

Notice in Figure 5.58 that the plate acceleration at mode K (482 Hz) is roughly 8 dB below that of the beam. However, this plate mode is only visible as a slight disturbance in the beam spectrum and would likely go undetected without evaluation of the plate spectrum. This is different from what was observed for beams 3 and 2, where plate modes were generally visible in the beam spectrum when the plate acceleration was within roughly 20 dB that of the beam.

100 Grams Coupling Mass : Figure 5.59 shows the effect of adding 100 grams coupling mass. Comparison with the unperturbed case shows practically no effect on either the beam, plate, or pressure spectra. Consistent with what was previously observed for beam 3 and beam 2, hydrophone response is repeatable for similar beam and plate acceleration spectra.

800 Grams Coupling Mass : Figure 5.60 shows the effect of adding 800 grams coupling mass. Comparison with the unperturbed condition reveals that plate mode K experiences a 3 Hz reduction in frequency and is now farther away from beam mode J. This separation of modes J and K results in a roughly 7 dB reduction in acoustic pressure near mode J, and a roughly 2 dB reduction in acoustic pressure near mode K.

4000 Grams Coupling Mass : Figure 5.61 shows the effect of 4000 grams coupling mass. Comparison with Figure 5.60 shows a further reduction (7 Hz over Figure 5.60) in the frequency of plate mode K (to 479 Hz). Additionally, beam mode J experiences a 1 Hz

frequency reduction to 501 Hz. These changes result in plate mode K and beam mode J being 6 Hz farther apart than in Figure 5.60. As a result, a 5 dB drop in acoustic pressure occurs near mode K. No further drop in the acoustic pressure is observed at beam mode J.

7 Grams Tuning Mass Plus 4000 Grams Coupling Mass : The addition of 7 grams tuning mass plus 4000 grams coupling mass is shown in Figure 5.62. Here we see a 6 Hz reduction in frequency for beam mode J (to 495 Hz), and a 3 Hz increase in frequency for plate mode K (to 482 Hz). As a result of these changes, plate mode K and beam mode J are now 8 Hz closer together than shown in Figure 5.61. The acoustic pressure near mode J increases about 4 dB. The acoustic pressure near mode K, however, does not increase. The likely reason for this is that at 482 Hz, mode K now appears centered over an anti-resonance of the acoustic water tank pressure response. This explanation is further supported by Figures 5.40 through 5.44 which also reveal a sharp pressure drop near 482 Hz.

In Figure 5.62 we see that the addition of tuning mass has increased the frequency of plate mode K. For beams 3 and 2, tuning mass resulted in decreased resonance frequencies for plate modes.

5.4.3 Beam 1 - Results in Air

Beam Spectra Overview

Figure 5.63 shows the beam drive point acceleration spectrum in air for the conditions of 0, 3, and 7 grams tuning mass added to the free end of beam 1 (no coupling mass applied). Results very similar to those obtained for beam 3 and 2 are also observed for beam 1. The unperturbed condition shows resonance modes at 53, 499, and 1472 Hz. The airborne spectra

and waterborne spectra (Figure 5.53) are very similar, with the waterborne resonance frequencies being slightly higher. Additionally, consistent with previous results, the differences between airborne and waterborne spectra are more pronounced at the high frequency mode.

400-600 Hz Frequency Range

Figures 5.64 through 5.67 compare beam and plate acceleration spectra in water and in air as coupling and tuning mass is added. For beam 1 we see that airborne acceleration levels are slightly higher (on the order of 2 dB) than waterborne acceleration levels. For beams 3 and 2, airborne and waterborne acceleration levels were comparable. Consistent with what was observed for beams 3 and 2, the frequency separation between globally reacting modes J and K varies from the waterborne to airborne case. For example, in Figure 5.62 we see the separation in air is 21 Hz vice 13 Hz in water. Additionally, in Figure 5.65 through 5.67 we see that another plate mode (labeled mode L) appears closer to the beam mode in the airborne case than in the waterborne case.

Figures 5.65 and 5.67 clearly show an inflection point just to the right of the beam mode. This indicates the likely existence of a plate mode which went undetected during investigation of the waterborne data. For identification purposes, the inflection point has been labeled mode M in Figures 5.65 and 5.67.

5.4.4 Beam 1 - Summary

Similarities with Previous Results

a) Beam mode J and plate mode K appear to react as a global pair with regard to radiated sound. As these modes are separated, acoustic pressure decreases. As these modes are brought together, acoustic pressure increases. However, consistent to what was found for beam 2, the existence of plate mode K would go undetected based on beam drive point spectrum data alone.

b) Similar to results for beam 2, the beam mode (mode J) is only slightly affected by coupling mass (1 Hz reduction after 4000 grams coupling mass). As discussed previously for beam 2, the likely reason for this is that the plate is already appearing as an infinite impedance to the beam. As such, the addition of coupling mass has little or no effect on the beam mode frequency.

c) Consistence to what was observed for beams 3 and 2, waterborne and airborne spectra appear similar. Additionally, modes appear to respond to coupling and tuning masses in a similar manner for the two cases. However, the frequency spacing between globally acting modes can vary considerably between the two cases.

Differences from Previous Results

a) A major difference from previous results is the fact that mode K was not detectable in the beam spectrum even though it was within 8 dB of the beam acceleration. Additionally, it appears that a plate mode (mode M) very close in both amplitude and frequency to beam mode J went undetected in the plate spectrum during waterborne testing. These differences

from the results of testing beams 3 and 2 may be due to the fact that the plate acceleration levels are much lower when the shaker is mounted on beam 1 compared to beams 3 and 2 (see Table 5-1). As such, the plate modes are much weaker acting and, therefore, are harder to detect in both the beam and plate spectra.

b) For beam 1, the addition of tuning mass increased the frequency of plate mode K. Also, the addition of coupling mass decreased the frequency of beam mode J. These changes were opposite of the effects on plate and beam modes observed for beams 3 and 2. It appears that the effects of tuning and coupling masses on mode frequency will vary from mode to mode, and probably can not be generalized.

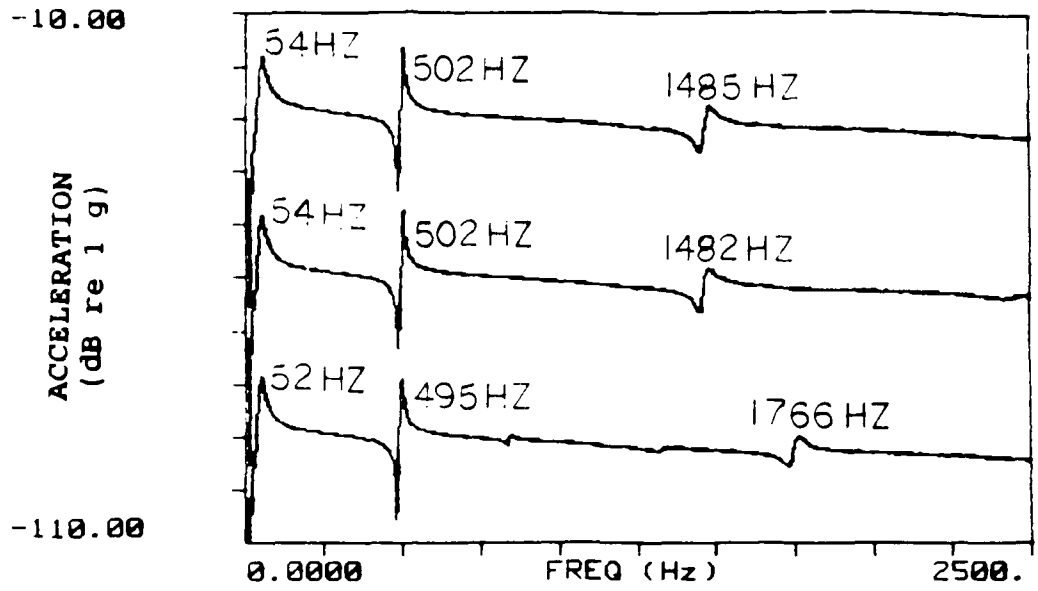

Figure 5.53 Beam 1 Waterborne. Beam drive point acceleration. From top: 0, 3, and 7 grams tuning mass.

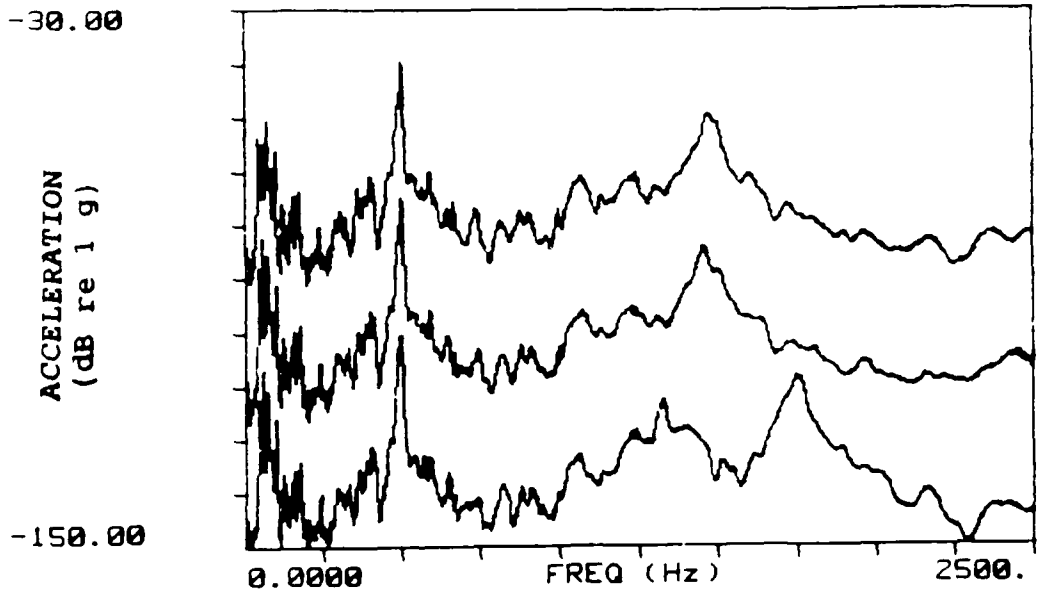

Figure 5.54 Beam 1 Waterborne. Mean plate acceleration. From top: 0, 3, and 7 grams tuning mass.

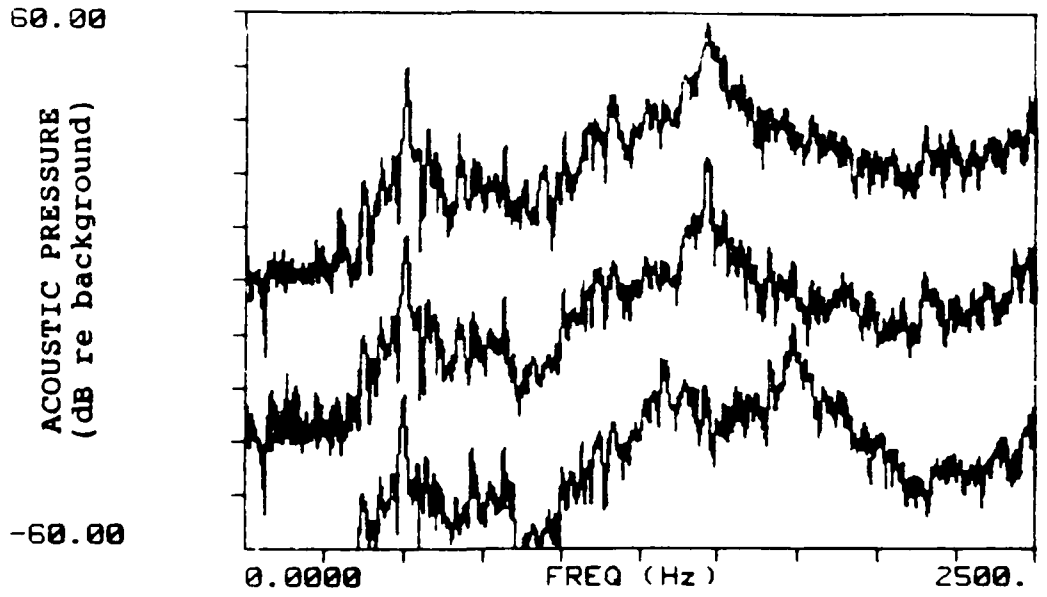

Figure 5.55 Beam 1 Waterborne. Mean acoustic pressure. From top: 0, 3, and 7 gram tuning mass.

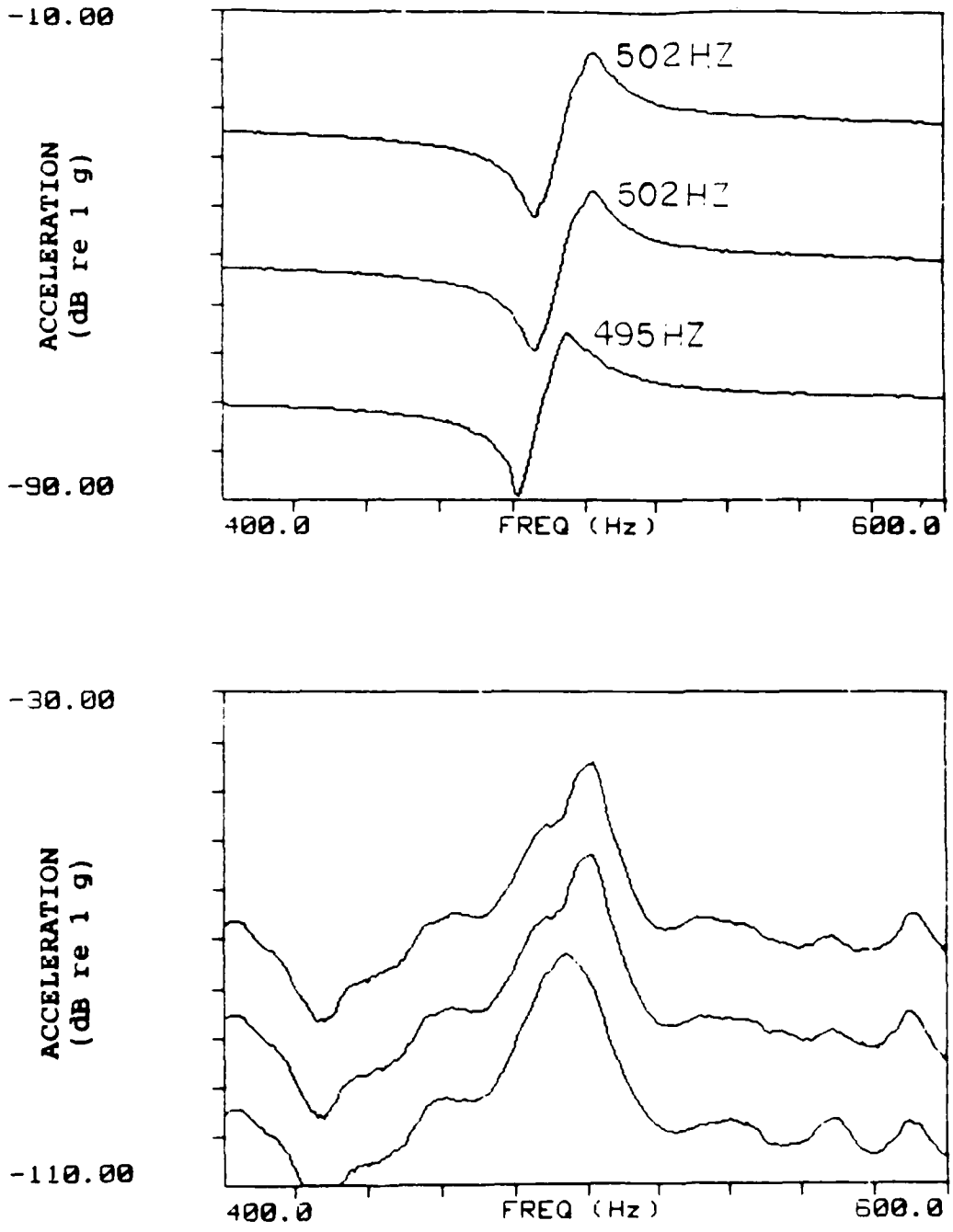

Figure 5.56 Beam 1 Waterborne. Beam drive point acceleration (top graph) and mean plate acceleration (bottom graph). From top in each graph: 0, 3, and 7 grams tuning mass.

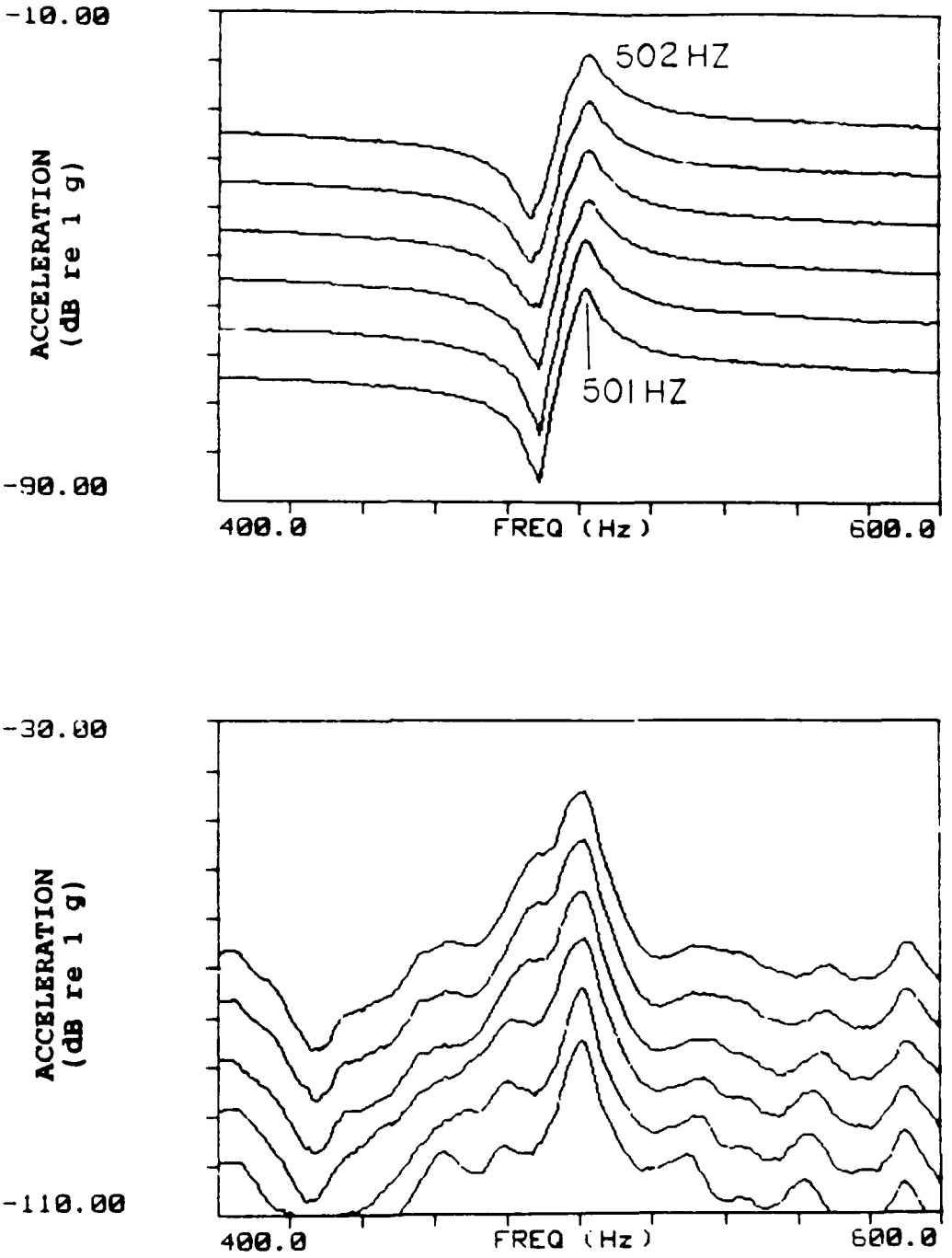

Figure 5.57 Beam 1 Waterborne. Beam drive point acceleration (top graph) and mean plate acceleration (bottom graph). From top in each graph: 0, 100, 400, 1200, 2000, and 4000 grams coupling mass.

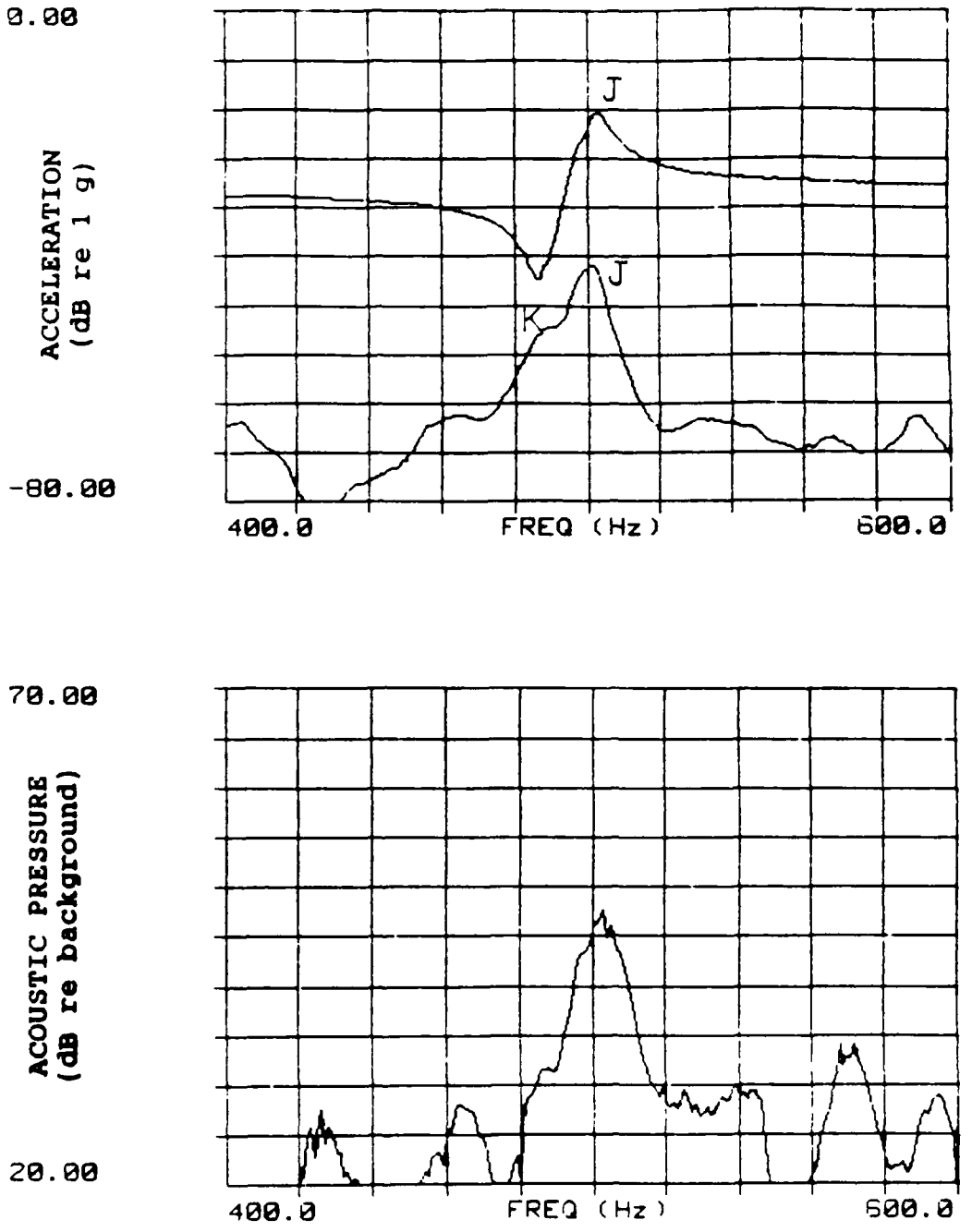

Figure 5.58 Beam 1 Waterborne. Unperturbed condition (no mass). From top: beam acceleration, mean plate acceleration, and mean acoustic pressure.

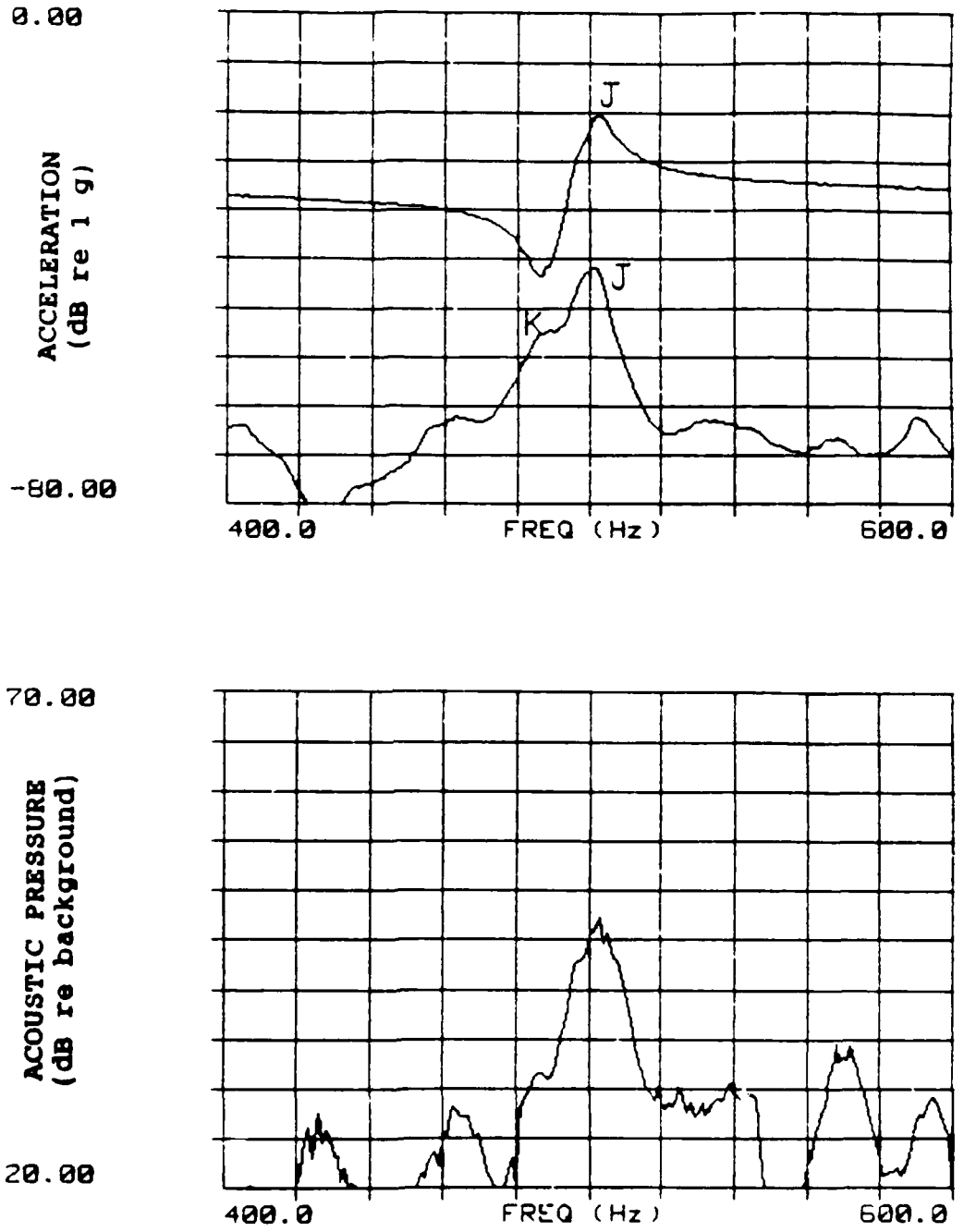

Figure 5.59 Beam 1 Waterborne. 100 grams coupling mass. From top: beam acceleration, mean plate acceleration, and mean acoustic pressure.

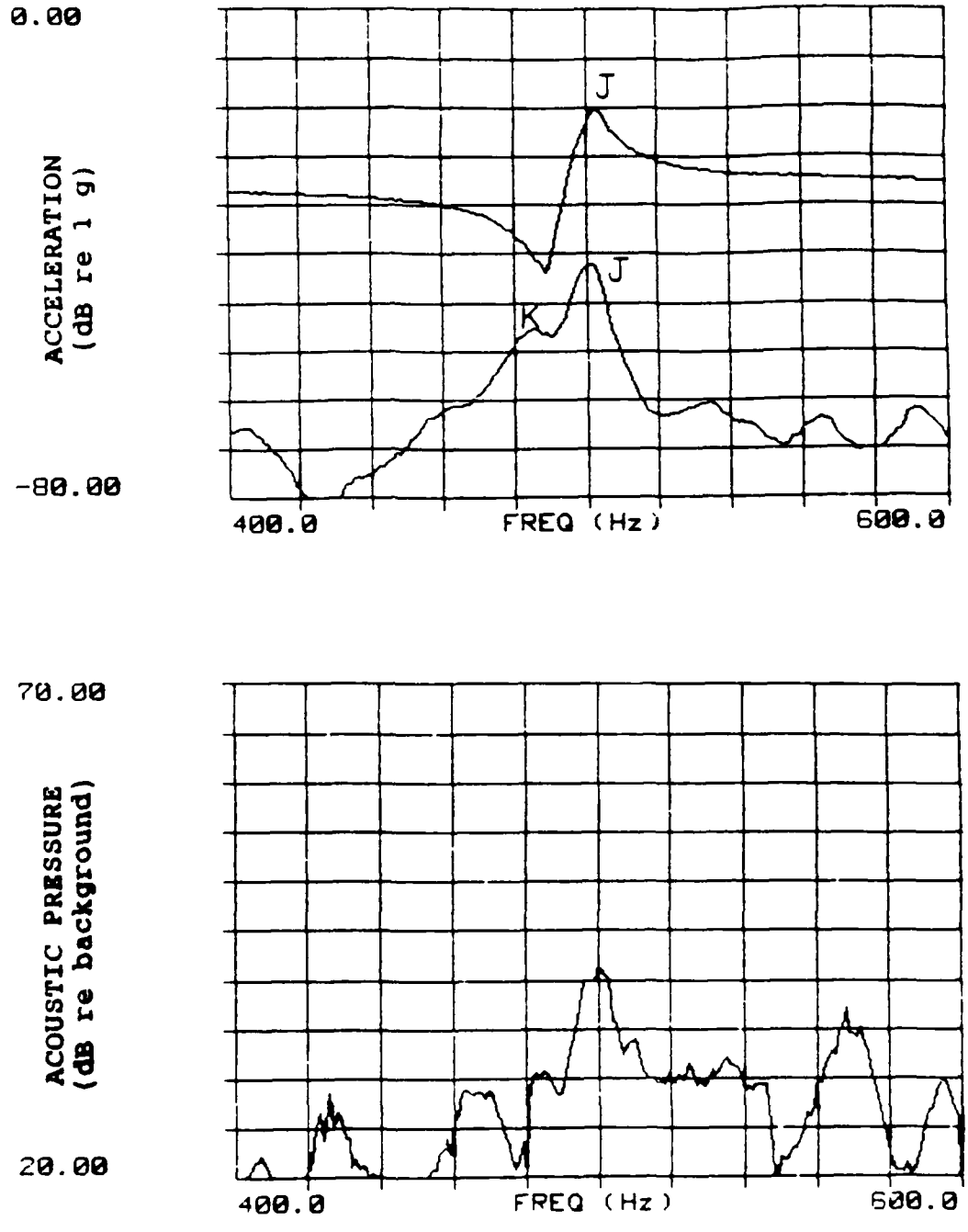

Figure 5.60 Beam 1 Waterborne. 800 grams coupling mass. From top: beam acceleration, mean plate acceleration, and mean acoustic pressure.

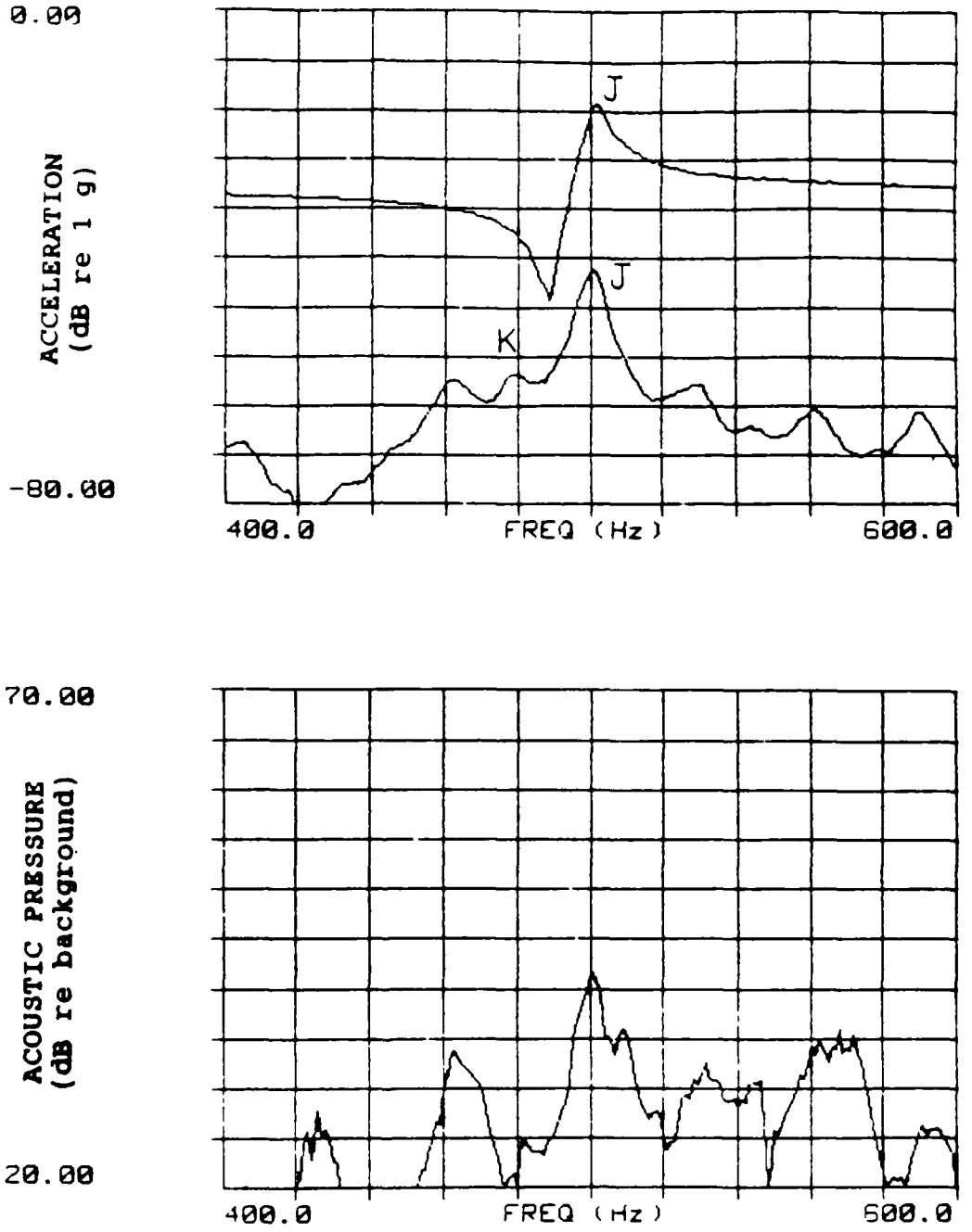

Figure 5.61 Beam 1 Waterborne. 4000 grams coupling mass. From top: beam acceleration, mean plate acceleration, and mean acoustic pressure.

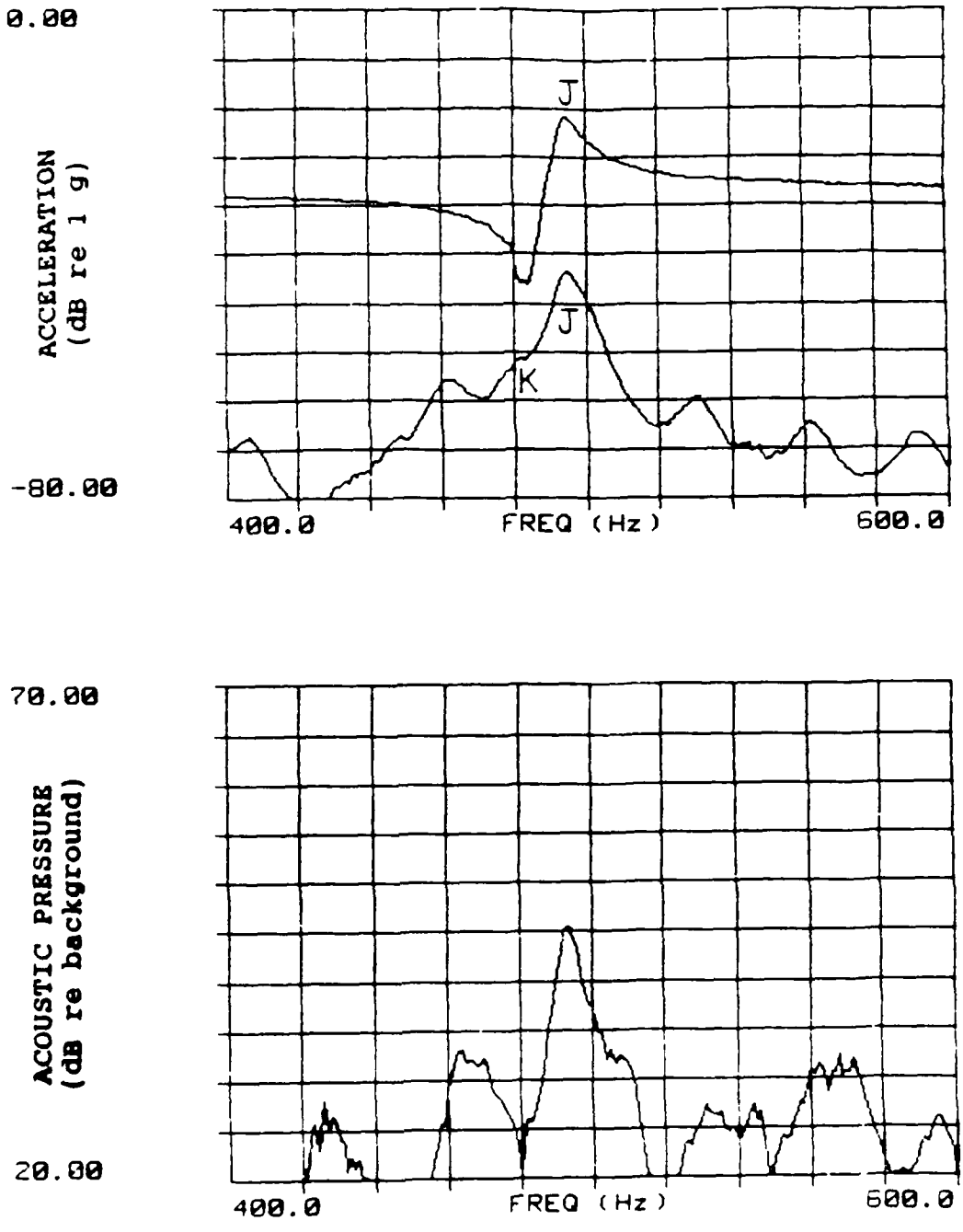

Figure 5.62 Beam 1 Waterborne. 7 grams tuning mass plus 4000 grams coupling mass. From top: beam acceleration, mean plate acceleration, and mean acoustic pressure.

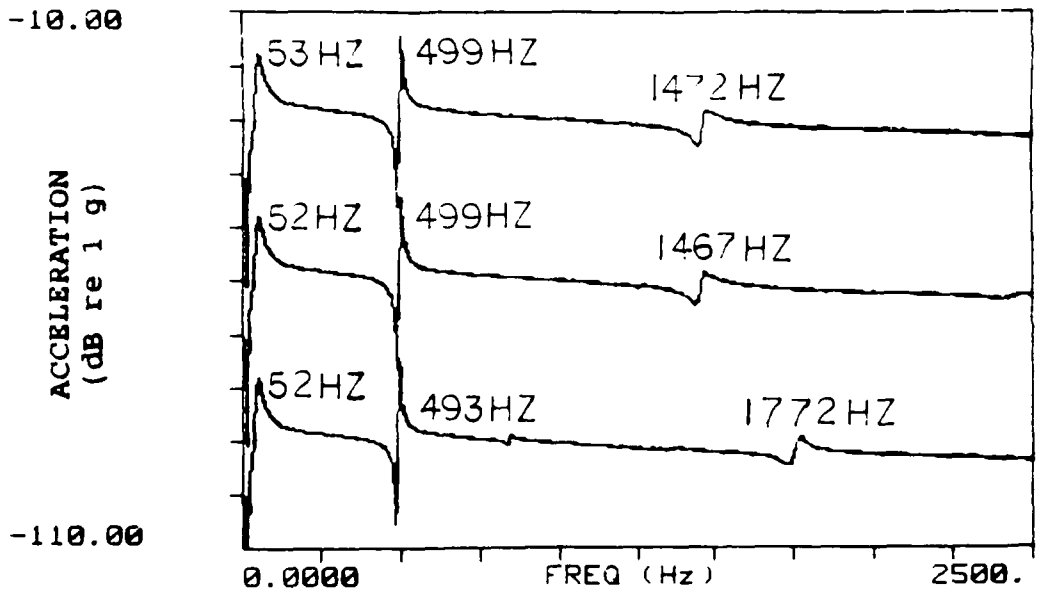

Figure 5.63 Beam 1 Airborne. Beam drive point acceleration. From top: 0, 3, and 7 grams tuning mass.

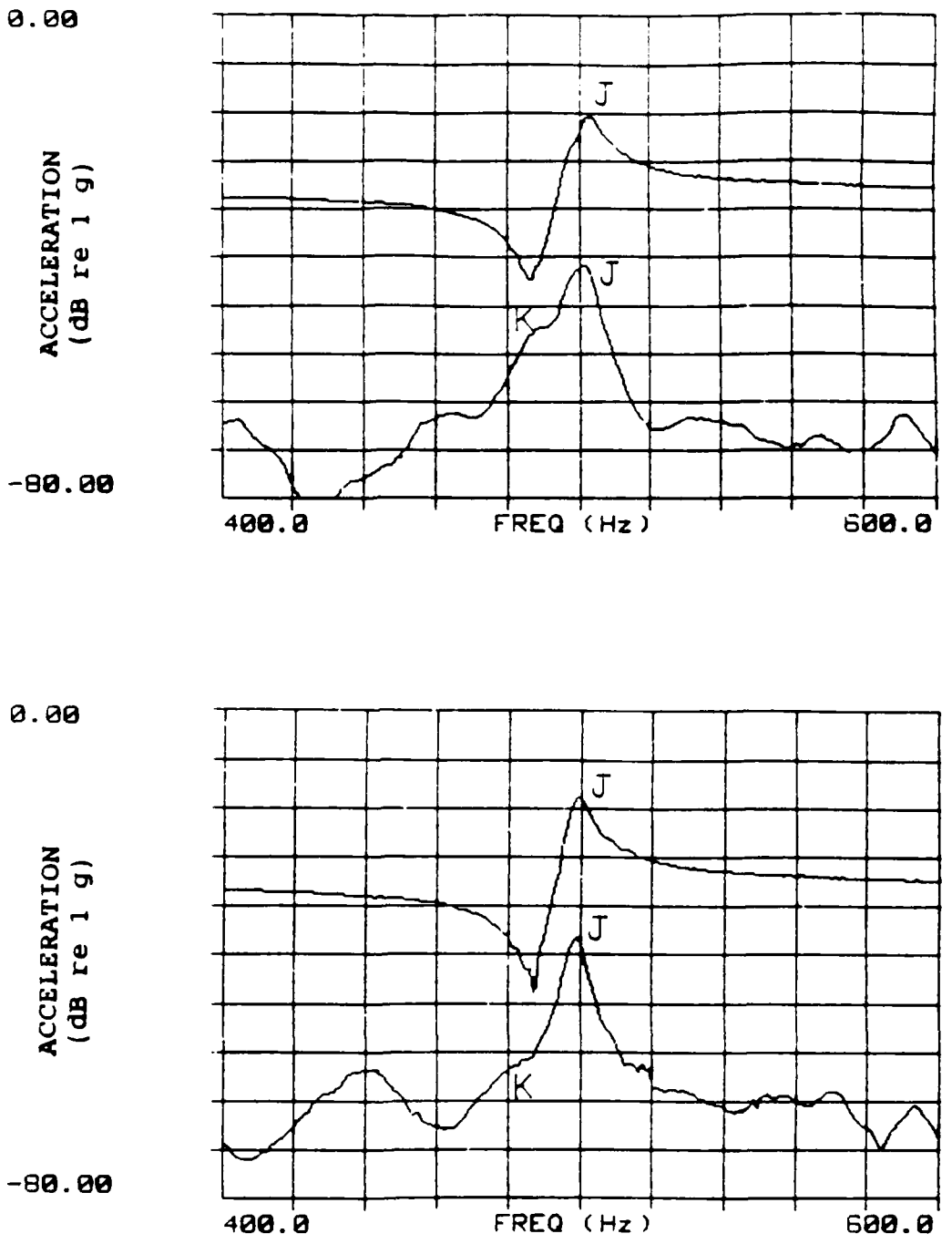

Figure 5.64 Beam 1 Waterborne (top graph) and Airborne (bottom graph). Unperturbed condition (no mass). From top in each graph: beam drive point acceleration, and mean plate acceleration.

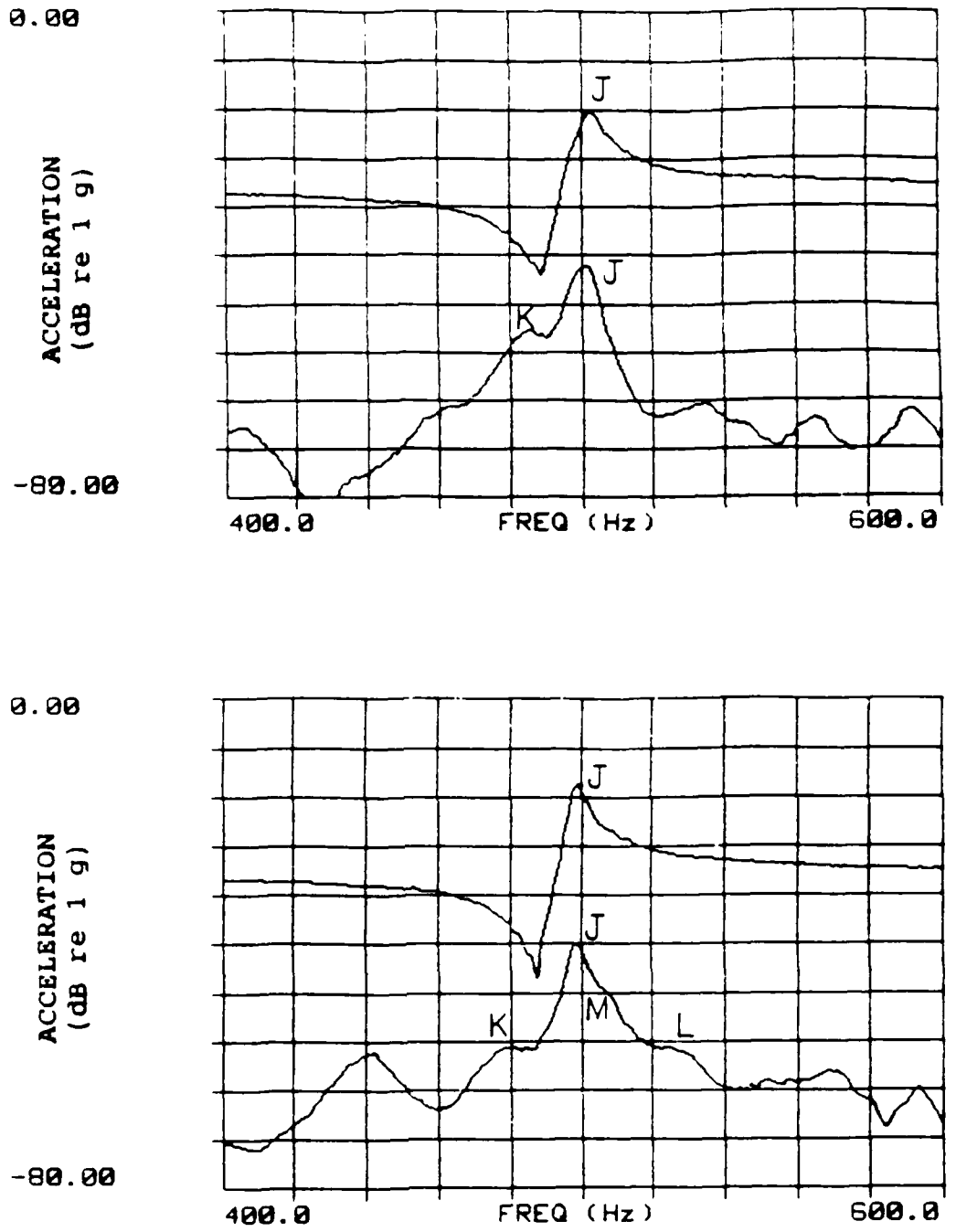

Figure 5.65 Beam 1 Waterborne (top graph) and Airborne (bottom graph). 800 grams coupling mass. From top in each graph: beam drive point acceleration, and mean plate acceleration.

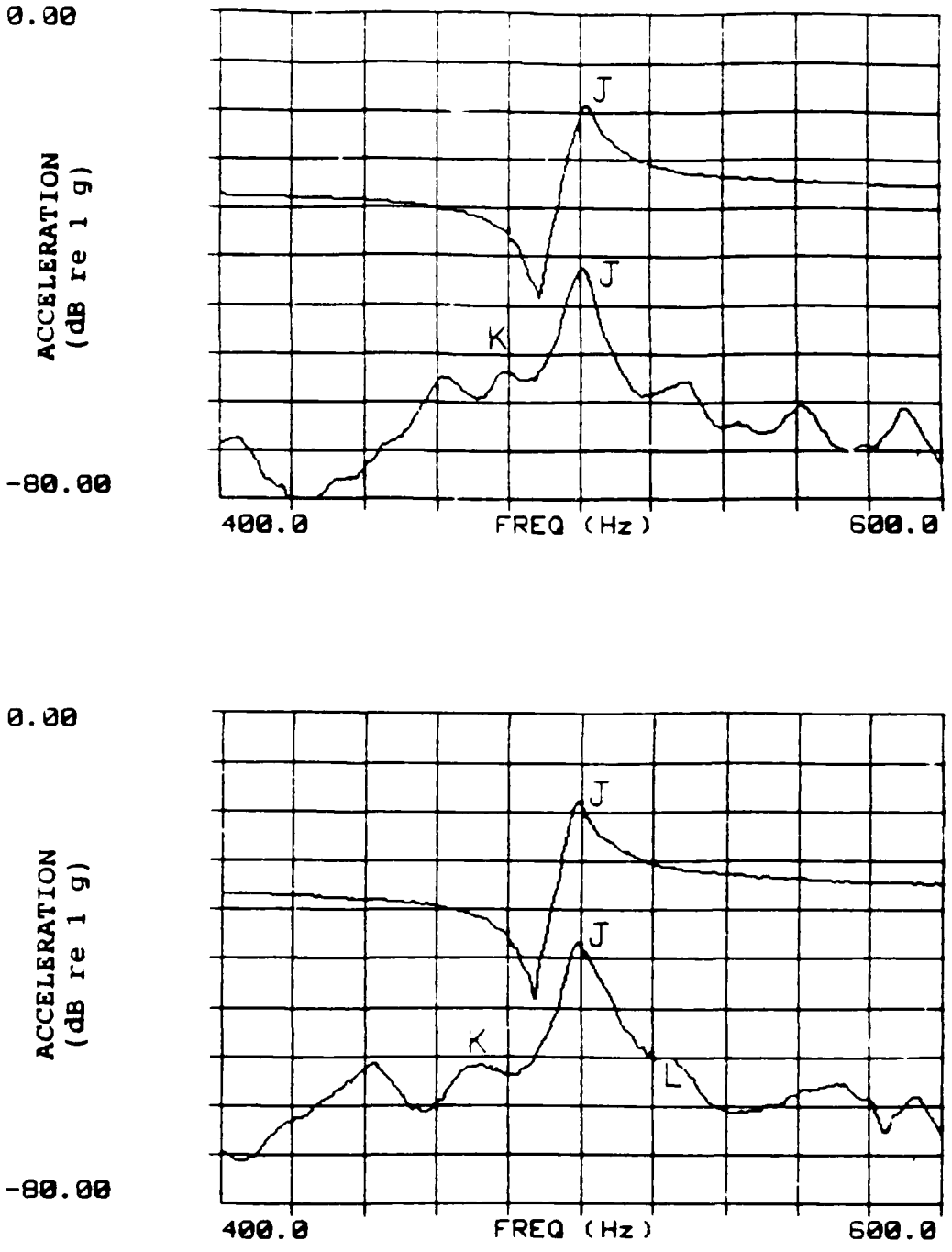

Figure 5.66 Beam 1 Waterborne (top graph) and Airborne (bottom graph). 4000 grams coupling mass. From top in each graph: beam drive point acceleration, and mean plate acceleration.

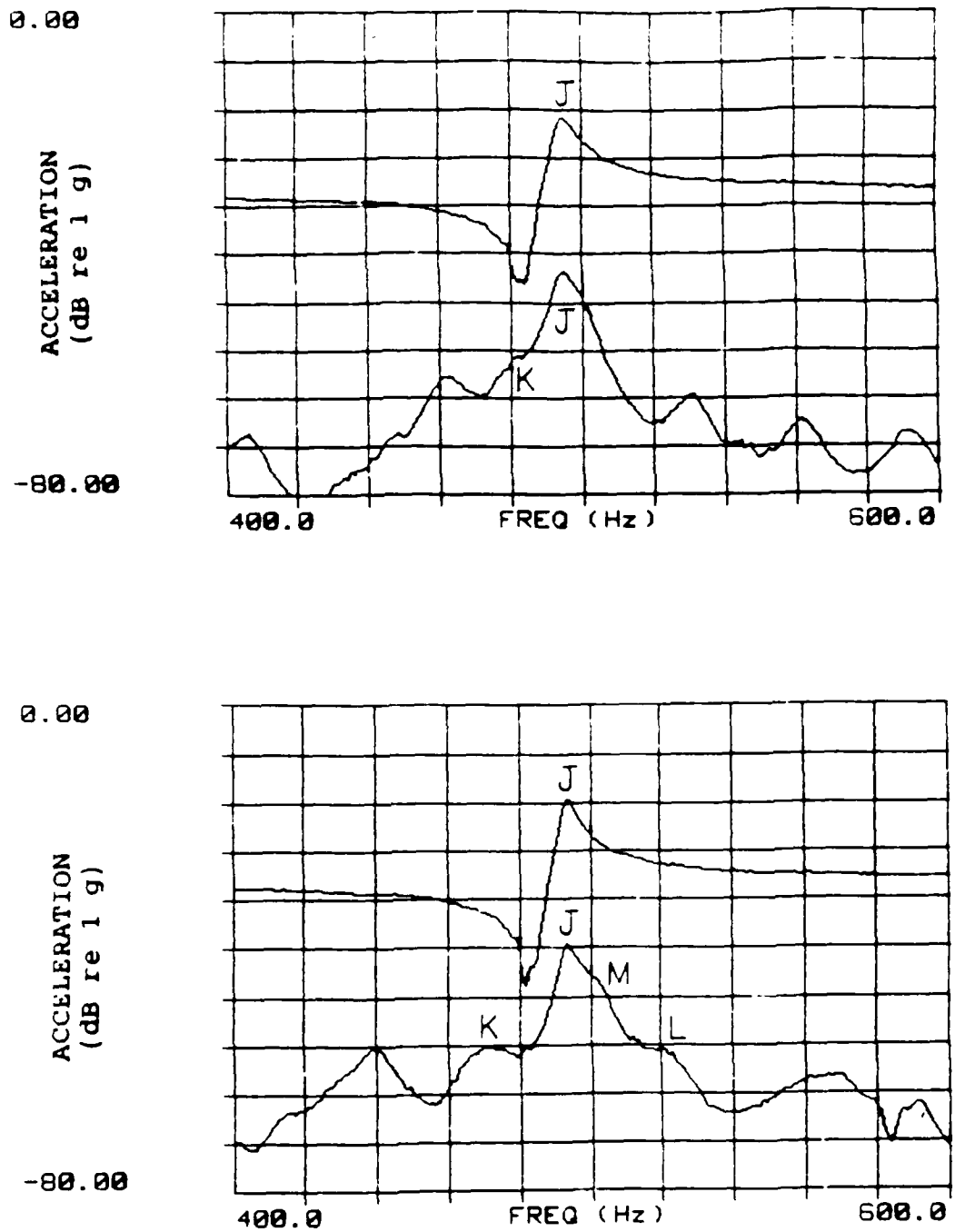

Figure 5.67 Beam 1 Waterborne (top graph) and Airborne (bottom graph). 7 grams tuning mass plus 4000 grams coupling mass. From top in each graph: beam drive point acceleration, and mean plate acceleration.

5.5 Beam 4 Results

Beams 1, 2, and 3 previously studied exhibited relatively "clean" beam drive point acceleration spectra. The beam modes were dominant and easy to detect. Plate modes which were present in the beam spectra were generally less in magnitude than the beam modes. Plate modes became more evident in the beam spectrum as the size of the beam increased. We will now see that for beam 4, plate modes are very evident in the beam drive point acceleration spectrum, making it more difficult to distinguish between beam and plate modes. Additionally, we will see that small amounts of coupling mass (on the order of 200-400 grams) will have pronounced effects on the beam and plate spectra.

Sections 5.5.1 through 5.5.3 below discuss in detail the results of testing the model in water and in air with the shaker mounted at the free end of beam 4. Section 5.5.4 summarizes the conclusions reached based on testing beam 4.

5.5.1 Beam 4 - Spectra Overview (Waterborne)

Figure 5.68 shows the drive point acceleration spectrum for beam 4 for the conditions of 0, 50, 100, and 200 grams tuning mass added to the free end of beam 4 (no coupling mass added). Figures 5.69 and 5.70 show the mean plate acceleration and mean water tank acoustic pressure spectra for the 0, 50, 100, and 200 grams tuning mass conditions. The following comments pertain to Figures 5.68, 5.69, and 5.70:

a) The most notable difference from test results for the 3 smaller beams is the clear presence of numerous plate modes evident in the beam spectrum. From Table 4-1, at 500 Hz

the average frequency separation ($\overline{\delta f}$) between beam modes is expected to be roughly 1170 Hz. Therefore, in Figure 5.68 one beam mode is likely near the peak around 100 Hz, and another beam mode is likely one of the peaks in the range 1000-1200 Hz.

b) Starting with the addition of 100 grams tuning mass (19 percent of beam mass), the beam spectrum becomes "distorted" near 2000 Hz. It appears that an anti-resonance from a mode above 2500 Hz is being shifted to the left as additional tuning mass is added.

c) The mean plate acceleration spectra shown in Figure 5.69 do not show a clear dominant peak in the frequency range 1000-1200 Hz. The acoustic pressure spectra shown in Figure 5.70, however, do show a dominant peak in this range.

Based on the above, it is not obvious which modes are plate modes and which are beam modes. Since the modes below 400 Hz are below the reverberant frequency range of the water tank, the discussion that follows will only concern the higher frequency modes. We will now investigate the frequency range 900-1300 Hz and apply tuning and coupling masses to identify and alter the plate and beam modes and determine if any global pairs exist.

5.5.2 Beam 4 - 900-1300 Hz Range (Waterborne)

Beam and Plate Acceleration Spectra

Figure 5.71 provides a close-up view of the beam drive point acceleration and mean plate acceleration spectra showing the effects of 50, 100, and 200 grams tuning mass. The addition of tuning mass noticeably perturbs both the beam and plate spectra, with 200 grams tuning mass causing gross changes.

Figure 5.72 shows the effect of adding coupling mass amounts of 100, 200, 400, 600, and 800 grams to the base of beam 4. Again, we see noticeable changes in both the beam and plate spectra as coupling mass is added. Here we see amplitude changes after 200 and 400 grams coupling mass is applied. Beams 1, 2, and 3 did not experience similar amplitude changes after addition of such relatively small amounts of coupling mass. After 800 grams coupling mass is applied, the spectrum appears grossly distorted compared to the unperturbed condition.

Figures 5.71 and 5.72 show that the addition of tuning and coupling mass affects many modes in both the beam and plate spectra. We will now closely study the effect of such mass additions on the frequency and amplitude of each mode and the radiated sound pressure.

Beam, Plate and Pressure Spectra

Figures 5.73 through 5.77 show the beam drive point acceleration spectrum, the mean plate acceleration spectrum, and the mean water tank acoustic pressure spectrum for the conditions ranging from the unperturbed to 100 grams tuning mass plus 1000 grams coupling mass.

Unperturbed Condition : Figure 5.73 shows that the acoustic pressure peaks near 1140 Hz. Near this pressure peak, the beam spectrum reaches a maximum with a wide bandwidth that appears to consist of two modes (labeled modes N and O). Since the pressure peaks in this range, we will focus on modes N and O and adjacent modes P and Q. These four modes span roughly 100 Hz.

Comparison of the levels observed in Figure 5.73 with those listed in Table 5-1 for beams 1, 2, and 3 reveals that the peak beam and plate acceleration levels for beam 4 (-28 dB and -45 dB respectively) are much lower than those for beams 1, 2, and 3. However, the 63 dB peak acoustic pressure level for beam 4 is much higher than peak pressure levels for beam 1 (48 dB), beam 2 (55 dB), and beam 3 (47 dB). Here again, we see that acoustic pressure levels can not be predicted based on beam or plate acceleration levels.

To identify the beam mode, we will now apply increasing tuning mass (with no coupling mass applied) to determine which mode is most affected.

50 Grams Tuning Mass : Figure 5.74 shows the effect of adding 50 grams tuning mass. Mode N now appears distinct at 1126 Hz in both the beam and plate spectra and has been reduced in amplitude about 2 dB. Mode O now appears as an inflection point to the right of mode N and has also been reduced in amplitude. The acoustic pressure near modes N and O has been reduced by about 2 dB. Mode P experiences a small frequency and amplitude increase. Mode Q experiences a 3 dB amplitude decrease, but no frequency change. The predominant change in Figure 5.74 as compared to Figure 5.73 is the shape and amplitude changes at modes N and O.

100 Grams Tuning Mass : Figure 5.75 shows the effect of adding 100 grams tuning mass. Here we see a 3 Hz frequency reduction and a roughly 3 dB amplitude reduction at mode N in both the beam and plate spectra. Mode O still appears as an inflection point in the beam spectrum and its amplitude has been reduced again by at least 4 dB (difficult to quantify since the mode is not distinct). The acoustic pressure near modes N and O again decreases by about 5 dB. Mode P experiences practically no change in frequency or amplitude. Mode Q experiences no change in frequency and a 5 dB amplitude reduction.

Comparison of Figure 5.75 with Figure 5.73 (unperturbed condition) shows practically no frequency or acceleration amplitude changes at mode P in response to 100 grams tuning mass. The acoustic pressure at mode P changes very little as well. Mode Q shows no frequency change, but does show a decreased amplitude. This is most likely due to the overall amplitude reduction to the right of mode N as tuning mass is added. Modes P and Q appear to be plate modes.

Modes N and O do undergo significant changes as tuning mass is added. Mode N experiences a 3 Hz frequency reduction and a 5 dB acceleration amplitude reduction. Based on this 3 Hz frequency reduction, it appears that mode N is a beam mode. Mode O went from being a high amplitude distinct mode, to an indistinguishable reduced amplitude mode. Based on this, it appears that mode O is a globally acting plate mode.

Although it is hard to quantify, modes N and O have been separated in frequency and amplitude (in the beam spectrum) by the addition of 100 grams tuning mass. As a result, the acoustic pressure near these modes has been reduced about 7 dB. We will now apply coupling mass to the 100 grams tuning mass condition to further perturb modes N and O and evaluate the effect on the acoustic pressure.

100 Grams Tuning Mass Plus 600 Grams Coupling Mass : In Figure 5.76 we see that the addition of 600 grams coupling mass results in mode O starting to become distinct and close in amplitude to beam mode N in the beam spectrum. This causes the acoustic pressure near these modes to increase slightly. Note that 600 grams coupling mass affects the amplitude of all modes visible in the 900-1300 Hz frequency range.

100 Grams Tuning Mass Plus 1000 Grams Coupling Mass : Figure 5.77 shows that the addition of 1000 grams coupling mass results in mode O being fully distinct and of comparable

amplitude to beam mode N in the beam spectrum. As a result, the pressure increases again by 2 dB at mode N and 4 dB near mode O. The acoustic pressure at these modes increases even though the acceleration levels at these modes decrease in both the beam and plate spectra. It appears we are seeing a strong coupling of these modes to the sound field. Note that globally acting modes N and O are more clearly visible in the beam spectrum than in the plate spectrum.

5.5.3 Beam 4 - Results in Air

Spectra Overview

Figures 5.78 and 5.79 present the beam drive point and mean plate acceleration spectra in air for the conditions of 0, 50, 100, and 200 grams tuning mass. Comparison of Figures 5.78 and 5.79 with Figures 5.68 and 5.69 for the waterborne case shows similar spectra response to the addition of tuning mass. However, for the airborne case more plate modes are evident in the beam spectra in the range 900-1300 Hz. From Table 4-5, the plate damping loss factor (η) is less for the airborne case than for the waterborne case in the 1000 Hz (η=0.017 vice 0.019) and 1250 Hz (η=0.012 vice 0.015) 1/3 octave bands. This reduced damping loss factor results in reduced modal overlap for the airborne case.

900-1300 Hz Frequency Range

Figures 5.80 through 5.83 compare beam and plate acceleration spectra in water and in air as tuning and coupling mass is applied. The top graph in each figure applies to the waterborne case; the bottom graph in each figure applies to the airborne case. Individual modes are labeled N, O, P, and Q, consistent to what was presented previously for the

waterborne case.

Unperturbed Condition : Figure 5.80 compares beam and plate spectra for the unperturbed (no mass) condition. Here we see that modes are much farther apart in the airborne case than in the waterborne case. For example, globally acting beam mode N and plate mode O are roughly 44 Hz apart in the airborne case and roughly 12 Hz apart in the waterborne case. Additionally, the effect of fluid loading results in both amplitude and frequency changes. Note that previously identified plate modes O and Q both experience a 4 dB amplitude reduction when the model is placed in water. Beam mode N experiences practically no amplitude change (as would be expected for a beam mode) but does undergo a frequency increase when waterborne (consistent with results for beams 1, 2, and 3).

100 Grams Tuning Mass : Figure 5.81 compares response to 100 grams tuning mass. For the airborne case, mode N experiences an 8 Hz frequency reduction and a small amplitude reduction. Mode O also experiences an 8 Hz frequency reduction and an 8 dB amplitude reduction in the airborne case. Mode P experiences practically no changes. In the airborne case, mode Q undergoes a 3 Hz frequency reduction and an amplitude reduction which appears to be part of an overall spectrum amplitude reduction near mode Q.

Comparison of Figures 5.80 and 5.81 shows that previously identified globally acting beam mode N and plate mode O undergo the most significant frequency and amplitude changes in response to tuning masses in both the airborne and waterborne cases.

100 Grams Tuning Mass Plus 600 Grams Coupling Mass : Figure 5.82 compares response to the addition of 600 grams coupling mass over the condition presented in Figure 5.81. Modes N and O respond to coupling mass in a similar manner in both the airborne and waterborne cases. In both cases, mode N is reduced in frequency and amplitude, and mode

O is reduced in amplitude. Additionally, these modes are comparable in amplitude (with mode N being slightly higher) in both the airborne and waterborne cases. Note also that these modes are more clearly defined in the beam spectra than in the plate spectra.

100 Grams Tuning Mass Plus 1000 Grams Coupling Mass : In Figure 5.83 we see again that modes N and O respond to coupling mass in a similar manner for the airborne and waterborne cases. Both cases show a reduction in the amplitude at mode N compared to Figure 5.83, and an increase in amplitude at mode O. Again, these modes are better defined in the beam spectra than in the plate spectra.

The fact that relative amplitude relationship between globally acting modes generally agree between the airborne and waterborne cases is important. We have consistently seen that globally acting modes appear to couple well to the sound field when they are close in both frequency and amplitude. Accordingly, it would be desirable to predict relative amplitude relationships between global modes based on airborne testing alone.

5.5.4 Beam 4 - Summary

Similarities with Previous Results

a) Beam mode N and plate mode O appear to react as a global pair with regard to radiated sound. We have seen acoustic pressure decreases on the order of 7 dB as these two modes are separated in frequency and amplitude. Acoustic pressure increases result as these modes are brought together.

b) The successive applications of tuning and coupling masses enabled classification of modes as plate, beam, and global. This was accomplished even though many plate modes of comparable amplitude to the beam mode were present to increase the difficulty of classifying the modes.

c) Waterborne and airborne beam and plate acceleration spectra appeared very similar. Even though fluid loading effects resulted in frequency shifts and modal overlap, corresponding modes in both the waterborne and airborne spectra could be identified. Additionally, the modes reacted to coupling and tuning masses in a similar manner in both the waterborne and airborne cases. However, the frequency separation between modes (practically globally acting modes N and O) varied greatly between the waterborne and airborne cases. However, relative amplitude levels between modes N and O appeared similar in both the waterborne and airborne cases.

Differences from Previous Results

a) Small amounts of coupling mass (200-400 grams) had a pronounced effect on the amplitude of the beam and plate acceleration spectra. As theorized in Chapter 4, since the beam impedance is comparable to that of the plate, additional impedance at the junction in the form of coupling mass has a big effect on both the beam and plate spectra. We have seen gross spectrum changes as a result of 800 grams tuning mass applied to the base of beam 4. Such changes were not observed with the addition of 4000 grams coupling mass at the base of beams 1, 2, or 3.

b) In addition to the increased sensitivity of all modes to coupling mass effects, the addition of tuning mass resulted in amplitude reductions for all modes and, in the airborne

case, resulted in a significant frequency reduction (e.g., 8 Hz after application of 100 grams tuning mass) for global plate mode O. For the three smaller beams, the addition of tuning mass resulted in small scale changes to plate modes.

c) Plate modes were as evident, if not more evident in some cases, in the beam drive point acceleration spectrum as in the mean plate acceleration spectrum. This enabled following and classifying modes strictly on the basis of the beam spectrum. The amplitude of the mean plate acceleration spectrum was roughly within 16 dB of the beam acceleration amplitude. This difference was much lower than that for beams 1, 2, and 3 (see Table 5-1). This difference in beam and plate acceleration levels appears to increase as the size of the beam decreases, thereby making it harder to detect plate modes in the beam spectrum.

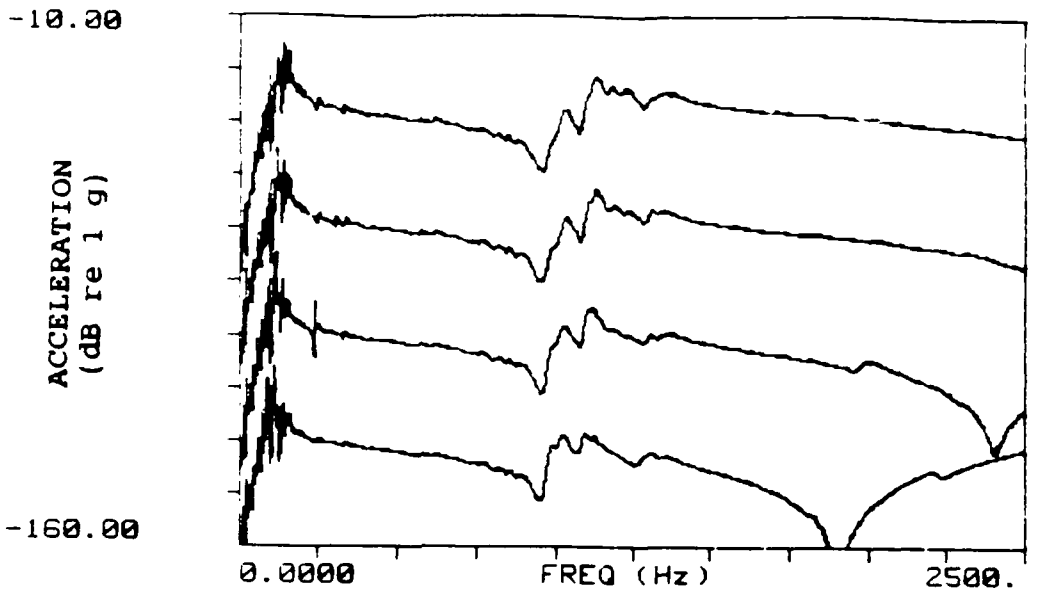

Figure 5.68 Beam 4 Waterborne. Beam drive point acceleration. From top: 0, 50, 100, and 200 grams tuning mass.

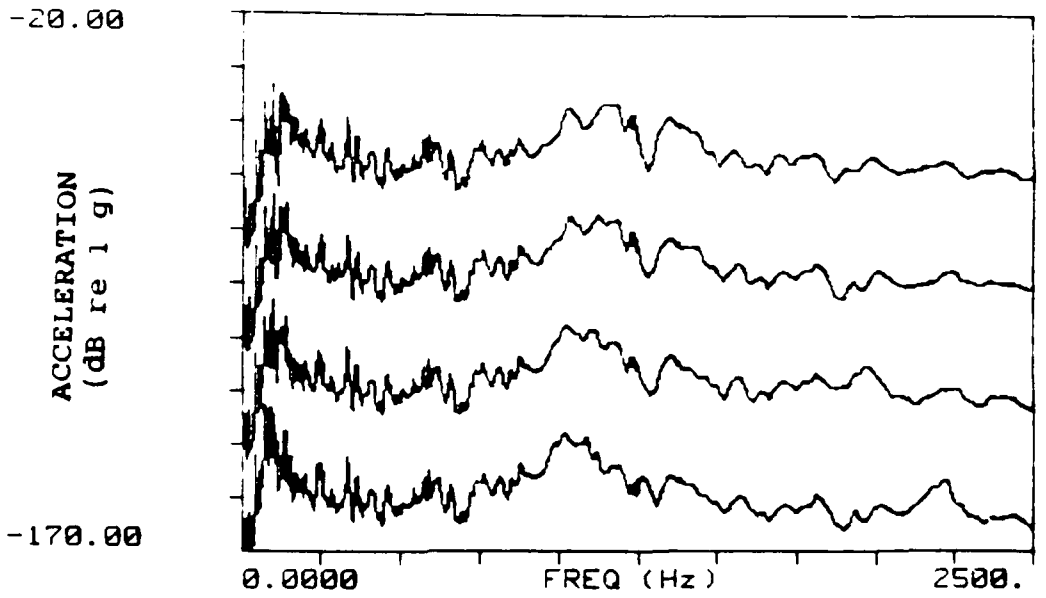

Figure 5.69 Beam 4 Waterborne. Mean plate acceleration. From top: 0, 50, 100, and 200 grams tuning mass.

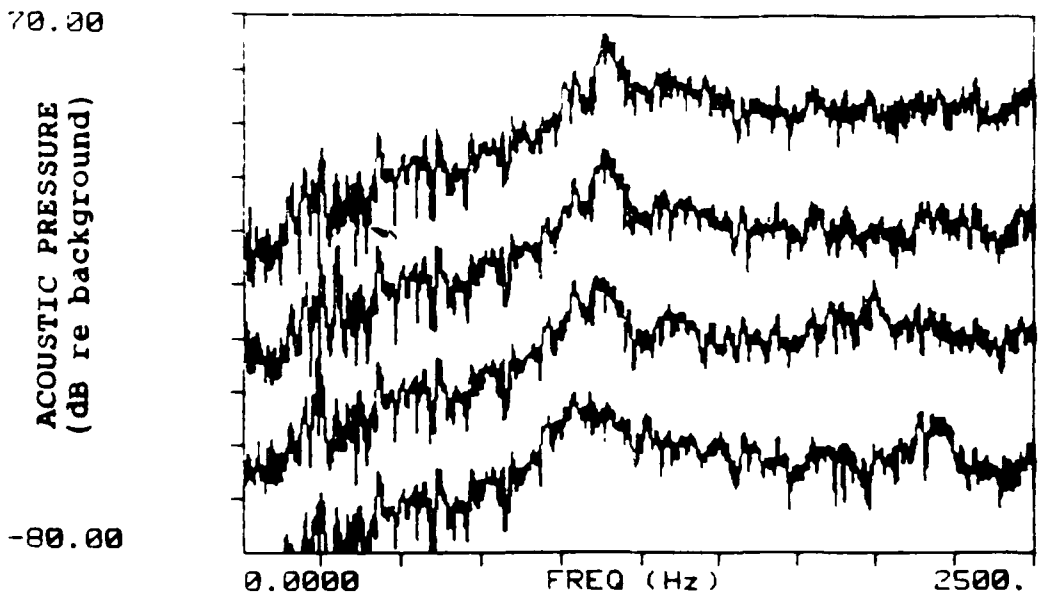

Figure 5.70 Beam 4 Waterborne. Mean acoustic pressure. From top: 0, 50, 100, and 200 gram tuning mass.

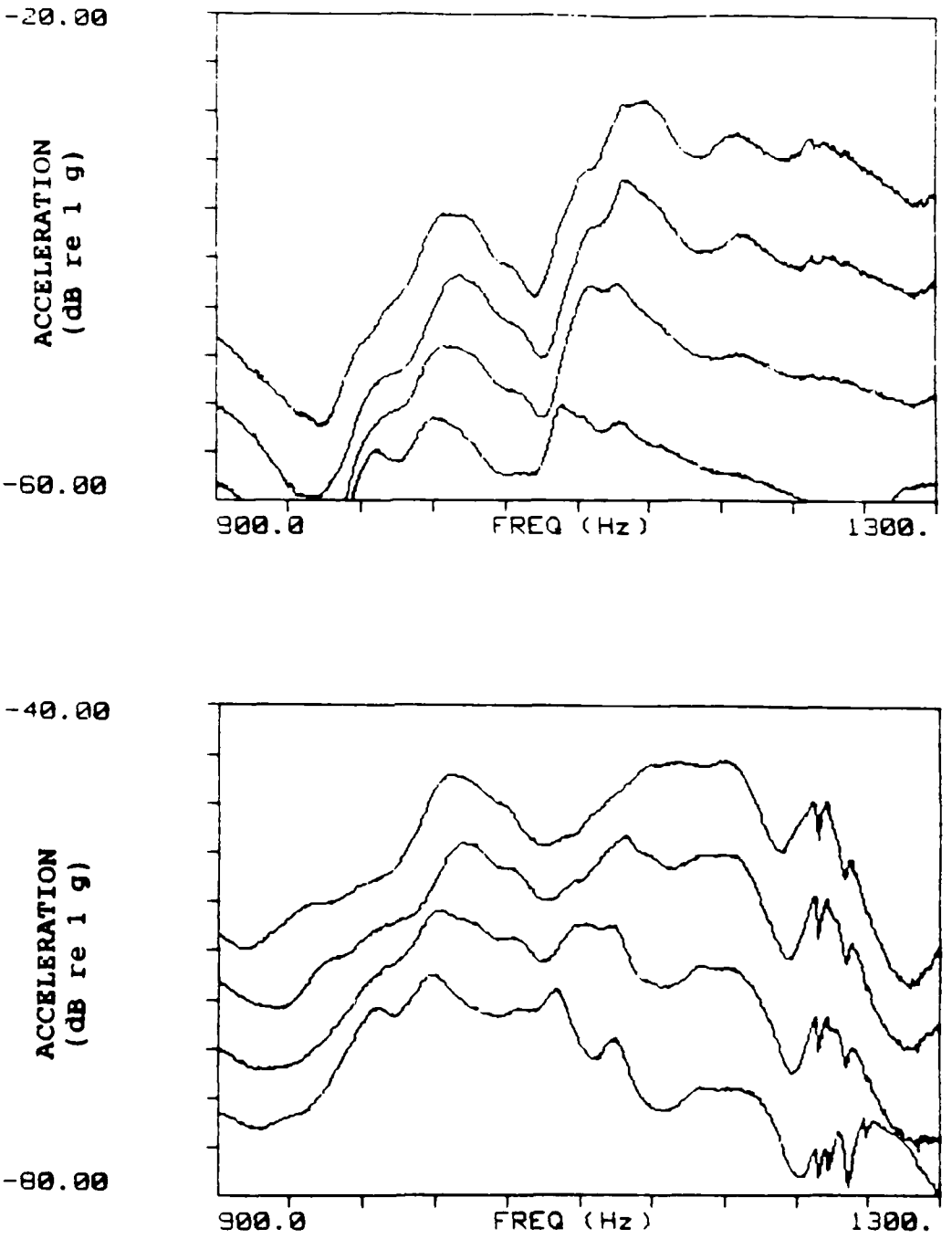

Figure 5.71 Beam 4 Waterborne. Beam drive point acceleration (top graph) and mean plate acceleration (bottom graph). From top in each graph: 0, 50, 100, and 200 grams tuning mass.

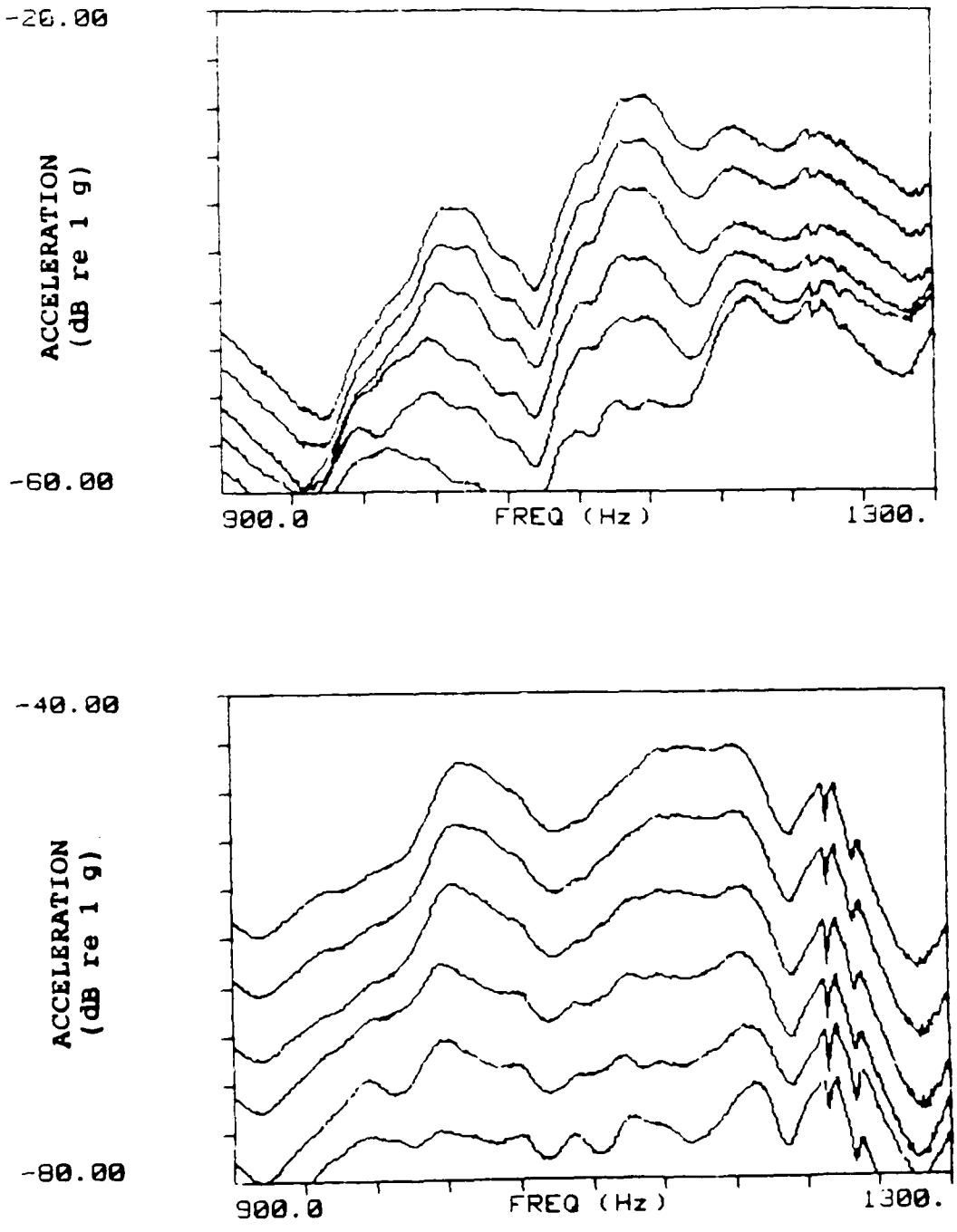

Figure 5.72 Beam 4 Waterborne. Beam drive point acccleration (top graph) and mean plate acceleration (bottom graph). From top in each graph: 0, 100, 200, 400, 600, and 800 grams coupling mass.

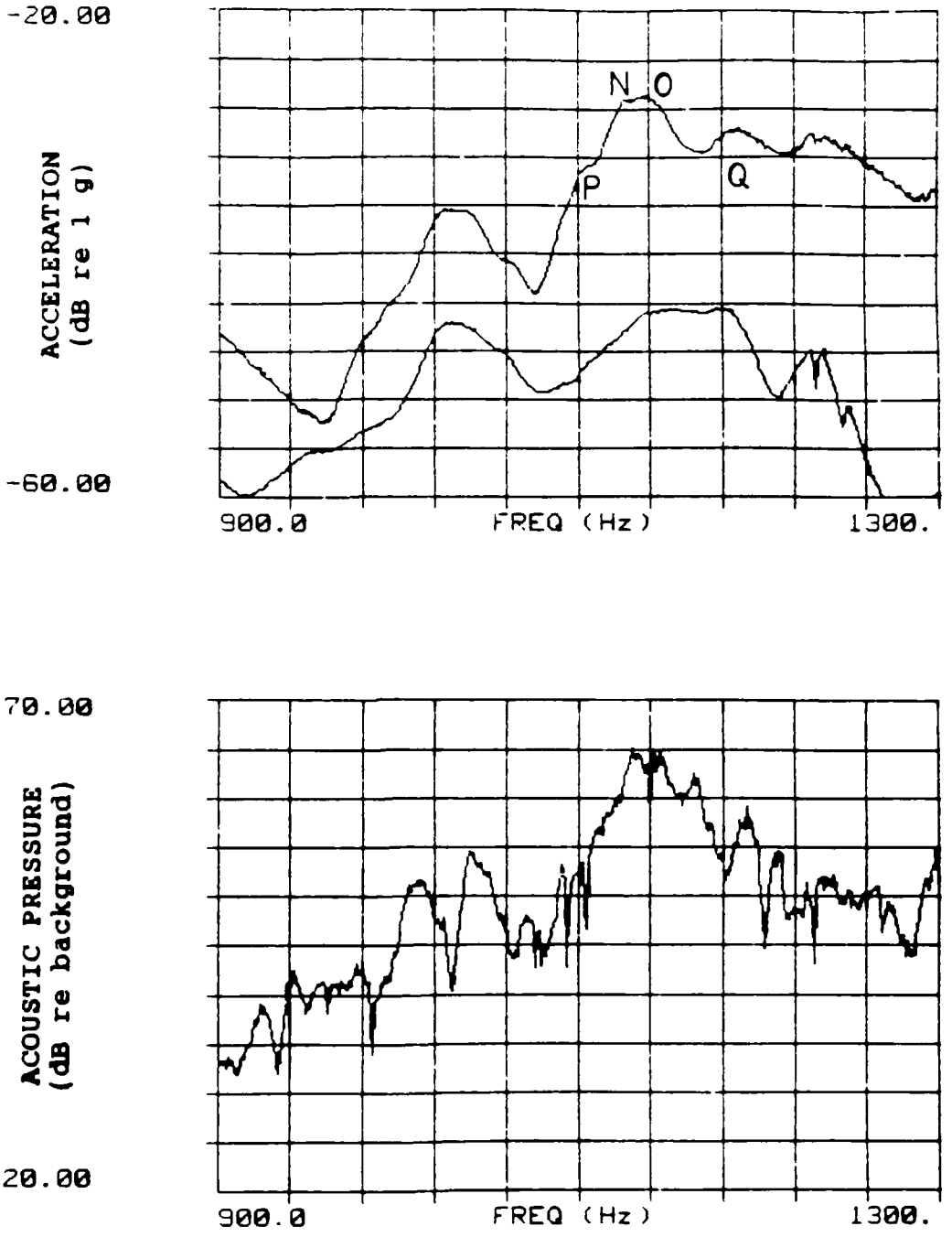

Figure 5.73 Beam 4 Waterborne. Unperturbed condition (no mass). From top: beam acceleration, mean plate acceleration, and mean acoustic pressure.

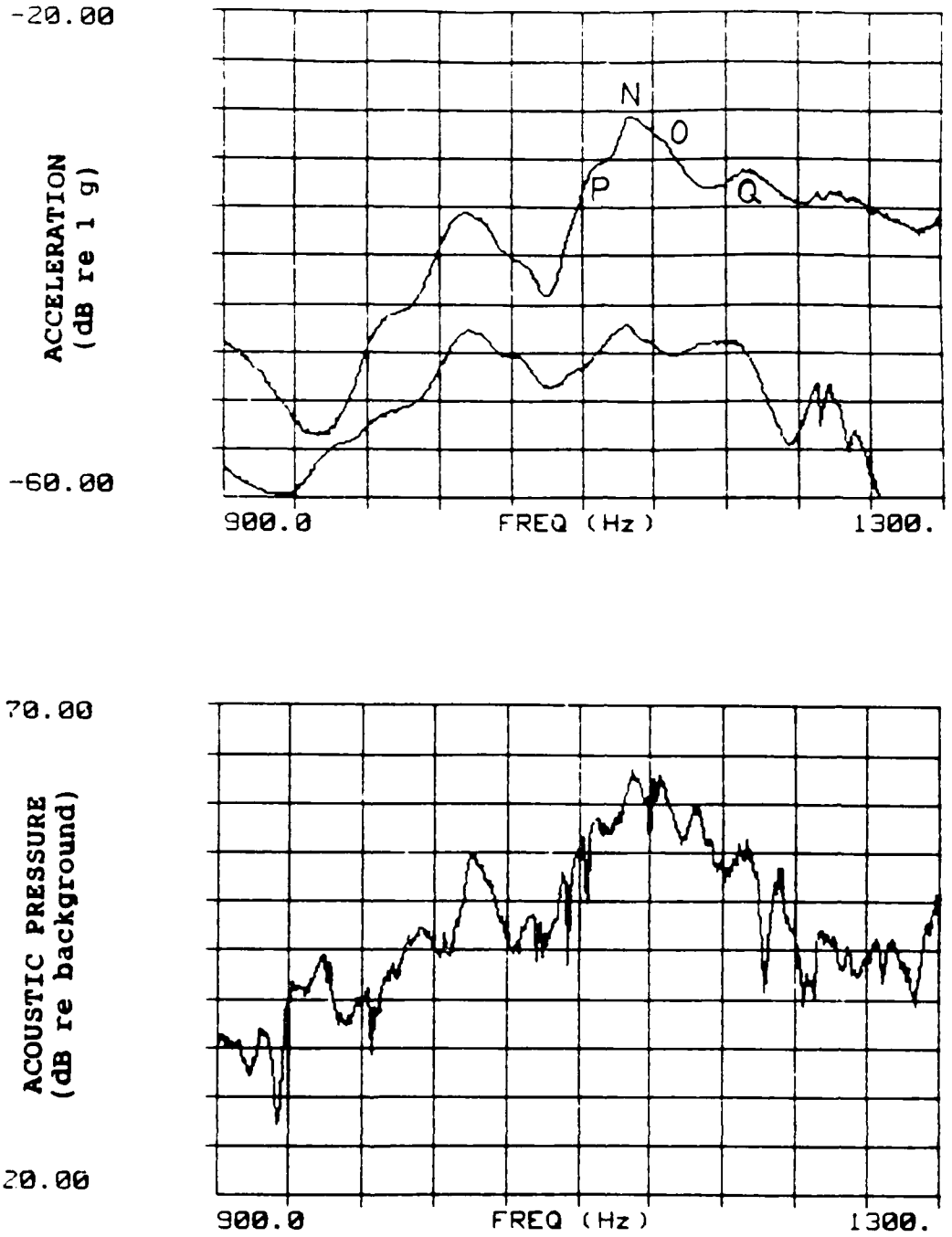

Figure 5.74 Beam 4 Waterborne. 50 grams tuning mass. From top: beam acceleration, mean plate acceleration, and mean acoustic pressure.

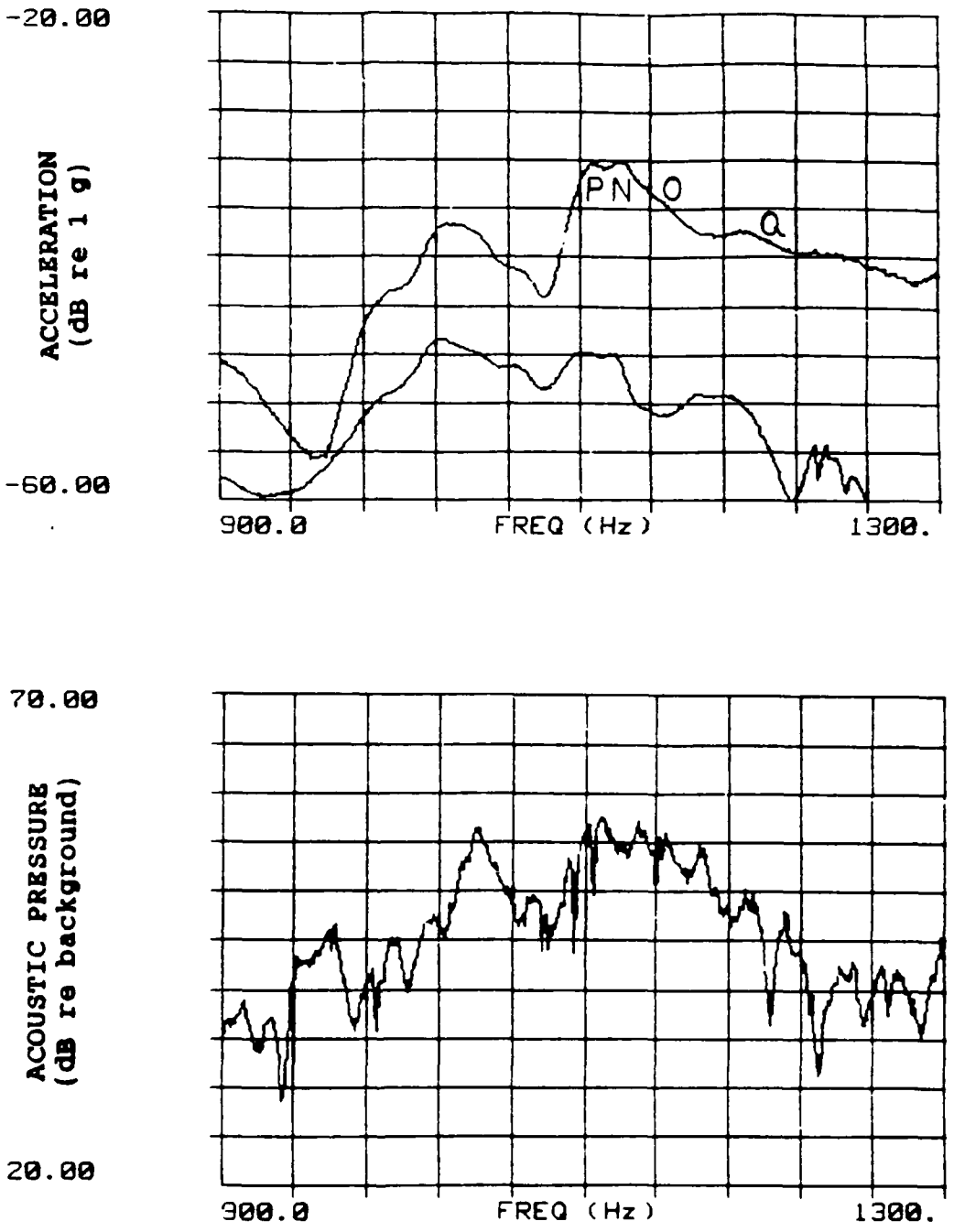

Figure 5.75 Beam 4 Waterborne. 100 grams tuning mass. From top: beam acceleration, mean plate acceleration, and mean acoustic pressure.

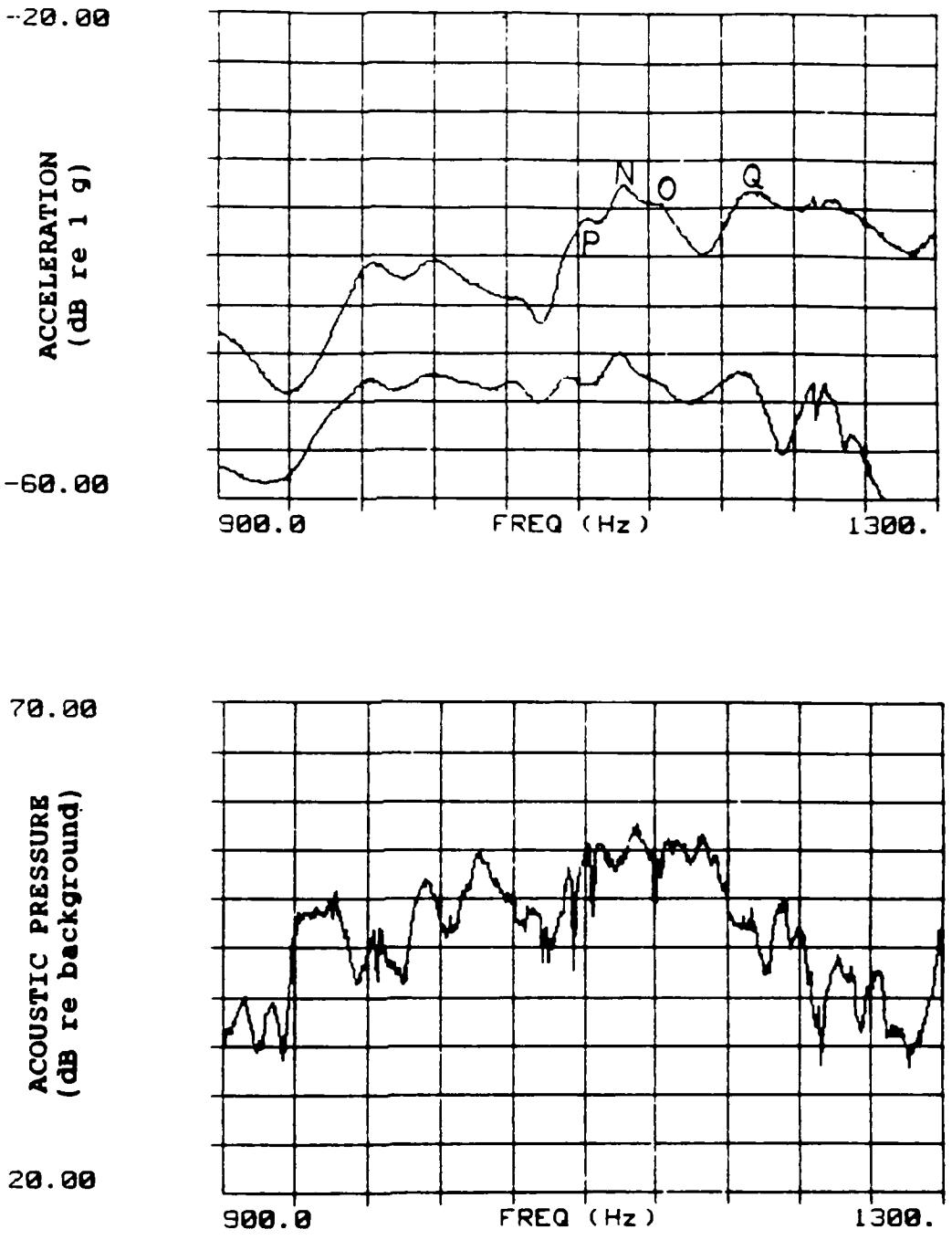

Figure 5.76 Beam 4 Waterborne. 100 grams tuning mass plus 600 grams coupling mass. From top: beam acceleration, mean plate acceleration, and mean acoustic pressure.

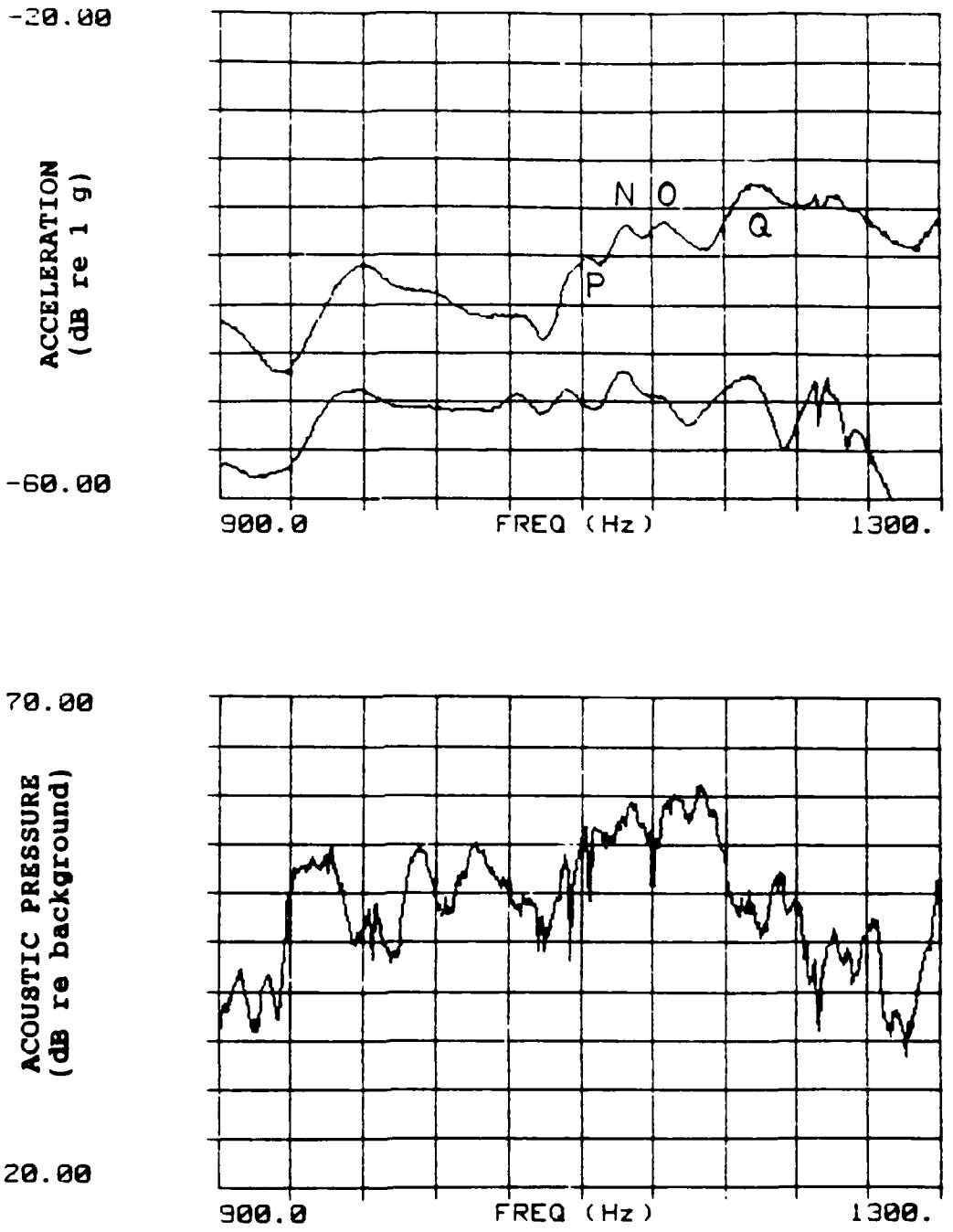

Figure 5.77 Beam 4 Waterborne. 100 grams tuning mass plus 1000 grams coupling mass. From top: beam acceleration, mean plate acceleration, and mean acoustic pressure.

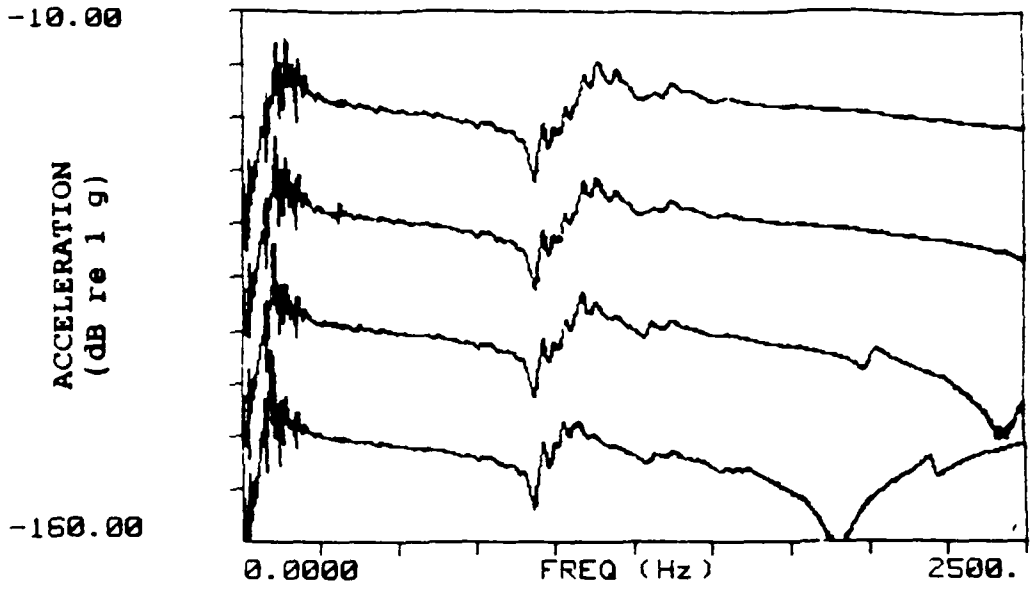

Figure 5.78 Beam 4 Airborne. Beam drive point acceleration. From top: 0, 50, 100, and 200 grams tuning mass.

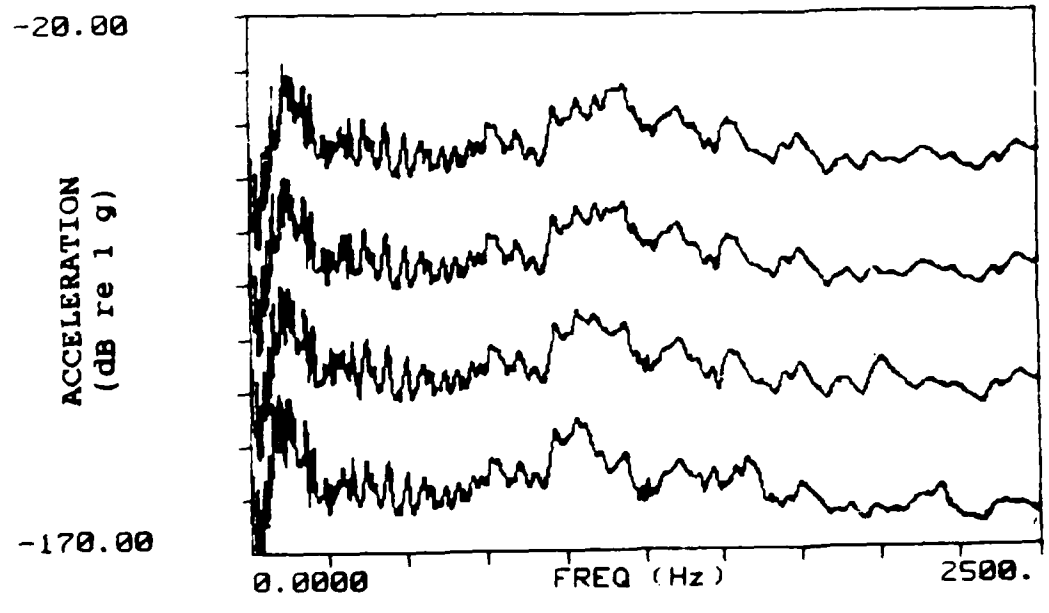

Figure 5.79 Beam 4 Airborne. Mean plate acceleration. From top: 0, 50, 100, and 200 grams tuning mass.

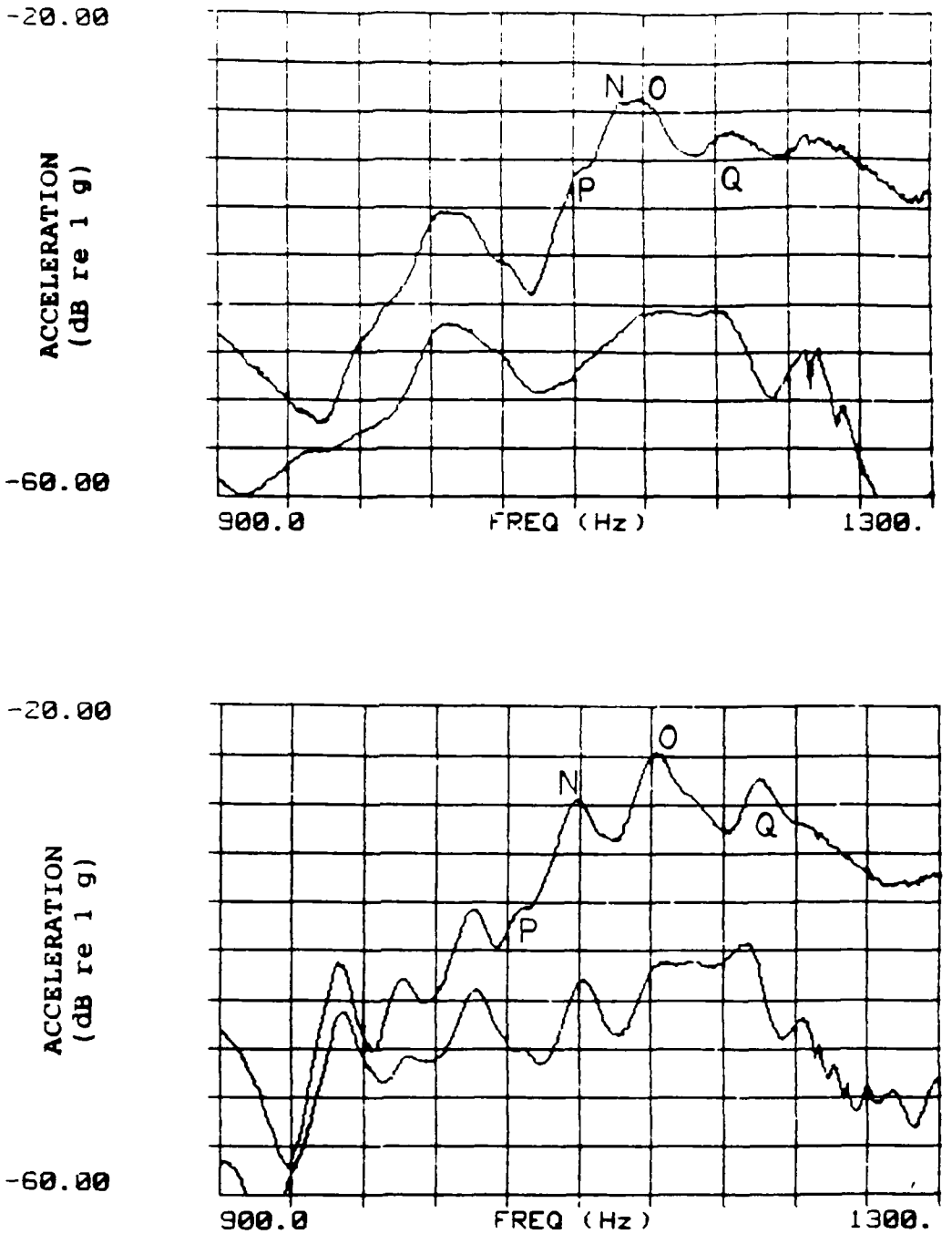

Figure 5.80 Beam 4 Waterborne (top graph) and Airborne (bottom graph). Unperturbed condition (no mass). From top in each graph: beam drive point acceleration, and mean plate acceleration.

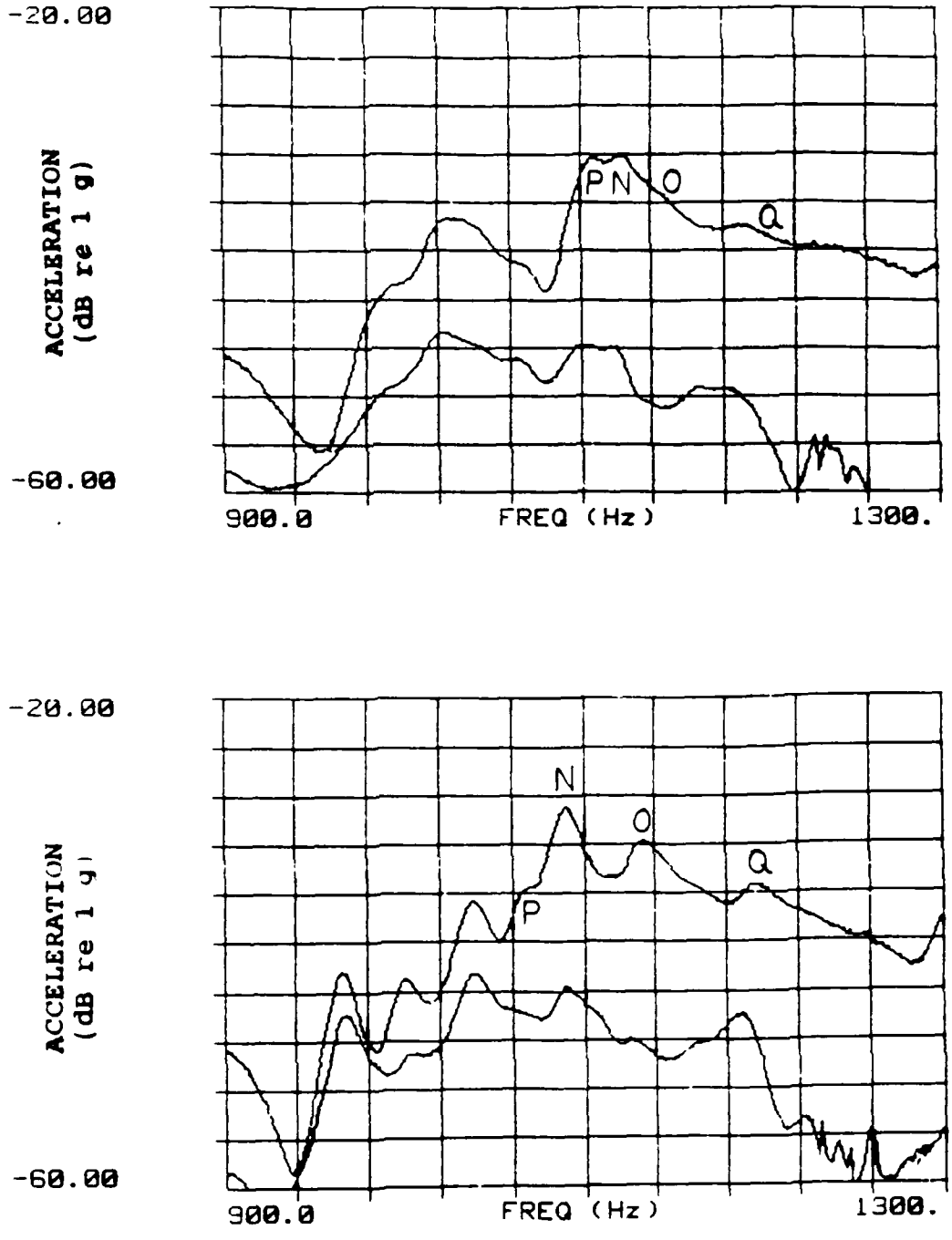

Figure 5.81 Beam 4 Waterborne (top graph) and Airborne (bottom graph). 100 grams tuning mass. From top in each graph: beam drive point acceleration, and mean plate acceleration.

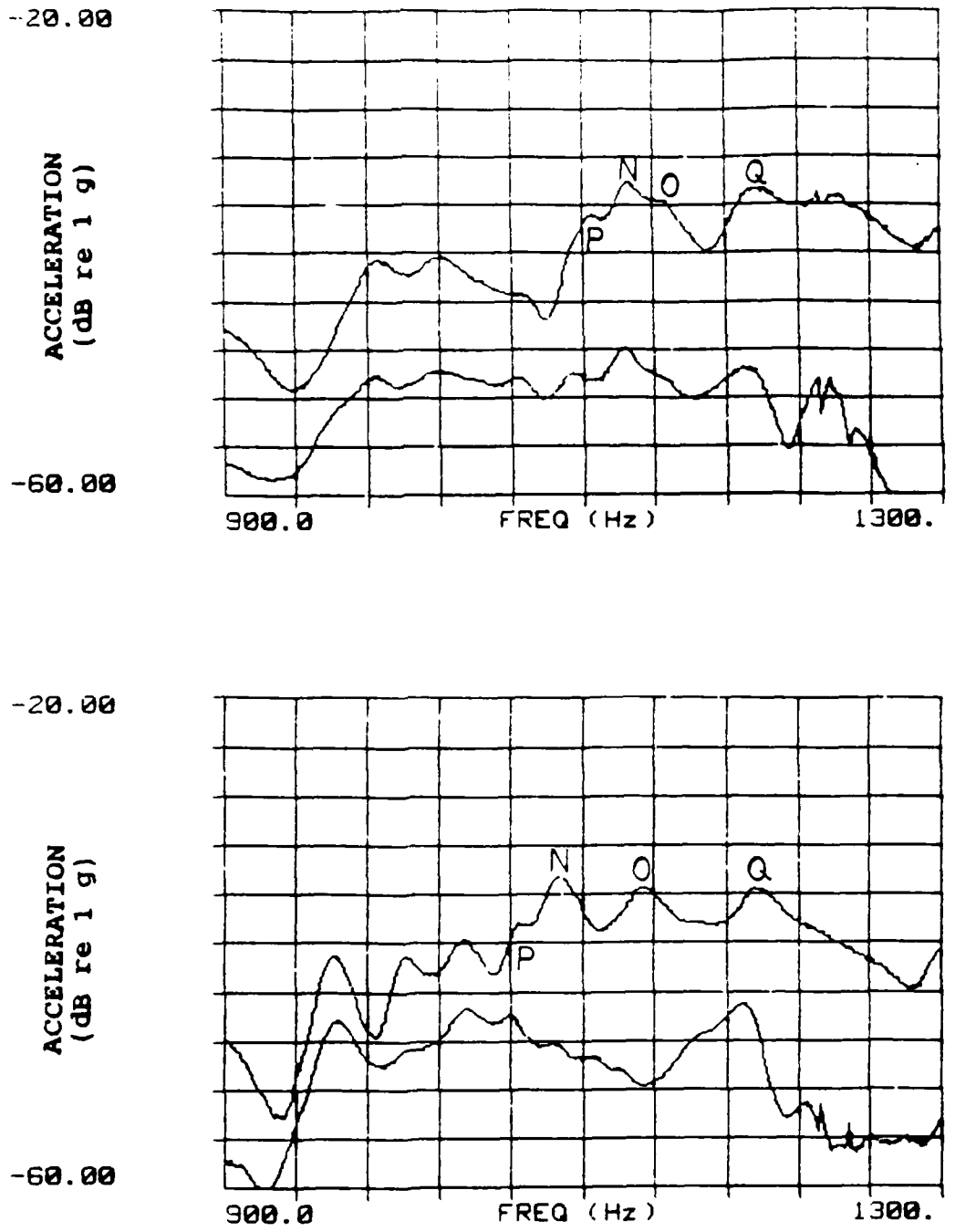

Figure 5.82 Beam 4 Waterborne (top graph) and Airborne (bottom graph). 100 grams tuning mass plus 600 grams coupling mass. From top in each graph: beam drive point acceleration, and mean plate acceleration.

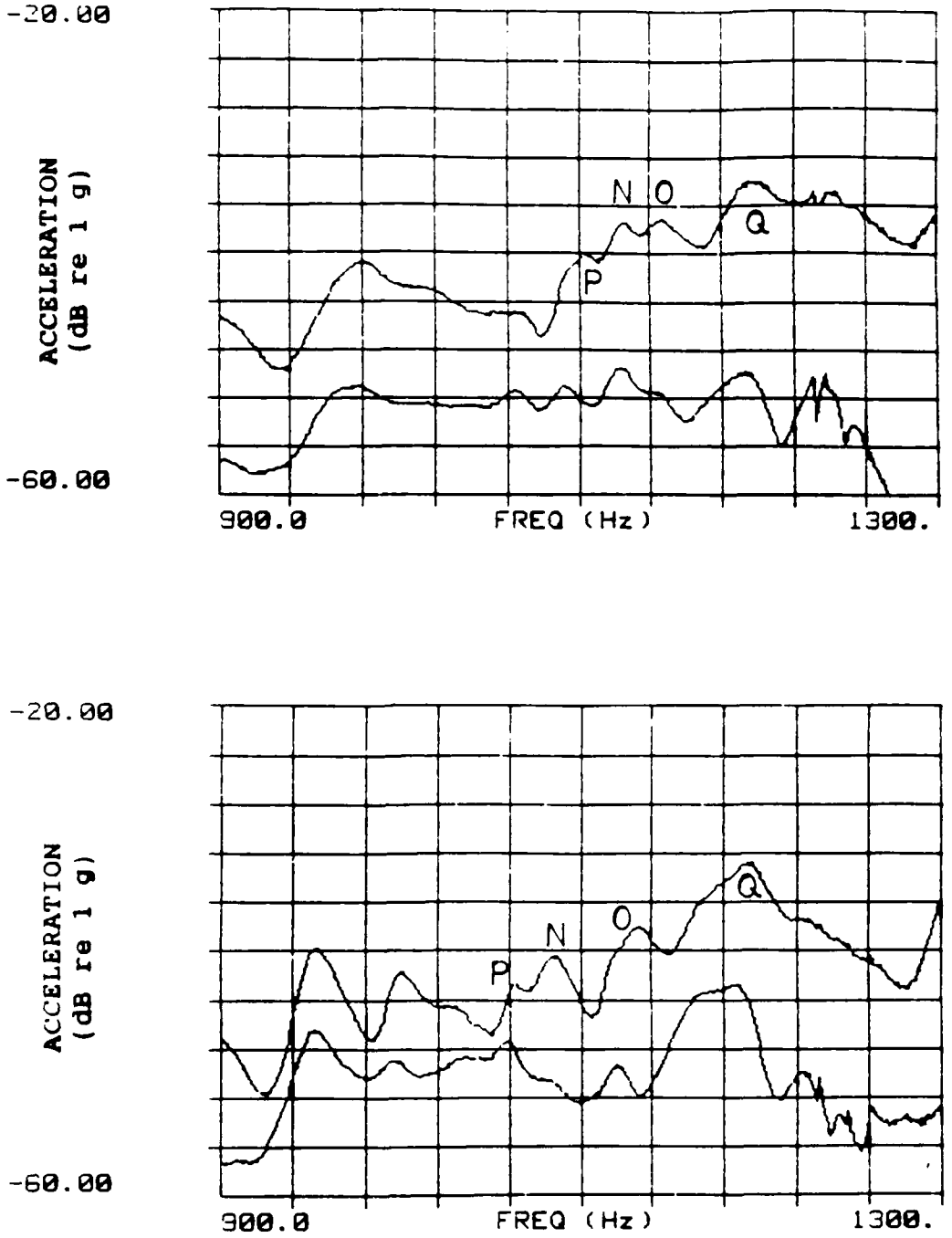

Figure 5.83 Beam 4 Waterborne (top graph) and Airborne (bottom graph). 100 grams tuning mass plus 1000 grams coupling mass. From top in each graph: beam drive point acceleration, and mean plate acceleration.

6 CONCLUSION

6.1 Discussion of Results

The experimental results presented in chapter 5 show that by applying small masses, it is possible to identify modes as predominantly plate (hull), beam (foundation), or a global combination of both the beam and the plate. As the size of the beam increases and its moment impedance approaches that of the plate, this identification can be performed by means of beam drive point spectrum data alone. For smaller beams with moment impedances on the order of 1 percent that of the plate, plate spectrum data is required to ensure globally acting plate modes are identified.

We have observed that sound radiation from global mode pairs changes dramatically (e.g. 12 dB in some cases) in response to small mass additions as both frequency and amplitude separation between the modes is varied. As the modes come close in frequency and amplitude, sound radiation increases. As the modes are separated in frequency and amplitude, sound radiation decreases. This close coupling of the global modes plays a more important role in sound radiation than beam or plate acceleration levels. We have repeatedly observed that beam and plate acceleration levels are not an accurate indicator of the sound radiation

The results presented in Chapter 5 also showed that global modes respond to tuning and coupling masses in a similar manner when the structure is waterborne or simply supported in air. The effects of fluid loading while waterborne are not so severe as to prevent identifying or following individual modes. However, the frequency separation between global mode pairs can vary dramatically between the waterborne and airborne cases.

The significant changes in sound radiation observed suggest that the methods applied during this research have potential application as a "fix" for structures with high waterborne sound radiation, in addition to use as a diagnostic tool for identifying potential waterborne sound problems during construction.

6.2 Suggested Further Research

The next logical step towards development and qualification of a method to identify and alter global modes in a full scale ship is to study the response of an experimental model more closely approximating a shipboard hull/foundation structure. The simple beams used for this research should be replaced with a multi-legged structure having multiple (e.g., 3 or 4) interfaces with the plate (hull). The existing experimental model used for this research could easily be modified as such to support continued research.

REFERENCES

[1] R. H. Lyon and J. B. Song, "Determination of Foundation/Hull Coupling from Foundation Mobility Functions", RH LYON CORP Report LC-122, 1 November 1987.

[2] R. H. Lyon and E. Eichler, "Random Vibration of Connected Structures", J. Acoust. Soc. Am., Vol. 36, No. 7, 1344-1354, July 1964.

[3] L. Cremer and M. Heckl, "Structure-Borne Sound", Springer-Verlag, New York, 1973.

[4] R. H. Lyon, "Machinery Noise and Diagnostics", Butterworths, Boston, 1987.

[5] Private Discussions with D. Goldsmith, David Taylor Research Center, Annapolis, Maryland, October 1988.

[6] R. H. Lyon and P. W. Smith, Jr., "Sound and Structural Vibration", NASA Contractor Report CR-160, March 1965.

[7] J. M. Komrower and L. Mitchel, "Recommended Procedure for Modal Testing of Noise Critical Naval Ship Systems and Foundations", NKF Engineering, Inc., NKF Report No. 8350-006B.

[8] M. C. Junger and D. Feit, "Sound, Structures, and Their Interaction", MIT Press, Cambridge, Massachusetts, 1972.

[9] C. M. Harris and C. E. Crede, "Shock and Vibration Handbook", McGraw-Hill, New York, 1976.

[10] M. R. Schroeder, "New Method of Measuring Reverberation Time", J. Acoust. Soc. Am., Vol. 37, No. 3, 409-412, March 1965.

[11] A. Levi, "Effect of Internal Fluid Containers on Sound Radiated Externally from a Surface Ship", M. Sc. Thesis, MIT, Dept. of Ocean Eng., January, 1989.

APPENDIX A - DAMPING LOSS FACTOR MEASUREMENT

A.1 Introduction

The purpose of this Appendix is to document the method used to determine the damping loss factor, η, for the experimental model. The Integrated Impulse method of obtaining acceleration decay rates is introduced and explained in Section A.4. Additionally, Section A.5 contains a listing for a program which calculates and displays the Integrated Impulse on a GenRad 2515 spectrum analyzer.

A.2 Experimental Setup

The setup used to determine damping loss factor for the experimental model is shown in Figure A.1.

A.3 Loss Factor and Acceleration Decay Rate

The equation for decay rate in dB/sec (DR) developed in [4] in terms of the damping loss factor (η) and center band frequency (f) is

$$DR = 27.3f\eta \tag{A.1}$$

Accordingly,

$$\eta = \frac{DR}{27.3f} \tag{A 2}$$

Since the reverberation time (T_{60}) is the time required for a 60 dB decay in vibration amplitude, Equation A.1 can be modified to yield

$$T_{60} = \frac{60}{DR} = \frac{2.2}{f\eta} \tag{A.3}$$

The decay rate for the plate in each 1/3 octave frequency band can be read directly off a plot of plate acceleration squared versus time when dB units are used to express acceleration squared.

Figure A.2 depicts the acceleration decay curve (dB/sec) for the plate in air in the 800 Hz 1/3 octave band. The prominent "humps" are the result of plate ringing. A decay rate can easily be determined from this decay curve. This frequency band is roughly 184 Hz wide (23 % of center frequency for 1/3 octave band). Since the average separation between plate modes is roughly 13 Hz, roughly 15 modes (on average) are decaying and interacting in the 800 Hz band. In such a case with many modes, the effect of a few modes coming into or out of phase with each other has very little impact on the decay curve.

When few modes are present (i.e. 2 or 3), however, wide amplitude fluctuations can occur at the accelerometer location due to in phase and out of phase conditions dominating the response. This situation can make it difficult to determine a decay rate from the acceleration response curve.

Figure A.3 depicts the acceleration decay curve (dB/sec) for the plate in air in the 100 Hz 1/3 octave band. Although a decay rate can be approximated from this curve, it is not as clear as in the case shown in Figure A.2. This can lead to inaccuracies in the calculated damping loss factor.

A.4 Integrated Impulse

To improve the accuracy of the acceleration decay rate determination, the plate could be impacted several t mes in the desired frequency band and the average decay rates obtained from each of the individual acceleration decay curves. This can be time consuming. An alternate method, the Integrated Impulse method, can be used to obtain accurate decay rates from a single measurement.

The Integrated Impulse method, developed in detail in [10], makes use of the fact that although the amplitude of the squared acceleration response may fluctuate wildly, the area under the squared response curve from time τ to infinity is decreasing at a relatively steady rate. In fact, from [10], the area under the squared response curve from any time τ to infinity is equal to the ensemble average of the squared acceleration response at that time τ. Therefore, the acceleration decay rate, and hence the damping loss factor, can be determined from integrating the acceleration response curve.

The validity of the Integrated Impulse method can easily be seen for the simple case of exponential decay, which is expected for a structure such as the steel plate used for this research. For example,

$$a^2(t) = a_0^2 e^{-\beta t} \tag{A.4}$$

where, a_0 is the acceleration at time t=0

β is the time constant for decay

Integration as described above yields:

$$\int_{\tau}^{\infty} a^2(t)dt = -\frac{a_0^2}{\beta} e^{-\beta t} \Big|_{t=\tau}^{\infty} = \frac{a_0^2}{\beta} e^{-\beta \tau} \tag{A.5}$$

Therefore, the area under the squared acceleration response curve from time τ to infinity decays with the same time constant as the squared acceleration response. Since the area decay curve is not subject to the wide fluctuations that the squared response curve experiences, the area decay curve will yield a better indication of the decay rate.

Figures A.4 and A.5 show the squared acceleration response decay curves for the 800 Hz and 100 Hz 1/3 octave bands along with the Integrated Impulse decay curves plotted above the response curves. As can be seen, the Integrated Impulse provides a clearer indication of the decay rate, and therefore, it is a better tool for calculation of the damping loss factor.

A.5 Program Listing for GenRad 2515 Analyzer

During the course of this research, the program listed on the next 2 pages was developed to calculate and display the Integrated Impulse of an acceleration time signal. This program is written in the Time Series Language (TSL2) programming language for the GenRad 2515 spectrum analyzer. The program is included here for information and use by others.

```
CREATE II
10 !
20 ! ---------------------------------------------------------------
30 !   Program to calculate and plot the Integrated Impulse
40 !   of an acceleration response signal.
50 !
60 !   Written by Kevin M. McCoy, Spring 1989
70 !
80 !   Ensure Subroutine 'MODLAC' (file access utility) is loaded.
90 !
100 ! ---------------------------------------------------------------
110 BLKCLR
120 ERASE
130 !
140 !  Identify and open the desired data file
150 !
160 PRINT 'ENTER THE FILE NAME TO ACCESS (e.g. DY0:DATA)'
170 INPUT A5
180 MODLAC 'OPEN',A5
190 !
200 PRINT 'ENTER THE NUMBER OF DISCREET TIME SAMPLES (e.g. 8192)'
210 INPUT I1
220 PRINT 'ENTER SOURCE & RECEIVER LOCATION FOR PLOT LABEL (40 CHAR)'
230 INPUT A1
240 ERASE
250 PRINT 'ENTER MIN,MAX TIME RANGE FOR X AXIS'
260 INPUT R9,R10
270 !
280 ! Initialize the dB scale range for the plot
290 !
300 I2=-100
310 I3=100
320 R1=R9
330 R2=R10
340 !
350 ! Display a listing of the chosen data file
360 !
370 MODLAC 'LIST'
380 !
390 ! Select the record number to plot
400 !
410 PRINT 'ENTER THE RECORD NUMBER TO PLOT'
420 INPUT I10
430 !
440 ! Read the chosen record number into data Block B1
450 !
460 MODLAC 'R',B1,'R',I10
470 ERASE
480 PRINT 'ENTER 1/3 OCTAVE BAND CENTER FREQUENCY (e.g. 100)'
490 INPUT A2
500 !
510 ! Square the acceleration response.
520 !
530 B2=B1*B1
540 !
550 ! Integrate the squared acceleration response from t=0 to tau
560 !
570 B3=INTG(B2)
580 !
```

Integrated Impulse Program for GenRad 2515 Analyzer

```
590 ! Integrate the squared acceleration response from t=0 to infinity
600 !
610 I5=I1-1
620 R8=B3[I5]
630 B5=R8-B3
640 R3=0
650 R4=R3/10
660 R5=EXP(R4)
670 B6=B5*R5
680 !
690 ! Plot the squared acceleration response
700 !
710 DISPLY B2,'FG','L100','DB','EX',R1,R2,'EXY',I2,I3,'XLAB','TIME (SEC)','AREA'
,200,589,210,410,'G','R'
720 !
730 ! Plot the Integrated Impulse
740 !
750 DISPLY B6,'SE','L100','DB','EX',R1,R2,'EXY',I2,I3,'XLAB','TIME (SEC)','AREA'
,200,589,210,410,'G','R'
760 I6=0
770 PRINT
780 I6=I6+1
790 IF I6,17,770,800,800
800 PRINT '      ACCELERATION & INTEGRATED IMPULSE - ',A1
810 PRINT '      ',A2,'HZ 1/3 OCTAVE BAND CENTER FREQUENCY'
820 !
830 ! Allow the user to change the plot
840 !
850 PRINT
860 PRINT
870 PRINT 'CHANGE PLOT ?  (<CR>=YES, 1=NO)'
880 INPUT I4
890 IF I4,1,900,1040,900
900 PRINT 'ENTER NEW MIN,MAX TIME RANGE - <CR>=',R1,',',R2
910 INPUT R6,R7
920 IF R7,0.930,950,930
930 R1=R6
940 R2=R7
950 PRINT 'ENTER NEW MIN,MAX DB RANGE - <CR>=',I2,',',I3
960 INPUT I7,I8
970 I8=I8-I7
980 IF I8,0,990,1010,990
990 I2=I7
1000 I3=I8+I7
1010 PRINT 'ENTER DB AMOUNT TO OFFSET INTEGRATED IMPULSE - <CR>=0'
1020 INPUT R3
1030 GOTO 650
1040 PRINT
1050 !
1060 ! Allow the user to plot another record number
1070 !
1080 PRINT 'PLOT ANOTHER RECORD NUMBER FROM FILE',A5,' ? (0=no, 1=yes)'
1090 INPUT I4
1100 IF I4,1,1130,1110,1110
1110 BLKCLR
1120 GOTO 300
1130 BLKCLR
1140 MODLAC 'CLOSE',A5
1150 RETURN
END
>
```

Integrated Impulse Program for GenRad 2515 Analyzer

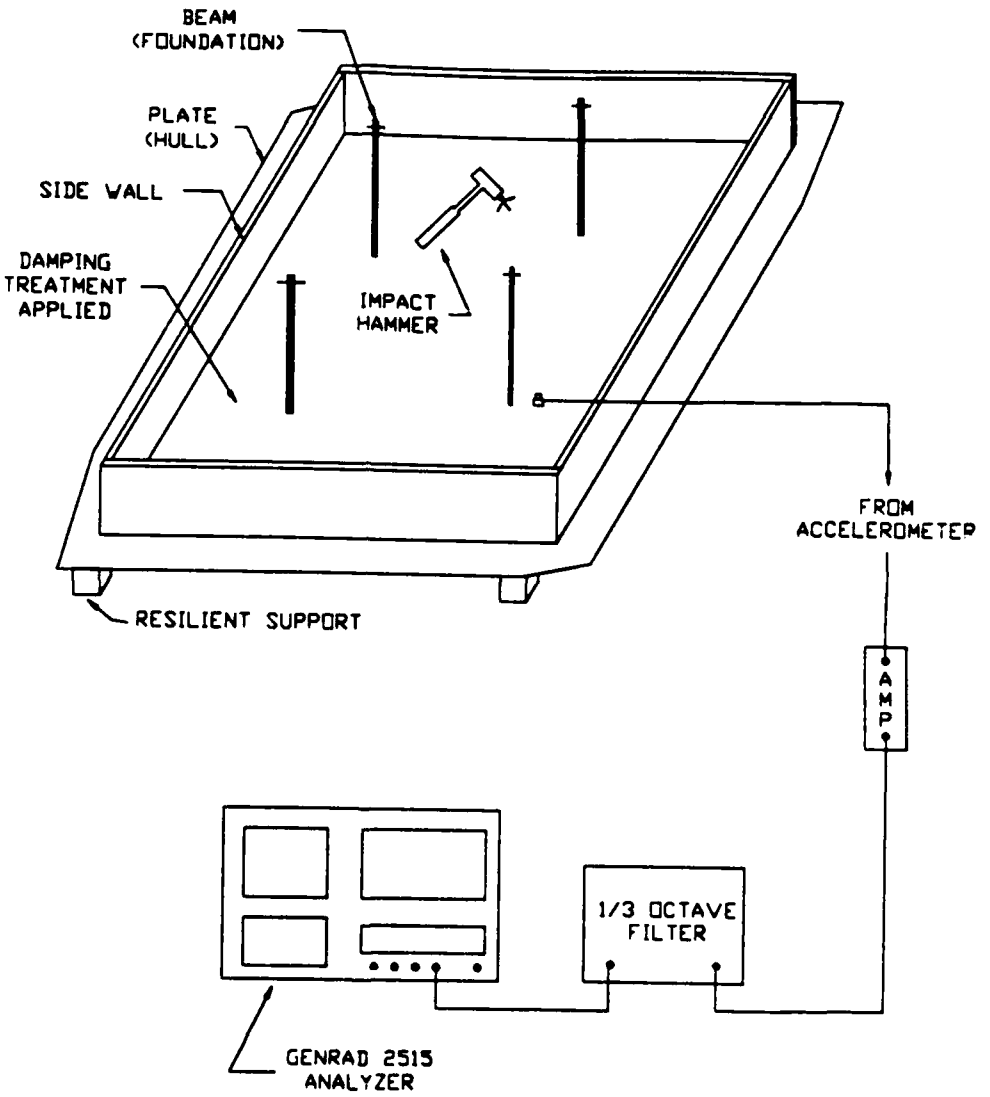

Figure A.1 Setup used to determine the damping loss factor as a function of frequency for the experimental model.

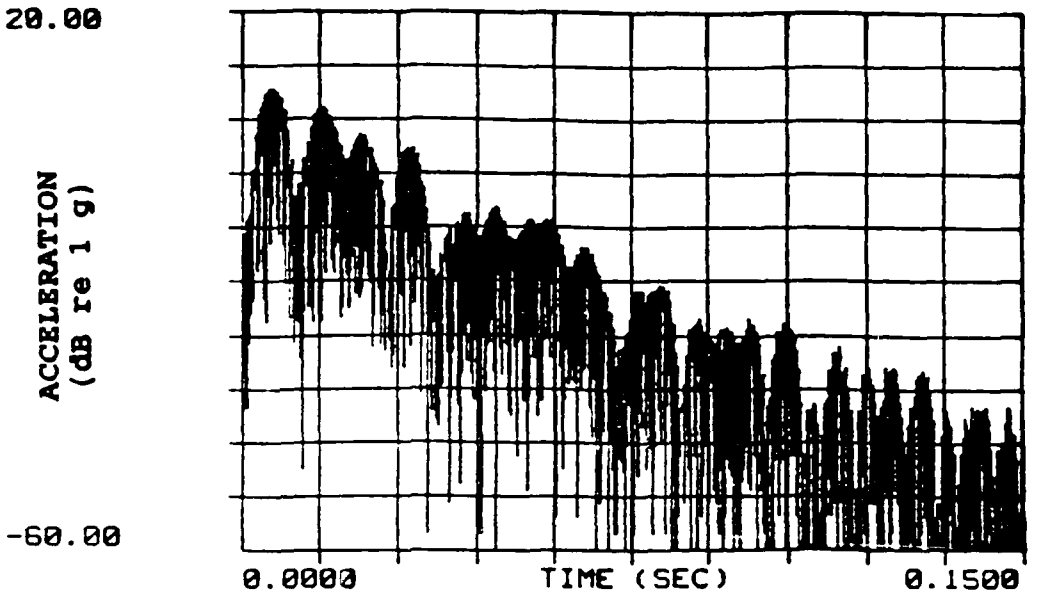

Figure A.2 Plate acceleration decay in air in the 800 Hz 1/3 octave band.

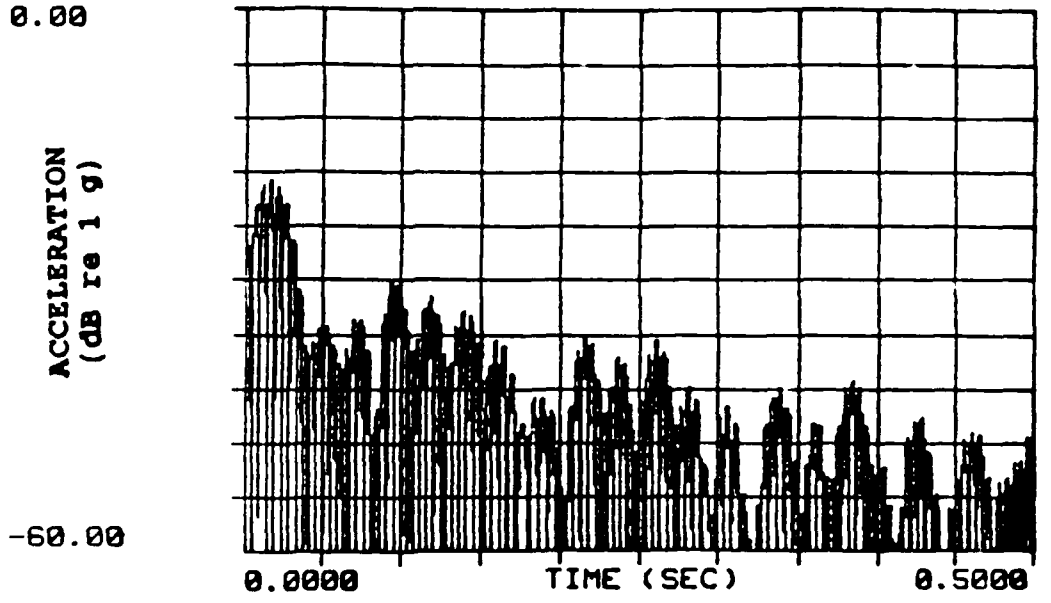

Figure A.3 Plate acceleration decay in air in the 100 Hz 1/3 octave band.

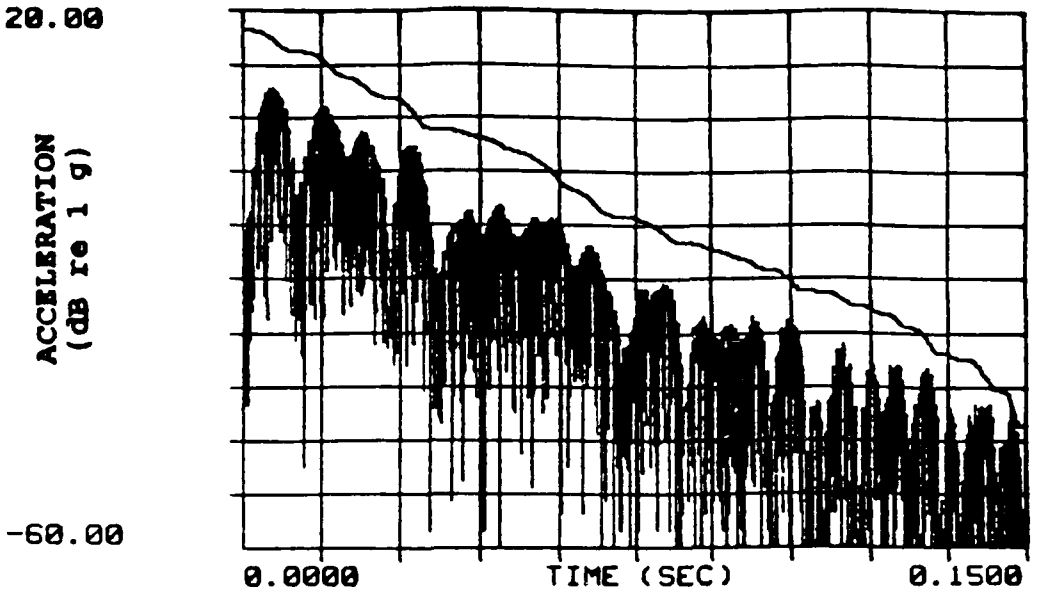

Figure A.4 Integrated Impulse (top) and plate acceleration decay (bottom) in air in the 800 Hz 1/3 octave band. The decay rate is 370 dB/sec; $\eta = 0.017$.

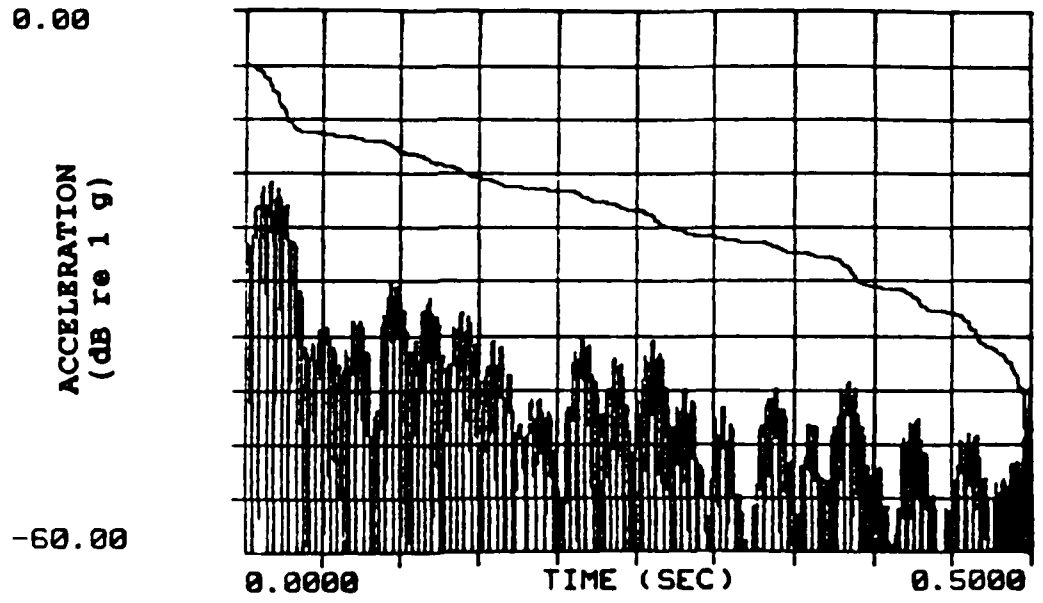

Figure A.5 Integrated Impulse (top) and plate acceleration decay (bottom) in air in the 100 Hz 1/3 octave band. The decay rate is 45 dB/sec; $\eta = 0.016$.

APPENDIX B - GENRAD 2515 PLOTTING PROGRAM

```
CREATE PLOT
10 !
20 !  ------------------------------------------------------------
30 !   Program to plot up to 6 spectra on a single graph.
40 !   This program will accommodate real (e.g., auto spectra)
50 !   or complex (e.g., transfer functions), or a combination
60 !   of real and complex data from up to 6 files.
70 !
80 !   The 6 data ranges can be offset a specified amount
90 !   in magnitude for discrimination.
100 !
110 !
120 !        Written by Kevin M. McCOY, MIT, Spring 1989
130 !
140 !  Ensure Subroutine 'MODLAC' (file access utility) is loaded.
150 !
160 ! ------------------------------------------------------------
170 !
180 !
190 ERASE
200 BLKCLR
210 !
220 ! Identify and open the desired data files.
230 !
240 !
250 PRINT 'ENTER NUMBER OF DATA RANGES (6 MAX)'
260 INPUT I1
270 PRINT 'ENTER THE NUMBER OF DIFFERENT FILES TO ACCESS'
280 INPUT I2
290 IF I2,1,300,300,570
300 PRINT 'ENTER THE FILENAME (e.g. DL1:TEST.DAT)'
310 INPUT A1
320 MODLAC 'O',A1
330 PRINT 'ENTER FIRST RECORD NUMBER'
340 INPUT I5
350 MODLAC 'R',B1,'R',I5
360 IF I1,2,880,370,370
370 PRINT 'ENTER SECOND RECORD NUMBER'
380 INPUT I5
390 MODLAC 'R',B2,'R',I5
400 IF I1,3,880,410,410
410 PRINT 'ENTER THIRD RECORD NUMBER'
420 INPUT I5
430 MODLAC 'R',B3,'R',I5
440 IF I1,4,880,450,450
450 PRINT 'ENTER FOURTH RECORD NUMBER'
460 INPUT I5
470 MODLAC 'R',B4,'R',I5
480 IF I1,5,880,490,490
490 PRINT 'ENTER FIFTH RECORD NUMBER'
500 INPUT I5
510 MODLAC 'R',B5,'R',I5
520 IF I1,6,880,530,530
530 PRINT 'ENTER SIXTH RECORD NUMBER'
540 INPUT I5
550 MODLAC 'R',B6,'R',I5
560 GOTO 880
570 FOR I6,1,I1
580 PRINT 'ENTER THE FILENAME FOR RANGE',I6,'   (e.g. TEST.DAT)'
590 INPUT A1
```

```
600 PRINT 'ENTER THE RECORD NUMBER FOR RANGE',I6
610 INPUT I5
620 IF I6,2,630,670,710
630 MODLAC 'O',A1
640 MODLAC 'R',B1,'R',I5
650 MODLAC 'C'
660 GOTO 870
670 MODLAC 'O',A1
680 MODLAC 'R',B2,'R',I5
690 MODLAC 'C'
700 GOTO 870
710 IF I6,4,720,760,800
720 MODLAC 'O',A1
730 MODLAC 'R',B3,'R',I5
740 MODLAC 'C'
750 GOTO 870
760 MODLAC 'O',A1
770 MODLAC 'R',B4,'R',I5
780 MODLAC 'C'
790 GOTO 870
800 IF I6,6,810,850,850
810 MODLAC 'O',A1
820 MODLAC 'R',B5,'R',I5
830 MODLAC 'C'
840 GOTO 870
850 MODLAC 'O',A1
860 MODLAC 'R',B6,'R',I5
870 NEXT I6
880 ERASE
890 !
900 !
910 !  Enter the desired plot parameters and labels.
920 !  Note, these can be changed after viewing the plot.
930 !
940 !
950 PRINT 'ENTER MIN,MAX FREQUENCY RANGE'
960 INPUT I3,I4
970 PRINT 'ENTER MIN,MAX DB RANGE'
980 INPUT I5,I6
990 IF I1,2,1020,1000,1000
1000 PRINT 'ENTER DB OFFSET FOR EACH RANGE'
1010 INPUT R3
1020 PRINT 'ENTER PLOT DESCRIPTION - FIRST LINE (40 CHAR)'
1030 INPUT A1
1040 PRINT 'ENTER PLOT DESCRIPTION - SECOND LINE (40 CHAR)'
1050 INPUT A2
1060 PRINT 'ADD A GRID TO THE PLOT ? (<CR>=NO, 1=YES)'
1070 INPUT I11
1080 !
1090 !
1100 !  Determine if the data is real or complex.  If complex,
1110 !  the data is converted to real and squared (dB=10 log).
1120 !  Real spectrum data is stored in its squared form by RTA.
1130 !
1140 !
1150 BIBSET B1,8,i1
1160 IF i1,2,1200,1170,1170
1170 B7=CABS(B1)
1180 B7=B7*B7
1190 GOTO 1210
```

Plotting Program for GenRad 2515 Analyzer

```
1200 B7=B1
1210 IF I1,2,1620,1220,1220
1220 BIBSET B2,8,i1
1230 IF i1,2,1270,1240,1240
1240 B8=CABS(B2)
1250 B8=B8*B8
1260 GOTO 1280
1270 B8=B2
1280 IF I1,3,1620,1290,1290
1290 BIBSET B3,8,i1
1300 IF i1,2,1340,1310,1310
1310 B9=CABS(B3)
1320 B9=B9*B9
1330 GOTO 1350
1340 B9=B3
1350 IF I1,4,1620,1360,1360
1360 BIBSET B4,8,i1
1370 IF i1,2,1410,1380,1380
1380 B10=CABS(B4)
1390 B10=B10*B10
1400 GOTO 1420
1410 B10=B4
1420 IF I1,5,1620,1430,1430
1430 BIBSET B5,8,i1
1440 IF i1,2,1480,1450,1450
1450 B11=CABS(B5)
1460 B11=B11*B11
1470 GOTO 1490
1480 B11=B5
1490 IF I1,6,1620,1500,1500
1500 BIBSET B6,8,i1
1510 IF i1,2,1550,1520,1520
1520 B12=CABS(B6)
1530 B12=B12*B12
1540 GOTO 1620
1550 B12=B6
1560 !
1570 !
1580 !  Calculate the dB offset and plot the data.
1590 !
1600 !
1610 !
1620 IF I11,1,1650,1630,1630
1630 DISPLY B7,'FG','L100','DB','EX',I3,I4,'EXY',I5,I6,'XLAB','FREQ (Hz)','AREA'
,200,589,210,410,'G','R'
1640 GOTO 1660
1650 DISPLY B7,'RES','L100','DB','EX',I3,I4,'EXY',I5,I6,'XLAB','FREQ (Hz)','AREA
',200,589,210,410,'G','R'
1660 IF I1,2,1960,1670,1670
1670 R4=R3/10
1680 R4=EXP(R4)
1690 B8=B8/R4
1700 DISPLY B8,'SE','L100','DB','EX',I3,I4,'EXY',I5,I6,'XLAB','FREQ (Hz)','AREA'
,200,589,210,410,'G','R'
1710 B8=B8*R4
1720 IF I1,3,1960,1730,1730
1730 R5=R3/5
1740 R5=EXP(R5)
1750 B9=B9/R5
1760 DISPLY B9,'SE','L100','DB','EX',I3,I4,'EXY',I5,I6,'XLAB','FREQ (Hz)','AREA'
,200,589,210,410,'G','R'
```

Plotting Program for GenRad 2515 Analyzer

```
1770 B9=B9*R5
1780 IF I1,4,1960,1790,1790
1790 R6=0.3*R3
1800 R6=EXP(R6)
1810 B10=B10/R6
1820 DISPLY B10,'SE','L100','DB','EX',I3,I4,'EXY',I5,I6,'XLAB','FREQ (Hz)','AREA
',200,589,210,410,'G','R'
1830 B10=B10*R6
1840 IF I1,5,1960,1850,1850
1850 R7=0.4*R3
1860 R7=EXP(R7)
1870 B11=B11/R7
1880 DISPLY B11,'SE','L100','DB','EX',I3,I4,'EXY',I5,I6,'XLAB','FREQ (Hz)','AREA
',200,589,210,410,'G','R'
1890 B11=B11*R7
1900 IF I1,6,1960,1910,1910
1910 R8=R3/2
1920 R8=EXP(R8)
1930 B12=B12/R8
1940 DISPLY B12,'SE','L100','DB','EX',I3,I4,'EXY',I5,I6,'XLAB','FREQ (Hz)','AREA
',200,589,210,410,'G','R'
1950 B12=B12*R8
1960 FOR I9,1,17
1970 PRINT
1980 NEXT I9
1990 PRINT '      ',A1
2000 PRINT '      ',A2
2010 PRINT
2020 PRINT
2030 !
2040 !
2050 !  Allow the user to change the plot.
2060 !  Carriage return (<CR>) defaults to the previous value.
2070 !
2080 !
2090 PRINT 'CHANGE GRAPH (<CR>=YES, 1=EXIT)'
2100 INPUT I9
2110 IF I9,1,2120,2550,2120
2120 PRINT 'ENTER NEW MIN,MAX FREQUENCY RANGE  - <CR>=',I3,',',I4
2130 INPUT I9,I10
2140 IF I10,1,2170,2150,2150
2150 I3=I9
2160 I4=I10
2170 PRINT 'ENTER NEW MIN,MAX DB RANGE  - <CR>=',I5,',',I6
2180 INPUT I9,I10
2190 I10=I10-I9
2200 IF I10,0,2230,2230,2210
2210 I5=I9
2220 I6=I9+I10
2230 PRINT 'ENTER NEW DB OFFSET  - <CR>= ',R3,'   FOR ZERO OFFSET ENTER 99 '
2240 INPUT R9
2250 IF R9,0,2260,2320,2280
2260 R3=R9
2270 GOTO 2320
2280 IF R9,99,2290,2310,2290
2290 R3=R9
2300 GOTO 2320
2310 R3=0
2320 IF I11,1,2330,2360,2360
2330 PRINT 'ADD GRID ? (<CR>=NO, 1=YES)'
```

Plotting Program for GenRad 2515 Analyzer

```
2340 INPUT I11
2350 GOTO 2410
2360 PRINT 'DELETE GRID ? (<CR>-NO, 1-YES)'
2370 INPUT I13
2380 IF I13,1,2390,2400,2400
2390 GOTO 2410
2400 I11=0
2410 PRINT 'CHANGE TITLES ?  (<CR>- NO, 1-YES)'
2420 INPUT I9
2430 IF I9,1,1620,2440,2440
2440 PRINT 'CHANGE FIRST LINE ?  (<CR>-NO, 1-YES)'
2450 INPUT I9
2460 IF I9,1,2490,2470,2470
2470 PRINT 'ENTER PLOT DESCRIPTION - FIRST LINE (40 CHAR)'
2480 INPUT A1
2490 PRINT ' CHANGE SECOND LINE ? (<CR>-NO, 1-YES)'
2500 INPUT I9
2510 IF I9,1,1620,2520,2520
2520 PRINT 'ENTER PLOT DESCRIPTION - SECOND LINE (40 CHAR)'
2530 INPUT A2
2540 GOTO 1620
2550 RETURN
END
>
```

Plotting Program for GenRad 2515 Analyzer